QiR
" Quality in Research "

Proceeding

THE 10th INTERNATIONAL CONFERENCE ON QUALITY IN RESEARCH (QIR)

"Research For Future Better Life"



Faculty of Engineering

Engineering Center University of Indonesia, Depok

4 - 6 December 2007

Special Session on Electronics Engineering
&
Information & Communication Technology

Supported by :

LEMTEK FT UI

FOREWORDS
Dean of Faculty of Engineering, University of Indonesia

The Quality in Research (QIR) Conference is the annual event organized by the Faculty of Engineering, University of Indonesia. Since started in 1998, it has become an excellent forum of discussion for all researchers from research institutions and universities all over the nation of Indonesia. The 1st and 6th QIR Conferences had been successfully organized as the high quality national conferences, and starting from the 7th QIR conference, has been organized to invite international research papers.

The 10th Quality in Research International Conference having a theme of "Research for future better life" is to provide an international forum for exchange of the knowledge, information, experience and result as well as the review of progress and discussion on the state of the art and the future trend various issues and the developments in the multi-fields of scientific and technology. The main purposes of this conference are to provide a forum for free discussion of new ideas, development and applications, including techniques and methods to stimulate and inspire pioneering work, to provide opportunities for students and young engineers to meet their experienced peer and to provide a meeting that will enforce progress, stimulate growth and advance the state of knowledge in the multi-fields of science and technology.

We would like to express our heartiest to thank to all authors and participants for their active participations in the 10th on Quality in Research (QIR) International Conference 2007, and also to all the paper reviewers, member of the technical committees, and member of the organizing committees, for their support to the success of this conference. Last but not the least; we would also like to invite all participants to the next on Quality in Research (QIR) Conference.

Faculty of Engineering, University of Indonesia
Dean,

Prof. Ir. Rinaldy Dalimi, Ph.D

FOREWORDS
Chairman of 10th International Conference on QIR 2007

The 10th Quality in Research International Conference will provide an international forum for exchange the knowledge, information, experience and recent researches of various fields. With a strong support and presentations from academic, industry and entrepreneurs, the conference will provide an ideal platform to learn various fields and understand technological trends in the region.

The 10th Quality in Research (QIR) International Conference has a theme of "Research for Better Future Life" being the third time to go internationally, has invited limited papers from other nations such as Korea and Malaysia. The conference is organized in parallel sessions focusing on the 8 (eight) research areas such that many researchers and peer groups may focus their discussion on the relevant topics. All submitted papers had been reviewed by the technical committees and had been arranged into 8 (eight) sub-themes according to the following fields:

- **Energy, Process and Environmental Engineering and Management:** Energy and environmental issues, combustion technology, fluids mechanics and thermal fluid machinery, thermodynamics and heat transfer, geotechnical and environmental engineering, etc.
- **Industrial, Manufacturing, Material Engineering, and Management:** Production Engineering, Supply Chain Management, Innovation System, Maintenance System, Quality Management System, Human Factors Engineering, Organizational System, Fabrication and Industrial Automation, Manufacturing System: Control Management and Information Technology, etc
- **Biomaterial, Biomedical Engineering and Biotechnology:** Biomedical numerical modeling, Biomaterial, Biosensor, Biocompatibility, Biomechanics, Biotechnology, Biomedical Instrumentation, Biomedical Imaging
- **Design and Infrastructure Engineering and Management:** Product design and development, composite: Materials and applications, structural dynamics, mechanics of materials, Construction Management, Public Infrastructures and Services, Structural Engineering, etc
- **Special Session on Electronics Engineering**
- **Information and Computation Technology**
- **Sustainable Architecture**
- **Nanomaterials and Nanotechnology:** Nano structured material, Nanotechnology, Nanocomposite, MEMS, Self Assembled Monolayer, Thin Film, etc

The main purposes of this conference are to provide a forum for free discussion of new ideas, development and applications, including techniques and methods to stimulate and inspire pioneering work, to provide Opportunities for students and young engineers to meet their experienced peer and to provide opportunities for students and young engineers to meet their experienced peer and to provide a meeting that will enforce progress, stimulate growth and advance the state of knowledge in the multi-fields of science and technology.

Depok, 4 December 2007
The Organizing Committee,
Chairman,

Gunawan Wibisono, Ph.D

Steering Committee

1. Prof. Dr-Ing. Axel Hunger, Universitaet, Duisburg-Essen, Germany
2. Prof. Dr. Carlo Morandi, Universida Degli Studi de Parma, Italy
3. Prof. Dr. Iwao Sasase, KEIO University, Japan
4. Prof. Kim Kyoo-ho, Yeungnam University, Korea
5. Prof. Dr. Ir. Irwan Katili, University of Indonesia
6. Prof. Dr. Ir. Bambang Suryawan, MT, University of Indonesia
7. Prof. Dr. Ir. Dadang Gunawan, M.Eng, University of Indonesia
8. Prof. Dr. Ir. Johny W Soedarsono, DEA, University of Indonesia
9. Prof. Ir. Gunawan Tjahjono, M.Arch, Ph.D, University of Indonesia
10. Prof. Dr. Ir. M. Nasikin, University of Indonesia
11. Isti Surjandari, Ph.D, University of Indonesia
12. Prof. Dr. Ir. Budi Susilo Soepandji, University of Indonesia
13. Prof. Dr. Ir. Sutanto Soehodho, University of Indonesia
14. Prof. Dr. Ir. Sulistyoweny Widanarko, Dilp. SE. MPH, University of Indonesia
15. Prof. Dr. Ir. I Made Kartika Dipl. Ing, University of Indonesia
16. Prof. Dr. Ir. Tresna P. Soemardi, University of Indonesia
17. Prof. Dr. Ir. Sardy, M.Eng, M.Sc, University of Indonesia
18. Prof. Dr. Ir. Bagio Budiardjo M.Sc, University of Indonesia
19. Prof. Dr. Ir. Djoko Hartanto, M.Sc, University of Indonesia
20. Prof. Dr. Ir. Eddy Siradj, M.Eng, University of Indonesia
21. Dr. Ir. Kemas Ridwan K, University of Indonesia
22. Prof. Dr. Widodo Wahyu P, DEA, University of Indonesia
23. Ir. Boy Nurtjahyo M.,MSIE, University of Indonesia
24. Dr. Ir. Dedi Prihadi DEA, University of Indonesia
25. Ir. Hendri D.S. Budiono, M.Eng, University of Indonesia
26. Dr. Ir. Sigit Pranowo Hadiwardoyo, DEA, University of Indonesia
27. Dr. Ir. Herr Soeryantono, University of Indonesia
28. Prof. Rinaldy Dalimi, Ph.D, University of Indonesia

Chairman of the Conference

Ir. Gunawan Wibisono, M.Sc, Ph.D

Technical Committee

1. Ir. Gunawan Wibisono, M.Sc, Ph.D
2. Dr. Yosia Irwan
3. Dr. Engkos Kosasih
4. Purnomo Sidi P, Ph.D
5. Abdul Muis, Ph.D
6. Badrul Munir, Ph.D
7. Tania Surya Utami, MT
8. Ir. Beatrianis, M.Si

TABLE OF CONTENTS

ICT-07 Characteristics of Non Uniform FBG in C-band region Using Transfer Matrix Method
by: Qadriyyah, Ary Syahriar

ICT-08 DNA-Based Application Design for Secure-Mobile Network
by: Muhammad Suryanegara, Dadang Gunawan

ICT-09 A High Performance Wireless MIMO Communication System
by: Ahmad Taqwa, Soegijardjo Soegijoko, Sugihartono, and Suhartono Tjondronegoro

ICT-10 The Development of DSP Algorithm for Virtual Surround Sound using TMS320 C6713 DSK
by: Fajar Dwi Satyo, Muhammad Suryanegara, Dadang Gunawan

ICT-11 Evaluation of Indoor HSDPA Performance Applying FEC Turbo Code
by: Muhammad Suryanegara and Moh. Harry Prabowo

ICT-12 Performance Analysis Of SPIHT Compressed Image Transmission with Diversity Selection Combining on Radio Frequency
by: Baharuddin

ICT-13 Simulation and Analysis of IPTV Video Transmission and Video Quality Assessment with MPQM Method
by: F. Dwi S and M. Asvial

ICT-14 Intrusion Detection of Mobile Ad-Hoc Network (MANET): A Literature review
by: Satria Mandala, Md. Asri Ngadi, Abd. Samad bin Haji Ismail, and A. Hanan Abdullah

ICT-15 Planning of digital Televison System With DVB-T-Tecnology in Indonesia
by: Denny Setiawan, Adis Alifiawan

ICT-16 SPIHT Compressed Image Transmission with Diversity Selection Combining Method On Wavelet Domain
by: Baharuddin

ICT-17 On the Design, Implementation and Evaluation of Networking System for Context Sensitive Classroom
by: Kalamullah Ramli

ICT-18 XML Transformation for Adaptive M-Learning
by: Sri Wahjuni, Kalamullah Ramli

ICT-19 Performance Evaluation of Weighted Round Robin based Scheduler over Wimax
by: Riri Fitri Sari, I Gde D, Nur Mukhayaroh, Dewi Laksmita

ICT-20 SIMPLE-O: Web based automated essay grading system using latent semantic analysisi method for Indonesia language considering wieghtr word and word synonym
by: Anak Agung Putri Ratna, Adhe W Astato, Bagio Budiardjo, Djoko Hartanto

ICT-21 On the Development of Mobile User Interface for VeRAS: Programmable Universal Remote Access System with Context-Sensitive Approach
by: Kalamullah Ramli

ICT-22 Design of Ultra Wideband Microstrip Antennas Using Genetic Algorithm
by: Sofian Hamid

ICT-23 Studies on technical selection and tariff model for implementation of mobile number portability
by: Djamhari S, Gunawan W, and Zuhad Kurniawan

ICT-24 Wavelength Dependence in Three Waveguides Directional Coupler Using Method of Lines
by: Helmi Adam, Ary Syahriar

ICT-25 Circularly Polarised Equilateral Triangular Patch Microstrip Antenna for Quasi Zenith Satellite
by: M. Darsono and Eko Tjipto R

ICT-26 V-Shaped Linear Tapered Slot Antenna with CPW Feed for Ultra Wideband Applications
by: Fitri Yuli Zulkifli, Bayu Aji, Eko Tjipto Rahardjo

ICT-27 Audio video processing on tapeless on-air television system
by: Dodi Sudiana and M. Sudiantoro

ICT-28 Dual Frequency Equilateral Triangular Microstrip Antenna for Indoor GSM Application
by: Fitri Yuli Zulkifli, Agus Rahmatullah, Eko Tjipto Rahardjo

ICT-29 Synchronization Mechanism in software for optical component analyzer
by: Z. Akbar and B. Widiyatmoko

ICT-30 A Preliminary Implementation of Joint Source and Channel Coding in MIMO System
by: Lydia Sari, Gunawan Wibisono, Dadang Gunawan

ISSN: 1411-1284

A mm-wave signal generation using laser diode : preliminary study

Bambang Widiyatmoko, Tomi Budi Waluyo and Masbah R.T Siregar

Research Center for Physics, Indonesia Institute of Sciences
Komplek PUSPIPTEK, Cisauk, Tangerang
Tel. 021-7560570, fax. 021-7560554 email : bamb039@lipi.go.id

Abstract– We proposed a technique for generating microwave signal by beating two laser diodes. Two lights from distributed feedback (DFB) laser diodes combined in intensity and polarity using a polarization maintained fiber coupler and detected by high speed photodetector. By tuning one of the laser frequency the generated microwave signal can be swept or selected from DC to 8.5 GHz.

Keywords– Laser frequency, mm-wave, heterodyne detection

I. INTRODUCTION

Signal in in the upper mm-wave region is interesting for short range communication such as for radio on fiber, as well as for spectroscopy and imaging application. However, it is difficult to generate clean signal which typically using frequency multiplier technique of low frequency signal source and will increase the phase noise of the signal.

In another side, laser is high frequency oscillator with high Q-factor, so it can be used as reference oscillator. However, the laser frequency is far from usual used microwave frequency. We can not count laser frequency as well as microwave signal.

We propose tecnique to generate mm-wave using heterodyne mixing between two stabilized laser. In this method, the generated mm-wave can tuned and synthezed by controlling one of the laser frequenc.

Preliminary study was done using two DFB laser. The results of preliminary experiment will be presentaed in this paper.

II. BASIC THEORY

Laser or optical wavelength is very short, and correspond to very high carrier frequency. In communication increasing the carrier frequencytheoritically increases the available transmission bandwidth. As a results, frequencies in optical range may have potential bandwidths of approximatically 105 times that of a carrier in the rf range[1].

Take example two lasers that haves frequency ν_0 and ν_s and its signal of electrics field E_0 and E_s that can form in equation as follows

$$E_0 = A_0 \cos(\varpi_0 t)$$
$$E_s = A_s \cos(\varpi_s t + \theta)$$

where $\omega_0=2\pi\nu_o$ dan $\omega_s=2\pi\nu_s$.

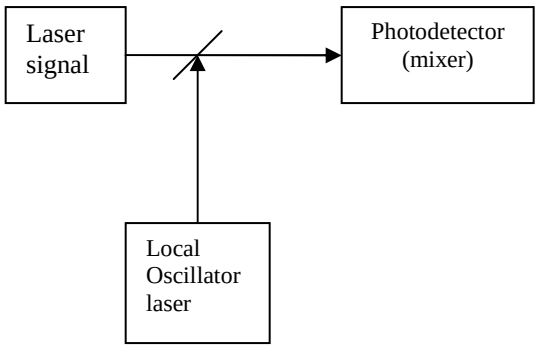

Figure 1. Scematic of heterodyne detection

Basic principle of heterodyne detection or mixing as shown in figure 1. Two laser which one of them as local oscillator is mixed each other at the photodetector. If the local oscillator (LO) is the same wavelength as the received optical signal, and in addition is in phase with optical carriers, the detection is called homodyne detection. If frequencies of the LO and received signal are different, then is called heterodyne detection. The heterodyne detector converts phase changes in optical carriers to phase changes in optical intencity, which are reproducced in the detected current waveform. If two beams are spatially well aligned, there is optical inteference on the photodetector surface, resulting the intensity

$$I \approx (E_s + E_l)^2 \quad \text{.....(1)}$$

This inherent squaring operation of the photodetector produces a photodetector current at intermediate frequecy. If the local oscillator and carrier beams are alight perpendicular to the photodetector surface, the expression of the field incident on the detector is :

$$E(t) = E_s(t)\cos[\varpi_s(t) + \phi_s] + E_l(t)\cos[\varpi_l(t) + \phi_l] \quad \text{.....(2)}$$

The photodetector output current is propotional to the detector resposivity and the optical intensity. The resposivity is given by:

$$\Re = \frac{e\eta_q}{h\nu} \quad \text{.....(3)}$$

Where e is electron charge, η_q is the detector quantum efficiency, h is Plack constans and n is laser frequency. Therefore.

$$i(t) = \frac{e\eta_q}{h\nu}[E(t)]^2 \quad \text{.....(4)}$$

$$E^2(t) = [E_S(t)\cos\{\varpi_S(t) + \phi_S\} + E_l(t)\cos\{\varpi_l(t) + \phi_l\}]^2 \quad \text{.....(5)}$$

High frequency intensity components has frequency twice of optical locak frequency are eliminate, because that frequency is much greater than the frequency response of photodetector. The generate photocurrent is propotional to the average optical intensity, therefore:

$$i(t) \propto 2E_l(t)E_s(t)\cos\{(\varpi_S(t) - \varpi_l)t + (\phi_l - \phi_S)\} \quad \text{.....(6)}$$

From equation (6) the detected current is depend on the laser power and its frequency is same with frequency different between two lasers. From this relation, it means that from two different frequency laser can generate microwave or mm-wave signal. This principe is used in this experiment.

II. EXPERIMENTAL SET UP

Figure 2 shown the experiment set-up. Two laser diode that current and temperature operation are precisely controlled was used in this experiment. Laser 1 is DFB laser, that the laser wavelength can tuned continuesly and don't have mode hope is the range of more then 2 nm. DFB laser 1 has maximum power 20 mW, coupled by polarization maintenance fiber. Laser 2 is DFB laser that has fix wavelength of 1552 nm. Laser was coupled with PM fiber. Two laser was combined by 90:10 fiber coupler. One port of 10% was used for monitoring the laser spectrum using optical spectrum analyzer. Another port coupled to high speed photodetector to generate microwave signal. In this experiment photodetector type R402 product Discovery semiconductor was used. This photodetector has frecuency respons from 100 Khz to 10 GHz which opitcal input was coupled by single mode fiber. Microwave signal was measured using RF spectrum analyzer which has frequency range of dc to 8.5 GHz.

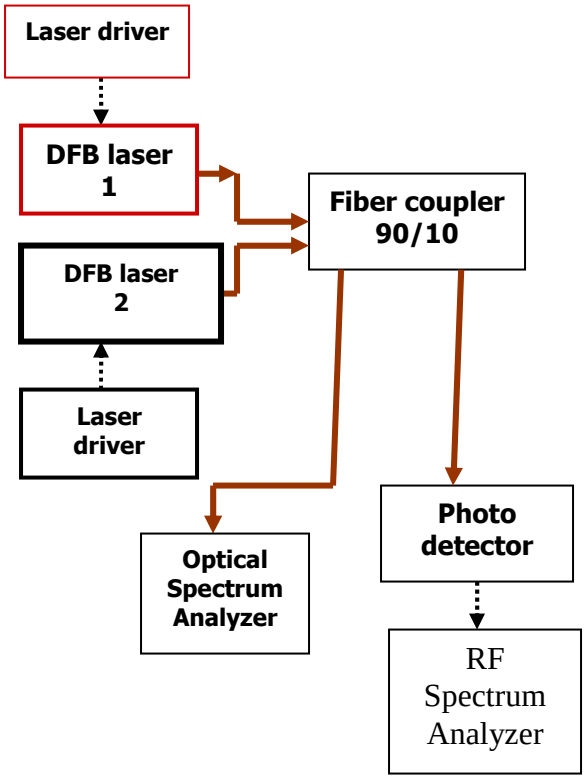

Figure 2. Block diagram of experiment set-up

III. EXPERIMENTAL RESULTS AND DISCUSSION

The optical spectrum of two laser when different frequency between them is far from bandwidth of photodetector is shown in figure 3a and 3b. In this experiment wavelength of the DFB laser 1 is fixed by control the injectin current and operating temperature. Figure 3a is spectrum when wavelength of DFB laser 2 is shorter then DFB laser 1 and figure 3 b spectrum when wavelength of the DFB laser is longer then DFB laser 2. Figure 4 shown the two lasers spectrum when different frequency between them is lower then frequency response of photodetedctor. By adjusting the wavelength of DFB laser 2 by changed the operation temperature , the beat signal in microwave frequency is detected by photodetector. Figure 5 a, b shown the RF spectrum of beat signal measured by RF spectrum analyzer. Figure 5a is RF spectrum when operating temperatur of laser was 26.2^{o}C, the beat signal frequency was 2,5 GHz and figure 5 b is RF spectrum when operating temperature was 27.1^{o}C and the

beat frequency was 8.4 GHz. The frequency change coefficient of the DFB laser was calculate as 80 GHz/^{o}C.

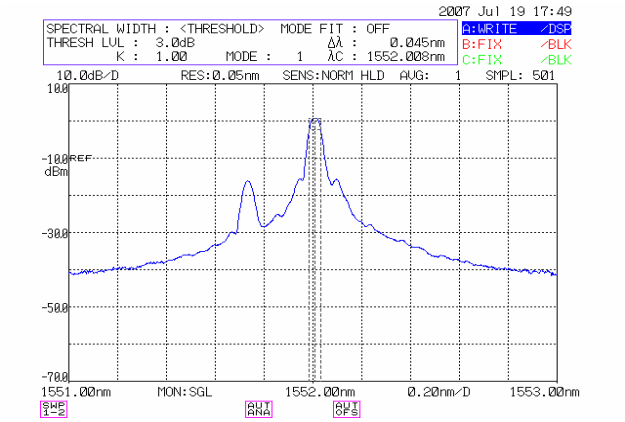

(a)

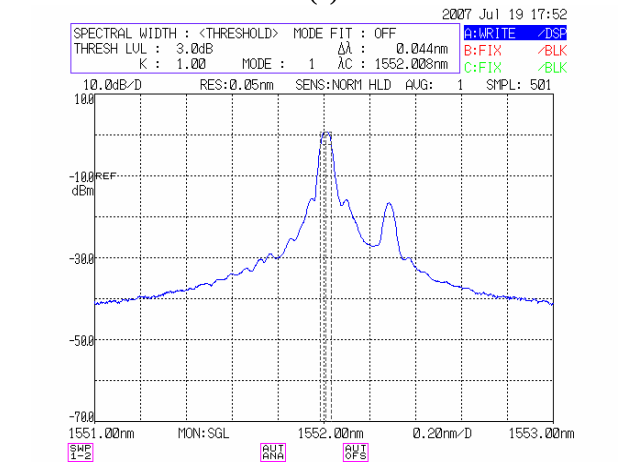

(b)

Figure 3. Optical spectrum of two combined lasers

As shown that the S/N of beat signal in frequency 8.5 GHz was only 10 dB. In frequency higher 3.5 GHz, the noise floor of RF spectrum analyzer is 20 dB higher then the lower frequency. As a result, the measured S/N of the generated microwave signal is low. In priciple, the maximum beat signal frequency is depends on the bandwidth of used photodetector and we can generate mm-wave signal using this teqnique by using high speed photodetector such as Unitraveling-carrier photodiode.

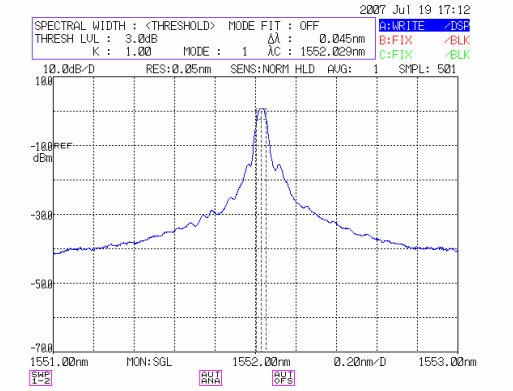

Figure 4. Laser spectrum when the two laser is combined within frequency response of photodetedctor

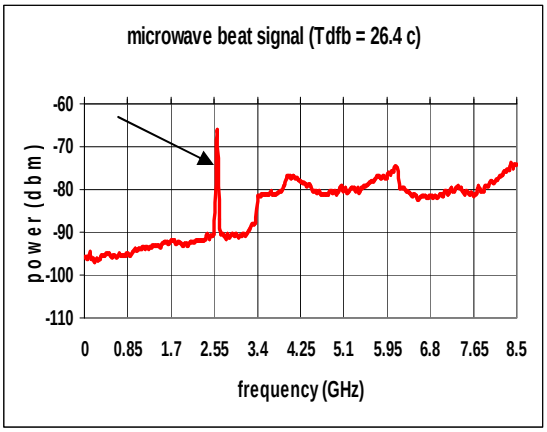

(a)

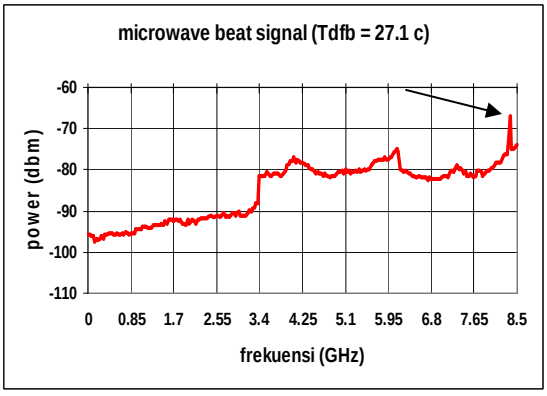

(b)

Figure 5. Spectrum of beat signal (microwave signal)

IV. CONCLUSIONS

We propose mm-wave signal generation using two laser diodes. Experiment results shown that the microwave signal is generated and tunable from dc to 8.5 GHz. This frequency is limiten by bandwidth of photodetector.

REFERENCES

[1] S.Fukushima et.al, "Optoelectronic Millimeter-Wave synthesis using an optical frequency comb generator, optically injecteion locked laser, and a unitraveling-carrier photodiode" Journal of Lightave technology, vol 21, no 12, 2003

[2] T.Kuri, et.al, " Characteristics of supercontinuum light souece for WDM Millimeter-Wave-Band Radio on Fiber System" IEEE Photonics Technology Letters, Vol 17, No 5, June 2005

[3] Y.Doi et.al. Compact 60-GHz photonics millimeter wave emitter module for fiber radio link", In Tech. Dig. 2002 Int. Topical Metting Microwave Photonics, Awaji Japan, Nov 2002, W4-6, pp 65-68.

ISSN: 1411-1284

The Effect of Humidity on the Worker Productivity: A Study at Malaysia Electronics Industry

[1]A. R. Ismail*, [2]M. R. A. Rani, [3]Z. K. M. Makhbul and [1]B. M. Deros

[1]Dept. of Mech. and Mat. Eng., Fac. of Eng., National University of Malaysia, 43600 UKM Bangi, Malaysia. Tel. 60389216775, fax 60389259659, email: arasdan@eng.ukm.my
[2]Dept. of Manuf. and Ind. Eng., Fac. of Mech. Eng., Universiti Teknologi Malaysia, 81310 UTM Skudai, Malaysia
[3]Sch. of Business Mgmt., Fac. of Econ. and Business, National University of Malaysia, 43600 UKM Bangi, Malaysia

Abstract– **The objective of this study is to determine the effects of humidity on the operators' productivity at Malaysian electronic industry. One electronic components assembly factory had been chosen as a subject for the study. The subjects were workers at the assembly section of the factory. The environment examined was the relative humidity (%) of the surrounding workstation area. Two sets of representative data, the relative humidity (%) and production rate were collected during the study. The production rate data were collected through observations and survey questionnaires while the relative humidity (%) was measured using BABUC equipment. The correlation and linear regression analysis were conducted in order to obtain the relationship between the effects of relative humidity (%) and the worker productivity. The results from the correlation analysis revealed there is a linear relationship between the relative humidity (%) and the productivity of the workers. The linear regression analysis further reveals that there is a linear equation model with positive slope to describe the relationship of relative humidity (%) and workers productivity for the assembly section involved. The linear regression line obtained is Y = 2.5863X – 28.896.**

Keywords– productivity, humidity, relationship

I. INTRODUCTION

Improving workers' productivity, occupational health and safety are major concerns of industry, especially in developing countries. However, these industries are featured with improper workplace design, ill-structured jobs, mismatch between workers' abilities and job demands, adverse environment, poor human-machine system design and inappropriate management programs [11].

Such conditions could lead to workplace hazards, poor worker health, disabilities, and affect the productivity of workers and quality of products. Work injuries create significant economic and humanitarian consequences to our society. Furthermore, work injuries have been associated with psychological distress, decreased participation in daily living activities and negative effects on family well-being [6].

Light, noise, air quality and the thermal environment were considered factors that would influence the acceptability and performance on the occupants of premises [9]. [2] stated that lower emotional health is manifested as psychological distress, depression and anxiety, whereas lower physical health is manifested as heart disease, insomnia, headaches, and infections. These health problems could lead to organizational symptoms such as job dissatisfaction, absenteeism, and poor work quality. Irritated, sore eyes and throat, hoarseness, stuffy congested nose, excessive mental fatigue, headache and unusual tiredness were all signs of the negative workplace environmental conditions [12].

Previous research done by [3] showed that the work environments were associated with perceived effects of work on health. This research used a national sample of 2,048 workers who were asked to rate the impact of their respective jobs job on their physical and mental health. Regression analyses proved that the workers' responses were significantly correlated with health outcomes. In addition to this, [11] pointed out that there was high correlation between performance indicators and health, facilities, and environmental attributes. In other words, companies with higher health, facilities, and environmental problems could face more performance related problems such as low productivity, and high absenteeism. Employees with complaints of discomfort and dissatisfaction at work could have their productivity affected, result of their inability to perform their work properly [7].

According to the [4], productivity was one of the most important factors affecting the overall performance to any organization, from small enterprises to entire nations. Increased attention had focused on the relationship between the work environment and productivity since the 1990s.

Laboratory and field studies showed that the physical and chemical factors in the work environment could have a notable impact on the health and performance of the occupants, and consequently on the productivity. Workplace environmental conditions, such as humidity, indoor air quality, and acoustics have significant relationships with workers' satisfaction and performance [12], [8], [5]. Indoors air quality could have a direct impact on health problems and leads to uncomfortable workplace environments [1], [10], [13].

II. METHODOLOGY

Selection of Location and Subjects

A Japanese based electronics company had been selected as a place of study. A line producing a product over a period of time and under the effects of certain relative humidity was chosen. This criterion is essential in order to obtain the relationship of the relative humidity on the worker productivity based on output of assemblies among operators. The production line was consist of 10 woman operators. Their task is to assemble an electronics parts on the circuit board for the television system tuner. Figure 1 shows the production line layout while in Figure 2 shows the flow chart of work sequences on the production line. The standard production rate determined by the previous feasibility study to assemble a complete television tuner was 250 units for every hour of production.

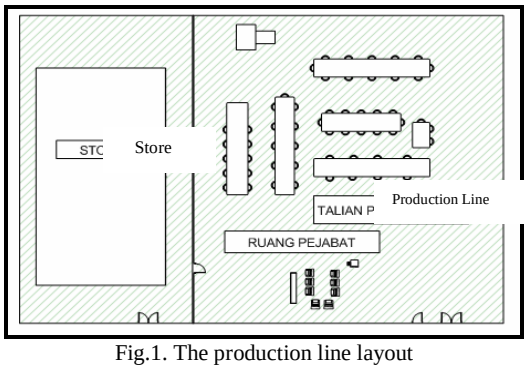

Fig.1. The production line layout

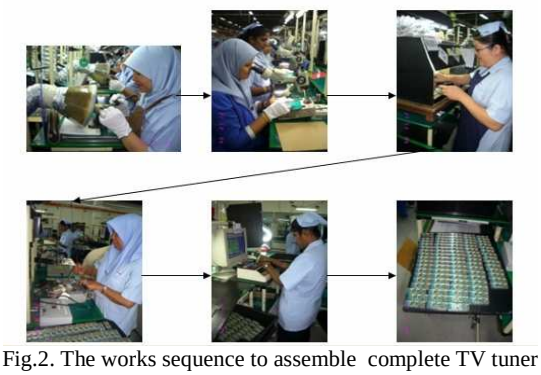

Fig.2. The works sequence to assemble complete TV tuner

Data Gathering and Analysis

Inferential statistics (i.e. the number of production rate and illumination level) were computed to gain a generalization of relationship between production rate and illumination levels. Further correlation and simple regression analysis were performed to obtain the relationship and hence the testing of the hypotheses**.** The alpha for all hypotheses testing was 0.05. The variables in this study were production rate and relative humidity. Correlation analysis procedure was used to examine if there was any relationship between relative humidity and production rate (i.e. whether the relationship was linear (either positive or negative). The simple regression analysis was conducted to obtain the mathematical equation in order to present the effect of illuminance on the production rate at that particular production line. Lastly, for hypotheses testing, ANOVA and t-test have been administered. The hypotheses of this study were:

H1: There is a relationship between production rate and relative humidity in the population studied.

H2: The relationship between relative humidity and production rate is significant.

The sample was inclusive of 10 female operators whose age were in the range between 20 – 30 years old comprised mostly of local citizen of non-degree holders and had been working with the organizations for less than 5 years. Majority of the respondents reported that they work for more than 49 hours per week. The measurements ofrelative humidity (%) was performed using BABUC environmental equipment. The workers' performance level was represented by the production rate. The amount of the products assembled were recorded for every 30 minutes and data was compared to the levels of relative humidity.

III. RESULTS

The result of this study was based on the case study conducted on the production line in the electronic factory. The hypotheses for this study was the production rate that have a direct relationship with the relative humidity. The relative humidity level were taken to identify the effect of humidity on the worker performances.

Table 1 shows the data of production rate, ,relative humidity (%) and the time taken for every 30 minutes. A graph was plotted to show the relationship between the production rate and the illuminance level. Figure 3 shows the graph to describe the relationship between production rate versus illuminance level. Based on the graph in Figure 3, we can note that the production rate were increases as we increase the relative humidity.

The model of equation used is $\hat{Y} = ß_0 + ß_1X$. The result from the analysis revealed the regression

linear equation obtained is Y = 2.5863X – 28.896 where the Y representing production rate and X representing relative humidity level. A hypothesis testing was conducted in order to determine if there is a relationship or not between productions rate (Y) and relative humidity (X). The hypotheses were:

H_o : $\rho = 0$ (There is no relationship between production rate and relative humidity (%) in the population studied).

H_a : $\rho \neq 0$ (There is a relationship between production rate and relative humidity (%) in the population studied).

From Figure 3, the correlation coefficient r, is 0.857613 which indicates a strong linear relationship between the production rate as a dependant variables and relative humidity (%) level as an independent variables to a significant level of 0.05 ($p < 0.05$). The coefficient of determination, r^2 at 0.77355 indicate that 77.35% of the production rate variance had relationship with relative humidity (%) variance. The value of correlation coefficient, r is then compared to the value from the Table of Critical Correlation Coefficient Value. The significance level was selected at 0.05 ($\alpha = 0.05$). The value of degree of freedom (n-2) is 7. The correlation coefficient, r from the analysis exceeds the critical value of r at 0.666 (according to Table of Critical Correlation Coefficient Value) thus that H_o is rejected. We can conlude the production rate and relative humidity (%) has positive significant ($r_{(8)} = 0.88142$, $p < 0.05$) relationship. The results based on the correlation analysis is presented in Table 2.

In order to understand the significance of the regression relationship between relative humidity (%) and the production rate for the area of population, an F-test was conducted. The results for regression, ANOVA and t-test analysis were presented in Table 3. The hypothesis were:

H_o: $\beta = 0$(The relationship between relative humidity (%) and production rate is not significant)

H_a: $\beta \neq 0$(The relationship between relative humidity (%) and production rate is significant)

Table 1. Data on the Relative Humidity, Production Rate and Time

Time (Hrs)	Production Target (Units)	Production Rate (Units)	Relative Humidity (%)
8.25-8.55	125	124	61.01
8.55-9.25	125	128	59.93
9.25-9.55	125	126	59.30
10.55-11.25	125	120	58.87
11.25-11.55	125	126	59.30
11.55-12.25	125	129	59.05
13.40-14.10	125	113	55.48
14.10-14.40	125	117	55.26
14.40-15.10	125	111	55.37

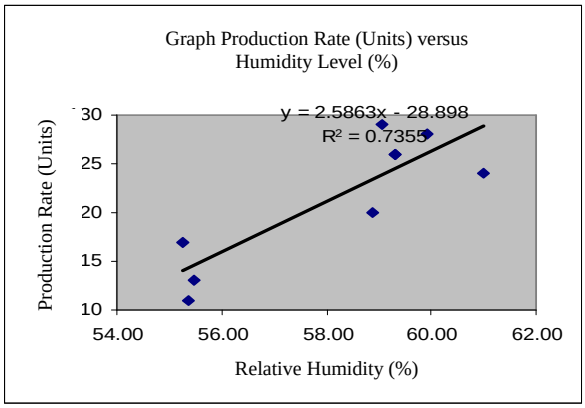

Fig.3.Graph of Production Rate versus Relative Humidity (%)

Table 2. Correlation Analysis

	Column 1	Column 2
Column 1	1	
Column 2	0.857613	1

Table 3. Regression, ANOVA and t-test Analysis

Regression Statistics

Multiple R	0.85761288
R Square	0.73549985
Adjusted R Square	0.697714122
Standard Error	3.63777459
Observations	9

ANOVA

	df	*SS*	*MS*	*F*	*Significance F*
Regression	1	257.5883943	257.5884	19.465014	0.00311158
Residual	7	92.63382794	13.2334		
Total	8	350.2222222			

	Coefficients	Standard Error	t Stat	P-value
Intercept	-28.87002176	34.11684108	-0.84621	0.42541446
Relative Humidity	2.58576732	0.586086991	4.411917	0.00311158

* $p < 0.05$

The F value from the ANOVA is 19.4650. The value of the significance level was selected at 0.05 (α

= 0.05). Based on the Table Critical Value F Distribution, the $F_{[0.05]}$ is equal to 5.59. Since the F(model) = 19.4650 > $F_{[0.05]}$ = 5.59, we can reject H_o: $\beta = 0$ in favor of H_a: $\beta \neq 0$ at the 0.05 significance level. It suggests strong evidence of significant relationship between the relative humidity and the production rate. Hence there is a strong evidence that the simple linear model relating production rate and relative humidity (%) is significant. A t-test was conducted to determine the significance of regression coefficient, $ß_1$. The value of t from the analysis is 4.411917. This value is significant under testing level of 0.05. It shows that the power of prediction for the equation model is significant ($t = 4.90$, $p < 0.05$).

IV. DISCUSSION

From the literature, only a few studies have been conducted in the area to establish an equation model related of environmental effect to productivity. The authors believe the study had achieved the objective to obtain an equation model to relate the relative humidity (%) to production rate in a quantitative way by inferential statistical analysis. The finding from the current investigation corresponds to the result of study by [12] The equation model is useful to manufacturing engineers as a guideline to determine the relative humidity (%) during the feasibilities study to allow production line achieves the optimum output.

The equation model is also useful to engineers in design air conditioning systems in order to minimize the use of power and control without disregard the productivity of workers. The equation model obtained is only applicable to present the current condition for the selected area of assembly workstation at Malaysian electronics industries. From the results of hypotheses testing, it can be concluding that there is a significant relationship between relative humidity (%) and production rate. Further test proved that the equation model could be strongly used to predict the production rate based on a certain relative humidity (%) provided by air conditioning systems in a particular organization.

V. CONCLUSIONS

Research on the relationship of workplace environmental factors to the productivity or performance is very limited and characterized by a short time perspective or perception with emphasis on survey methods, statistical analysis, satisfaction and the preferences measurement. This study is done to prove empirically the previous perception studies based on the role of environmental factors to productivity. It is expected that this study would be beneficial to the electronic manufacturing industries in Malaysia. The research findings are restricted to the Malaysian workplace environment, where the awareness among workers on productivity is still low. The results might vary for tests carried out for different sample sizes, types of industries and countries.

REFERENCES

[1] Chubaj, C.A (2002). School Indoor Air Quality. Journal of Instructional Psychology **29**(4): 317-321.

[2] Dua, J.K (1994). Job Stressors and Their Effects on Physical Health, Emotional Health, and Job Satisfaction in a University. Journal of Educational Administration. **32**(1): 59-78.

[3] Ettner, SL. and Grzywacz, JG. (2001). "Workers' perceptions of how jobs affect health: a social ecological perspective", Journal of Occupational Health Psychology, **6**(2): 101-131

[4] Fisk W.J. and Rosenfeld A.H. (1997). Estimates of improved productivity and health from better indoor environments. Indoor Air **7**: 158-172.

[5] Fisk, W. J. (2000). Health and Productivity Gains From Better Indoor Environments and Their Relationship with Building Energy Efficiency. Annual Review of Energy & The Environment. **25**(2): 537-566.

[6] Kirsh, B.and Mckee, P. 2003. "The needs and experiences of injured workers: A participatory research study", Work, **21**:221-231.

[7] Leaman, A. (1995). "Dissatisfaction and office productivity", Facilities, **13**(2):13-19.

[8] Marshall, L., Erica, W., Alan, A. and Sanborn, M. D. (2002). Identifying and Managing Adverse Enviromental Health Effects: 1. Taking an Exposure History Canadian Medical Association Journal. **166**(8): 1049-1055.

[9] Olesen, B. W. (1995). International standards and the ergonomics of the thermal environment. Journal of Applied Ergonomics. **26**:293-302.

[10] Shiaw-Fen Ferng, L. W. L. (2002). Indoor Air Quality Assesment of Day – Care Facilities with Carbon Dioxide, Temperature, and Humidity as Indicator. Journal of Environmental Health. **65**(4): 14-18.

[11] Shikdar, A. A. and Sawaqed, N. M. (2003). "Worker productivity, and occupational health and safety issues in selected industries" , Computers and Industrial Engineering, **45** (4) : 563-572.

[12] Tarcan, E. Varol, E.S. and Ates, M. (2004). A Qualitative Study of Facilities and Their Enviromental Performance Management of Environmental Quality: An International Journal. **15(**2): 154-173.

[13] Wilson, S. (2001). Graduating to Better AQ. Consulting-Specifying Engineer. **29**(6): 24-28.

ISSN: 1411-1284

Developing A Digital Current Controller For Optical Amplifiers Using FPGA

{Sardjono Trihatmo, Irwan R. Husdi, Fadjar Rahino, Ary Syahriar, Andria Ginting }[#] and Sholeh Hadi Pramono *

[#]Center for Information Technology and Communication
Agency for the Assessment and Application of Technology of the Republic of Indonesia
Gedung BPPT 2, Lantai 21, Jl. MH Thamrin no 8, Jakarta 10340
sardjono@inn.bppt.go.id, irwan@inn.bppt.go.id
[*)]Department of Electrical Engineering, Brawijaya University

Abstract–**The Wavelength Division Multiplexing (WDM) technology enables to establish an optical network to fulfill the need of a broadband communication in Indonesia. The important component for the network is the optical amplifier. It is an optical signal repeater that amplifies a modulated signal laser beam directly without optoelectronic and electro-optical conversion. It is more efficient rather than using optoelectronic amplifier devices. However, for the domestic market in Indonesia, this optical device is still imported and its cost is relative high. The research group of BPPT has been trying to develop a low cost optical amplifier but robust, reliable and performs as well as a high cost one. To realize the objective, it needs some engineering works. It includes the simplification of the technical design of the laser driver and developing a digital current controller. In addition it must be able to be implemented using market ready electronic components. At the recent state, this optical amplifier reaches the gain up to 30 dB. At the previous approach, the electric current for driving the pump laser is stabilized and controlled by using a microprocessor. Now we are developing the controller using a Field Programmable Gate Array (FPGA) to reduce the cost and increase the performance.**

Keywords– EDFA, optical amplifier, control, current control, digital control, FPGA

I. INTRODUCTION

The need of a low cost and broadband communication system in the Indonesian requires an appropriate solution. The optical fibre network is the appropriate one. The technology for optical fibre production becomes shopisticated so that the cost of fiber optics decreases and consequently the bandwidth increases significantly.

The newest technology in the fiber optic communication is the Wavelength Division Multiplexing (WDM). Using the WDM technology some signal carrier of different wavelength can be transmitted through a fiber optic simultaneously[5]. Consequently, the bandwidth capacity of communication medium is broader.

Like in other transmission media, there is signal attenuation in fiber optics. To amplify a highly broad bandwidth optical signal, the use of an optical repeater or optical amplifier is essensial and beneficial. An optical amplifier amplifies signal using pure photonic process. It does not need optical-electronical- optical (OEO) conversion so that it increase the efficiency and the reliability of communication systems [4].

Unfortunately, for the domestic market in Indonesia, the optical amplifiers need still to be imported and it costs very high. The engineers in the optical communication research group of BPPT have been trying to develop a low cost optical amplifier but it is reliable and robust and performs like a high cost optical amplifiers. In order to achieve this requirement, it needs some engineering work. It includes the simplification and optimization of the technical design of either the optical part or the electronic part that drives the pump laser and support additional features. In addition, the technical design must be able to be implemented as long as possible using domestic market ready components.

The main objective of this engineering work is to develop a reliable and robust low cost optical amplifier with a high gain in broad optical spectrum. The other objective is to endorse the national communication industry for market competitiveness in order to support the policy of the Indonesian government about the optimation of local content in the telecommunication infrastructures.

II. BASIC THEORY

The developed optical amplifier uses Erbium Doped Fiber (EDF) as the main optical component. It amplifies signals in C band. The EDF is driven by a

powerful laser beam (pump laser) that is generated by a laser diode.

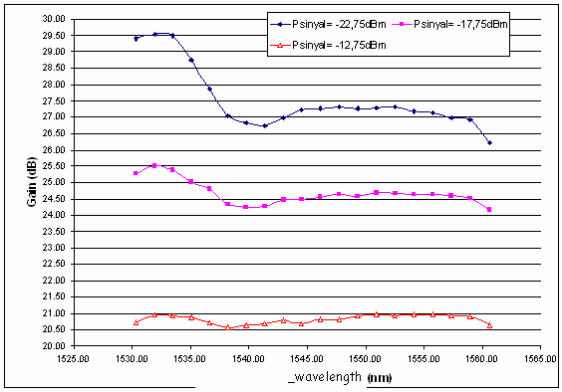

.

.Fig. 1 EDFA Characteristic 13m long and for signalsl: -22,75dBm, -17,75 dBm, dan -12,75 dBm at 20 mW pumping

The characteristic of the optical amplifier using the EDF can be seen in figure 1. The problem occurs since the laser diode needs a pretty high electric current to pump a powerful laser beam. A high value current that flows through the laser diode and through the laser driver will produce heat. Since they are semiconductor devices, the heat will influence the characteristics of the device itself. The following effect is the unstable current. The unstable current affects the power of the laser beam and finally the gain of the optical amplifier. There is a gain controlled optical as described in [2].

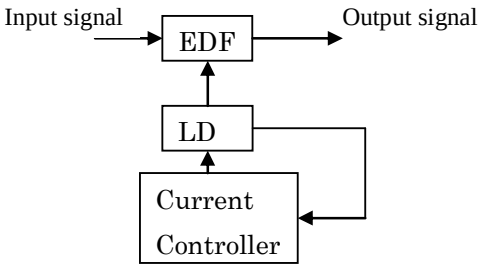

Fig. 2.Block diagram of the optical amplifier

Since the dynamic of the current much faster than the change of the gain, the current must be controlled. Figure 2 shows the block diagram for the controlled optical amplifier. The laser driver (LD) in the block diagram is established using only one transistor as the current source. The circuit can be seen in figure 3. The system (input voltage and diode current) builds a non linear system. However, if the system works in a fixed operating point and the disturbance is small around that point, we may approximate the system as a linear one. So we can implement the most widely used control algorithm, namely the digital PI controller. The formulation of the digital PI controller is shown as:

$$u(k) = u(k-1) + K[e(k) - e(k-1)] + \frac{KT}{T} e(k) \quad (1)$$

This formula is implemented using FPGA. The recent technology makes vendors possible to produce FPGA massively and cheaply. FPGA increases also the flexibility of hardware programming and it can be used to process high speed signals. Those are the reason why we have been trying to subtitute the microcontroller that we used in the first approach [1] and [3] with the FPGA.

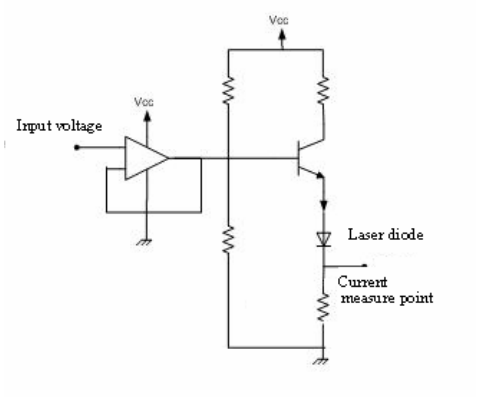

Fig. 3.Schematic diagram of the laser driver.

Figure 4 and 5 show the design of PI controller and its integration to the laser driver. The design is automatically generated by hardware description language compiler. We used the VHDL code to create the controller.

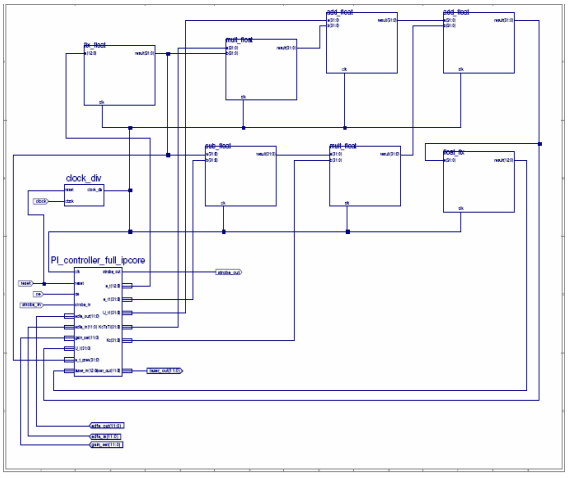

Fig. 4.Design of PI Controller using VHDL

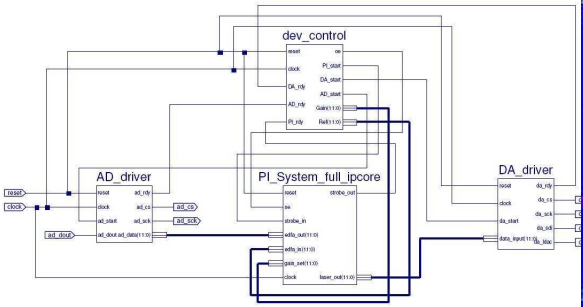

Fig. 5.Design of PI Controller using VHDL

III. EXPERIMENTAL RESULTS

The laser diode and the transistors in laser driver are semiconductor devices and their characteristics are influenced by temperature. Since the value of the current for pumping is high enough, then temperature increases significantly for a couple hours. Even a fan does not help to keep the current constant. Furthermore, the system shows inappropriate transient behavior. Once the system switches to another operating point, there is a pretty high overshoot. The figure 6 shows the step response of the system. The overshoot reached a value about 50% of a value in steady state.

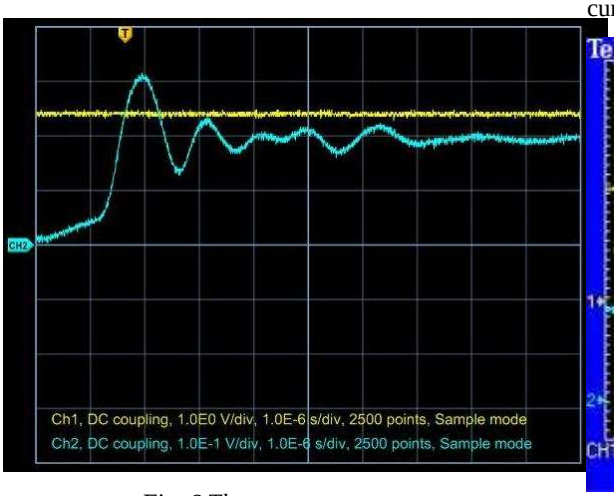

Fig. 6.The system response

According to the step response, the system can be approximated as a system with dominant conjugation complex poles. It causes an badly damping oscillation at the system before it reaches the steady state. Using a simple control analysis [6] the parameters of controller are set to get an appropriate damping factor so that the overshoot is reduced up to 5%.

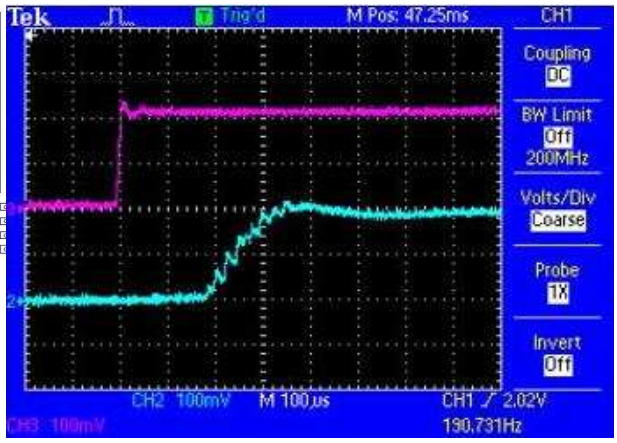

Fig. 7.The system response using feedback PI controller

Using the PI controller with parameter Ti = 0.0004s, overshoot reduced below 5% as can be seen in figure 7. The probably obviously delay time of the step response might be caused by the delay time of the ADC and an additional filter for noise suppression.

The primary goal of the current controller is to keep the current constant. In the experiment, the system operated in an operating point, and at a certain moment the load was changed. It caused permanent current drop as can be seen in figure 8.

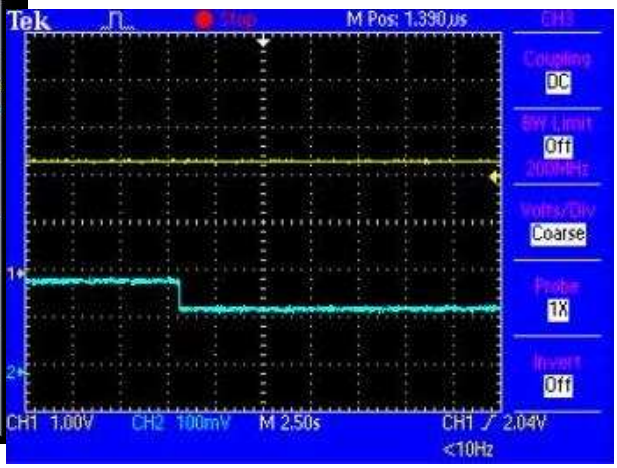

Fig. 8.The system response under the occurrence of permanent load/disturbance

With a controller, the current is recovered to the reference value automatically after the occurrence of a permanent load as can be seen in the picture 6. Through an appropriate PI parameter setting, the effect of a permanent load is not remarkable. The picture 7 shows the final result.

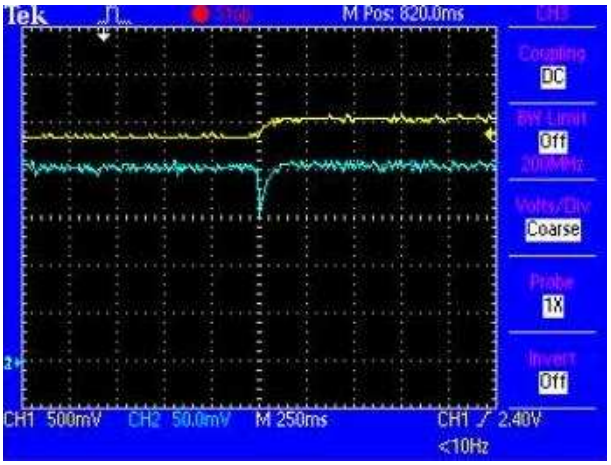

Fig. 9.The system response under permanent load using feedback PI controller

With PI controller, the current is recovered to the reference value automatically after the occurrence of a permanent load as can be seen in the picture 9. Through an appropriate PI parameter setting, the effect of a permanent load is not remarkable. The picture 10 shows the final result.

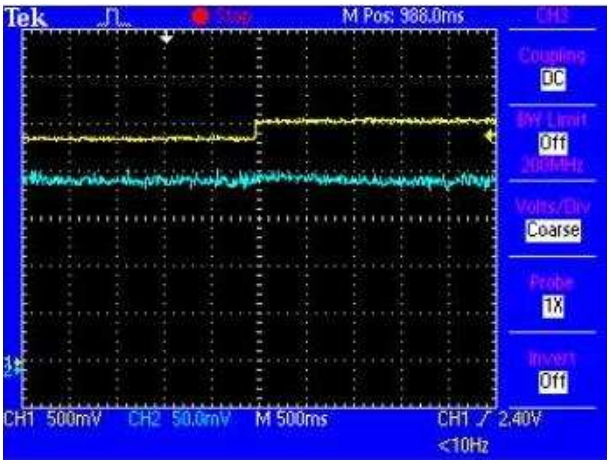

Fig. 10.The system response under permanent load using feedback PI controller

IV. CONCLUSIONS

The work on developing an optical amplifier has been done successfully. The gain of the amplifier reaches a practical value at 30 dB in a broad spectrum. Using a simple PI feedback control system that is implemented using FPGA, the current can be kept stable although there is perturbation around an operating point. It keeps the gain of optical amplifier remain constant. The transient behavior of the system is better through the reduction of the overshoot below 5% so that it keep the lifetime of the laser long.

REFERENCES

[1]. Trihatmo S. et all, "Microprocessor based Current Controll for EDFA," Proc. International Conference on Telecommunications, STT Telkom, Bandung October, 2007

[2]. Lijie Qiao and Paul J. Vella , "ASE Analysis and Correction for EDFA Automatic Control", Journal of Lightwave Technology, Vol. 25, No. 3, March 2007

[3]. NN, "Device Engineering", Technical Report, BPPT, 2006.

[4]. Sun, Y et all, "Optical Fiber Amplifier for WDM Optical Networks, Bell Labs Tech. J., 1999.

[5]. Desurvire. E, "Erbium Doped Amplifiers: Principles and Applications", John Wiley & Sons. 1994.

[6]. Weinmann A,"Regelungen. Analyse and Technischer Entwurf" Springer, 1998.

ISSN: 1411-1284

Simulink Analysis Of Blood Glucose Regulation As The Basic Concept Of Non-Invasive Blood Glucose Sensor Design

Soegianto, Johanes Calvinus, Djoko Hartanto

Sensor Device Research Group, Faculty of Engineering, University of Indonesia.
UI Campus, Depok, 16424.
Tel. 7270078 ext 111, fax. 7270077 email : djoko@eng.ui.ac.id

Abstract - **The conventional technique to quantize blood glucose utilizes blood samples extracted from a subject for further analysis by chemical determination method. Penetration of the syringe through the skin, though negligibly sensed on a single performance, will result in augmentation of sensation felt as pain after several repetitions. This uncomfortable feeling, hence reluctance to pursue a series of blood tests, might prevent the progress a 24 hour blood glucose monitoring by invasive investigation. To overcome this problem, a non-invasive device such as the impedance or dielectric spectroscopy sensor [1] adhered to the skin is intended as a practical solution.**

This research is a re-investigation based on Natal van Riel [2] method to observe blood glucose regulation, applying a modified Simulink Matlab 7.1.3 program. The electronic blood glucose parameters thus obtained will be applied in designing a non-invasive sensor device.

Key words: blood glucose, non-invasive sensor device, dielectric spectroscopy.

I. INTRODUCTION

The minimal model of glucose that analyzed by Van Riel, proved the amount of glucose which have received, gave an effect to the insulin and would stimulate close loop system, so the level of glucose rate which is increase can turn into normal condition. We refer to FSIGTT (Frequently Sample Intravenous Glucose Tolerance Test) data which developed by Dr. Richard. N. Bergman in 1970's in Fig.1.

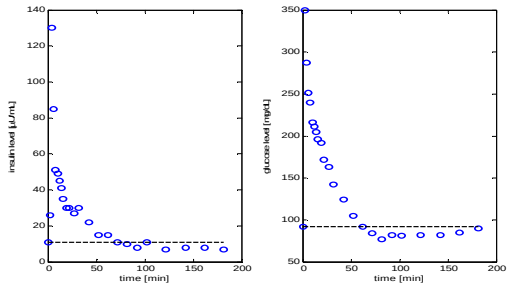

Fig.1. FSIGTT data on Normal Subject

The result revealed, when a subject received a glucose injection, thus the insulin rate amount will increase in order to keep a glucose rate at a normal condition which is called "basal". Van Riel was using Matlab Editor to simulate minimal model of glucose that shown on Fig. 2.

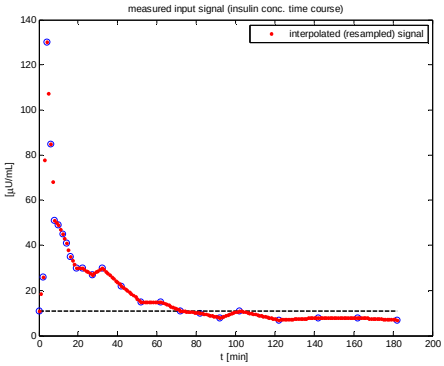

Fig. 2. Interpolated data of Insulin

For analysis, a review of Van Riel data [2] using Simulation MatLab Editor, shows results on Fig. 3.

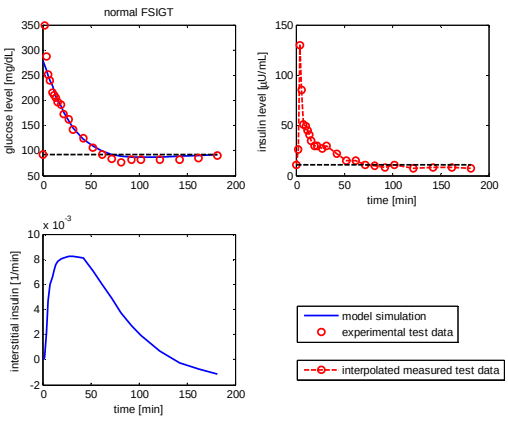

Fig.3. Van Riel Simulation using MatLab Editor

The amount of glucose can then be represented by mathematical formula :

$$\frac{dG_{(t)}}{dt} = k_1\left(G_b - G_{(t)}\right) - X_{(t)} \quad (1)$$

$$\frac{dX_{(t)}}{dt} = k_2\left(I_{(t)} - I_b\right) - k_i \quad (2)$$

$$\frac{dI_{(t)}}{dt} = \gamma\left(G_{(t)} - G_T\right)(t - t_0) -$$

If $G_{(t)} >$ $\frac{dI_{(t)}}{dt} = -kI_{(t)}$ (3)

Eq. (1) to Eq. (3) can be described in a block diagram , as shown in Fig. 4.

Plasma insulin were effected by interstitial insulin and amount of plasma glucose will effected not directly by interstitial insulin. Minimal Model of Glucose can be modelize to be MatLab Simulink that can make easily to modify any simulation.

II. Mathematical Model

Glucose Mathematics model are :

$$\frac{dG_{(t)}}{dt} = k_1\left(G_b - G_{(t)}\right) - X_{(t)}G_{(t)} \quad (4)$$

In Laplace form:

$$S.G_{(s)} = k_1\left(G_b - G_{(s)}\right) - X_{(s)}G_{(s)}$$

$$S.G_{(s)} = k_1G_b - k_1G_{(s)} - X_{(s)}G_{(s)}$$

$$S.G_{(s)} + k_1G_{(s)} = k_1G_b - X_{(s)}G_{(s)}$$

$$(S + k_1)\,G_{(s)} = k_1G_b - X_{(s)}G_{(s)}$$

$$G_{(s)} = \frac{k_1G_b - X_{(s)}G_{(s)}}{(S + k_1)} \quad (5)$$

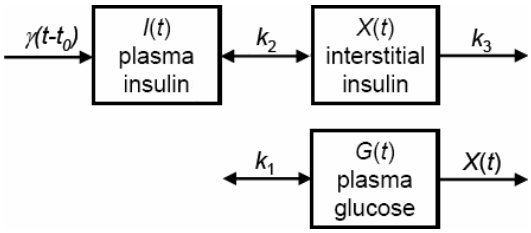

Fig. 4. Minimal Model of Glucose Block Diagram

Interstitial Insulin Mathematics model are :

$$\frac{dX_{(t)}}{dt} = k_2\left(I_{(t)} - I_b\right) - k_3X_{(t)} \quad (6)$$

In Laplace form:

$$S.X_{(s)} = k_2\left(I_{(s)} - I_b\right) - k_3X_{(s)}$$

$$S.X_{(s)} + k_3X_{(s)} = k_2I_{(s)} - k_2I_b$$

$$(S + k_3)X_{(s)} = k_2I_{(s)} - k_2I_b$$

$$(S + k_3)X_{(s)} = k_2I_{(s)} - k_2I_b$$

$$X_{(s)} = \frac{k_2I_{(s)} - k_2I_b}{(S + k_3)} \quad (7)$$

Based on Eq. (4) to Eq. (7), the Model will be shown in Fig. 5.

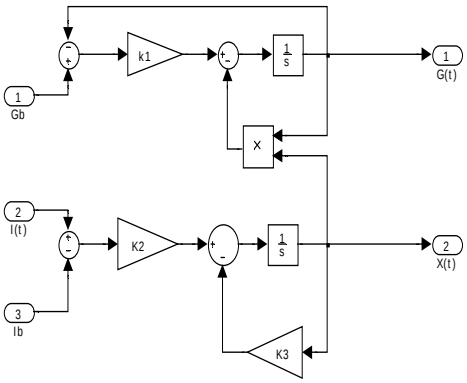

Fig. 5 Simulink Model (Glucose)

For insulin mathematics model are :

$$\frac{dI_{(t)}}{dt} = \gamma\left(G_{(t)} - G_T\right)(t - t_0) - kI_{(t)} \qquad (8)$$

In Laplace form:

$$S.I_{(s)} = \gamma\left(G_{(s)} - G_T\right)e^{-t_0} - kI_{(s)}$$

$$S.I_{(s)} + kI_{(s)} = \gamma\left(G_{(s)} - G_T\right)e^{-t_0}$$

$$(S + k)\, I_{(s)} = \gamma\left(G_{(s)} - G_T\right)e^{-t_0}$$

$$I_{(s)} = \frac{\gamma\left(G_{(s)} - G_T\right)e^{-t_0}}{(S + k)} \qquad (9)$$

Based on Eq. (8) - Eq. (9), the Model will be shown in Fig. 6.

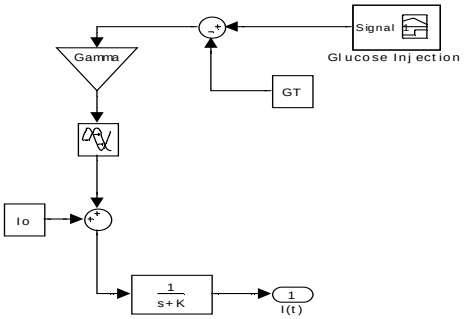

Fig. 6. Simulink Model (Insulin)

III. Minimal Model of Glucose Kinetics

From Eq. (1) to Eq. (9) then the Simulink Program for Minimal Model of Glucose Kinetics can be constructed as shown in Fig. 7.

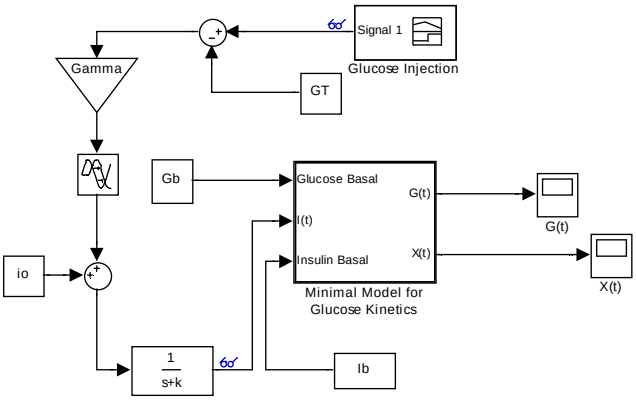

Fig. 7. Simulink Diagram Block for Minimal Model of Glucose Kinetics

Executing simulink model in Fig. 7, we will get graphs of important parameter i.e $X_{(t)}$, $G_{(t)}$ and the Glucose injection, interstitial Insulin & Glucose level, will be shown in Fig. 8 to Fig. 10 respectively.

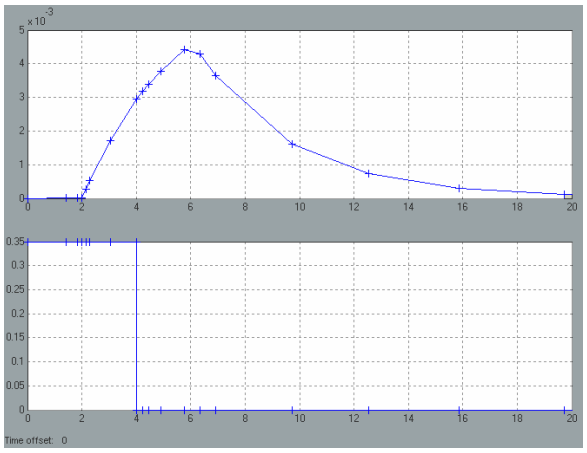

Fig. 8. Glucose injection

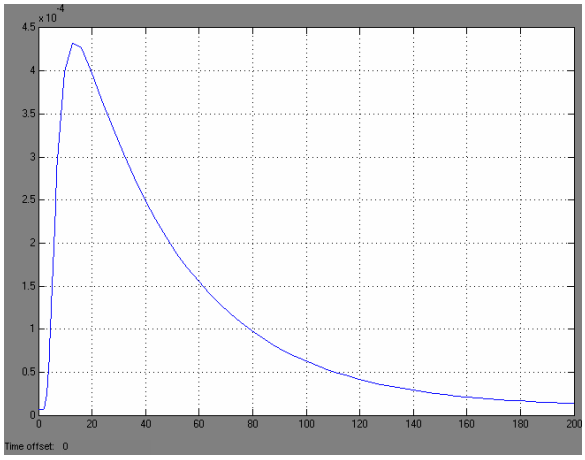

Graph. 9 Interstitial Insulin

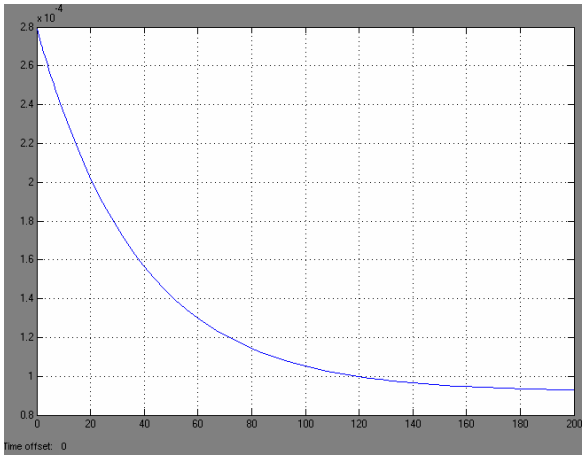

Fig.10. Glucose level

IV. Conclusion

From the graphs in Fig. 1.8- Fig. 1.3, it can be drawn conclusion i.e.: if glucose being injected to normal and then glucose will effect insulin to increase and when insulin level were growing up.

All graph above were in any scale of parameters. With shown all the graph, we can compare a graph that Van Riel done with Matlab Simulink Model are easily to use and modify if there's no accurate data.

REFERENCES

[1] A. Caduff, E. Hirt, Yu. Feldman, Z. Ali, L. Heineman, *First human experiments a novel non-invasive, non-optical continuous glucose monitoring system*, Biosensor and Bioelectronics (2003), **19**, 209-217.

[2] Natan van Riel, *Minimal models for glucose and insulin kinetics: a Matlab implementation*, Eindhoven University of Technology (2004).

Appendix.

Blood Glucose Minimal Model

MODIFY FROM VAN RIEL MATLAB ! FOR NORMAL SUBJECT

```
x0(2) = 0;
Gb = 92;
Ib = 11;
   % for normal subject
      x0(1) = 279;
      Sg = 2.6e-2;
      K3 = 0.025;
      Si = 5.0e-4;
      K2 = Si/K3 ;

p = [Sg, Gb, K3, Si, Ib];

   tgi = [ 0 92 11
           2 350 26
           4 287 130
```

```
  6 251 85
  8 240 51
 10 216 49
 12 211 45
 14 205 41
 16 196 35
 19 192 30
 22 172 30
 27 163 27
 32 142 30
 42 124 22
 52 105 15
 62 92 15
 72 84 11
 82 77 10
 92 82 8
102 81 11
122 82 7
142 82 8
162 85 8
182 90 7];

tu = tgi(:,[1,3]);
t_insu = tu(:,1);
u = tu(:,2);
t_gluc = t_insu;
gluc_exp = tgi(:,2);
insul_exp = tgi(:,3);

figure(1)
subplot(121); plot(t_insu,insul_exp,'o', 'Linewidth',2);
hold on
plot( [t_insu(1) t_insu(end)], [Ib Ib], '--k','Linewidth',1.5);
ylabel('insulin level [\muU/mL]'); xlabel('time [min]')

subplot(122); plot(t_insu,gluc_exp, 'o','Linewidth',2); hold on
plot( [t_insu(1) t_insu(end)], [Gb Gb], '--k','Linewidth',1.5)
ylabel('glucose level [mg/dL]'); xlabel('time [min]')


figure(2)
plot(t_insu, u, 'o'); hold on
plot( [t_insu(1) t_insu(end)], [Ib Ib], '--k','Linewidth',1.5)
xlabel('t [min]'); ylabel('[\muU/mL]')
title('measured input signal (insulin conc. time course)')
tspan = [0:1:200];
h = plot(tspan, interp1(tu(:,1),tu(:,2), tspan), '.r');
legend(h,'interpolated (resampled) signal')

%Simulation time vector:
tspan = t_insu;%tspan = union(t_insu, t_gluc);

ode_options = [];
[t,x] = ode45(@gluc_ode,tspan,x0,ode_options,tu,p);
%Output
gluc = x(:,1);

figure(3)
subplot(221);
h = plot(tspan,gluc,'-', 'Linewidth',2); hold on
plot( [tspan(1) tspan(end)], [Gb Gb], '--k','Linewidth',1.5)
ylabel('glucose level [mg/dL]'); title('normal FSIGT')

if exist('gluc_exp') %compare model output with measured data
h1 = plot(t_gluc,gluc_exp,'or', 'Linewidth',2);
legend([h,h1], 'model simulation','experimental test data')
end

u = interp1(tu(:,1),tu(:,2), tspan); %reconstruct used input signal
subplot(222); plot(tspan,u,'--or', 'Linewidth',2); hold on
plot( [tspan(1) tspan(end)], [Ib Ib], '--k','Linewidth',1.5)
ylabel('insulin level [\muU/mL]');xlabel('time [min]');
legend('interpolated measured test data')

subplot(223); plot(tspan, x(:,2), 'Linewidth',2)
xlabel('time [min]'); ylabel('interstitial insulin [1/min]')
```

ISSN: 1411-1284

The use of Carbon Nanotube (3,3) as Finger and Bus Bar at Silicon Solar Cell to Minimize Shadowing Loss Effect: A Theoretical Approach

Arief Udhiarto*, Marni, and Djoko Hartanto

* Fac. of Engineering, University of Indonesia, Depok 16424
Tel. 7270078, fax. 7270077 email : arief@ee.ui.ac.id

Abstract– **Shadowing loss is one of the factors which cause low of efficiency in Solar Cell. Shadowing loss is caused by metallic finger and bus bar which block the sun light to enter semiconductor. Carbon Nanotube (CNT) (3,3) is a CNT with metallic properties. The use of CNT (3,3) as finger and bus bar can minimize the shadowing loss effect.**

In this research we design a silicon solar cell and simulate the potential of CNT (3,3) as finger and bus bar. The calculation of n-type silicon concentration was made to make sure that silicon and CNT (3,3) has ohmic contact behavior. Other aspect as series resistance also considered to predict the potential of CNT (3,3) to increase solar cell efficiency.

From calculation and simulation we got the results that CNT (3,3) can be used as finger and bus bar in silicon solar cell. The maximum n-type silicon concentration to have ohmic contact behavior is 3.25 x 10^{11} /cm^2. The us of CNT (3,3) can minimize shadowing loss and hence increase solar cell efficiency.

Keywords– Shadowing loss, silicon solar cell, CNT, efficiency

I. INTRODUCTION

Solar cell efficiency are affected by many factors. One of them is power lose caused by shadowing loss effect. The power loss caused by shadowing loss is about 13.1% from the total power loss [1]. This shadowing loss is caused by finger and bus bar of solar cell which used to collect current from solar cell. Photon energy which expose solar cell is not entirely absorbs by the cell. Light which can enter into the cell will give its energy and make electron to be free. The other light cannot enter into cell caused by finger and bus bar which block the light. This phenomenon is known as shadowing effect which will cause shadowing loss.

On the other hand, the new inventions in nanotechnology give new challenge to enhance the efficiency of solar cell. One of the most popular inventions in nanotechnology is Carbon Nanotube (CNT). As the properties of the CNT become understood, the implementation of the CNT is become hot topic in many areas. Some of CNT has semiconductor properties and the other one has conductor properties. Using the superiority of CNT properties, the high efficiency solar cell may be obtained.

CNT (3,3) is a CNT with metallic properties. In this research, we analysis the use of CNT (3,3) to become finger and bus bar. By using this CNT the shadowing loss can be reduce.

II. BASIC THEORY

SOLAR CELL DESIGN

Solar cell is a device which directly converts the incident solar radiation into electricity. This alternative energy has many advantages as no noise, pollution or moving parts, making them robust, reliable and long lasting. Silicon is the most common Solar cell's material for terrestrial application. It is consists of two different types of semiconductor, n-type and p-type semiconductor.

The incident solar radiation will make electron to be come free. These free electrons will flow to connecting wire and make an electrical current. Unfortunately, not all photon energy can make electron to become free. Some of photons cannot enter into cell because of finger and bus bar. These fingers are known as metallic top contact and used to collect current. Using fewer fingers will allow more photon entering to the cell but it will make less free electron to reach finger. Using more fingers will guaranty free electron to reach finger but it is mean that fewer number of photon will enter into cell and release electron. The key design trade-off in top contact design is the balance between the increased resistive losses associated with a widely spaced grid and the increased reflection caused by a high fraction of metal coverage of the top surface [2].

To maximizing absorption and minimizing recombination, we need to minimize parasitic resistive loss. Parasitic resistive losses are caused by shunt and

series resistance. Shunt resistance is processing defect product rather than a design parameter. However, the series resistance is controlled by the top contact design and emitter resistance. We need to be carefully designed for each type and size of solar cell structure in order to optimize solar cell efficiency [2].

Figure (2) shows the series resistance of a solar cell. Finger and bus bar resistance dominate the overall series resistance and are therefore must be considered in solar cell design.

The design of the top contact involves not only the minimizations of the finger and bus bar resistance, but the overall reduction of losses associated with the top contact. These include resistive losses in the emitter, resistive losses in the metal top contact and shading losses. The critical features of the top contact design which determine how the magnitude of these losses are the finger and bus bar spacing, the metal height-to-width aspect ratio, the minimum metal line width and the resistivity of the metal. These are shown in the Figure 3. [2].

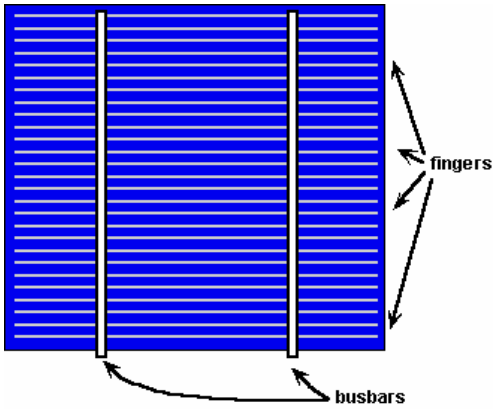

Fig.1. Top contact design in a solar cell [2]

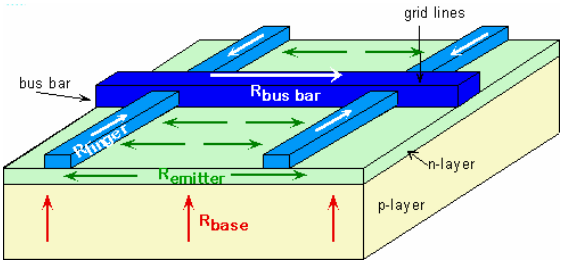

Fig.2. Bus bar, finger and current flows in solar cell [2]

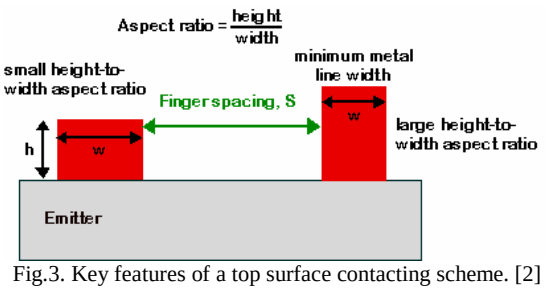

Fig.3. Key features of a top surface contacting scheme. [2]

Power loss caused by shadowing effect is calculated based on Equation 1 for finger shadowing loss and Equation 2 for bus bar shadowing loss.

$$p_{sf} = (1 - t_f)\frac{W_f}{S} \quad (1)$$

$$p_{sb} = (1 - t_b)\frac{n_t W_b}{W_c} \quad (2)$$

Doping concentration under metal contact must match with the metal to make ohmic contact behavior instead of blocking contact.

CARBON NANOTUBE

CNT is made from concentric cylinder of graphene layer. It can be metallic, semiconducting, or semimetal depend on rolling direction. Based on its rolling direction CNT can be zig-zag, armchair, or chiral. Two types of single-wall nanotubes (SWNTs) have a pure axial symmetry, so-called armchair (A) and zigzag (Z) nanotubes. The graphene rectangle shown in Figure 3(B), gives an armchair (A) nanotube when wrapped from top to bottom Figure 4 and a zigzag (Z) nanotube when wrapped from left to right. Any other type of nanotube is chiral.[3]

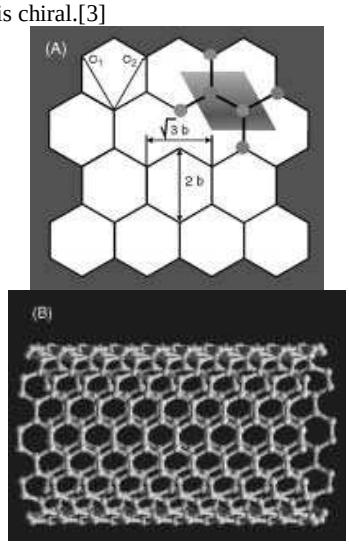

Fig.3. (A) Honeycomb lattice structure of graphene. (B) Lattice structure of [10,10] armchair SWNT. [3]

Because of its size, CNT is transparent to light [4].

III. EXPERIMENTAL RESULTS

The design of solar cell is based on structure shown in Figure 1. Finger and bus bar are CNT (3,3)

The analysis of used of CNT (3,3] was done based on theoretical approach. CNT (3,3) was chosen because it has metallically properties. This CNT (3,3) is used as finger and bus bar. CNT (3,3) has work function 4.5 ev [5]. By using n-type silicon semiconductor material as emitter and using Equation (3), (4) and (5) the maximum doping concentration for n-type silicon semiconductor is 3.25×10^{11}/cm3. Above

this concentration, the junction will become blocking contact instead of ohmic contact.

$$E0\text{-}Efn = (E0\text{-}Ec) + (Ec\text{-}Ei) - (Efn\text{-}Ei) \quad (3)$$

$$Efn\text{-}Ei = (E0\text{-}Ec) + (Ec\text{-}Ei) - E0\text{-}Efn) \quad (4)$$

$$N_D = ni\, e^{(Efn\text{-}Ei)\,/\,kT} \quad (5)$$

Every electron which already free is needs to travel onto finger to become current. When traveling onto finger some of them are recombine with hole. This recombination will reduce number of electron to become current. To reduce this recombination, space between fingers must be less than electron diffusion length.

Space between fingers was designed to be a half of electron diffusion length or about 10^{-6}cm. Finger spacing was designed to be less than electron diffusion length. Using Equation (6) the resistive loss for finger is 10^{-15} W.

$$P_{rf} = \frac{1}{m}\frac{J_{mp}}{V_{mp}}\frac{B^2 \rho_{smf}}{W_F} S \quad (6)$$

Equation (7) is used to find bus bar resistive loss.

$$P_{rb} \cong \frac{A^2 B \frac{\rho_s}{t}}{W_B} \quad (7)$$

Thickness of the doping layer is made in the order of micrometer, so bus bar resistive loss is about 10^{-16}.

Loss contact in this research is only calculated in finger by assuming that all electrons will flow only through finger, and then the current flow to the bus bar is neglected. Contact loss is calculated using Equation (8):

$$P_{cf} = \rho_c \frac{J_{mp}}{V_{mp}}\frac{S}{W_F} \quad (8)$$

ρc = Specific contact resistance or specific inter facial resistance can be obtained using Equation (9)

$$\rho c = \rho_i(TE) = \rho_1 e^{q\phi_B / kT} \quad (9)$$

Theoretically contact loss is affected by doping concentration, but the doping concentration in this case is low enough and then contact loss is not affected by doping concentration. This case is to be known as thermionic emission.

Finger spacing in this research is made lower than 10^{-6} cm, and then the contact loss can be neglected.

Finger shadowing loss is calculated using Equation (1). As the transparent coefficient of CNT is almost 1, then finger shadowing loss is almost 0.

Equation (2) is used to calculate bus shadowing loss. By using tb near to 1, the bus shadowing loss is almost 0.

From the previous research conduct by Daisuke Uchida, Faculty of Technology, Tokyo University of Agriculture and Technology, the maximum value of shadowing loss is 13.1% [6]. Using CNT (3,3) as finger and bus bar in solar cell can reduce this loss to almost 0 and then increase total solar cell efficiency.

IV. CONCLUSIONS

The use of CNT (3,3) for finger and bus bar can increase the efficiency of solar cell. The significant increase is obtained from the fact that the use of CNT (3,3) can reduce parasitic resistive include resistive loss, top layer loss, contact loss, and shadowing loss. To make sure that CNT (3,3) has ohmic contact properties, the maximum doping concentration for n-type semiconductor is 3.25 x 10^{11} /cm^2.

REFERENCES

[1] Chaudhari V. A. and C. S. Solanki, "Study of different top metal contact designs for concentration solar cells", Energy Systems Engineering Indian Institute of Technology Bomba, India,

[2] Honsberg, Christina and Stuart Bowden, "Photovoltaic: Devices, Systems, and Application PVCDROM 1.0." University of new south Wales 1999.

[3] William A. Goddard, at al, "Handbook of Nanoscience, Enginering, and Technology", ch11.4, CRC Press, 2003

[4] Michael W. Rowel, Mark A. Topinka, Michael D. McGehee" Organic solar cells with carbon nanotube network electrodes" Applied physics letters 88, 233506., 2006

[5] Bin Shan, Kyeongjae Cho "First Principles Study of Work Functions of Single Wall Carbon Nanotubes". Stanford University, Stanford CA, USA, 94305-4040

[6] Daisuke Uchida, Kenji Otani, Kosuke Kurokawa."Evaluation of effective shading factor by fitting a clear-day pattern obtained from hourly maximum irradiance data", Electrotechnical Laboratory, Tokyo University of Agriculture and Technology

ISSN: 1411-1284

Design and Implementation Artificial Intelligence of Path Searching Robot Based on Microcontroller BASIC Stamp

Harry Sudibyo Soetjokro*, and Gede Indrawan†

* Fac. of Engineering, Universitas Indonesia (UI), Depok, 16424
Tel. 62-021-7270077, fax. 62-021-7270077, email: harisudi@ee.ui.ac.id
†Fac. of Engineering, Universitas Pendidikan Ganesha (Undiksha), Singaraja - Bali
Tel. 62-0362-22570, fax. 62-0362-25735, email: gede.indrawan@gmail.com

Abstract– **Artificial intelligence in robotics, as a smart algorithm programmed into the robot, is needed by the robot to help human to do some work automatically and in autonomous way. In this research, the implanted artificial intelligence is designed for path searching, included in mapping activity, from starting point at corner to destination point at center, in controlled environment like maze. General speaking, this research want to contribute in knowledge development under robotics domain of autonomous position-sensing and navigation.**

Robot design for this artificial intelligence consists of two aspects, i.e. robot prototype itself, and maze environment where path-searching robot will run. Implementation of robot involves three aspects, i.e. input (sensor to capture information from the environment), process (processor and its supporting system as robot brain for data processing), and output (as result of data processing, it can be signal for controlling the motor, etc).

The artificial intelligence in this research is implemented using PBASIC programming language, with BASIC Stamp BS2px from Parallax as targeted microcontroller. Multi bank programming style is used to utilize 16 KB internal EEPROM resource, comprise of eight memory bank with 2 KB capacity respectively, to save program code. This code supports robot function for path searching in maze, by using Flood-Fill algorithm and modified Flood-Fill algorithm as main algorithms. Flexibility and scalability are two concepts of this artificial intelligence to accommodate features addition and to anticipate more complex maze environment.

Keywords– Artificial Intelligence, robot, autonomous position-sensing and navigation, microcontroller, PBASIC, Basic Stamp, multi bank programming, Flood-Fill algorithm¸modified Flood-Fill algorithm

I. INTRODUCTION

Robot, to associate behaviors with a place (localization) requires to know where it is and to be able to navigate point-to-point. Such navigation began with wire-guidance in the 1970s and progressed in the early 2000s to beacon-based triangulation.

For indoor application, current commercial robots autonomously navigate based on sensing natural features. The first commercial robots to achieve this were Pyxus' HelpMate hospital robot and the CyberMotion guard robot, both designed in the 1980s. These robots originally used manually created CAD floor plans, sonar sensing and wall-following variations to navigate buildings. The next generation, such as MobileRobots' PatrolBot and autonomous wheelchair both introduced in 2004, have the ability to create their own laser-based maps of a building and to navigate open areas as well as corridors. Their control system changes its path on-the-fly if something blocks the way [1].

At the other side, outdoor autonomy is most easily achieved in the air, since obstacles are rare. Cruise missiles are rather dangerous highly autonomous robots. Some of unmanned aerial vehicles (UAVs) are capable of flying their entire mission without any human interaction at all except possibly for the landing where a person intervenes using radio remote control. But some drone aircraft are capable of a safe, automatic landing also.

Outdoor autonomy is the most difficult for ground vehicles, due to: a) 3-dimensional terrain, b) great disparities in surface density, c) weather exigencies, and d) instability of the sensed environment. The Mars rovers MER-A and MER-B can find the position of the sun and navigate their own routes to destinations on-the-fly by: a) mapping the surface with 3-D vision, b) computing safe and unsafe areas on the surface within that field of vision, c) computing optimal paths across the safe area towards the desired destination, d) driving along the calculated route, e) repeating this cycle until either the destination is reached, or there is no known path to the destination

II. BASIC THEORY

The objective of this research is to create artificial intelligence for path searching robot from starting cell at corner to destination cell at center of the maze without breaking 2-dimension walls, represented by black line that exist in different side on each cell (Fig.1a). Fig.1b illustrates how at starting cell, robot has no information about walls except at the current cell where robot is standing on and detect wall using its sensors.

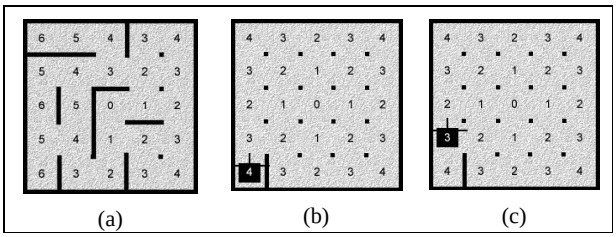

Fig.1. (a) Maze with wall (b) Maze view by robot at start (c) Robot move to other cell

To solve this path searching problem, Flood-Fill algorithm and modified Flood-Fill algorithm are used as main algorithms for this artificial intelligence.

The Flood-Fill algorithm involves assigning values to each of the cells in the maze where these values represent the distance from any cell on the maze to the destination cell without breaking the wall. The destination cell, therefore, is assigned a value of 0. If the path searching robot is standing in a cell with a value of 1, it is 1 cell away from the goal. If the robot is standing in a cell with a value of 3, it is 3 cells away from the goal. Fig.1b represents initial value for every cell known by robot at start with initial assumption there is no wall at all.

For the maze at Fig.1, we would have 5 rows by 5 columns = 25 cell values. Therefore we would need 25 bytes to store the distance values for a complete maze. Actually, for this research, we have designed other data needed by a cell, as shown by Table 1 below.

Table 1. Cell data design (put in Scratchpad RAM)

CoordinateValue (Address: 0 - 24)	
7 6 5 4 3 2 1 0	x-axis = nibble1 (bit 7 … 4) y-axis = nibble0 (bit 3 … 0)
DistanceValue (Address: 25 - 49)	
7 6 5 4 3 2 1 0	Minimum = 0 (00000000b) Maximum = 255 (11111111b)
WallValue (Address: 50 - 74)	
7 6 5 4 3 2 1 0 0 0 = facing North 0 1 = facing East 1 0 = facing South 1 1 = facing West	Bit 7 - 6 = Robot orientation Bit 5 = Side wall check status Bit 4 = Checkpoint status Bit 3 = West wall existence Bit 2 = South wall existence Bit 1 = East wall existence Bit 0 = North wall existence

When it comes time to make a move, the robot must examine all adjacent cells which are not separated by walls and choose the one with the lowest distance value. In Fig.1c above, the robot would ignore any cell to the West (left side) because there is a wall, and it would look at the distance values of the cells to the North, East, and South since those are not separated by walls. The cell to the North has a value of 2, the cell to the East has a value of 2 and the cell to the South has a value of 4. The routine sorts the values to determine which cell has the lowest distance value. It turns out that both the North and East cells have a distance value of 2. That means that the robot can go North or East and traverse the same number of cells on its way to the destination cell. Since turning would take time, the robot will choose to go forward to the North cell. Fig.2a gives generic algorithm for that case.

Furthermore, every interior wall is shared by two cells so when robot update the wall value for one cell, robot can update the wall value for its neighbor as well (Fig.2b).

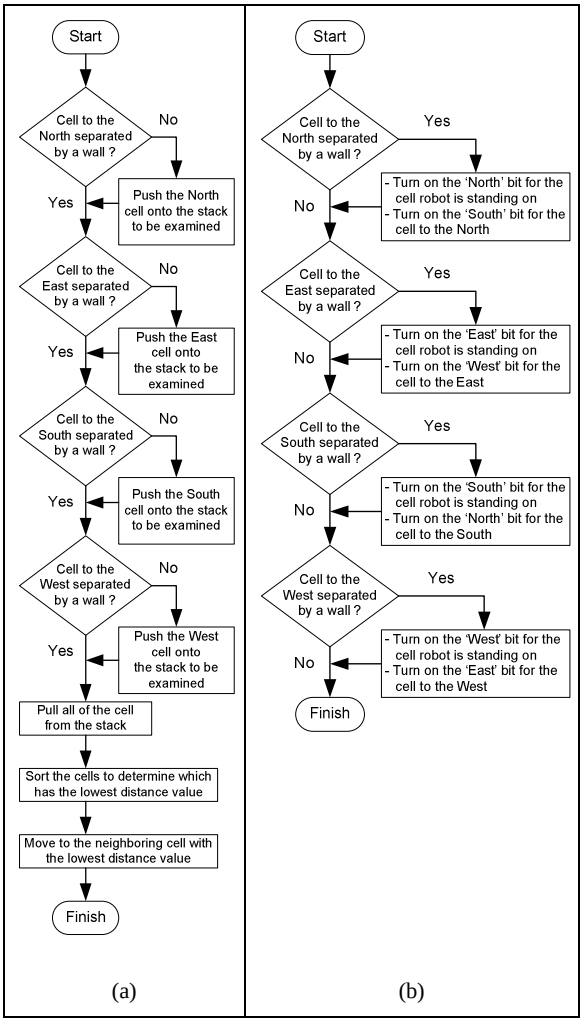

Fig.2. (a) Deciding lowest distance value (b) Updating wall map

The instructions for flooding the maze with distance values could be like algorithm at Fig.3 below.

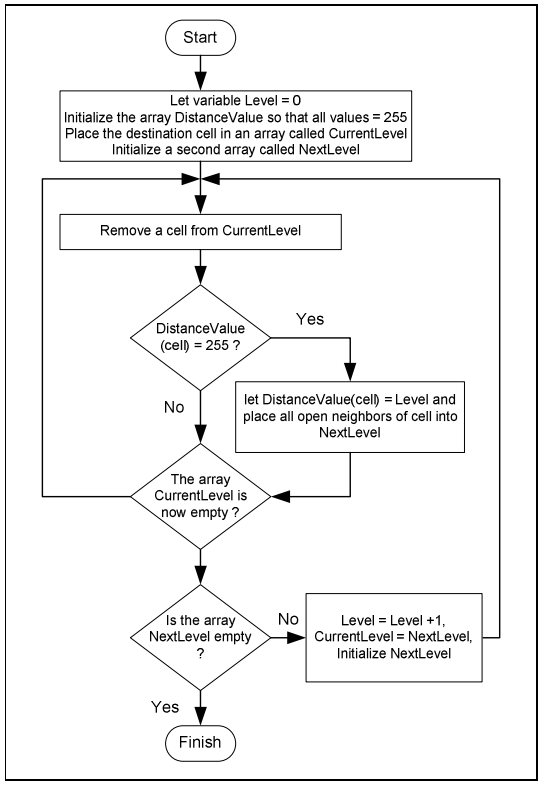

Fig.3. Flooding with distance values for Flood-Fill algorithm

The modified Flood-Fill algorithm at the other side is similar to the regular Flood-Fill algorithm in that the robot uses distance values to move about the maze. The distance values which represent how far the robot is from the destination cell, are followed in descending order until the robot reaches its goal. As the robot finds new walls during its exploration, the distance values need to be updated. Instead of flooding the entire maze with values, as is the case with the regular Flood-Fill, the modified Flood-Fill only changes those values which need to be changed.

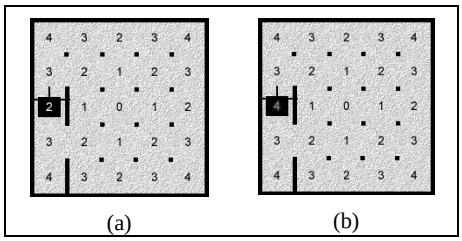

Fig.4. (a) Old distance value (b) New distance value

Fig.4 shows how our robot moves forward one cell and discovers a wall. The robot cannot go West and it cannot go East, it can only travel North or South. But going North or South means going up in distance values. So the cell values need to be updated. When the robot encounters this, it follows this rule: *"If a cell is not the destination cell, its value should be one plus the minimum value of its open neighbors"*. In the case above, the minimum value of its open neighbors is 3. Adding 1 to this value, results in 3 + 1 = 4. The maze now looks like Fig.4b.

There are times when updating a cell's value will cause its neighbors to violate the *"1 + minimum value"* rule and so they must be checked as well. We can see in our example above that the cells to the North and to the South have neighbors whose minimum value is 2. Adding a 1 to this value results in 2 + 1 = 3 therefore the cells to the North and to the South do not violate the rule and the updating routine is done. Now that the cell values have been updated, the robot can once again follow the distance values in descending order.

So our modified Flood-Fill procedure for updating the distance values is looked like Fig.5 below.

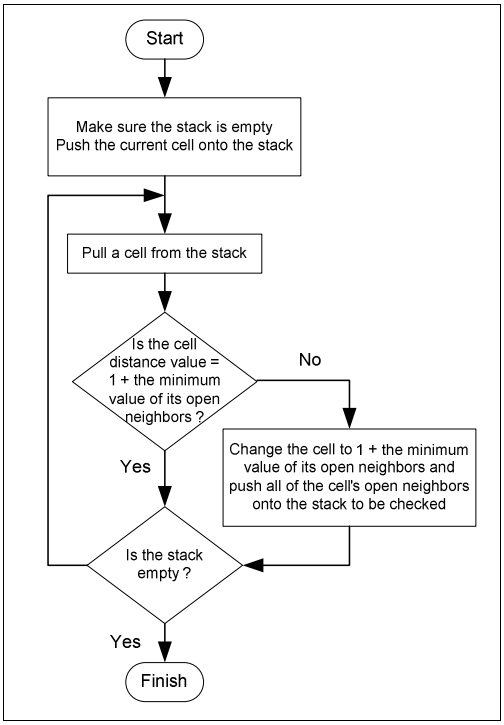

Fig.5. Flooding with distance values (if necessary) for modified Flood-Fill algorithm

As summary for both of algorithm, every time robot arrives in a cell, the Flood-Fill algorithm will perform the following steps [2], i.e.: 1) Update the wall map, 2) Flood the maze with new distance values (if necessary for modified Flood-Fill algorithm), 3) Decide which neighboring cell has the lowest distance value, 4) Move to the neighboring cell with the lowest distance value.

III. EXPERIMENTAL RESULTS

In this research, experiment is conducted to confirm the functionality of our artificial intelligence for path searching robot from starting cell to destination cell in the maze.

The artificial intelligence itself will control the system with simple diagram block (Fig.6a) that always consist of input, process, and output section.

Input section receives wall information from the maze using infra red reflective object sensor Fairchild Semiconductor QRD1114 and Honeywell HOA708-1.

Output section for robot maneuver -- in order to avoid breaking the wall, is handled by continuous rotation servo that received signal from Process section to control motor speed and direction.

Process section is handled by microcontroller BASIC Stamp BS2px and its supporting system. Here, the artificial intelligence is implanted with two main algorithms, as shown by Fig.6a. Information of maze map size, with initial distance value for every cell, also initialized at this section. Of course, at initialization, robot does not know about wall map information.

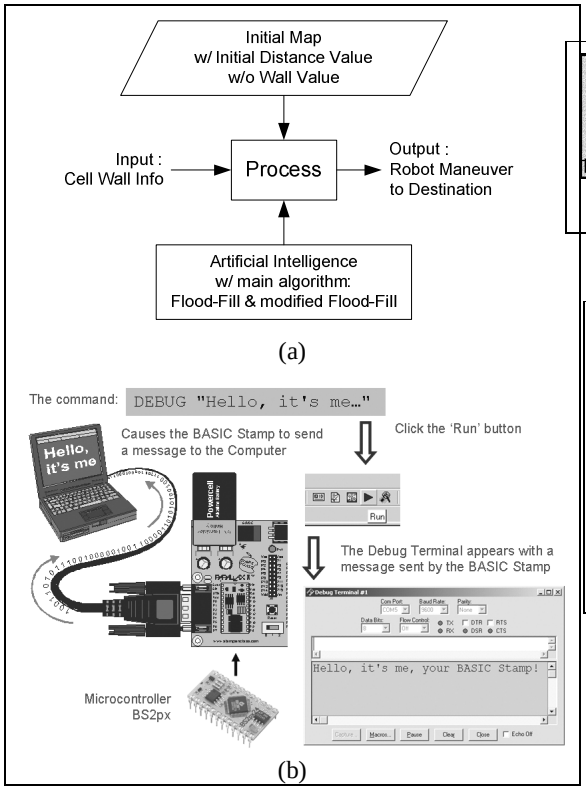

Fig.6. (a) System diagram block (b) Implementation of block process in BS2px development environment [3]

Fig.6b illustrates how the artificial intelligence was developed and implanted to the microcontroller BS2px with specification provided by Table 2.

Table 2. BS2px Specification [4]

Package	24-pin DIP
Package Size (L x W x H)	1.2" x 0.6" x 0.4"
Environment*	0º - 70º C (32º - 158º F)
Microcontroller	Parallax SX48
Processor Speed	32 MHz Turbo
Program Execution Speed	~19,000 instructions/sec.
RAM Size	38 Bytes (12 I/O, 26 Variable)
Scratch Pad RAM	128 Bytes
EEPROM (Program) Size	8 x 2K Bytes, ~4,000 inst.
Number of I/O pins	16 + 2 Dedicated Serial
Voltage Requirements	5 - 12 vdc
Current Draw @ 5V	55 mA Run / 450 µA Sleep
Source / Sink Current per I/O	30 mA / 30 mA
Source / Sink Current per unit	60 mA / 60 mA per 8 I/O pins
PBASIC Commands***	63
PC Programming Interface	Serial (19200 baud)
Windows Text Editor	Stampw.exe (v2.2 and up)

* 70% Non-Condensing Humidity
*** Using PBASIC 2.5 for BS2-type models

Experiment is conducted using some maneuvers as illustrated by Fig.7 and internal data processing is monitored via PC using serial communication, as shown by Fig.8a. Monitoring system itself involves debugging code that was embedded to the artificial intelligence, so it will make life easier to detect and repair any existing bug. Fig.10 shows the monitoring system in detail.

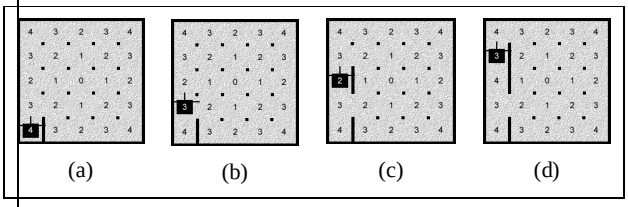

Fig.7. Prototype maneuver

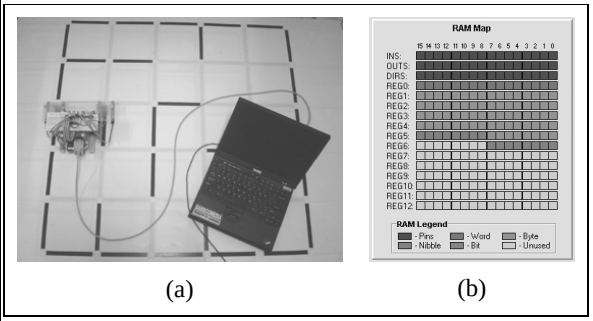

Fig.8. (a) Prototype testing (b) Usage of RAM

Microcontroller BS2px has three types of internal memory resource, i.e. 1) EEPROM for storing program code, 2) RAM for assigned and temporary variables, and 3) Scratchpad RAM for storing cell's data (see Table 1). Fig.8b shows internal RAM resource used by assigned variables that construct this artificial intelligence. RAM itself has total capacity of 13 Words (REG0 - REG12).

Using multi bank programming style, program code for artificial intelligence is stored from EEPROM bank 0 to bank 3 with its own usage percentage shown by Fig.9. Internal EEPROM itself comprised of eight memory banks (bank 0 to bank 7)

with capacity 2 KB in each, together form total capacity of 16 KB.

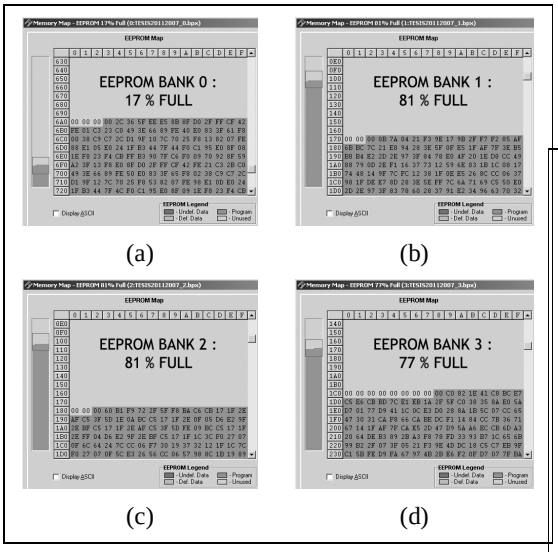

Fig.9. Usage of EEPROM Bank

Fig.10 shows the monitoring process for some maneuvers of path searching robot, as illustrated by Fig.7. At robot position like Fig.7c, monitoring result is shown by Fig.10a. At robot position like Fig.7d, monitoring result is shown by Fig.10b.

What monitoring process want to tell us is that modified Flood-Fill algorithm has already work. As summary for that algorithm, every time robot arrives in a cell, the Flood-Fill algorithm will perform the following steps:

1. Update the wall map
Fig.10a gives Wall value = 00011010b at cell with Coordinate value = (0, 2). From Table 1, it means that robot facing North because bit (7-6) = 00b. The cell has already been checked for side wall and front-rear wall (has reach checkpoint) because bit (4) = 1 and bit (5) = 1. Based on that, it is no need again for gathering wall info that has already got, i.e. there are walls at West and East side because bit (3) = 1 and bit (1) = 1.

2. Flood the maze with new distance values (if necessary)
The cell at (0, 2) need to update its distance value because its recent distance value = 2, violates rule: "*If a cell is not the destination cell, its value should be one plus the minimum value of its open neighbors*". Artificial intelligence updates this value. Fig.10b show updated distance value = 4.

3. Decide which neighboring cell has the lowest distance
Fig.10a shows there are two open neighboring cells with lowest distance = 3, i.e. cell at (0,1) and (0,3). The artificial intelligence choose cell (0,3) to move on because robot just go forward rather than turning that take more time.

4. Move to the neighboring cell with the lowest distance
Fig.10b shows robot move from cell at (0,2) to cell at (0,3). It proves this step.

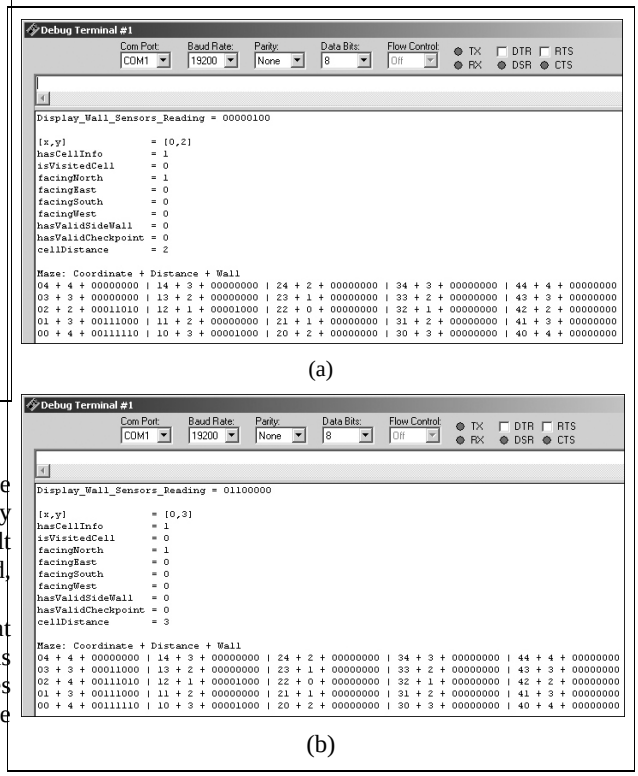

Fig.10. Monitoring for prototype maneuver

IV. CONCLUSIONS

Path searching from starting cell to destination cell has been accomplished by the artificial intelligence using Flood-Fill algorithm and modified Flood-Fill algorithm.

REFERENCES

[1] Wikipedia, "Autonomous robot", 2007, http://id.wikipedia.org/wiki/Robot
[2] Steve Benkovic, "*Hints, Ideas, Inspiration for Mice Builders*", 2007, http:// micromouseinfo.com/.
[3] Andy Lindsay, "*Robotics with the Boe-Bot, Student Guide*", Parallax, Inc. Press, California, 2004.
[4] Parallax Inc., "*Stamp Specifications*", 2007, http://parallax.com/Portals/0/Downloads/docs/prod/stamps/stampscomparison.pdf.

ISSN: 1411-1284

Design of Electro-Absorption Optical Modulator Incorporated with Waveguide MQW AlGaSb/GaSb and Fabry-Perrot Grating Cavity Structure for Fiber-Optics 1.55 µm Communication System.

P. S. Priambodo, Harry Sudibyo and Djoko Hartanto
Department of Electrical Engineering, Universitas Indonesia, Indonesia

Abstract — **Electro-absorption optical modulator based on waveguide structure incorporated with MQW AlGaSb/GaSb and Fabry-Perrot (FP) grating cavity structure has been designed for fiber-optics 1.55 µm communication systems. Different to the transversal modulator structure, where the Fabry-Perrot cavity is in the form of thin film layer Bragg Reflector, the modulator with waveguide structure is incorporating Fabry-Perrot cavity with grating mirror. The advantage of waveguide modulator in comparison to the transverse structure one is the improvement on the on/off ratio and further being able easily to be integrated with semiconductor laser source and semiconductor amplifier, which are grown on top of the same GaSb substrate. This paper contributes in the development of electro-absorption waveguide modulator design software.**

Keywords — **electro-absorption, optical modulator, Fabry-Perrot cavity, waveguide MQW, waveguide grating.**

I. INTRODUCTION

Interest in high-performance optical modulators has increased since 1990s due to increased performance demands of communication systems that use them. For long haul communication systems, where the bandwidth of fiber optics reaches THz and conversion speed between optical and electronic have increased to tens of GHz, has led to search for reliable high-speed modulators. Modulation technique by directly injecting semiconductor lasers is not accepted since it cause non-stability and creates chirps that result in low speed performance [1]. The answer for the demands is only external modulators. In the field of optical computing and communication systems, the need for encoding and delivering large amount of data and switching light with low energy, has encouraged to seek for compact optoelectronic devices.

There are at least four types of external optical modulators have been developed by researchers, which are based on electro-optics, acousto-optics, magneto-optics and electro-absorption. Electro-optics modulators have been developed since 1970s. The electro-optics modulators mostly work based on Pockel's and Kerr's effects. The disadvantage of this type of modulators is that it is not able to be grown and integrated with semiconductor lasers and light amplifier on top of the same substrate. The other disadvantages are the need of very high drive voltage and require longer light interaction, which cause higher device capacitance [2]. The higher drive voltage requires an extra power supply to the modulator, which is not compatible with the high-speed electronic circuits (5V or less) [3]. On the other side, higher capacitance causes low-speed device. This makes electro-optics modulators not the final answer.

Advances in material growth and processing have made it possible to fabricate thin layers of semiconductor with very high precision. For instances, molecular beam epitaxy (MBE) and metal organic chemical vapor deposition (MOCVD) have the capabilities to grow high purity semiconductor heterostructure layers with smooth interfaces. This technology makes the quantum mechanical effect possible to happen. One of the significant of this semiconductor layering technology is the development of semiconductor multi quantum well (MQW) electro-absorption modulators. Electro-absorption on semiconductor structure is the most ultimate technology applied for optical modulators. Its operation principle is based on Franz-Keldysh effect [4], i.e., a change of the absorption spectrum caused by an applied electric field, which change the band-gap energy. This mechanism effect is called tunneling process. The theory states that the material absorption threshold shifted to the long wavelength due to applied voltage on the material. However, usually the applied electric field does not involve the excitation carriers. In the earlier time, the development of electro-absorption modulator was started with bulk material. Further, it was known that the effect of electro-absorption is increased several folds by using multi-quantum well structures in the modulator [3]. The quantum well creates a confinement effect on electrons and holes, which are trapped inside the wells. The multi-quantum well structure, consists of barrier and well, each approximately 70Å thin, cause electrons and holes limited in 2-D movement. The movement limitation on the other dimension (perpendicular direction to the quantum well structure) creates quantization on

electrons and holes density state function in the structure. This sharpens the absorption curve and definitely improves the modulator more effective [1]. A photon with sufficient energy will be absorbed and will create a pair of electron and hole and called as an exciton. Because trapped inside a quantum-well, the exciton-energy bonding increases. Because of the quantization energy and the high-exciton energy bonding, it will sharpen the absorption curve. To increase the effect of quantum well, researchers increase the number of quantum well become multi-quantum wells. The most fundamental effect due to the applied voltage is decrement of the zero-point energy of the electron-hole quantization energy in the quantum well. This effect is called quantum-confined Stark effect (QCSE) [5].

More over, there are two fundamental structures in the development of electro-absorption optical modulator. The first structur structure of vertical cavity surface emitting laser (VCSEL) and ideal for 2D-array interconnection and computing applications [6]. The disadvantage of transversal structure modulator is that the light-material interaction is very short, as short as the thickness of the MQW layer; this makes the on/off ratio low. To improve light material interaction, it mostly uses asymmetric Fabry-Perrot (FP) cavity structure [7-9]. Where the back reflector on the substrate is Bragg stack quarter wavelength thin film layer 99% reflectivity and the front reflector is mostly a simple air and semiconductor interface 30% reflectivity. In general, transversal modulator is designed for reflectivity modulator [7-10]. The second type is waveguide modulator, where the light-material interaction is longer than the transversal modulator; it means it has higher on/off ratio. Another advantage of waveguide type modulator is possibility to be integrated with laser and semiconductor optical amplifier, and grown them on top of the same substrate [5]. Transversal and waveguide type modulators have their own advantages and disadvantages. Nevertheless, for the sake of device integration, higher on/off ratio and good speed reasons, the author has chosen waveguide type modulator to achieve high speed and efficient optical modulators.

II. DESIGN AND CALCULATION

Since a waveguide type optical modulator has a long light-material interaction, hence, most researcher use a single-pass method for the light interacts with the electro-absorptive region. They never need to reuse the absorptive region. This is definitely different to the transversal type modulator, where it has only very short light-material interaction region. To improve on/off ratio on transversal structure, the one needs to reuse the electro-absorptive region by applying FP cavity structure [7-9]. However, for technical reasons, only asymmetric FP cavity structure can be implemented on the transversal modulator.

The new idea brought in by this paper is applying FP cavity structure on waveguide type modulator as shown on Figure-1. By implementing the FP cavity structure on the waveguide modulator, it will reduce the length of light-material interaction region. Reduction of the interaction region results in smaller bias contact area, which finally reduces the capacitance and smaller capacitance means higher speed.

Different to the one applied on transversal modulator, which use asymmetric FP cavity, in this waveguide modulator structure, it uses symmetric FP cavity. The reason that the transversal modulator uses asymmetric FP cavity is due to requirement as a reflectance modulator. On the other side, the waveguide structure is required to be a transmittance modulator.

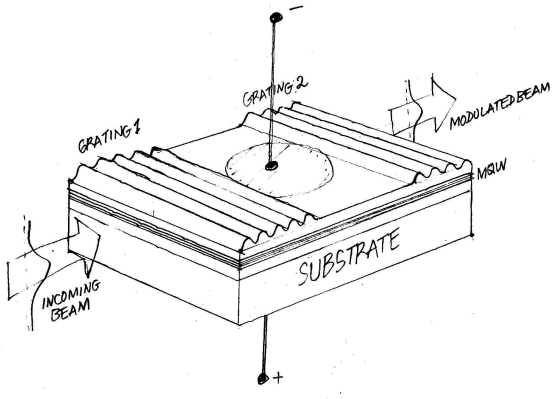

Figure-1. Electro-absorption waveguide type modulator incorporated with a symmetric Fabry-Perrot cavity structure and grating mirrors.

There are at least 3 important things to calculate such that the modulat working. The first is a design such that only a single fundamental mode running the waveguide modulator. Since the waveguide itself consist of many layers of superlattice and MQW, it needs an averaging estimation of the effective index of the waveguide. The optical properties of subwavelength repetitive thin layer stack can be explained approximately by using effective medium theory [11-13]. In the limit of $d/\lambda \rightarrow 0$, where d is the thickness of each superlattice or MQW layer, the effective waveguide refractive index is

$$n_{wg} = [n_L^2 + f(n_H^2 - n_L^2)]^{0.5} \quad (1)$$

where f is the ratio of $d_H/(d_H+d_L)$ and d_H and d_L are the thickness of the high and low refractive index layer respectively.

The second, after knowing the effective refractive index of the waveguide, then continuing to calculate the number of modes inside the waveguide

by using the following dispersion equation [14]:

$$2\,k\,n_{wg}\,h\cos\theta - 2\,\Phi_s - 2\,\Phi_c = 2q\pi \qquad (2)$$

where q is an integer (0,1,2, …), which identifies the mode number. The phase-shifts Φ_s and Φ_c are phase-shifts at the interface substrate and cover and represent the function of θ. For near symmetric film structure such as in our design, the number of modes in waveguide can be derived from Eq.2, to be [14]

$$N = \frac{2d}{\lambda}\sqrt{n_{wg}^2 - n_s^2} \qquad (3)$$

where N is integer number and $N = q+1$. Further on, the exact value of θ can be solved computationally by using Eq.2.

The detail structure of the electro-absorption waveguide modulator design is shown in Figure-2. Opposite to the forward bias for laser semiconductor, it uses reversed bias for electro-absorption modulator. The structure is expected to support only the fundamental mode.

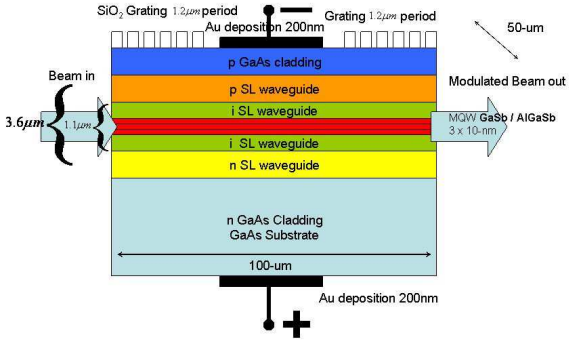

Figure-2. The detail structure of the electro-absorption waveguide modulator design

The third, the grating structures act as the front and back mirror in symmetric FP cavity. The design of this grating mirror is based on the perturbation theory of coupled modes in optical waveguide [15]. Basically the principle of the grating mirror is to couple the incident wave mode to the reflected wave mode as shown in Figure-3.

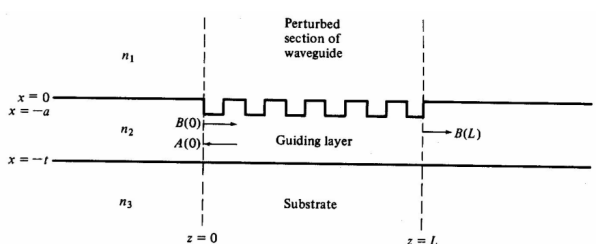

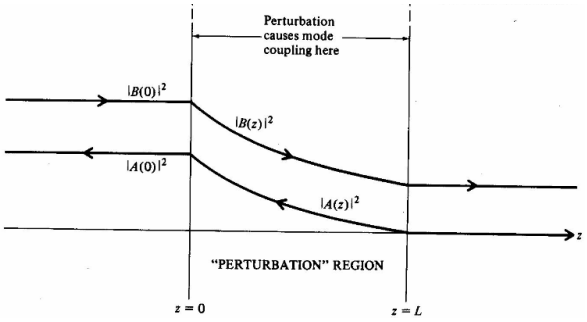

Figure-3. (*Upper*) Grating mirror as a part of FP cavity, (*lower*) the coupling between the forward and backward intensities inside the corrugated section.

The coupling between the backward B(z) and the forward A(z) can be described by [15]

$$\frac{dA}{dz} = \kappa_{ab} B e^{-i2(\Delta\beta)z} \qquad (4\text{-a})$$

$$\frac{dB}{dz} = \kappa_{ab}^{*} A e^{+i2(\Delta\beta)z} \qquad (4\text{-b})$$

Where κ_{ab} is coupling between wave A to B. The solution of Eq. 4 for the case subject to $A(L) = 0$ and under matching condition $\Delta\beta = 0$, it has

$$A(z) = B(0)\frac{\kappa_{ab}}{|\kappa_{ab}|}\frac{\sinh\left[\kappa(z-L)\right]}{\cosh \kappa L} \qquad (5\text{-a})$$

$$B(z) = B(0)\frac{\cosh\left[\kappa(z-L)\right]}{\cosh \kappa L} \qquad (5\text{-b})$$

To obtain grating mirror with $R = T = 50\%$, z = L. Thus from Eq. 5-b, we have

$$\cosh \kappa L = 4\cosh 0 = 4 \qquad (6)$$

It means that $L = 2.063/\kappa$. To solve how long is the requirement of grating length, it needs to solve the coupling coefficient κ, which is governed by the following equation []:

$$\kappa = \frac{i\omega\varepsilon_0 a_l}{4}\int_{-\infty}^{\infty}\Delta n^2(x)\left[\xi_y^s(x)\right]^2 dx \qquad (7)$$

Eq.7. tells us that the coupling coefficient between mode depends on several parameters, i.e.: (1) $\Delta n(x)$ the difference high-low refractive index of the grating materials; (2) ω frequency; (3) a_l Fourier component of grating contributes for the coupling and (4) ξ_y is the part of guided mode overlaps on the grating. Once finishing calculation for the grating, it has done for the waveguide and FP cavity structure.

There are three parameters that would like to be

the goals for the design: device capacitance, on/off ratio and internal insertion loss. The capacitance value is readily available by computing the area of the bias contact, the thickness of the intrinsic region of the waveguide and finally the dielectric constant average of the waveguide. The analysis for parameters such as on/off ratio and internal insertion loss needs information about the absorption curve of the MQW. In the first stage of design, for the sake simulation, we can make some assumption regarding to the absorption curve as shown in Figure-4. To calculate the on/off ratio, the effect of FP cavity on the transmittance intensity must be calculated first.

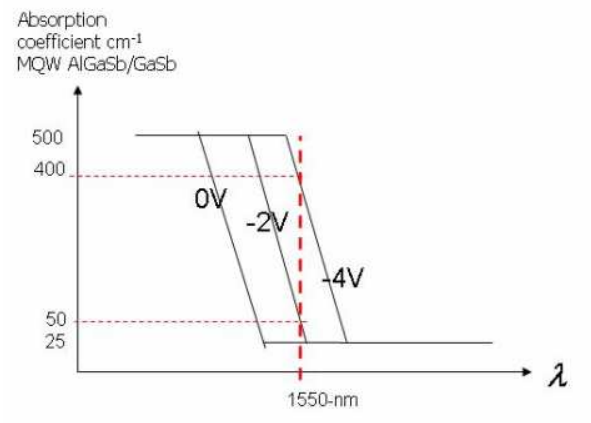

Figure-4. Assumption of electro-absorption curves of the MQW at several reverse biased values (0, -2V and -4V).

If the incoming mode has intensity of I_0, after passing the FP cavity, the outgoing mode will have [2]

$$I = \frac{rI_0}{\left|1 - r \cdot e^{j\varphi} \cdot e^{-\alpha L}\right|^2} \tag{8}$$

where r is reflectance of each mirror and φ is phase difference of the beam phasors, α is absorption and L is light-material interaction length. We design φ is 2π, thus Eq. 8 can be rewrote

$$I = \frac{rI_0}{(1 - r \cdot e^{-\alpha L})^2} \tag{9}$$

For a single-pass of 50 μm absorption length device, the on/off ratio is:

$$On/Off = \frac{e^{-\alpha_{ON} L}}{e^{-\alpha_{OFF} L}} = e^{-(\alpha_{ON} - \alpha_{OFF})L} \tag{10}$$

The gain of FP cavity is $1/(1 - r \cdot e^{-\alpha L})^2$ times. It means that the use of FP is equal to reuse the absorption region $\ln(1/(1 - r \cdot e^{-\alpha L})^2)$ times. Hence the on/off ratio is increased and rewrote as

$$On/Off = \frac{e^{-\alpha_{ON} L}}{e^{-\alpha_{OFF} L}} = e^{-(\alpha_{ON} - \alpha_{OFF})L \cdot \ln\left(1/\left(1 - re^{-\alpha L}\right)^2\right)} \tag{11}$$

The internal insertion loss is simply

$$IIL = \frac{r(1-r)}{(1 - r \cdot e^{-\alpha L})^2} \tag{12}$$

III. RESULT

During the process of development the design software, it is found that not only fundamental mode exist in the waveguide modulator, but also several fundamental modes exist in the quantum well structures due to symmetrical layers on the active layers. These multi fundamental modes can interfere each other and degrade the speed of the device. However, the multi fundamental modes which exist in the MQW, easily can be kicked out by the grating structure of the FP cavity.

This is the prove that the symmetrical FP cavity applied on electro-absorption waveguide modulator is not only improving the on/off ratio and reducing the capacitance, but also cleaning up the unused fundamental modes guided in the MQW.

The software is still under development, hopefully the full design of electro-absorption waveguide modulator can be completed soon.

IV. CONCLUSIONS

A new idea of electro-absorption waveguide modulator incorporating FP cavity with grating mirrors was presented, promises to improve the on/off ratio, reducing capacitance and finally improve the speed. As long as the writer knows, this is the first idea proposed.

Since waveguide modulator is possible to be integrated with laser source and semiconductor optical amplifier, the development of this device will be very interesting in the future.

V. ACKNOWLEDGEMENTS

The authors acknowledge Dr. Preston P. Young and Dr. K. Alavi of University of Texas at Arlington for their contributions to this work. This research was supported by the Ministry of Research and Technology, Republic of Indonesia, under Research Incentive Program.

REFERENCES

[1] T.H. Wood, “Multiple quantum well (MQW) waveguide modulators,” Journal of Lightwave Technology, Vol. 6, No. 6, June 1988, pp. 743-757.

[2] B.E.A. Saleh and M.C. Teich, “Fundamentals of photonics,” John Wiley & Sons,Inc., ISBN 0-471-83965-5, 1991.

[3] M. Whitehead, A. Rivers and G. Parry, ”Very low voltage, normally-off asymmetric Fabry-Perot reflection modulator,” Electronics Letters, Vol. 26, No. 19, 13th September 1990, pp. 1588-1590.

[4] H. I. Ralph, “On the theory of the Franz-Keldysh effect”, J. Phys.C (Proc. Phys.Soc), Ser. 2, Vol. 1, 1968, pp. 378-386.

[5] M. Bass and E.W. van Stryland, “Fiber Optics Handbook,” Optical Siciety of America, McGraw-Hill, ISBN 0-07-138623-8, 2002, pp. 4.57-4.63.

[6] R.H. Yan, R.J. Simes and L.A. Coldren, “Surface-normal asymmetric electroabsorption reflection modulators using asymmetric Fabry-Perot structures,” IEEE Journal of Quantum Electronics, Vol. 27, No. 7, July 1991, pp. 1922-1931.

[7] P. Zouganeli, M. Whitehead, P.J. Stevens, A.W. Rivers, G. Parry and J.S. Roberts, “High tolerance for low-voltage, high-contrast, low-insertion-loss asymmetric Fabry-perot modulators,” IEEE Photonics Technology Letters, Vol. 3, No. 8, August 1991, pp. 733-735.

[8] K.K. Law, J.L. Merz and L.A. Coldren, “Superlattice surface-normal asymmetric Fabry-Perot reflection modulators: optical modulation and switching,” IEEE Journal of Quantum Electronics, Vol. 29, No. 2, Februray 1989, pp. 727-740.

[9] R.H. Yan, R.J. Simes and L.A. Coldren, “Electroabsortive Fabry-perot reflection modulators with asymmetric mirror,” IEEE Photonics Technology Letters, Vol. 1, No. 9, September 1989, pp. 273-275.

[10] M. Whitehead, A. Rivers and G. Parry, “Low-voltage multiple quantum well reflection modulator with on:off ratio > 100:1,” Electronics Letters, Vol. 25, No. 15, 20th July 1989, pp. 984-985.

[11]S. M. Rytov, "Electromagnetic properties of a finely stratified medium," *Soviet Physics JETP*, vol. 2, pp. 466-475, 1956.

[12]E. N. Glytsis, T. K. Gaylord, and D. L. Brundrett, "Rigorous coupled-wave analysis and applications of grating diffraction," in *Diffractive and Miniaturized Optics*, vol. CR49, S. H. Lee, Ed.: SPIE, pp. 3-31, 1994.

[13]D. L. Brundrett, E. N. Glytsis, and T. K. Gaylord, "Homogeneous layer models for high-spatial-frequency dielectric surface-relief gratings: conical diffraction and antireflection designs," *Applied Optics*, vol. 33, pp. 2695-2706, 1994.

[14] T. Tamir, “Integrated Optics”, Springer-Verlag, 1979

[15] A. Yariv, “Optical Communications”, Oxford, 1991

ISSN: 1411-1284

Flight Control System Based on Laser Gyro's Technique Applied to Takeoff phase on Wing In Surface Effect craft (WiSE-craft)

Sayuti Syamsuar Usman* And Purnomo Sidi Priambodo**

*Agency For The Assessment And Application of Technology (BPPT)
BPPT 2nd Building 10th Fl Jalan MH Thamrin 8 Jakarta, 10340 INDONESIA
Phone/Fax: +62-21-316 9342 E-mail: sayutisyam@webmail.bppt.go.id
** Department of Electrical Engineering University of Indonesia
KAMPUS UI DEPOK INDONESIA
E-mail: pspriambodo@ee.ui.ac.id

Abstract. **Flight control system based on laser gyro's technique has been developed and will be applied for the takeoff phase of Wing In Surface Effect (WiSE) craft. In this system, laser gyro's sensors will be used to measure the real time alpha, α and theta angles, θ, heading direction, ψ and altitude, h of WiSE-craft, where this data will be used as the output for the flight control system. To obtain an accurate design, the aerodynamic model equations for longitudinal state of remote control craft NA-5 model will be simulated. Further on the simulation data such as speed, V, altitude, h and heading, ψ are compared to the real flying test data of model NA-5 which carrying a portable Global Positioning System (GPS). The comparison between simulated and real flying test data are used to improve the accuracy of laser gyro's LTN-92 and the whole flight control system. The 5 (five) conditions that the flight control system is need during takeoff on WiSE craft 8 seaters configuration, i.e (i). the center of gravity limitation, (ii). the resistance of hump drag on the water, (iii). the low altitude range on surface effect, (iv). upper engine position on fuselage, (v). the negative stability margin about -0.1. The prototype of WiSE craft 8 passengers have been building since 2006.**

Keywords – Aerodynamic model, real flying test, flight control, hump drag, negative stability margin, Global Positioning System, laser gyro's LTN-92.

1. INTRODUCTION

The concept design of flight control system by using laser gyro's LTN-92 optics sensory is applied to remote control model NA-5 during takeoff phase. The aerodynamics parameter such as Lift coefficient, CL, Drag coefficient, C_D and Moment coefficient, C_M calculated by DATCOM referred to airfoil and wing configurations. While, the non dimensional stability derivative must be calculated to fulfill the block diagram of the closed loop digital flight control system. The graphics of drag polar C_L versus C_D of WiSE craft performance to known the engine efficiency and optimum cruise speed. The theoretical background as a basic mathematical analysis to six degree of freedom from Eulers equation and presented as figures, where the force and moment acting on each axis in the WiSE craft.

The 5 (five) problems of remote control model NA-5 configuration are found during the flight test activities. These problems becomes from (i). weight and balance referred to center of gravity limitation (flight envelope), (ii). Hump drag of water resistance during high speed taxiing, (iii). the engine installation on the upper fuselage position, (iv). the altitude range on the surface effect not more than wing span, and (v). the negative stability margin of Irodov criterias are around -0.1 for moderate static and dynamic stability.

The data measurement during flight testing such as altitude, h, speed, V and true heading, ψ are recorded by portable Global Positioning System (GPS) are presented in several graphics. The purpose of the whole flight control design by using sensors laser gyro's LTN-92 to know the altitude, h, speed, V and true heading, ψ are more accurately and faster than portable GPS. The feedback of flight control system and others mechanical system affected by the response of the control surface such as elevator deflection, e and throttle of engine, th on the longitudinal mode as an input deflections. The optic sensor laser gyro's are measures the altitude, h as parameter output on the flight control system beside parameter angle of attack, alpha , theta and heading. The flight environmental conditions during RC model flight testing is found with the wind calm, zero wind or not more than 10.0 [knots] and the water wave not height than 30.0 [cm]. If this conditions are not found, pursuit the flight testing in the early morning.

The basic design of the topics, become from the mathematical model of configuration, aerodynamic and hydrodynamic model testing, remote control model testing and prototype flight testing. In the same time, the specialist are defined the engine specification and mounting, flight control and handling system, instrumentation and electrical also data monitoring systems to handle the WiSE craft operational. The safety factor is mandatory during flight testing activity, while the test Pilot handle conducting the flight test development and certification program. In normally, the sensory system and on board data acquisition on the WiSE craft "flying test bed" fully instrumented and to get the air data system is recommended by using the laser gyro's LTN-92 sensory system. While, these laser gyro's system more compactable and accurately if its using in the closed loop flight control system. The force and moment acting on each aerodynamic, body and inertial axis in WiSE-craft measured in-direct by using other electronic and mechanical sensory systems. These data measurement must be calculated to get the physically value. For example,

the drag polar: Lift coefficient, C_L versus Drag coefficient, C_D graphics of flight testing become from airspeed measurement in subsonic region times air density and wing dimensional of WiSE craft. And then, the Lift, Drag and Moment acting on each axis WiSE craft could be calculated from these value. The center of gravity, c.g envelope calculate by the WiSE craft designer depend on the Maximum Takeoff Weight, MTOW, all of WiSE craft dimension, load factor, nz and speed endurance need. The thrust power of engine calculated by specialist and by the theoretically equation of Thrust (T)/ Weight (W) ratio to fulfil the Aspect Ratio, AR is 3.5.

The first step of our activity is to understand how the WiSE craft takeoff on the surface effect in the water runway. By theoretical aerodynamic, its found the results that the WiSE craft flown in the optimal altitude as high as width of its wing chord. In this case, the remote control model NA-5 is better flight in the level 30.0 [cm] above sea level. The power of 1 (one) engine utilize about 11.0 [HP] installed on the upper of fuselage. After liftoff, the remote control model WiSE craft airborne with level flight while the wave of water not more than 20.0 [cm] height and wind speed not more than 5.0 [knots]. Normally, this condition will found in the morning early, between 06:00 to 09:00 o'clock. In the test period since 2 years ago having 6 (six) wing configurations and 2 (two) step positions on the hull related to the center of buoyance, c.b location in the body axis of WiSE craft. The Maximum Takeoff Weight, MTOW of remote control model NA-5 configurations around 42.0 [kg] included fuel, ballast, engine and others component such as portable Global Positioning System (GPS) to get the airspeed, V, altitude, h, and true heading, ψ as measuring and recording system. The specifically of this model when WiSE craft liftoff from the water, while the craft is tendence have maneuvering with high agility. The dynamics flight response during airborne after liftoff have been recorded by portable GPS and gave a good results. And, comparing to the Irodov criteria, the negative stability margin about -0.1 have a better results. Figure 1 is remote control model NA-5 demonstrator.

Figure 1
Remote control model NA-5 configurations .

Figure 2 is GPS portable was installed in the remote control model NA-5. The flight test results at 28 till 31 May 2007 such as altitude, h, speed, V and heading, ψ during RC model NA-5 takeoff and airborne are presented. The time histories, (t) data are recorded by portable GPS looks better and without speck.

Figure 2
A portable Global Positioning System (GPS) installed in the remote control model NA-5.

Figure 3 is the fuselage of WiSE craft 8 seaters prototype. The WiSE craft have been fabricating in Serpong. The next activities is to improve and preparating the prototype flight testing. The flight control system of the WiSE craft is depend on the aerodynamic Lift, Drag and Moment coefficients versus angle of attack, α graphics. The stability aerodynamic stability parameter are presented too and calculated by DATCOM software.

Figure 3
The prototype of WiSE-craft 8 seaters have been building since a years ago in Serpong.

2. THE WiSE CRAFT MATHEMATICAL MODEL

The mathematical model longitudinal mode during takeoff phase without hydrodynamic, turbulence model but purely aerodynamic parameters. While, the focus to the problem it self and monitored the flight characteristics after liftoff is the first priority. The block diagram of non dimensional stability derivative model are presented while its supported by aerodynamic parameter calculated from DATCOM software. Also, the non dimensional stability derivative parameter including in this program. The optimum high altitude of WiSE craft prototype not more than 2.0 [m]. The flight control system maintains this altitude to keep aerodynamic lift is constant. The elevator deflection and throttle deflection, th of the power engine as output feedback on the closed loop are gived automatically by the signal response of actuator systems.

The Wieselsberger and Tani method is one of several method that concentrate in the aerodynamic surface effect. This theoretical calculation method are also implemented in the wind tunnel software while the aerodynamic model scaling down must be tested before build up the prototype of WiSE craft. The calculation of aerodynamic coefficients, like aerodynamic lift coefficient, C_L, aerodynamic drag coefficient, C_D and aerodynamic moment coefficient, C_M are calculated by DATCOM software.

The wind tunnel model testing as shown in Figure 4. The dimensions of wind tunnel model testing must be scale down (1 : 8), and the weight of the model is not corellable depend on the strength of material structure.

Figure 4
Wind tunnel model testing of WiSE craft 8 seaters on the Indonesian Low speed Tunnel, LAGG in PUSPIPTEK, Serpong.

2.1 Dynamic analysis during takeoff phase

The first step of dynamic analysis of WiSE craft takeoff phase become from the non dimensional stability derivative that calculated by hand and than make it the digital simulation in the flight control closed loop system to get the transfer function of input and output response. The sensor laser gyro's LTN-92 axis are linked to the body axis Xb Yb Zb. The Thrust, (T) and Weight, (W) are acting in the body axis are referable also. The second step are observed by the graphics of aerodynamic parameter during theoretical analysis, wind tunnel test results and the remote control flight testing results. The second step on this discussions are giving a quickly analysis. Figure 5 is the trayectory of WiSE craft takeoff phase.

Figure 5
The trayectory of WiSE-craft takeoff phase on the water surface.

2.2 Dynamic motions during takeoff phase

The dynamic mathematical equations are solving problems of forces and moments on the reference axis by using the body axis, X_b Y_b Z_b. Define the several parameters, such as:

- Mass, (M) of WiSE craft is constant.
- WiSE craft is the rigid body.
- Earth as reference Inersial axis, and atmosphere is not moving from the Earth.
- The forces acting on the axis of WiSE craft becomes from Weight, (W), Thrust, , (T), and Inersial, (I).
- The moments acting on the WiSE craft are reffered to center of gravity, c.g location.

The Newton's Law II on the WiSE craft are as follows:

The force equation is $$\sum \Delta F = \frac{d}{dt}(mV)$$

Where, V is speed and m : mass.

The moment equation is $$\sum \Delta M = \sum \Delta .F.X$$

Where, X is distance to c.g

All of the dynamics time response, (t) motion of WiSE craft are referred to the body axis Xb Yb Zb.

The Eulerian angles of flight performance and stability during flight control system design is shown in Figure 6.

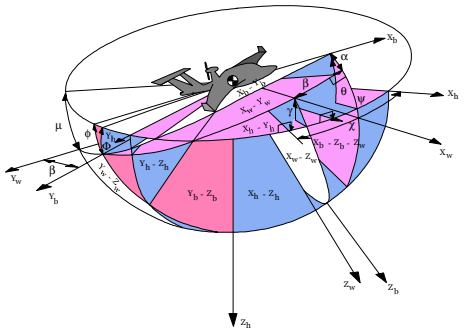

Figure 6
Eulerian angles.

2.3 The static and dynamic stability criterian in the longitudinal mode

The static stability criteria in the longitudinal mode is defined as:

$C_{m_\alpha} < 0$ is static pitch stability.

The static height stability that used in Irodov criteria are calculated by DATCOM software[9].

The Irodov criteria during dynamic motions:

$$X_\alpha - X_h < 0$$

where,

$$X_\alpha = \frac{C_{m_\alpha}}{C_{L_\alpha}}$$

$$X_h = \frac{C_{m_h}}{C_{L_h}}$$

Parameter is called stability margin. This value normally -0.1 base on experience.

3. THE SIMULATION RESULTS OF DATCOM

The digital simulation results calculated by DATCOM software for WiSE craft 8 seaters; V = 80 [knots] and c.g = 17 %). Cma between - 0.04 to - 0.01 are fulfil to the static stability criterian. The C_L and C_M versus angle of attack, α are presented in Figure 7 and 8. Diagram C_L versus C_D in Figure 9.

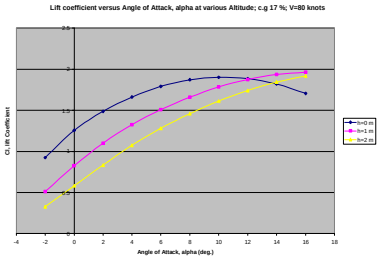

Figure 7
Lift coefficient, C_L versus angle of attack, α at speed 80.0 [knots]; center of gravity, c.g 17 % and altitude 0.0, 1.0 and 2.0 [m][9]

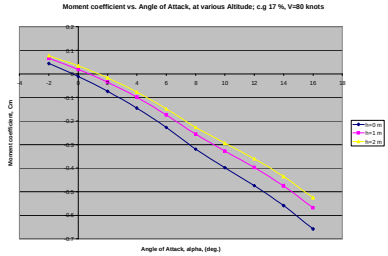

Figure 8
Moment coefficient, C_M versus angle of attack, α at speed 80.0 [knots]; center of gravity, c.g 17 % and altitude 0.0, 1.0 and 2.0 [m][9].

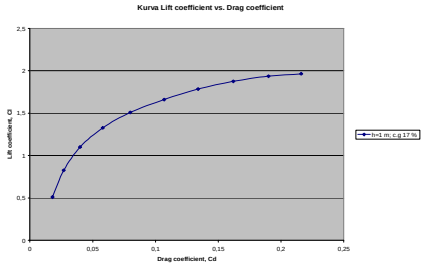

Figure 9
Lift coefficient, C_L versus Drag coefficient, C_D at altitude, h=1 [m] and Center of gravity, c.g 17 %[9].

4. THE REMOTE CONTROL MODEL NA-5 FLIGHT TEST RESULTS

The next graphic are the flight test results of remote control model NA-5 recording by GPS portable. The altitude, h, speed, V and true heading, ψ during flight testing are given in Figure 10, 11 and 12.

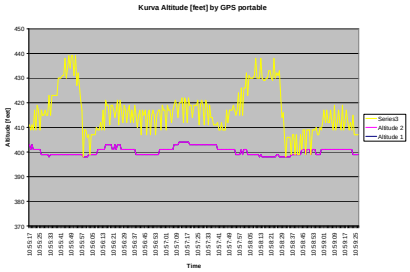

Figure 10
Altitude, h 1 and altitude, h 2 versus time, (t).

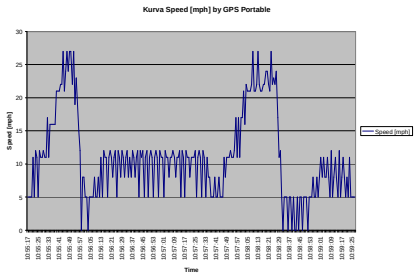

Figure 11
WiSE-craft speed, V versus time, t during takeoff.

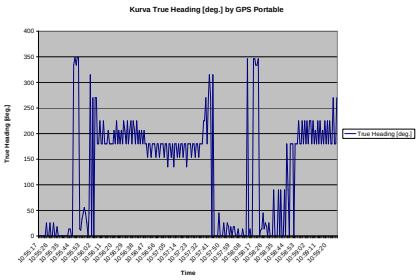

Figure 12
True heading, ψ on remote control model NA-5; run 1.

5. THE DIAGRAM BLOCK AND TRANSFER FUNCTION OF FLIGHT CONTROL SYSTEM

The methodology of this research is reffered to flight control system on the Alpha Jet fighter aircraft with the alpha maximum control system during its maneuvering in the air. This packet software was installed in the Simulink-MATLAB. See Figure 13. The mathematical model of WiSE craft 8 seaters became from DATCOM analysis and the graphic are to known the WiSE craft 8 seaters performance and static-dynamic stability. The conclusions of that problematic should be answered. The constraints during flight testing are: (i). the satic and dynamic characteristic are moderate stable, (ii). The optimum flight surface around 30.0 [cm] of RC model NA-5, (iii). the center of gravity, c.g range between 16.0 to 28.0 %, (iv) and maximum takeoff weight not more than 42.0 [kg]. Its could be found that the laser gyro's LTN-92 is recognize to be installed on the WiSE craft as a part of flight control system in the literature.

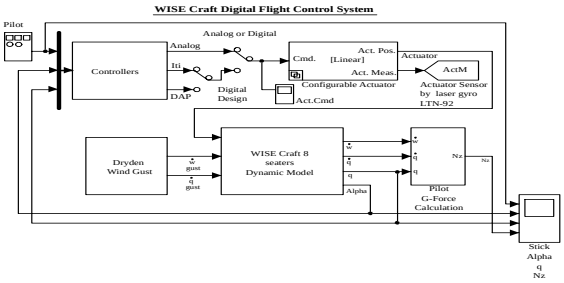

Figure 13
WiSE craft flight control system refferd to Alpha Jet fighter diagram block.

The WiSE craft conditions during performance analysis in the airborne conditions after liftoff with the cruise speed, VC. The stability analysis by using non-dimensional aerodynamic/ stability derivative in stability axis Xs Ys Zs. The equation of motion on the longitudinal mode during takeoff phase by using the frequency response, (f) and Laplace, (s) transformation. The fourth order transfer function of aerodynamic derivative diagram block as a dynamic model of WiSE craft with the input are elevator deflection, and throttle deflection. See Figure 14.

Figure 14
Laser gyro's LTN-92 for WiSE craft 8 seaters prototype.

The flight control system during takeoff by using laser gyro's LTN-92 sensor is recommended from others sensory systems to accomplish a better WiSE craft performance. The LTN 92 Inertial Navigation System is the world leading laser gyro's replacement for the transport aircraft. The LTN-92 uses three ring laser gyro's, force rebalanced accelerometer, and three high speed digital microprocessor to provide an advance technology all altitude, worldwide navigation system offering up to five times reliability of mechanical inertial navigation systems reliability.
The technical specification such as physical, INU, CDU, MSU and MCDU at several size are given.

6. CONCLUSIONS

Based on the prediction analysis and the remote control flight test results, give the actual conclusions for the development of WiSE craft 8 seaters construction:

- All of the static and dynamic stability criteria from theoretical background analysis are fulfilled the design criterian.
- All of the flight test results of GPS portable recording of remote control model NA-5 are fulfilled enough. And, the flight test results are combined to the performance analysis, but the response are not referable.
- During remote control flight testing experience, the flight test engineer should be prepare the weight and balance procedures to get center of gravity, c.g limitation.
- The laser gyro's LTN-92 sensor measuring latitude during flight testing.
- All of the research activities such as theoretical background analysis, windtunnel test model and remote control model flight testing are available.
- The laser gyro's LTN-92 as an output latitude sensory system in the next flight control systems longitudinal mode during takeoff phase on the WiSE craft prototype are available.
- The digital flight control system by using laser gyro's LTN-92 is useful to applied in the WiSE craft 8 seaters prototype.

REFERENCES

1. John J Anderson Jr., Fundamentals of Aerodynamics, Second Edition, Mc Graw-Hill, Inc., New York, 1991.
2. Sighard F Hoerner, Fluid dynamic drag, New York, 1966.
3. Ir. R F Scheltema, Buoyancy and Stability of Ships, Culemborg, The Netherlands, 1969.
4. F Bruhn, Analysis and Design of Flight Vehicle Structures, Tri State Offset Co., USA, 1965.
5. Nikolai Kornev, Konstantin Matveev, Complex Numerical Modeling of Dynamics and Crashes of Wing in Ground Vehicles, AIAA 2003-600, California Institute of Technology, Pasadena, USA , 2003.
6. Bernard Etkin, Dynamics of Flight Stability and Control, 2nd edition, John Wiley & Sons, University of Toronto, 1982.
7. G J J Ruijgrok, Elements of Airplane Performance, Delft University, Netherlands, 1994.
8. Donald Mc Lean, Automatic Flight Control Systems, Prentice Hall International (UK), London, 1990.
9. Tim WiSE LPPM-ITB, Laporan Akhir Desain Konfigurasi, Preliminary Design Part II-A, WiSE 8 Aerodynamic Prediction Based on DATCOM, ITB, Bandung, 2005.

Noise Recovery Cage to Reduce High Noise of Control valve Using Sound Pressure Level

Baskoro Abie Pandowo, PhD Candidate of EE Department, University of Indonesia,
Jl. Salemba Raya 4, Jakarta 10430
Tel. 330188, fax. 3918115 email : baskoro.abie@eng.ui.ac.id
Faculty of Engineering
Jakarta, November 25, 2007

Abstract– **One of sources of control valve noise is mechanical vibration of trim valve.**
Vibration of trim valve is a result of random pressure fluctuation within the valve body and/or fluid impingement upon the movable or flexible trim valve. Source of noise resulting from mechanical vibration is the lateral movement of the valve plug relative to the guide surfaces.
In this article explains a high noise of trim valve in oil and gas industries at the gas compressor application.
Service condition data is simulated by sound pressure level with using firstvue version 1.0ab software. The simulation result tells that control valve CV-3 and CV-5 have high noise before using noise recovery cage, the noise is 92.2 dBA and 100.5 dBA, then after using noise recovery cage, the noise will be 80.4 dBA and 83.7 dBA.

Keywords– Control valve, Noise, Recovery Cage, Sound Pressure Level (SPL).

I. INTRODUCTION

Control valve is defined by ISA (International Standard Association as "A power operated device which modifies the fluid flow rate in a process control system. It consists of a valve connected to an actuator mechanism that is capable of changing the position of a flow controlling element in the valve in response to a signal from the controlling system".

In other words, a control valve automatically responds to some feedback from a sensing element which measures a variable in the process loop. The variable may be temperature, pressure, flow or level of the process fluid. The sensing element sends a signal, either directly or through intermediate instrumentation to the actuator. The actuator which is often pneumatically operated responds to the signal and adjusts the position of the valve.

Noise has always been present in control valve. It is a natural side effect of the turbulence and energy absorption inherent in control valve. One of major sources of control valve noise are mechanical vibration noise. Mechanical vibration noise generally results from the plug vibration. Vibration of valve component (trim valve) is a result of random pressure fluctuations within the valve body and/or fluid impingement upon the moveable or flexible trim valve.

The major problem with industrial people is its effect on people. If there are no people to hear a noise and if the noise does not damage the equipment, there is no noise problem.

The U.S. Occupational Safety and Health Act (OSHA), establishes maximum permissible noise levels for all industries whose business affects interstate commerce. Notice in Table 1.1 that the maximum permissible levels depend upon the duration of exposure. These maximum sound levels have become the accepted noise exposure standard for most regulatory agencies. Thus they have become the standard by which much noise generating equipment has been specified and measured.

Table 1.1. OSHA regulations provide maximum noise exposures for personnel in the work place as a function of noise level and exposure time

Duration In Hours per day	**Sound Level dBA**
8	90
6	92
4	95
3	97
2	100
1-1/2	102
1	105
1/2	110
¼ or less	115

II. BASIC THEORY [1]

Noise Prediction

The establishment of an accurate technique for predicting noise is perquisite for good noise abatement program. The technique for predicting the ambient noise resulting from flow of fluid thru a control valve fir any given set of service conditions.

The technique gives consideration to flow parameters relevant to noise generation. These parameters are pressure differential across the valve, flow coefficient, ratio of pressure differential to inlet pressure, valve geometry and size and schedule of adjacent piping. This technique is called Sound Pressure Level (SPL) as equation 2.1.

Noise coefficients used in the equation 2.1 are unique values that must be determined by laboratory tests for both compressible and incompressible fluids as s function of valve geometry.

$$SPL = SPL_{\Delta P} + \Delta SPL_{Cg} + \Delta SPL\,\Delta P/P1 + \Delta SPL_{k} + \Delta SPL_{P2} \quad \text{……..…….. (2.1)}$$

The information needed to determine SPL of the control valve is valve style, trim type, size and schedule of adjacent piping, service condition (inlet pressure, pressure drop, temperature, flow rate).

Noise Control

In closed systems (not vented to atmosphere) any noise produced in the process becomes airborne only transmission through the valves and adjacent piping that contain the flow stream. The flow stream forces these solid boundaries to vibrate. The vibrations cause disturbances in the ambient atmosphere that are propagated as sound waves.

Noise control employs either *Source treatment* or *Path treatment*.

Source treatment, preventing or attenuating noise at its source, is the most desirable approach. There are several manners of source treatment available for valves with recovery cage-style trim as shown Figure 2.1.

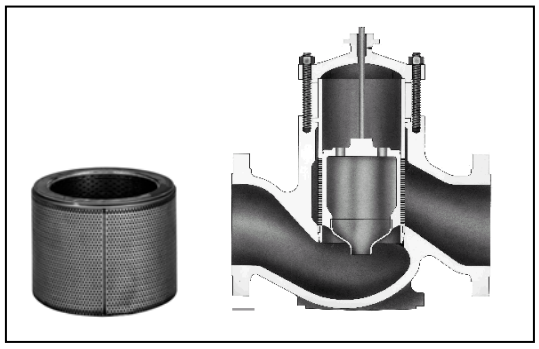

Figure 2.1. Recovery Cage Style Trim for Gas/Steam Application

Source treatment for noise problems associated with control valves handling liquid is directed primarily at eliminating or minimizing cavitation as Figure 2.2.

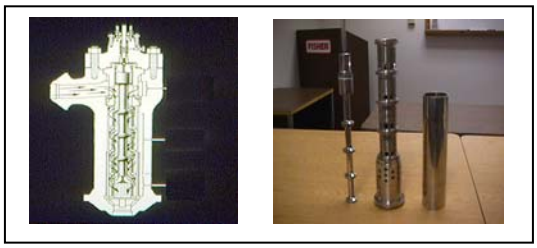

Figure 2.2. Cage Style Trim for Liquid Application

Second approach to noise control is that of path treatment. The fluid stream is an excellent noise transmission path. When critical flow exists, the vena contracta acts as a barrier to the propagation of sound upstream via the liquid. At sub-critical flow, valve noise can be propagated in the upstream direction almost as efficiently as it is downstream. The impedance to the transmission of noise upstream at sub-critical flow is primarily a function of valve geometry.

Path treatment consists of increasing the impedance of the transmission path to reduce the acoustic energy that is communicated to the receiver.

In gas transmission system, inline silencers effectively dissipate the noise within the floe stream and attenuate the noise level transmitted to the solid boundaries, as shown Figure 2.3.

Figure 2.3. Path Treatment as Silencer & Resistant plate

III. EXPERIMENTAL RESULTS

Application System in Oil-Gas Industry

Gas compressor is a mechanical device that increases the pressure of a gas by reducing its volume. Compression of a gas naturally increases its temperature.

Gas compressor is similar to pump, both increase the pressure on a fluid and both can transport the fluid through a pipe. A gases are compressible, the compressor also reduces the volume of a gas. Liquids are relatively incompressible, so the main action of a pump is to transport liquids. Generic compressor station is as Figure 3.1.

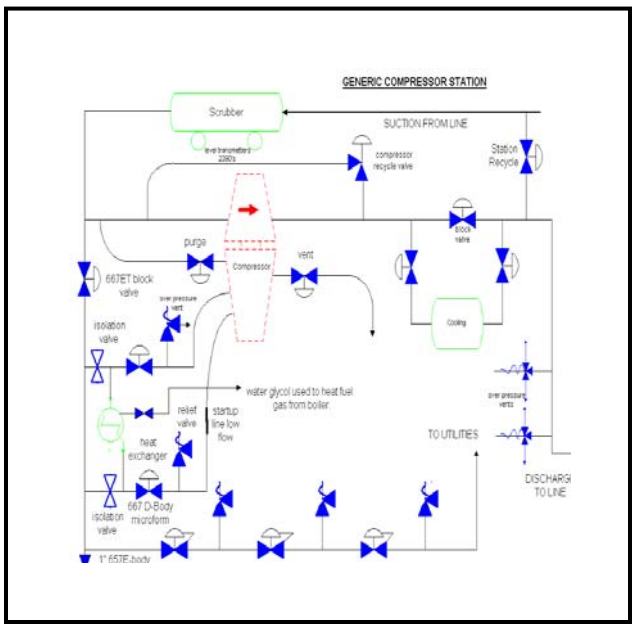

Figure 3.1. Generic Gas Compressor

As the Figure 2.1, the gas compressor station has six control valves. Every control valve has the dedicated service condition designed by the process licenser of oil and gas industry as shown Table 3.1, for selecting the control valve is suitable to this application.

Table 3.1. Service Condition Every Control Valve

SC	CV-1	CV-2	CV-3	CV-4	CV-5	CV-6
Q	400	2200	2500	500	14M	1M
P1	60	150	25	60	40	440
PD	35	110	5	20	20	290
T	95	95	95	95	95	95
V	0.439	0.252	0.719	0.439	0.847	0.771
PS	2	2	3	4	6	3
SC	40	40	40	40	40	40

The unit of service condition is flow (Q) in BPD (Barrel Per Day) or MMSCFD, inlet pressure (P1) in psig, pressure drop (PD) in psid, temperature (T) in deg.F, viscosity (V) in cP and piping size (PS) in inch.

SPL Sizing Calculation

From Table 3.1, we did the SPL sizing calculation for looking for SPL every control valve using Firstvue latest version 1.0.ab to identity the control valve package best suited to each set of service conditions as shown in Table 3.2. This valve sizing program software offers Export/ Import capabilities that let to take advantage of plant engineering, design and maintenance programs such as Intergraph Corporation's INtools and Instrument Data Manager.

Table 3.2. SPL Sizing Calculation Result

CONTROL VALVE	SPL [dBA]
1	86.8
2	76.0
3	92.2
4	80.9
5	100.5
6	79.0

Recovery Cage Application to Attenuate the High Noise

From Table 3.2 shows control valve CV-3 and CV-5 have noise higher than OSHA regulation 92.2 dBA and 100.5 dBA. To attenuate the high noise, both control valves should use the recovery cage style trim.

After SPL sizing calculation with recovery cage style trim, the high noise can be reduced to be the SPL value as shown in Table 3.3.

Table 3.3. SPL Sizing Calculation with Recovery Cage

CONTROL VALVE	SPL [dBA]
1	86.8
2	76.0
3	80.4
4	80.9
5	83.7
6	79.0

Discussion

Based on SPL sizing calculation, the gas compressor system has two control valves (CV-3 and CV-5) which have noise 92.2 dBA (CV-3) and 100.5 dBA (CV-5). This noise is bigger than OSHA regulations. Then

We took the service condition (inlet pressure, pressure drop, temperature and flow rate) for both control valves is same for doing the simulation with recovery cage style trim. Finally we got the noise reduction to be 80.4 dBA (CV-3) and 83.7 dBA (CV-5). In Figure 3.2 says control valve CV-3 and CV-5 which using recovery cage in same service conditions has better noise.

Other case, if we change the temperature to be 150 deg.F, the noise reduction to be 80.8 dBA (CV-3) and 84.1 dBA (CV-5).

Figure 3.2. SPL Curve of without/with Recovery Cage

IV. CONCLUSIONS

With temperature is kept constant 95 deg.F, it can give the reducing high noise, before using noise recovery cage, control valve CV-3 and CV-5 have the noise of 92.2 dBA and 100.5 dBA and after applying the noise recovery cage the noise can be reduced to 80.4 dBA and 84.1 dBA or 12.8% of control valve CV-3 and 16.7% of control valve CV-5.

Finally all six control valves are safe to protect peoples health and to prevent physical damage to control valves in gas compressor system application of the oil-gas industry.

REFERENCES

[1] "Control Valve Handbook", Fourth Edition, Emerson Process Management Solution, Marshalltown, Iowa, 2005.

[2] "Cavitation in Control Valve", Samson AG, Weismüllerstraße 3, 60314, Frankfurt, 2003

[3] Beal.O.Guy, Cook.Gerald. "Noniterative System Identification Applied to Wind Tunnel Valve Control. IEEE Transaction on Industrial Electronics. Vol.IE-32 No.1 February 1985.

[4] "Control Valve Engineering School. Fisher-Rosemount Singapore Pte Ltd, 1997

[5] Kaku.Bin, Mayashita.Ichiro, Sone.Satoru. "A Novel Prediction Method of Acoustic Magnetic Noise Based on Induction Motor's NHCC Function". (IEEE Transaction on Industrial Electronics. Vol.45 No.2. April 1999).

[6] James F.Buresh and Charles B.Schuder, "Development of Universal Gas Sizing Equation for Control Valve", Final Control Systems Research, Fisher Controls International Inc, Iowa, 1974

[7] Allen C.Fagerlund, "Use of Pipewall Vibrations to Measure Valve Noise", Final Control Systems Research, Fisher Controls International Inc, Iowa, 1988

[8] Paul Schafbuch, "Fundamentals of Flow Charac-terization", Final Control Systems Research, Fisher Controls International Inc, Iowa, 1974

[9] Marc Riveland, "Fundamentals of Valve Sizing for Liquids", Final Control Systems Research, Fisher Controls International Inc, Iowa, 1985

ISSN: 1411-1284

Solar Power Mobile Computer

N.R. Poespawati, J. Halomoan, G. Witjaksono

Department of Electrical Engineering, Faculty of Engineering, University of Indonesia
Kampus Baru UI-Depok 16424
Indonesia
Phone : +62-21-7270078, Fax: +62-21-7270077
Email : pupu@ee.ui.ac.id, juned_new@yahoo.com, witjaksono@ee.ui.ac.id

Abstract – **In modern information technology system it is used continued and uninterruptible power supply (in this case battery) for information technology system components, such as a mobile computer. The battery is a power storage which is produced from solar modules and used as power source for the mobile computer. In this paper we designed, simulated the solar power system by using Pspice Orcad Ver.9.1 and made it. The solar power system we made consists of photovoltaic module, a voltage regulator, short circuit protection, reverse polarity protection, and mobile computer as a load. Toshiba satellite Pro 6000 is chosen as mobile computer. The solar power system needs input voltage about 15V with input current 2A and able to charge internal battery 4400mAh of Toshiba satellite Pro6000 for 8 hours. To fulfill the load power and voltage requirement, system requires photovoltaic module which has the specification of minimum power equal to 40W or more. Added, electronic control circuit is used to supervise input minimum voltage system and control the connection between solar module and load. Overload is included in the system to protect system from short circuit current. And also indicator to give the user condition of system.**

Keywords- Solar power system modelling, linear regulator

I. INTRODUCTION

In modern information technology system it is used continued and uninterruptible power supply (in this case battery) for information technology system components, such as a mobile computer. Without the battery the mobile computer is not good function and less efficient so that it will cause useless and ineffective all information technology system. The battery is a power storage which is produced from solar modules and used as power source for the mobile computer. Recently, the price of world crude oil goes up drastically. It makes researchers compete to use conventional or renewable energy to cover energy requirement. Solar energy is one of the alternatives of renewable energy and has not been used fully yet. By using solar module, we can convert solar energy to electricity energy for area which has not been reached by transmission and electricity distribution network, like hinterland, desert, forest or remote areas. In information technology era, a lot of mobile computers like Palmtop, Notebook or Laptop have been used by people nowadays. Its power depends on electricity from wall plug and battery which lasts for 2 hours or more. So, in order mobile computer can have more runtime and improve its mobility. Solar power system for mobile computer is needed. Ideally, solar power system should have features like reverse current leakage protection to prevent current loss into solar modules at night, low-voltage load disconnect, system monitoring, overcurrent protection, system control, load control, temperature compensation, and MPPT (maximum power point tracking) using switching regulator[1]. There are still a little commercial solar power systems in solar cell market. Some of them are Sunwize Portable Energy System designed for mobile computer with output voltage about 18V [2,] Smart adaptor from LUNA II Apple Newton [3], and etc. Those commercial solar power systems are still expensive. So, in this paper we designed a solar power system that costs a little money, simple, portable, and has a high reliability. To help us in testing our design, an electronic simulator Pspice OrCad ver.9.1 is used.

II. SYSTEM DESIGN

In solar power system design, we should know the electrical characteristics of load that will be used. As explained earlier in abstract, we chose Toshiba Satellite Pro6000 which is used as load in solar power system. Actually, there is no detail electrical data about its computer from the manufacturer. The only electrical data we got are output voltage 15V and output current

4A from its AC power adapter. Therefore, we did some measurements in order to get more detailed the electrical data of mobile computer. In this case, we use AC power adapter from its manufacturer to operate the computer. As the results, we got input voltage of mobile computer measured below average of 15.2V. Besides that, input current is measured below average of 2A for mobile computer with internal battery and 1.5A without internal battery.

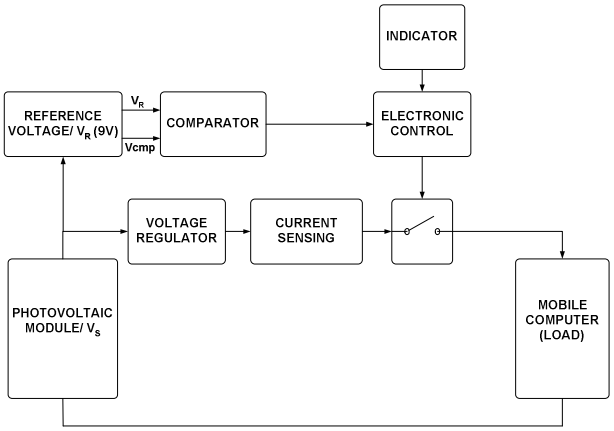

Fig 1. Diagram block system

From those measurement data, we conclude:

- Toshiba Satellite Pro6000 with internal battery requires:
  Input voltage = 15V
  Input current (min) = 2A
  Input current (max) = 4A
  Input power (min) = 30W
  Input power (max) = 60W
- Toshiba Satellite Pro6000 without internal battery requires:
  Input voltage = 15V
  Input current (min) = 1.5A
  Input current (max) = 4A
  Input power (min) = 22.5W
  Input power (max) = 60W.

After getting mobile computer specifications, we certainly design how the system works based on features mentioned in introduction. Some features that are considered in the system design are short circuit protection/over-current protection, monitoring system/ indicator, control system, voltage regulator using linear regulator, and low voltage load disconnect. To realize these features, we made a diagram block system to help us designing the system. As we can see in Fig.1, there are three main important things to design solar power system:

- Photovoltaic module
- Voltage regulator included reference voltage regulator
- Electronic control system included comparator, indicator, switching to control connection between electricity source (photovoltaic module) and load (mobile computer).

I.1. PHOTOVOLTAIC MODULE

As explained in section a, there are two condition measurement of electrical parameter data: mobile computer with internal battery and without internal battery. Mobile computer with internal battery requires more power. It happens because current flows to charge internal battery about 0.5A (depending condition of the internal battery) and operate computer itself. In order system can work well for both conditions with internal battery and without internal battery.

Table 1. Photovoltaic Mdule Specification

Electrical Characteristics*		
Module catalogue number		BP585
Open circuit voltage	V	22.30
Short circuit current	A	5.00
Voltage at maximum power	V	18.00
Current at maximum power	A	4.72
Nominal peak power	W	85
Thermal coefficient characteristics		
Coefficient of Voltage (V/°C)		-0.086
Coefficient of Current (A/°C)		+0.0025

So, we decided to use electrical parameter data of mobile computer with internal battery. To fulfill the requirement power that needed by computer, we chose photovoltaic module BP585-85W from BP Solar which has specification shown in Table 1[4]. BP585-85W was chosen because it was the only module that is available to be used for experiments. And moreover its specifications exceed the requirement power we need.

I.2. VOLTAGE REGULATOR

A lot of controller chargers for mobile computer in solar energy market are inverter or dc to ac converter. Inverter consumes a lot of power on step-up transformer and has complicated design. So, we chose voltage regulator to convert dc to dc. There are two ways dc to dc voltage regulator: linear regulator and switching regulator. The advantages of linear regulator are able to provide lower noise and higher bandwidth; their simplicity can sometimes offer a less expensive solution. Whereas, switching regulator has three main advantages compared to linear regulators: efficiency

better than linear regulator, smaller component, and energy stored by switchers can be transformed to any output voltages that can be greater than input, smaller than input, negative, etc. Anyway, switching regulator also has disadvantages: it can be noisy and require energy management in the form of a control loop [5]. We determine voltage regulator using linear regulator because its simplicity and linearity, easy to design, and get in electronic simulator. IC (integrated circuit) LM723 is one of linear regulator. We chose it as voltage regulator because it can handle input voltage up to 40V maximum, adjust output voltage from 2V to 37V, and limit current (overcurrent protection), its output current in excess of 10A possible by adding external transistors,[6]. For determining values of component in voltage regulator design using LM723 (with part reference U3), we used an equation [6]:

$$Vout = Vref\left(\frac{R_I + R_{18}}{R_{18}}\right) \quad (1)$$

Equation (1) is a formula to solve output voltage that we want. With R_{18}=10kΩ and V_{ref}=7.15V, we got R_I=11,2kΩ. In Fig.2, R_I=11,2kΩ represents combination of R_{15}, R_{16}, and R_{17}.

To achieve the output current 4A maximum, we add a pass transistor, 2N3055 which can handle continuous collector current up to 15A with heatsink required [7]. For reference voltage regulator, we use a zener diode 9.1V/ 1W with R_1= 390Ω to limit current.

I.3. CONTROL SYSTEM

One the most important part of diagram block system is control system. It has so many tasks: indicate the condition of system, control connection between voltage source and load, and detect the minimum input voltage requirement needed by voltage regulator. First of all, we analyze comparator part which detects the minimum input voltage requirement. The comparator is expected:

- If non inverting input voltage is bigger than reference voltage or inverting input voltage, output voltage will be the same positive input supply voltage of op-amp or 9.1V. It means the minimum input voltage requirement of voltage regulator fulfilled.
- If non inverting input voltage is smaller than reference voltage or inverting input voltage, output voltage will be the same negative input supply voltage of op-amp or 0V. It means the minimum input voltage requirement of voltage regulator not fulfilled. In order comparator can work well as explained before, we set low voltage load disconnect at V_{comp}=17.7V then:

$$V^+ = \frac{R_5}{R_4 + R_5} \times V_{comp(selsurya)} \quad (2)$$

With R_4=47kΩ, R_5=10kΩ, and V_{comp}=17.7V (see Fig.2), we got V^+=3.1V. So inverting input voltage should be set close to and more than 3.1V $\left(V^- > V^+\right)$. By varying value R_8, $\left(V^- > V^+\right)$ can be achieved (see Fig.2). Two two-input NAND Schmitt Trigger CD4093 (with part reference U2A and U2B) is added to enhance noise

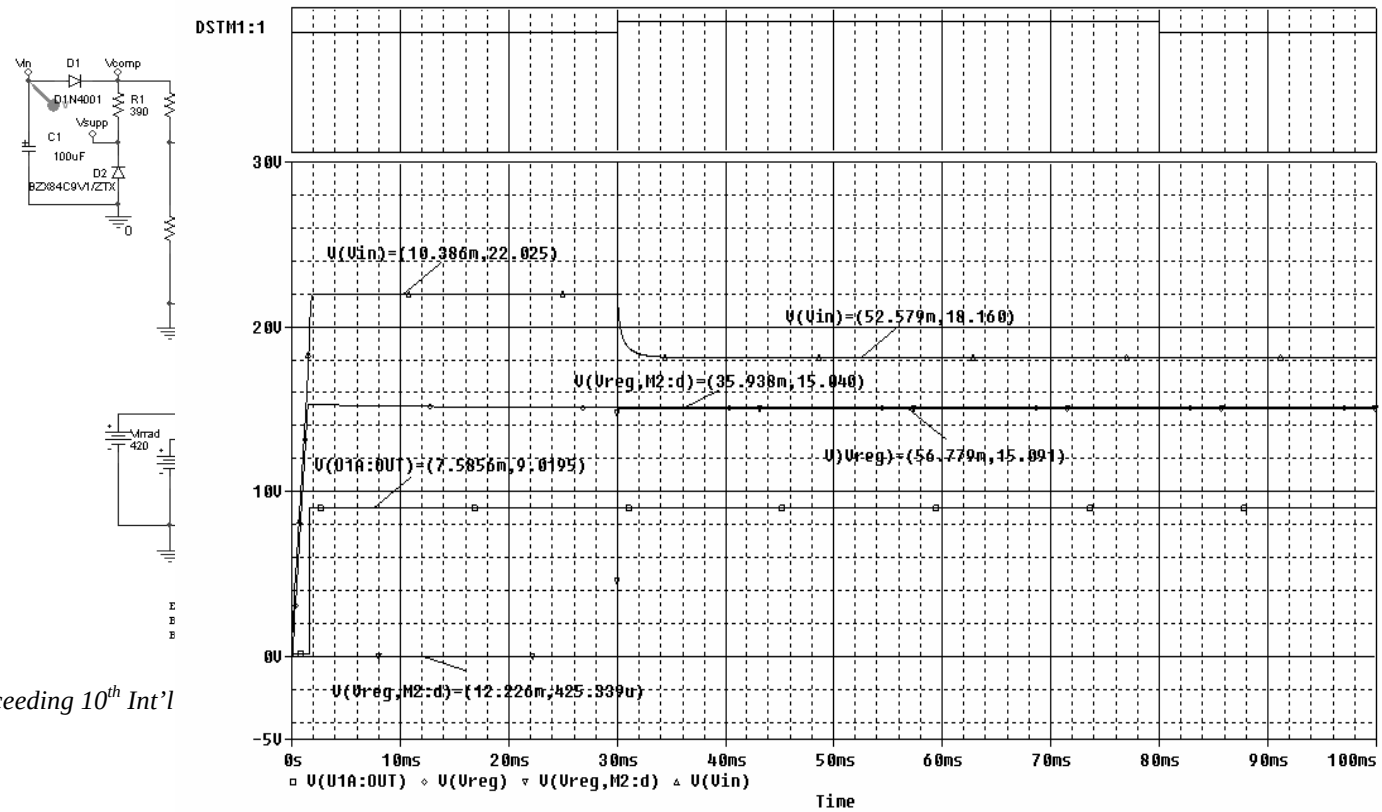

Fig 2. Solar Power system for mobile computer in Pspice simulation

immunity or square up the waveform of op-amp output voltage. Secondly, we analyze the connection control between voltage source and load. In this part, we chose D flip-flop CD4013 as latching component and MOS N-channel IRFZ44N as switching component which has R_{ds}=17.5mΩ [8]. For indicator in Fig.2, R_{13} represents green LED (light emitting diode) and R_{12} represents red LED because there is no LED component in Pspice Orcad Ver.9.1.

D flip- flop is used to latch the condition of system. It works:

- If input voltage pin "D" and "S" is 0V which means op- amp non inverting input voltage is bigger than inverting input voltage, D flip-flop output voltage (without a positive- going edge of the clock pulse) will be no change, indicator red LED will be on, green LED and mosfet will be off, and no current flows to load.
- If input voltage pin "D" and "S" is 0V which means op-amp non inverting input voltage is bigger than inverting input voltage, D flip-flop output voltage (with a positive-going edge of the clock pulse) will be 9.1V ($\overline{Q}$=1), indicator red LED will be off, green LED and mosfet will be on, and current flows to load.
- If input voltage pin "D" and "S" is 9.1V which means op- amp non inverting input voltage is smaller than inverting input voltage, D flip-flop output voltage (with or without a positive- going edge of the clock pulse) will be 0V ($\overline{Q}$=O), indicator red LED will be on, green LED and mosfet will be off, and no current flows to load.

All electronic components can be got in Pspice itself but photovoltaic module. So, we built a photovoltaic module library object using Pspice source code from modelling photovoltaic systems using Pspice book [9]. By using photovoltaic module library object, it made us easier to change electrical parameter data of photovoltaic module. All parameter data in Table 1 is used in simulation and irradiance value is set to 420W/m^2 (see Fig.2)

III. RESULTS AND DISCUSSION

As simulation results we can see output voltage of photovoltaic module going down rapidly from 22.025V (open circuit voltage) to 18.16V and staying at 18.16V because current flows to load (see Fig.3). Output voltage of regulator is about 15.091V. Input voltage of U2B two-input NAND Schmitt trigger is about 9.0195V which means op-amp non inverting input voltage is bigger than reference voltage or inverting input voltage and fulfilled minimum input voltage requirement for regulator .

Then output voltage of D flip-flop ($\overline{Q}$) toggles (with a positive- going edge of the clock pulse (see Fig.3) from $\overline{Q}$=0 to $\overline{Q}$=1 which means mosfet and green LED are on and current flows to load. Output load voltage between $V_{(Vreg)}$ node and $V_{(M2:\ d)}$ node is about 15.040V. In simulation, the solar power system can distribute electricity to mobile computer with minimum irradiance about 420W/m^2.

After doing simulation, we also realized the solar power system design into PCB (*printed circuit board*) as shown in Fig 4. Then we did some experiments at B2TE (*Balai Besar Teknologi Energi*)/Energy Technology center

Fig 4. Solar Power System with laptop Toshiba satellite Pro 6000

Fig 3. Pspice simulation results

Tangerang, Indonesia. As the results, we got that internal battery of mobile computer could be charged from 70% to 78% (computer was not operated) for 60 minutes and 71% to 73% (computer was operated) for 79 minutes. And with minimum irradiance about 395.833W/m^2, solar power system could power up the mobile computer. The performance of solar power system was affected by many factors such as variation changes of solar irradiance, moisture, temperature, velocity of wind, etc. Those factors made internal battery slowly charged up to 100%.

Ideally, photovoltaic modules used in solar power system should be small, foldable, portable, high reliability, and fulfilled the need power requirement. The minimum power is needed by mobile computer about 30W. So, photovoltaic module BP585- 85W, which is used, wasted much energy at solar irradiance of 1000W/m^2. Besides that, photovoltaic module BP585-85W is big and difficult to bring along with mobile computer. However, this module which produces a lot of energy could make the mobile computer operated at lower minimum solar irradiance.

Linear regulator of solar power system consumed a lot of energy and needed input voltage higher than output voltage. In the future design, solar power system will be regulated by switching regulator. Switching regulator offers many advantages like simpler design and consumed less energy.

IV. CONCLUSIONS

In summary, solar power system for mobile computer can be designed by using linear regulator. But it needs a high input voltage requirement (about 17.7V) than output voltage. And for this reason, we need photovoltaic module which has open circuit voltage more than 17.7V like BP585-85W. The minimum irradiance in simulations is 420W/m^2 while minimum irradiance in experiments is 395.833 W/m^2. It means that only a little error between simulations and experiments. In experiments, internal battery of mobile could be charged from 70% to 78% (computer was not operated) for 60 minutes and 71% to 73% (computer was operated) for 79 minutes. With this solar power system, mobile computer can be protected by variation changes of photovoltaic module output voltage and short circuit current. Pspice simulations have output value almost close to what we design.

REFERENCES

[1] P&R Technologies,"Controller", www.pr-tech.com
[2] Sunwize, "Sunwize Portable Energy System", www.sunwize.com
[3] Solar Energy Alliance, "laptop solar systems, SOLAR POWER
for your laptop, now the office can be the beach or the park",

http://www.gosolar.unet.com/Portable_solar_power_systems.htm
[4] BP Solar, "BP585- 85W", www.bpsolar.com
[5] Dallas semiconductor, "DC to DC converter Tutorial", http://pdfserv.maxim-ic.com/en/an/AN2031.pdf
[6] National Semiconductor Corporation, "LM723 Voltage Regulator"
[7] Motorola Inc., "NPN 2n3055"
[8] International Rectifier, "IRFZ44N"
[9] Luis Castaner and Santiago Silvestre, "Modelling photovoltaic systems using Pspice", John Wiley & Sons, LTD, ch.4, pp. 92-93.

ISSN: 1411-1284

Study on Robotic Motion Control with Microcontroller H8-3052

Abdul Muis

Electrical Engineering Dept., Faculty of Engineering, University of Indonesia
Kampus Baru UI Depok, 16424
Telp: 021-7270077, Fax: 021-7270078
Email : muis@ee.ui.ac.id

Abstract– **Obviously, microcontroller has power limitation compared with personal computer. Nevertheless, more control components are available within a small package in microcontroller. Nowadays, more small digital electronics known as embedded systems made based on microcontroller plus a small number of additional components such as in modern cars, video recorder, etc. Undoubtedly, controlling robot-motion through recent general purpose computer with additional external components provides more realistic performance with instant computation. Here, more real-time control computation and performance are realized, especially with high precision control components. On the other hand, computation performance on microcontroller is limited to the clock speed. Within this boundary, the high precision component is not necessary as it has no significant result for low speed computation. However, there are some constraints to be fulfilled for controlling robot motion in real-time. Here, this paper discusses necessary conditions to control robot motion from control unit perspective. A microcontroller H8-3052 is preferred as it has sufficient port devices compared to other microcontroller in the same class. At the end, this paper discuss the reliability of this microcontroller for robot motion control.**

Keywords– robotics, motion control, microcontroller, H8-3052

I. INTRODUCTION

Motion control mainly a sub-field of automation, in which the position and/or velocity of machines are controlled using some type of device such as linear actuator, or an electric motor. In addition, motion control is an important part of robotics and CNC machines tools. There are typically three uses for motion control; positioning, speed control, torque control. Here, robots are the most expensive form of motion control.

Robots are typically multi-axes actuator with one main controller that coordinates all of the axes. The robot controller also simplifies the programming by providing most of the calculation transparently. Determining the position of each axis takes a considerable amount of calculations. However, robots are the most flexible while perform the most complex control.

Controlling robot motion refer to controlling actuators of the robot so that the robot parts or the body move within desired motion. Here, the actuators are the plant of the robot. An open loop either closed loop control system may be applied. However for open loop control, the plant should be well calibrated such as step motor. Nevertheless, most precise system model and the effect of external disturbance are not known. Here, measuring the output through sensor and then comparing with the desired one known as closed-loop or feedback system are crucial. It has greater accuracy than open loop systems and less sensitive to disturbances and changes in the environment. In addition, the time response and the steady-state error can be controlled [2].

With the advent of the digital computer and low-cost microcontroller processing elements, control engineers began to use these programmable devices in control systems. A digital computer or a microcontroller can keep track of the various signals in a system and can make intelligent decisions about the implementation of a control strategy. However, most plants are analog while digital computer or microcontroller are digital. Thus, there should be analog-to-digital (A/D) and digital-to-analog (D/A) converter so that both may work together.

Nowadays, A general purpose computer has become cheaper and the computation power doubled in every two years. On the other hand, the speed of microcontroller has no such enhancement. Thus, a general purpose computer realizes more realistic performance with instant computation compared with microcontroller. However, one need to attach input/output device cards on general purpose computer. Nowadays, there are many microcontrollers that incorporate built-in A/D and D/A converter circuits and input/output ports. These microcontrollers can be connected directly to analog signals, and to the plant. Hence, microcontroller is more portable so that widely used as embedded system. Nevertheless, the microcontroller speed is too low compared with recent general purpose computer. Thus, we need to clarify how appropriate the microcontroller is for digital control especially for controlling robot motion.

For that purpose, in the following chapter this paper discusses the general requirement to be fulfilled to apply microcontroller for robot motion control. A microcontroller h8-3052 is considered in this paper as it has sufficient input/output devices compared with other

microcontroller in the same class. Chapter III discusses more briefly about this microcontroller. Chapter IV discuss H8-3052 implementation on robot motion control. At the end, the reliability of this microcontroller for robot motion control is summarized in Chapter IV.

II. MICROCONTROLLER CONSTRAINTS

In general, although almost any digital computer can be used for digital control there are some requirements that should be satisfied before a computer is used for such an application. Today, the majority of small and medium scale *Direct Digital Control* (DDC) –type applications are based on microcontrollers which are used as embedded controllers. Depend on digital control applications, choosing the appropriate microcontroller are limited to ;

- Central Processing Unit
  - Speed
  - Architecture
- Memory
  - Size
  - Bits wide of address bus, data bus
- Built-in circuits/function (how much and how precise)
  - D/A and A/D converter
  - I/O ports
  - Counter
  - Built-in timer
  - PWM
  - Interrupt logic
- Programming language
  - Assembly language
  - High level language

Dealing with robot motion control, one need to consider software techniques such as Polling where we keep waiting until a certain event occurs, and only then perform the required actions. This way, we wait for the next sampling time to occur and only then run the controller algorithm. This technique is crucial for robot motion control as hard real-time application. Each controller algorithm should be done at every sampling instant. The other precise technique is using timer interrupt from internal clock either external clock. Here the controller algorithm is written inside the timer interrupt service routine, and the timer is programmed to generate interrupt at regular intervals, equal to the sampling time. At the end of the algorithm control returns to the main program, which either waits for the occurrence of the next interrupt or perform other tasks (e.g. displaying data on an LCD) until the next interrupt occurs. The timer interrupt approach provides accurate control of the sampling time.

Generally, the microcontroller is used as controller for sampled data system operates on discrete-time. Here, all the signals enter and leave the microcontroller at the same fixed time, known as the sampling times. A typical sampled data control system is shown in Figure 1.

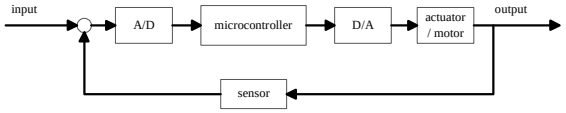

Figure 1. Sampled data control system

Digital control system are obviously real time in the sense that the controller output is to be generated as soon as possible after the input is available. In many applications multiple digital control tasks must be managed within an interrupt environment. Real-time control system must not only be reliable, but must also have fault recovery mechanisms and the ability to restart. This generally required physical redundancy for system reliability and maintainability. Most recent microcontroller has watchdog timer for that purpose.

III. OVERVIEW of H8-3052

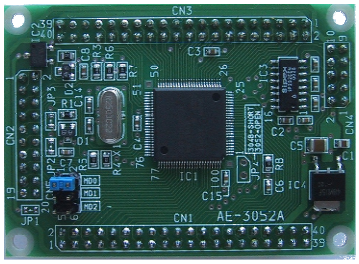

Figure 2. Microcontroller H8-3052 (5x7cm)

The H8-3052F is a series of microcontrollers (MCUs) with an H8/300H CPU core having an original Hitachi architecture. The minimum board with 5x7cm size, comes with internal voltage regulator as shown in Figure 2. It has a 32-bit internal architecture with sixteen 16bit general register. The on-chip system supporting function include 512kbytes ROM and 8kbytes of RAM. Nevertheless, it can address a 16-M linear address space. In addition, the on-chip system include 5 channel 16-bit integrated timer unit (ITU), 4 channel programmable timing pattern controller (TPC), a watchdog timer (WDT), two serial communication interface (SCI), 8 channel 10-bit A/D converter, 2 channel 8-bit D/A converter, 78 I/O ports, a direct memory access controller, refresh controller and other facilities.

The CPU comes with 25MHz maximum clock rate with 80ns, 560ns for add/subtract and multiply/divide operations respectively. In addition, the instruction support 8/16/32-bit data transfer, arithmetic, and logic instructions. In other words, this microcontroller is sufficient to support simple PD feedback control system with sampling time less than 5ms.

In order to realize hard real-time control system for robot motion, one needs to use timer interrupt. This microcontroller provides up to 5 channel 16-bit timer units. In addition, the operation of each channel can be done independently or synchronized. Also, PWM mode is available. Based on this integrated timer unit (ITU), 4 channel output programmable timing pattern controller (TPC) are available. Moreover, seven external interrupt pins and 30 internal interrupts are available. Least but not last, this microcontroller has watchdog timer with reset signal generated by overflow.

Having two channel serial communication interface (SCI), this microcontroller provide communication between microcontrollers or between microcontroller and PC. Moreover, a top-down distributed control system can be applied with this feature.

As most sensors in robotic applications comes with analog signal, 8 channel A/D input provided in this microcontroller is sufficient to feedback 8 environment conditions. In addition, 2 channel D/A available output is sufficient to drive two actuators. Common robot control especially the small one, requires at least one digital signal generated by PWM to drive the servo motor through H-bridge circuit. While the output position of the actuator can be sensed by incremental encoder or potentiometer. The incremental encoder with high number pulse per rotation is more precise than potentiometer. In addition, this optical encoder has more lifetime than potentiometer. The output of incremental encoder can be read through up to 5 channels ITU.

IV. ROBOT MOTION CONTROL WITH H8-3052

As discussed in preceding section, H8-3052 may be applied to robot motion control. As an extension of feedback control system as described in Figure 1, the realization with h8-3052 would be a combination of control structure as shown in Figure 3. For RC servo motor, the PWM output may directly applied, while for general DC servo motor, one need to add H-bridge circuit. The position of the output of the actuator may be sensed by potentiometer or incremental optical encoder. As for potentiometer, the microcontroller may read the signal through A/D input, while for incremental encoder through ITU counter.

As for the software, the control algorithm is executed through interrupt service routine to realize real-time performance with fixed sampling time.

IV. CONCLUSIONS

To realize robot motion control, one need to perform real-time control with garanted fixed sampling time. This

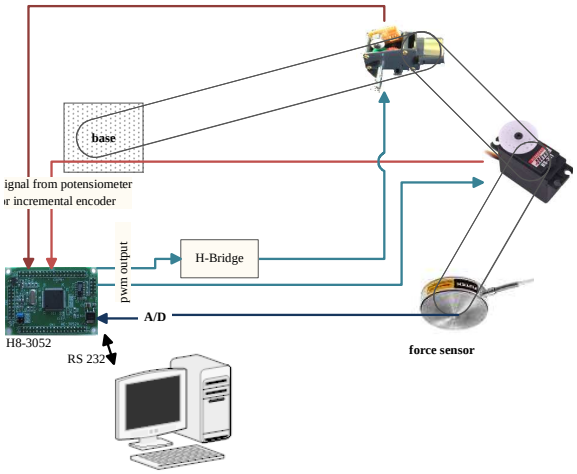

Figure 3. Robot motion control with h8-3052

can be realized through timer interrupt either from internal clock or from external clock. In addition to interact with the plant or the environment, the microcontroller should have interface to deal with such as A/D, D/A converter and I/O port. Moreover, most actuator are driven with PWM signal that should be provided by microcontroller. These requirements are satisfied in H8-3052. Thus in summary, this microcontroller has features needed to realize robot motion control in real-time.

REFERENCES

[1] A. Mahabuba, S. Balavishwakumar, S. Bharath, E. Arthi, and D. Brinda, “Microcontroller based Computer Control of Robot Arm for Sorting of Objects”, Proc. of Robotics and Applications (RA 2004), USA, 2004.

[2] Dogan Ibrahim, “Microcontroller based Applied Digital Control”, John Wiley & Sons, 2006.

[3] Houpis, C.H, and Lamont G.B., “Digital Control Systems: Theory, Hardware, Software”, 2nd edition McGraw-Hills, Inc, 1992.

[4] Hitachi Single-Chip Microcomputer H8/3052F-ZTAT hardware manual., 2001.

ISSN: 1411-1284

Design Fused Fiber Couplers 980 nm - 1550 nm For EDFA Pumping Schemes

Suci Rahmatia [1)] Ary Syahriar [1,2)]

[1)] Electrical Engineering Department, University al Azhar Indonesia
[2)] Center of Information Technology and Communication, Agency for the Assessment and Application of Technology of the Republic of Indonesia
Email : suci@uai.ac.id, ary@uai.ac.id

Abstract - **Erbium Doped Fiber Amplifier (EDFA) provides an attractive approach for implementation status and control communication in communication networks. The desired control signal is imposed as an amplitude over modulation on the payload communication signals propagating down the systems, via modulation of the EDFA pump power. To support such systems one important passive component based on fused couplers is needed as a wavelength division multiplexing devices.**

This paper explains the design of wavelength division multiplexing fused couplers in the wavelength range of 980 nm - 1550 nm. The couple mode theory has been used to design such couplers, where the coupled equations are solved numerically by using Runge-Kutta numerical scheme. To get exactly 980 nm-1550 nm splitting wavelength the coupling coefficient has been alter to desire the characteristics. Further effect can be achieve through the change of the taper region size.

Keyword: optical communications, fiber optics, coupled mode theory, fused fiber optics

I. INTRODUCTION

With the demand for longer transmission lengths, optical amplifiers have become an essential component in long-haul fiber optic systems. Semiconductor optical amplifiers (SOA), erbium doped fiber amplifiers (EDFA), and Raman optical amplifiers lessen the effects of dispersion and attenuation allowing improved performance of long-haul optical systems.

EDFA is a device that boosts the signal in an optical fiber. Introduced in the late 1980s, the EDFA was the first successful optical amplifier. It was a major factor in the rapid development of fiber-optic networks in the 1990s, because it extended the distance between costly regenerators. In addition, an EDFA amplifies all the channels in a WDM signal simultaneously, whereas regenerators require optical to electrical conversion for each channel.

The explosion of wavelength division multiplexing (WDM) applications make these optical amplifiers an essential fiber optic system building block. EDFA allow information to be transmitted over longer distances without the need for conventional repeaters. The fiber is doped with erbium, a rare earth element, that has the appropriate energy levels in their atomic structures for amplifying light. EDFA are designed to amplify light at 1550 nm. The device utilizes a 980 nm or 1480 nm pump laser to inject energy into the doped fiber. When a weak signal at 1310 nm or 1550 nm enters the fiber, the light stimulates the rare earth atoms to release their stored energy as additional 1550 nm or 1310 nm light. This process continues as the signal passes down the fiber, growing stronger and stronger as it goes.

From figure 1. We can see that EDFA boost the input regardless of the number of wavelengths. In several meters of doped fiber, the pump laser excites the doped atoms to higher orbits, and the input signal stimulates them to release excess energy as photons in phase and at the same wavelength (Illustration courtesy of Jeff Hecht).

Single mode fiber couplers is important component in WDM and the application of censor covering optical power splitting, optical filtering, optical reflecting, wavelength multiplexing/demultiplexing, and optical polarisation splitting [1], [2]. Public principle constituting fiber couplers was if delivery of light between two nearby fibre cores passed mechanism of waving evanescent coupling done at correct condition. That is when light launched at one of wave guide hence in driblets of dislocation stress field evanescent [3] is residing in cladding will move to other wave guide core, so that there will be displacement of power from wave guide one to other wave guide, and this takes place periodical. To get output division of power matching with requirement, the way wave parallelly at both wave guides must be stopped at certain point.

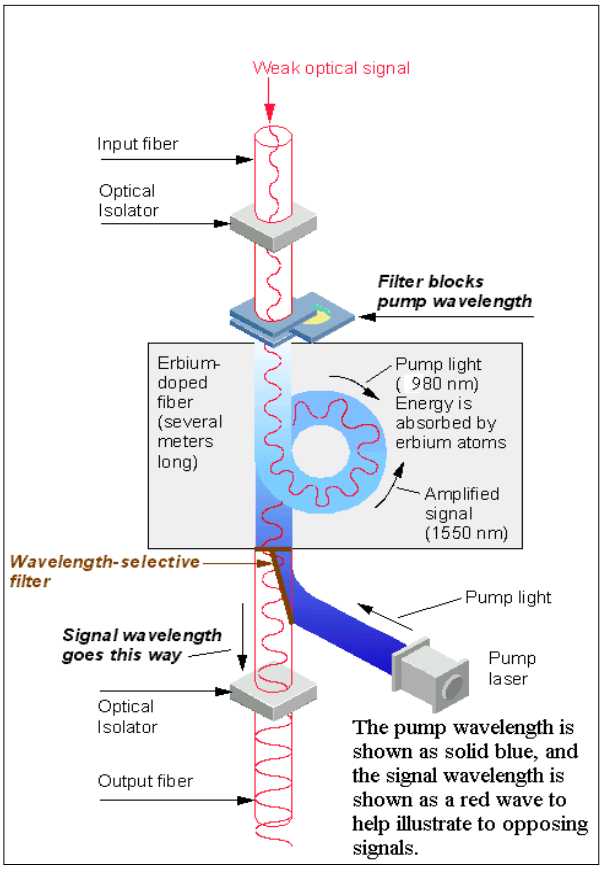

Figure 1. Erbium Doped Fiber Amplifier [4]

Optical fibre couplers is made with technology fusing and tapering two fibers which the application of his has many applied by components in optical fibre. At fused fiber couplers, form of taper is one of most importantly so that research to look for form of ideal taper always is done. Taper is formed by heating partly small fibers causing forms structures biconical [5]. This thing done to lessen loss power mode in core. At taper is in the form of this biconical, mode core move into mode cladding in district taper. This displacement causes loss power which will increase according to big of angle of taper. But, loss earns remain to be small if angle of taper is small.

Figure 2. explain about the structures fused fiber coupler for wavelength division. This component analysis generally applies the couple mode theory [6]. Principal thing which will be searched is coupling coefficient value determining how far aparted power can make a move entirely, then parameter characteristic of displacement power between wave guides will be found to look for at distance how much the wave guide has division of power matching with the one which we wish.

After the characteristic parameter value is gotten, hence component designer WDM FFC would easy to be done. This designer will be done by one wavelength range, that is 980 nm – 1550 nm productively certain propagasi distance.

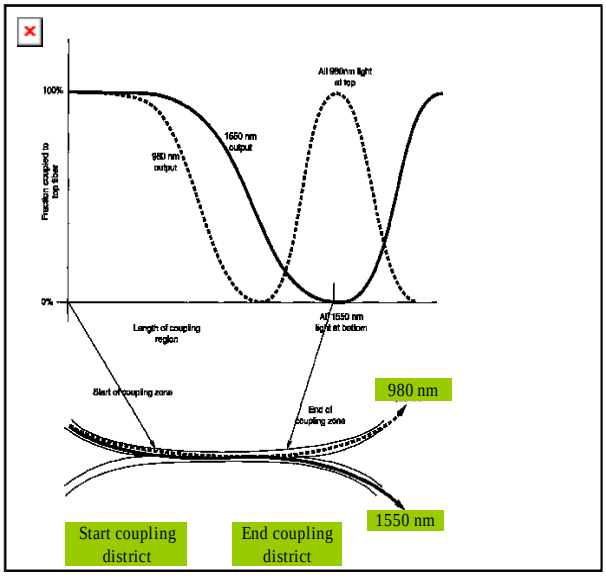

Figure 2. Fused fiber coupler structures for wavelength division

II. COUPLE MODE EQUATIONS

The Coupled Mode Equations [7] explains transformation of wave amplitude flow in each wave guide. From figure 3, we see that the directional couplers consist of two waveguides that closed each other with the distance *d*, direction length propagation *z* and length of coupling *L*. The exchange of power will happen periodicly as long as direct propagation.

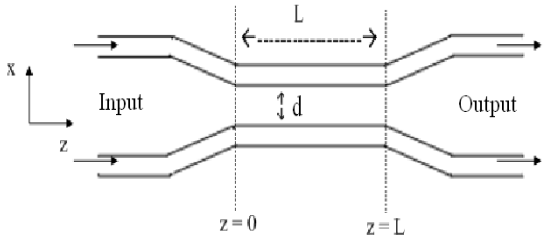

Figure 3. Directional Couplers Structures

The couple mode equations for directional couplers are described as follows :

$$\frac{\partial A_1}{\partial z} + j\kappa A_2 e^{(-j\Delta\beta z)} = 0 \qquad (1)$$

$$\frac{\partial A_2}{\partial z} + j\kappa A_1 e^{(+j\Delta\beta z)} = 0 \qquad (2)$$

Equation of continuity (1) and (2) called as couple mode equation with κ is coupling coefficient which is important parameter in coupler. The equation of continuity is as follows,

$$\kappa = (\frac{k_0^2}{2\beta_0})\left\langle (n_T^2 - n_2^2)E_2, E_1 \right\rangle / \left\langle E_1, E_1 \right\rangle \qquad (3)$$

So solution of equation output power from each wave guide becomes [8],

$$P_1 = A_1 \cos^2(\kappa z) \qquad (4)$$

$$P_2 = A_2 \sin^2(\kappa z) \qquad (5)$$

At this case, coupling coefficient has been assumed symmetry to coupling district. Reachable 3-dB value when $\kappa z = \pi/4$, temporary for delivery of complete power $\kappa z = \pi/2$ is required.

Coupling coefficient is important parameter at coupler because determining how far aparted wave guide can be coupling finely. Wave guide distance is arranged in such a manner to assess coupling coefficient is not too big or undersize so that displacement of dislocation stress field evanescent will take place maximumly and loss signal would smaller even uncared.

III. SIMULATION

In designing and analyses characteristic WDM fused couplers is required some parameters that is each other supports, there are core radius (*r*), refraction index of core (n_1) and refraction index of cladding (n_2), wavelength (λ), coupling length (*L*), direction length propagation (*z*), fibre core breadth (*h*) and space two fibre cores (*d*). This design will be done by 980 nm - 1550 nm productively certain propagasi distance. Value of *r*= 4 μm, *d* = 20 μm, *L* = 7 mm, *z*= 12 mm – 20 mm, n_1 = 1.463 – 1.465, n_2 = 1.458, dan *h* = 5. Tolerance stretch applied at refraction index of core and cladding that is Δn = 0.005 – 0.007. This thing aim in order to the value can measure up to single mode fibers. This property applied to analyse wave guide parameters that is in the end applied to design component WDM FFC. Calculation to determine optical fibre haves the character of single mode based on assumption V - number or called as frequency normalization to be valuable less than 2.405 at wave guide.

$$V = \frac{2\pi}{\lambda} n_1 r \sqrt{2\Delta} \qquad (6)$$

$$V \le 2.405 \qquad (7)$$

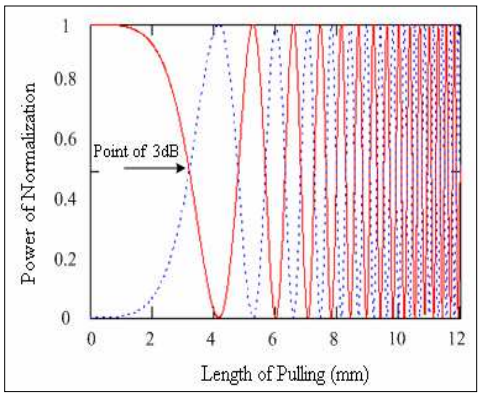

Figure 4. Power exchange in *fused fiber coupler* during fusing and tapering

As a whole designs graph at Figure 4 till Figure 6. is solution of equation of continuity (4) and (5) what depicts phase difference at second dislocation stress field amplitude of wave guide equal to 90°. Guided wave phase that is second wave guide always lag 90° to phase waving guiding that is first wave guide. The relation of second phase of this wave guide influenced by direction propagation taking place *z* continually so certain distance reachs value $\kappa z = \pi/2$. In that situation, all powers flown from first wave guide towards second wave guide. Then state returned, preceding second wave guide is finite first wave guide at distance $\kappa z = \pi$, and so further.

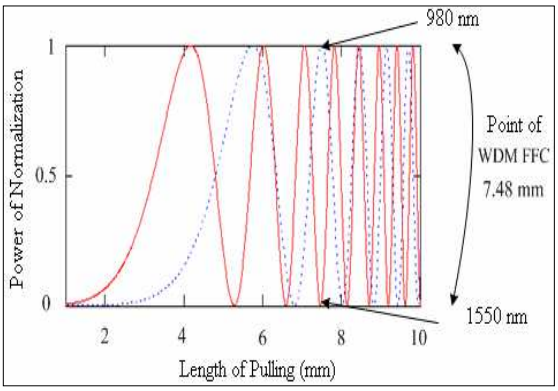

Figure 5. Wavelength 1310 nm-1550 nm as a function of pulling length

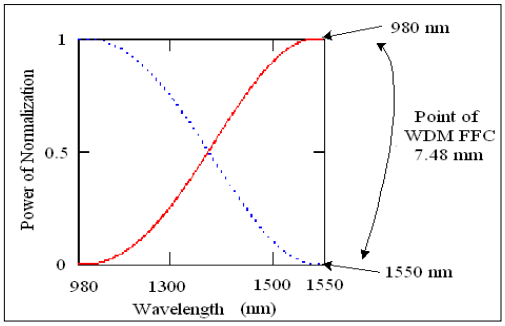

Figure 6. Wavelength responses to point of WDM FFC 7.48 mm
at power normalization

Figure 5. is combination two wavelength range 980 nm – 1550 nm yielding one point of direction value propagasi is residing in at two power tops is normalization. And figure 6. is wavelength responses to point of WDM FFC 7.48 mm at power normalization.

IV. CONCLUSION

The key to design fused couplers for the application of wavelength division multiplexing lays in election of wave guide are characteristic parameter and governing of coupling coefficient. All this thing did in order to be obtained the characteristic WDM at certain wavelength stretch. Till now WDM FFC still hardly is required one of for the application of EDFA.

REFERENCES

1. H. Zanger and Cynthia Zanger, *"Fiber Optics Communication and Other Applications,"* Macmillan Publishing Company, New York, 1991.
2. D. L. Lee, *"Electromagnetic Principles of Iintegrated Optics,"* John Wiley & Sons, New York, 1986.
3. J.R. Dutton, "Understanding optical communications", IBM Corp, New York, 1998.
4. http://content.answers.com/main/content/img/CDE/_EDFA.GIF
5. Bukhari. *"Simulasi Komponen Multi/Demultiplekser untuk Sistem Telekomunikasi Optik,"* Universitas Indonesia, Depok, 2002.
6. R. Syms, J. Cozens, "Optical guided waves and devices", McGraw Hill, London 1992J.
7. J. Dewynne, J. R. Ockendon, and P. Wilmott, *"On a Mathematical Model for Fiber Tapering,"* SIAM J. Appl. Mathematics, vol. 49, pp. 983-990, 1989.
8. A. K. Ghatak and K. Thyagarajan, *"Optical Electronics,"* Cambridge University Press, New Delhi, 1989

ISSN: 1411-1284

Fabrication of Wavelength Independence Fused Fiber Couplers Using Asymmetric Fiber Optics

Ary Syahriar

[1)] Center of Information Technology and Communication,
Agency for the Assessment and Application of Technology of the Republic of Indonesia
[2)] Electrical Engineering Department, University Al-Azhar Indonesia
ary@inn.bppt.go.id, ary@uai.ac.id

Abstract– We have fabricated low loss, high coupling ratio optical couplers for infrared light using single mode step-index fiber. Fusion technique similar to that commonly used with silica fibers have been employed. We have fabricated 3-dB wavelength independence coupler (WIC) with a wavelength range of 1310 nm-1550 nm. The first fiber has to be pre-pulled to reduce the fiber optics radius. This is done to achieve proper coupling ratio for broad range of wavelength.

Keywords– optical communication, optical fibers, optical fiber couplers, optical fiber devices.

I. INTRODUCTION

The widespread use of fiber couplers or splitters in a variety of optical fiber optic systems has become quite commonplace. Major market segments include telecommunications and cable TV, instrumentation and sensors. Of these, telecommunication sector has the largest market share today and still has the greatest potential for growth. It is also the toughest requirements for long-term reliability, with expected lifetime of twenty to forty years in an outside plant environment [1].

Over the past twenty years, the fused fiber coupler has provided the greatest number and variety of couplers into these market segments. The basic process, which basically consists of twisting and fusing two adjacent fiber optics by heating and pulling them until appropriate of power transfer is achieved, is very stable with low excess loss. However, the critical long-term reliability is not only depending on the basic process itself but also on the packaging process [2].
This paper explains the fabrication of single mode Wavelength independence coupler using fusing methods.

II. COUPLER DESCRIPTION

In most coupler under appropriate conditions light transfer can occur between the two adjacent fiber cores via a mechanism called evanescent wave coupling. When the two cores are put closely together the evanescent field travelling from the throughput fiber reaches the coupled fiber and excite mode in the coupled fiber. Figure 1 shows schematic diagram of fused fiber couplers.

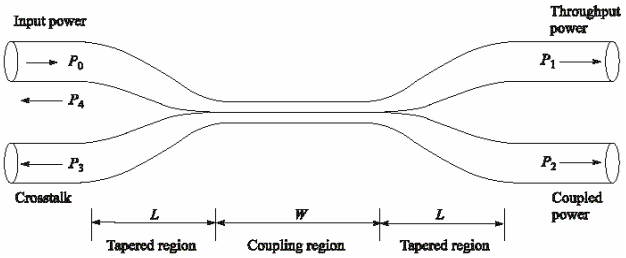

Figure 1. Schematic diagram of fused fiber couplers

When a mode in one fiber has the same propagation constant as that in the other, total power transfer may take place after some interaction length. If this mechanism continues beyond the first total power transfer length, the roles of the two fibers are reversed and the signal is coupled back into the throughput fiber until the entire signal is transferred after one coupling length. If the coupling length is even longer, the process repeats itself in a cyclical manner.

The coupled mode theory governs power exchange between the two fibers can be written as [4]-[6]:

$$\frac{dA}{dz} = -jMA \qquad (1)$$

Here, $A = \{A_1, A_2\}^T$ is a vector representing the amplitude of the two guided modes, M is 2x2 matrix with elements $m_{11} = m_{22} = \Delta\beta$, $m_{12} = m_{21} = \kappa$. Here, $\Delta\beta$ is the propagation constant mismatch and κ is the coupling coefficient, which is usually defined as [4]:

$$\kappa = \frac{\omega\varepsilon_0}{8}\iint \psi^* \Delta n^2 \psi \; dxdy \qquad (2)$$

where ψ^* and ψ are the two modes of the fibers, ω and ε have their usual definition. For fiber couplers the coupling coefficient κ can be derived using Equation (2) and the result is given by [4]:

$$\kappa = \frac{\lambda}{2\pi n_1}\frac{U^2}{a^2V^2}\frac{K_o(\frac{Wd}{a})}{K_1^2(W)} \quad (3)$$

here d is the separation between the fiber axes. K_o and K_1 are modified Bessel functions. The core and cladding parameters U and W are given by [5]:

$$U = k_o a\sqrt{n_1^2 - n_{eff}^2} \quad (4)$$

$$W = \sqrt{V^2 - U^2} \quad (5)$$

where $n_{eff} = \frac{\beta}{k_o}$ is the mode effective index.

III. EXPERIMENTAL SETUP AND RESULTS

Figure 2. shows the experimental set-up used to fabricate the couplers.

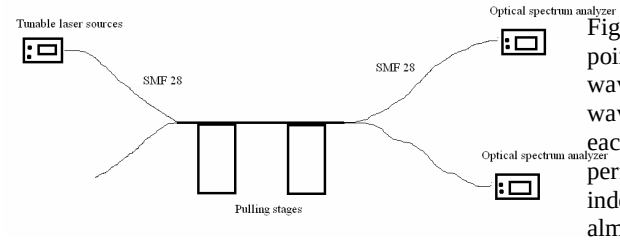

Figure 2. Experimental stage used in the experiments

To fuse two standard fibers, the protective jacket on each fiber has to be removed over a certain length without damaging the fiber itself. There are several methods that may be used, such as chemically removing the jacket or mechanically stripping the jacket by using a fiber stripper. The rule to make a good coupler is that the fiber must be perfectly clean before fusion. Debris of any kind between the fibers will prevent the fiber-to-fiber contact. Therefore an acetone solvent has been used to clean the fiber after it is stripped.

The hydrogen torch was applied to heat the two fibers; at the same time the two movable supports were pulling the two fiber ends. During tapering, laser with wavelength of 1310 nm and 1550 nm were launched into the input fiber to monitor the coupling online. The coupling ratio could be adjusted to the proper value by stopping the pulling length at the suitable moment. For the best result the fibers should be of matched cladding; a twist in a taper region is preferable. After fusion, the coupler are put in a lower refractive index material which, when set, protects the fused region [7]. In the case of producing wavelength independence couplers the first fiber need to be pre taper for
To produce a WIC the first fiber needed to be

Figure 3 shows power exchanges of two dissimilar fiber optics as a function of pulling length. The coupled power shows an oscillation during elongation. Total power transfer cannot be achieved between the two fibers this is because of a different in propagation constant on each fiber.

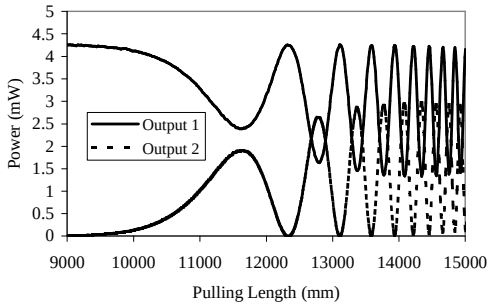

Figure 3. Power exchange as a function of elongation for dissimilar fiber optics.

Figure 4 shows an elongation that was stopped at 3 dB points, however the coupling ratio of second wavelength is not similar to those of the first wavelength. The glitch shows that power splitting on each wavelength is not similar. Figure 5. shows a perfect prepull and coupling ratio for wavelength independence couplers. The two wavelength give almost similar coupling ratio after similar elongation procedure.

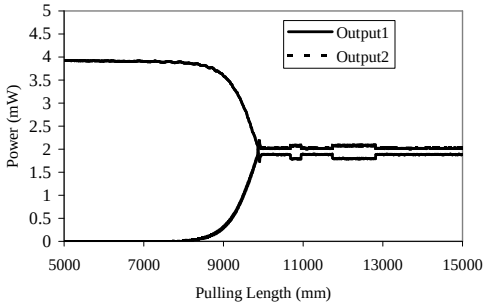

Figure 4. 3 dB power exchange but with a different coupling ratio of the couplers.

Figure 5 shows a perfect coupling ratio on both wavelength. This characteristic is expected to get better performances for WIC coupler.

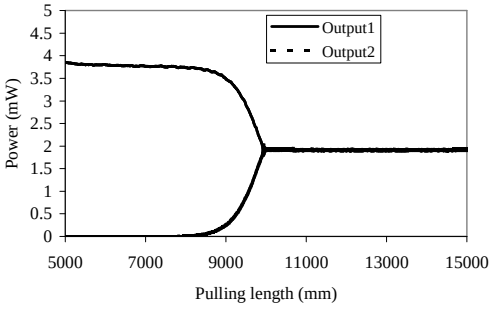

Figure 5. 3 dB power exchange with equal coupling ratio of the couplers.

To get a better understanding of fabricated WIC fused fiber couplers, it is then characterized using white light sources and scan along the wavelength of 1100 nm up to 1700 nm. It is found that WIC shows its perfect characteristics as expected. The coupling ration along such wavelength has not changed as shown in Figure 6. and Figure 7.

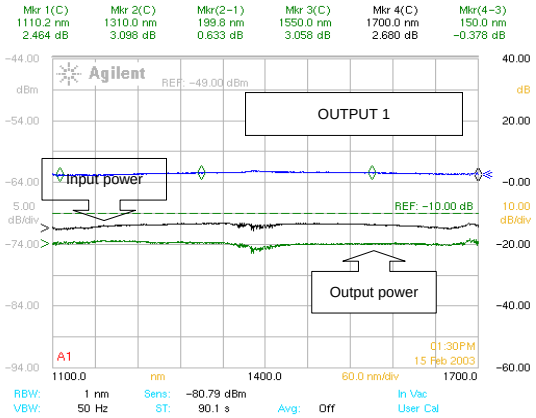

Figure 6. Output power at arm 1

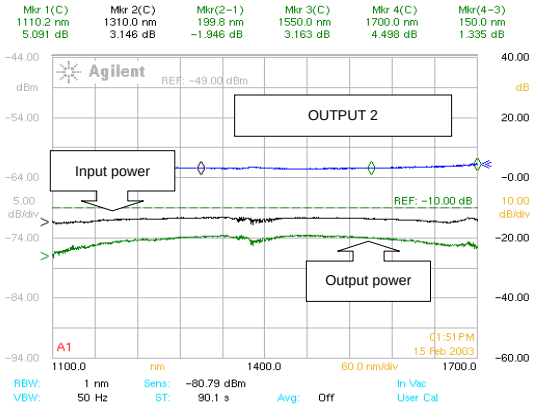

Figure 7. Output power at arm 2

IV. CONCLUSIONS

We have fabricated the WIC fused fiber couplers using asymmetric fiber optics. The results shows that the coupler has broad band characteristics with a very low loss and perfect coupling ratio. Further treatments are still needed to encapsulate the fused couplers using metal cap and glue so that it can become commercially ready to sell products.

REFERENCES

1. R. Ramaswami, "Optical fiber communication: from transmission to network", IEEE. Commun. Mag., 50th Anniversary comm. Issue, 138-147, 2002.
2. M.J. Yadlowsky, E.M. Deliso, V.L. Da Silva, "Optical fibers and amplifiers for WDM systems", Proc. IEEE, vol. 85, 1765-1779, 1997.
3. H.M. Presby, C.A. Edwards, "Packaging of glass waveguide silicon devices", Opt. Engng., vol 31, 141-143, 1992.
4. D. T. Schaafsma, J. A. Moon, J. S. Sanghera, and I. D. Aggarwal, "Fused taper infrared optical fiber couplers in chalcogenide glass", IEEE J. Lightwave Technol., vol. LT-15, 2242-2245, 1997.
5. D. Marcuse, *Theory of dielectric waveguides*, Academic Press, New York 1990.
6. W.P. Huang, "Coupled mode theory for optical waveguide: an overview", J. Optical Soc. Am. A, vol. 11, 963-983, 1994.
7. R. Syms, J. Cozens, "Optical guided waves and devices", McGraw Hill, London 1992.

ISSN: 1411-1284

Numerical Scheme to Solve the Population Density in Erbium Doped Fiber Amplifier

Octarina Nur Samijayani [2)]
Ary Syahriar [1, 2)]

[1)] Center of Information Technology and Communication, Agency for the Assessment and Application of Technology of the Republic of Indonesia
[2)] Electrical Engineering Department, University Al-Azhar Indonesia

Abstract– **Atomic three level system is the most basic theory that usually used to get better understanding on the amplification of Erbium Doped Fiber Amplifiers (EDFA). The basic process that begins the amplification process in EDFA is the population inversion.**

In this paper we will investigate how the population inversion mechanism is taking place in EDFA part. It is done by solving the population density rate equation numerically. The numerical scheme that is used based on fourth order Runge Kutta method. The number of ion density, the level of stimulated absorption and emission, also the spontaneous decay rate will be considered as the important parameters that influence the rate change of population density.

Keyword: EDFA, Amplification process, Population inversion, Population density.

I. INTRODUCTION

To obtain the amplification, the population inversion is the most important process of EDFA. The population inversion is influenced by some characteristics of material of the fiber, and also the parameter that chosen in EDFA configuration. To explain about the output of EDFA include the signal output power and the amplification gain, we need to know how the population inversion process take place inside EDFA.

The inversion is depending on the number of ion density, the level of stimulated absorption and emission, also the spontaneous decay rate. We will then numerically solve the population density equation to know how they influence the population inversion.

II. BASIC THEORY

Atomic three level system is extended to represent the part of the energy level structure of Er^{3+} that is relevant to the amplification process as depicted in fig.1.[1]. We consider the ground state is denoted by 1, the metastable state that has a long lifetime denoted by 2, and intermediate state labeled by 3 which energy is pumped. The number of population in each state are labeled N_1, N_2, and N_3 respect to their state. To initiate the amplification process inside, we need to get the population inversion between state 1 and state 2.

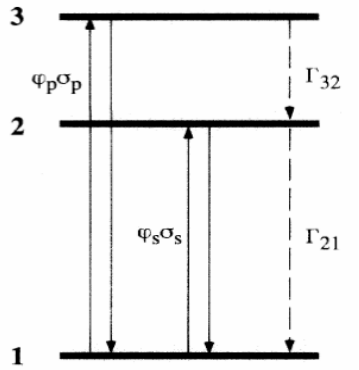

Fig.1. Atomic three level systems for amplification model

We will initially consider the problem with assume which the erbium ions distribution inside EDFA are constant in the transverse dimension over an effective cross sectional area of the fiber.

The pump light intensity at the frequency v_p, corresponding to the transition of the state 1 to state 3, is denoted as ϕ_p, i.e. the number of photons per unit time per unit area [1]. The signal light intensity ϕ_s, at the frequency v_s corresponding to the transition rate from state 1 to state 2.

The changes of population in each state are occurred by the absorption and emission of photons from the incident light field and from other pathway for energy to escape a particular level [1].

The transition probability from level 3 to the level 2 will be denoted as Γ_{32}, include the nonradiative and radiative transition probabilities. Γ_{21} is the transition probability from state 2 to state 1. This transition is related with the spontaneous emission. Both transition probabilities are depending on the lifetime of level that labeled as τ. The transition probabilities and the lifetime of each level has inversely proportional

relation, so we can define the value of $\Gamma_{21} = 1/\tau_{2,}$ and so for $\Gamma_{32} = 1/\tau_{3.}$

The absorption cross section for transition from state 1 to 3 is denoted by $\sigma_p^{(a)}$, i.e. the ability to absorb the pump photons per unit cross section area. The ability to absorb the signal photons per unit cross section area is denoted as $\sigma_s^{(a)}$. As the same consideration for the emission cross section then denoted for pump emission by $\sigma_p^{(e)}$, and $\sigma_s^{(a)}$ for signal emission cross section. This emission is stimulated by signal frequency so it called as stimulated emission.

The differences value of the absorption and emission cross section is depend on the thermal population distribution. Under the normal conditions, all material absorbs light rather than emit it [2]. The absorption process can occur if the photons energy hv of the incident light at frequency v is about the same as the energy difference, Eg, between two state energy level. The photons are absorbed by atoms which end up to the upper level.

The stimulated emission rate can exceed the absorption rate only when $N_2 > N_1$. This condition is referred as population inversion, and is never realized in thermal equilibrium condition [2].

The rate equations for population change are:

$$\frac{dN_1}{dt} = -N_1\phi_p^{(a)}\sigma_p^{(a)} - N_1\phi_s^{(a)}\sigma_s^{(a)} + N_2\phi_s^{(e)}\sigma_s^{(e)} + N_2\Gamma_{21} + N_3\phi_p^{(e)}\sigma_p^{(e)} \quad (1)$$

$$\frac{dN_2}{dt} = -N_2\Gamma_{21} - N_2\phi_s^{(e)}\sigma_s^{(e)} + N_1\phi_s^{(a)}\sigma_s^{(a)} + N_3\Gamma_{32} \quad (2)$$

$$\frac{dN_3}{dt} = -N_3\Gamma_{32} - N_3\phi_p^{(e)}\sigma_p^{(e)} + N_1\phi_p^{(a)}\sigma_p^{(a)} \quad (3)$$

To simplify the equation for the rate of absorption and emission, we can assume that:

$$\phi_p^{(a)}\sigma_p^{(a)} = R_p^{(a)} \text{ and } \phi_s^{(a)}\sigma_s^{(a)} = R_s^{(a)}$$

$$\phi_p^{(e)}\sigma_p^{(e)} = R_p^{(e)} \text{ and } \phi_s^{(e)}\sigma_s^{(e)} = R_s^{(e)}$$

So we produce the population density rate equation:

$$\frac{dN_1}{dt} = -N_1R_p^{(a)} - N_1R_s^{(a)} + N_2R_s^{(e)} + N_2\Gamma_{21} + N_3R_p^{(e)} \quad (4)$$

$$\frac{dN_2}{dt} = -N_2\Gamma_{21} - N_2R_s^{(e)} + N_1R_s^{(a)} + N_3\Gamma_{32} \quad (5)$$

$$\frac{dN_3}{dt} = -N_3\Gamma_{32} - N_3R_p^{(e)} + N_1R_p^{(a)} \quad (6)$$

These equations are indicates that the population in each state are added or reduced from other state, which is depending by absorption and emission process. For steady state we can calculate the equation above that becoming zero. Then we can get the number population at a certain time.

III. NUMERICAL SIMULATION

The simulation of population density on each level is done using Runge Kutte method. This method is usually used to solve the derivative and also to integrating the derivative equations. We used fourth order of this method because we consider the small enough error that permitted occurred in this numerical simulation. We will do the simulation with the certain initial parameter of EDFA as listed below.

Table.1 Initial parameter of EDFA used for the simulation

Cross section area	2.10^{-6} m^2
Er-doping density	1.10^{25} m^{-3}
Spontaneous time	10^{-3} s
Non radiative time	10^{-6} s
Absorption sross section ($\sigma_p^{(a)}$,$\sigma_s^{(a)}$)	(7.10^{-25}, 25.10^{-26})
Emission sross section ($\sigma_p^{(e)}$,$\sigma_s^{(e)}$)	(95 % from absorption)
Pump wavelength	980nm and 1480nm
Input signal wavelength	1510nm

The analysis is begin for the population density equation that depend on the time (time variant) based on eq. (4), (5) and (6), then we will see how the population density at steady state condition. Under the steady state, we simulate the population density equation that varies with some value of input pump power.

Based on simulation result as pictured in Fig.2 represents the number of Er density in state 1 is decreasing, because the pumping process to the upper level (to the state 2 and state 3). So N_2 is increased and so for state 3. But for population densities in state 3, after a short time it is become decaying, it means that the population which has pumped is moved back to the lower state (both to state 1 and state2) until close to zero. This phenomenon is the basic principle that can be used to reduce the atomic three level system to the atomic two level system.

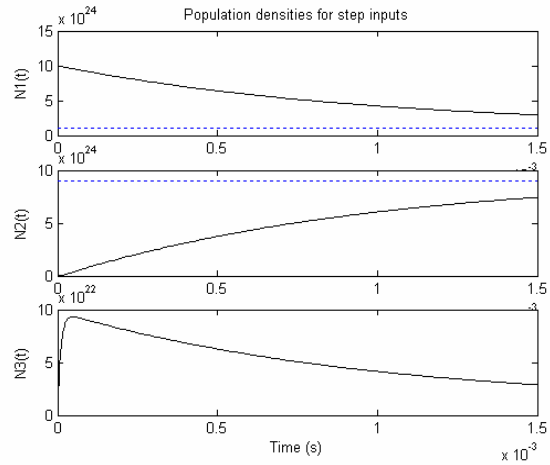

Fig.2 Population density with 10mW input pump power

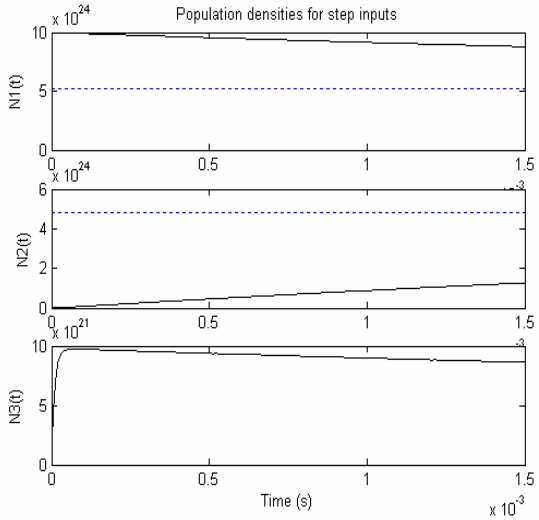

Fig.3 Population density with 1mW input pump power

Based on the Fig.2 and Fig.3, that shows the two population changes behaviors with different input pump power, (10mW for Fig.2 and 1mW for Fig.3), we see that the rate change for Fig.2 is faster then Fig.3. It means with higher pump power the population density will be more excited.

Then we simulate the population in state 3 that depict the number of population that has pumped by different input pump power. This explains that with the higher input pump power, it is stronger enough to exciting more number of populations from the ground state.

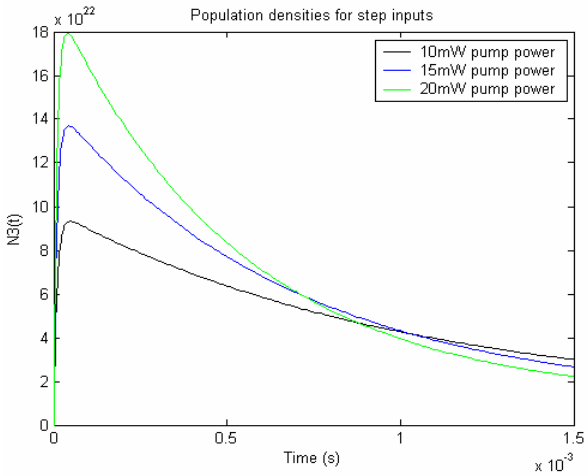

Fig.4 Population density in state 3, for different input pump power (10mW, 15mW, and 20mW)

Next simulation is explaining about the other factor that influences the rate change of population density, that is pump wavelength. The simulation is done for 980nm and 1480nm, the most efficient pump wavelengths, with the same input pump power. We obtain that for 980nm has better population inversion since it can excite more population from ground state to state 3.

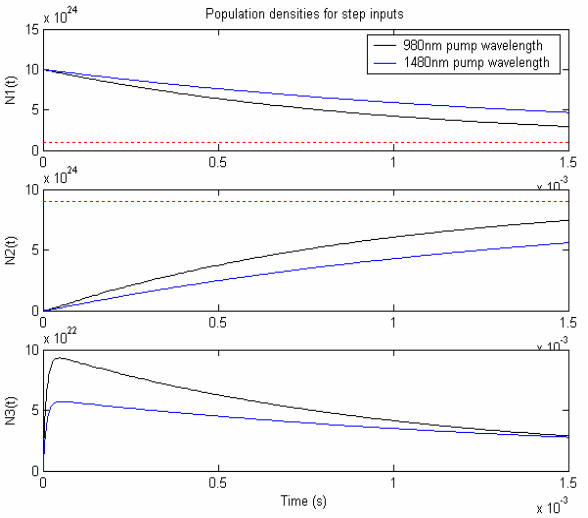

Fig.5. Population density for different pump wavelength (980nm and 1480nm)

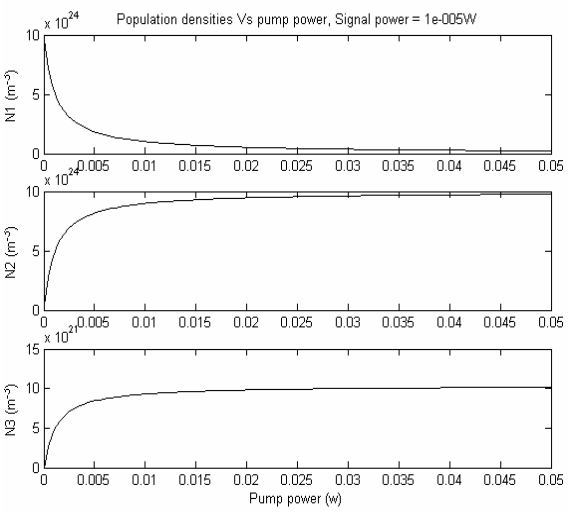

Fig.5. Population density under the steady state condition that varies with different input pump power.

Under the steady state condition we clearly see that at a certain time, the number of population that has pumped from the lower state to upper state is very depending on the input pump power. But the value of input pump power is has to be chosen appropriately in order to get higher inversion efficiently. Because, according to Fig.6, the increasing of inversion rate is not linearly proportional to the value of input pump power.

IV. CONCLUSION

The rate change of population density in each state is representing the population inversion rate. According to the simulation result, EDFA with higher input pump power, the population inversion is getting better. It means there are more number of populations that pumped to the upper energy level, so it can emits more light, and then it can perform the much higher amplification.

But we can not choose the very large level of pump power, because we need to consider the power efficiency and also the noise that come from the spontaneous emission. The other parameter that influences the population inversion is the pump wavelength. From the simulation, EDFA using 980nm pump wavelength can produce better population inversion than using 1480nm pump wavelength.

V. REFERENCES

[1] Becker,P.C. 1999. “Erbium-Doped Fiber Amplifiers: Fundamentals and Technology”, Academic Press, London.

[2] Agrawal,P Govind, 1951. “Fiber-Optic Communication Systems”, John Willey & Sons,Inc.

[3] Kiusalaas, Jaan. “Numerical Methods in Engineering With MATLAB”, Cambridge University Press.

[4] Clifford Pollock, 2003. “Integrated Photonics” Kluwer Academic Publisher.

[5] Qinghe Mao. 1998. “A theoretical analysis of amplification characteristics of bi-directional erbium-doped fiber amplifiers with single erbium-doped fiber”. Southeast UniÍersity, Nanjing.

ISSN: 1411-1284

Characteristics of Silica on Silicon Switching Devices Fabricated by Electron Beam Irraidiation

Ary Syahriar
[1)] Center of Information Technology and Communication,
Agency for the Assessment and Application of Technology of the Republic of Indonesia
[2)] Electrical Engineering Department, University Al-Azhar Indonesia
ary@inn.bppt.go.id, ary@uai.ac.id

Abstract– **We have characterized the optical switching devices fabricated by the electron beam irradiation. The structure consists of silica on silicon layers where on top of it the MgF2 cladding layers have been deposited to engulfed the core layers. It shows that switching time of 2.0 μs has been achieved.**

Keywords: photonic switching, silica on silicon, electron beam irradiation, optical communications

I. INTRODUCTION

Optical switches are key components in advanced optical communications networks. Many different optical switching technologies are currently available or under development. Stable switching operation with low driving power is also necessary. Switches with these characteristics can be realized using the electro-optic effect [1][2], the thermo-optic (TO) effect [3]-[5], or mechanical means [6]. Today, the leading technology for optical switching devices is Ti-diffusion in $LiNbO_3$, where switching is achieved using the electro-optic effect. For example, switched directional couplers based on $LiNbO_3$ devices are commercially available. These components can operate very fast, in the sub-nanosecond regime, but are generally polarization sensitive and expensive [2].

In some applications, polarisation insensitivity is more important than high switching speed (for example, by-pass switching in LAN's with ring topologies and circuit switching for video distribution [8]). In this case, optical waveguide switching using the polarisation independent TO effect, which gives switching times of the order of milliseconds, would be a good alternative.

The TO effect is the change in the optical index of refraction as a result of a temperature rise. Conventional TO phase shifters consist of a thin film heater deposited on the cladding of a buried channel guide. Since in a silica-on-silicon optical waveguide, the glass conductivity is larger than air, heat will be conducted to the silicon substrate, which acts as a heat sink. In the steady-state, the result is a linear temperature gradient between the heater and the substrate, which increases the average temperature of the core. However, relatively high power consumption is involved and lateral heat diffusion in the glass can cause a thermal crosstalk between two adjacent guides [9][10]. These difficulties can be reduced by using a bridge-suspended waveguide structure, which lowers the required drive power and reduces the thermal crosstalk [7]. However, device switching times are lengthened proportionally.

The main purpose of this article is to explain on thermo-optic switching using Mach-Zehnder interferometer (MZI) structures. A thermo optic phase shifter consisting of thin film heater deposited on top of one Mach-Zehnder arms has shown to be very effective to change the effective refractive index of MZI so that the switching occurs.

II. DEVICE CONFIGURATION

The Mach-Zehnder interferometer provides an elegant means of taking advantage of the thermo-optic effect. It consists of two back-to-back Y-junctions connected by two straight guide arms. The first Y-junction splits the input light into two components which travel along the straight guide and are recombined at the second Y-junction. Either or both the straight arms may have a heater to allow the relative phase of the recombining components to be altered. If the two are in phase, the guided output is high, and if they are out-of-phase, it is low.

The layout of the Mach-Zehnder 1x1 single mode optical switches used to investigate thermo-optic switching in irradiated waveguides is shown in Figure 1. The device has two straight arms of 10 mm length and an additional thin film of Ti metal, to act as a heater electrode.

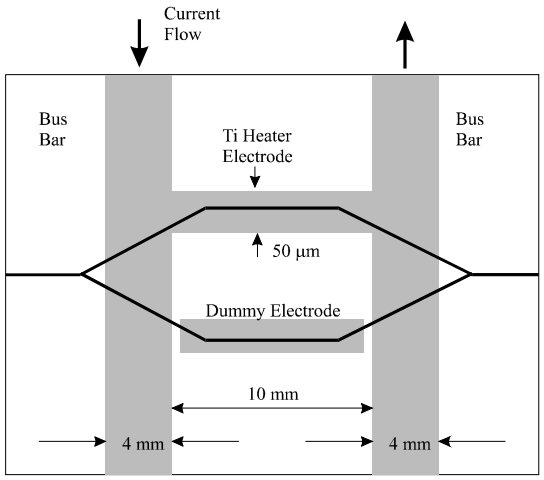

Figure 1. Layout of thermo-optic Mach-Zehnder interferometric switches

The waveguides were formed in PECVD silica-on-silicon obtained from BT Labs, which has characteristics intermediate between those of LETI and BNR material. Irradiation parameters of 1.06 C/cm^2 charge dose at 30 keV energy were chosen to obtain essentially polarization independent insertion losses of ≈ 1 dB at λ = 1.523 μm for 3.4 cm lengths of straight guide with an oil cladding. The guide width was 7 μm, and the index difference between the core and buffer layer was $\Delta n \approx 6x10^{-3}$. Insertion losses for an electrodeless interferometer measured using an oil cladding were 2.0 dB (TE) and 2.5 dB (TM), with the difference being ascribed to slight birefringence. The heater was deposited above one arm of each interferometer by patterning a 0.1 μm thick layer of sputtered Ti metal into 50 μm wide strips fed by 4 mm wide bus bars, and a dummy electrode was placed above the unheated arm to avoid any phase or amplitude imbalance [14].

III. MEASUREMENT OF SWITCHING CHARACTERISTICS

The measurement of switching characteristics was performed using a laser at a wavelength of 1.523 μm. The incident light was butt-coupled into the input end facet of the device using a single mode fibre. The circuit of Figure 5.8 was used to supply current to the heater and hence obtain a phase shift. The output light was detected using a photodetector, and the time variation of the detected signal was displayed on an oscilloscope.

Three types of experiment were carried out. In the first experiment, the variation of transmission with heater power was measured by applying a low frequency square-wave voltage of varying amplitude to the heater. In the second, faster-varying signals were used and the frequency response of the switch was measured. In the third, overdriven switching characteristics were measured.

Figure 2. shows the variation of normalised transmission with heater power, which follows the conventional sinusoidal form. Points are experimental data; the solid line represents the calculated transmission as given by a best fit to Equation (2). Switching performance was essentially similar to devices demonstrated by other technologies [3][15]. The lack of phase bias in the curve suggests that there is no phase shift between the two-interferometer arms, although the relatively poor extinction ratio (10 dB) suggests unequal splitting in the Y-junctions. The first extinction was obtained at a power of ≈ 0.5 W while the second was obtained at a power of ≈ 1.6 W.

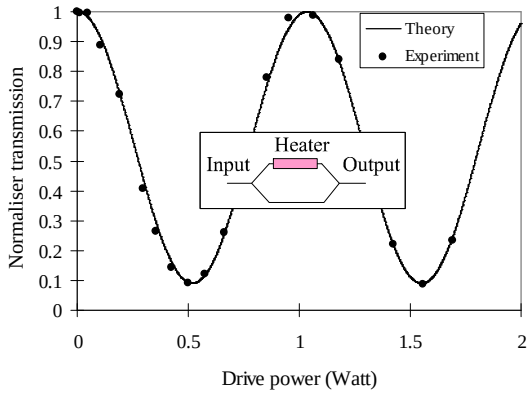

Figure 2. Variation of normalized transmission with heater power for a thermo-optic Mach-Zehnder interferometer modulator formed by irradiation of BT material.

Figures 3 (a), (b), (c) show switch characteristics obtained using a square wave heater drive at frequencies of 125 Hz, 500 Hz and 1 kHz, respectively. Complete switching is clearly achieved at the lowest frequency. However, as the drive frequency is raised, the relatively slow response of the switch quickly limit its ability to reach the ON and OFF states fully. Minimum switching times of ≈ 0.5 ms are slightly shorter than results obtained with topographic guides with a much thicker silica cladding, formed by flame hydrolysis deposition [17]

.

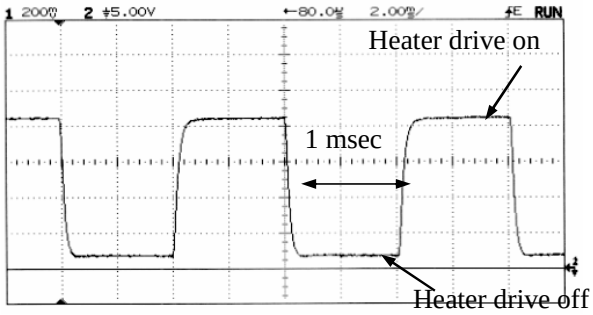

(a)

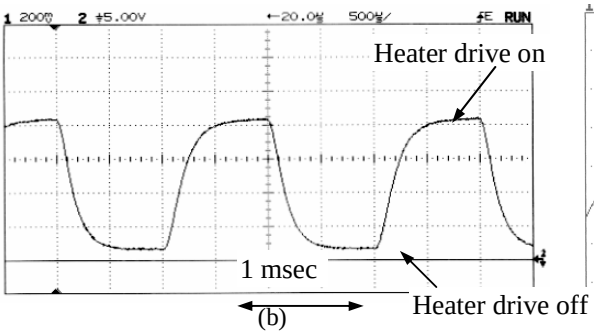

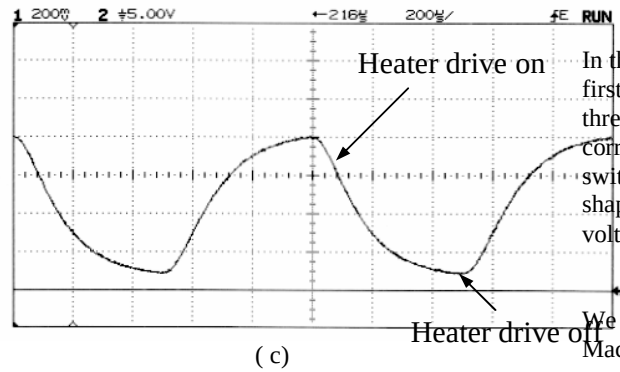

(c)

Figure 3(a). Interferometer switching characteristics obtained using a square wave heater drive at (a) 125 Hz, (b) 500 Hz, (c) 1 kHz.

In the previous set of experiments, the switch was driven using a voltage exactly sufficient to reach the first extinction. Faster switching speeds can in fact be achieved by using larger driving voltages. For example, Figure 4 (a) shows the switch characteristic obtained using a square wave of voltage 64 V at a frequency of 125 Hz. Here, the heater power is sufficient to drive the switch past the first extinction, through the following maximum, and then to the second extinction. Due to the increased drive power, the first extinction is reached extremely rapidly. Figure 4 (b) shows the corresponding trace obtained at 3 kHz.

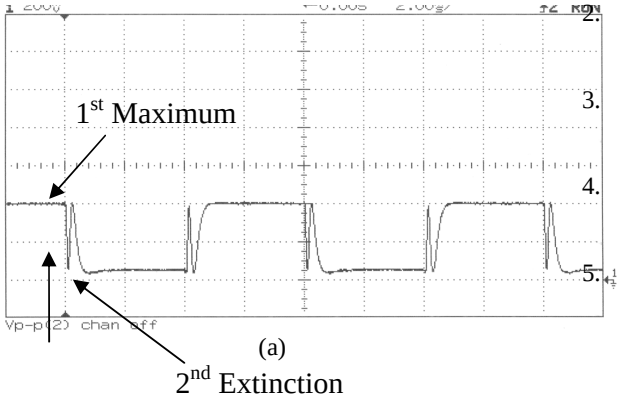

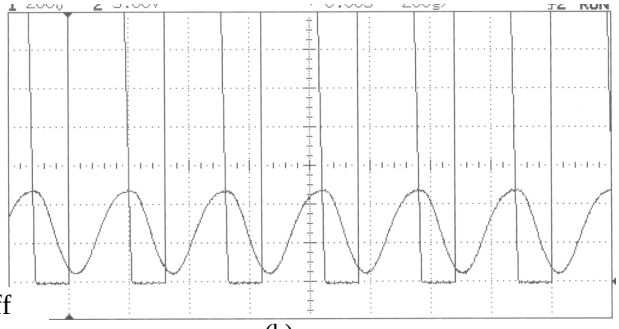

Figure 4. Overdriven switch characteristic obtained using a square wave heater drive with a voltage of 64 V and a frequency of (a) 125 Hz, (b) 3 kHz.

In this case, the drive signal falls to zero exactly as the first extinction is reached, allowing an approximately three-fold increase in modulation speed over the corresponding result shown in Figure 3 (c). A periodic switching at similar speed may be obtained using shaped drive pulse, where an initially large switching voltage is followed by a smaller holding voltage.

IV. CONCLUSIONS

We have characterized the switching devices based on Mach Zehnder interferometer where thin layers of evaporated MgF_2 can be used as a cladding for waveguides formed by electron beam irradiation of PECVD silica-on-silicon. Switching can be realized by using a thin film heater to induce refractive index changes in waveguide structures.

An unequal splitting in the Y-junctions results in poor extinction, however, a major disadvantage. Switches based on directional couplers would be a good alternative, but heating one waveguide without affecting the other in such a closely-spaced geometry is extremely difficult.

REFERENCES

1. H.S. Hinton, “Photonic switching using directional couplers”, IEEE Communication Mag., vol. 25, 16-26, 1987.
2. O. Mitomi, H. Miyazawa, K. Noguchi, “Waveguide-type $LiNbO_3$ high-speed optical switches”, NTT Review, vol. 7, 35-40, 1995.
3. M. Haruna, J. Koyama, “Thermooptic deflection and switching in glass”, Appl. Opt., vol. 21, 3461-3465, 1982.
4. M. Haruna, “Thermooptic waveguide devices”, JARECT Optical Devices & Fibers, vol. 17, 69-81, 1985.
5. M. Haruna, J. Koyama, “Thermo-optic waveguide interferometric modulator/ switch in glass”, IEE Proceedings Pt. H, vol. 131, 322-324, 1984.

6. E. Ollier, P. Lebeye, F. Revol, “Micro-opto mechanical switch integrated on silicon”, Elect. Lett., vol. 31, 2003-2005, 1995.
7. A. Sugita, K. Jinguji, N. Takato, K. Katoh, M. Kawachi, “Bridge-suspended silica-waveguide thermo-optic phase shifter and its application to Mach-Zehnder type optical switch”, IEICE Trans. Electron, vol. E-73, 105-109, 1990.
8. W.K. Ritchie, “Overview of local access development”, BT. Tech. J. vol. 7, 7-16, 1989.
9. T. Aoki, Y. Nishimura, “Technical trends on electromechanical devices”, IEICE Trans. Electron, vol. E77-C, 1536-1544, 1994.
10. Y. Inoue, K. Katoh, M. Kawachi, “Polarization sensitivity of a silica waveguide thermooptic phase shifter for planar lightwave circuit”, IEEE Photon. Lett., vol. 4, 36-38, 1992.
11. M. Okuno, A. Sugita, T. Matsunaga, M. Kawachi, Y. Ohmori, K. Katoh, “8x8 optical matrix switch using silica-based planar lightwave circuit”, IEICE Trans. Electron., vol. E76-C, 1215-1223, 1993.
12. Y. Hida, H. Onose, S. Imamura, “Polymer waveguide thermooptic switch with low electric power consumption at 1.3 □m”, IEEE Photon. Lett., vol. 5, 782-784, 1993.
13. M.B.J. Diemeer, J.J. Brons, E.S. Trommel, “Polymeric optical waveguide switch using the thermooptic effect”, IEEE J. Lightwave Technol., vol. LT-7, 449-453, 1989.
14. A. Syahriar, R.R.A. Syms, T.J. Tate, “Thermooptic interferometric switches fabricated by electron beam irradiation of silica-on-silicon”, IEEE J. Lightwave Technol., vol. LT-16, 841-846, 1998.
15. H.M. Presby, C.A. Edwards, “Packaging of glass waveguide silicon devices”, Opt. Engng., vol. 31, 141-143, 1992.
16. R.R.A. Syms, T.J. Tate, J.J. Lewandowski, “Near-infrared channel waveguides formed by electron-beam irradiation of silica layers on silicon substrates”, IEEE J. Lightwave Technol., vol. LT-12, 2085-2091, 1994.
17. M. Kawachi, “ Silica waveguide on silicon and their application to integrated optic components, “ Opt. Quant. Elect., vol. 22, 391-416, 1990.
18. N. Takato, K. Jinguji, M. Yasu, H. Toba, and M. Kawachi, “Silica-based single-mode waveguides on silicon and their application to guided-wave optical interferometers,” IEEE J. Lightwave Technol., vol. LT-6, 1003-1010, 1988.

ISSN: 1411-1284

Performance Evaluation of IEEE 802.11e EDCA based on Variable Priority Parameters

Riri Fitri Sari, Yan Maraden, Kamal Djunaedi

Department of Electrical Engineering. Faculty of Engineering. University of Indonesian
Kampus Baru UI Depok 16424 Indonesia
email: riri@ui.edu, archezus@yahoo.com, kamaldjunaedi@yahoo.com

Abstract– **This paper presents an evaluation of IEEE 802.11e Enhanced Ditributed Coordination Function (EDCA) traffic priority mechanism performance based on its priority parameter values. Simulation was conducted using ns2 (ns 2.29) platform and IEEE 802.11e EDCA patch [7]. Simulation result shows that changes on the value of priority parameter (AIFS, CWmin, CWmax) affect traffic's throughput. High priority traffic (in this paper, priority 0 is the highest) is guaranteed to get more bandwidth resource than any other lower traffic priority. However, IEEE 802.11e can not guarantee that a traffic in WLAN will always get the same service all the time for its QoS requirements. This is due to the fact that the total bit rate from all other lower priority traffic in the WLAN will affect (reduce) higher priority traffic throughput. Our simulation shows that bandwidth utilization within WLAN is only about 57% of maximum available bandwidth.**

Keywords– EDCA, DCF, 802.11e, WLAN

I. INTRODUCTION

IEEE 802.11 Wireless LANs (WLANS) has been a popular standard since 1990s [1], and play an important role in building a wireless broadband computing environment. The standard is composed of both Physical Layer (PHY) and Medium Access Control (MAC) specifications for wireless LANs. Many task groups under the IEEE 802.11 and some working groups have also revised the standard. The latest PHY specifications allows much higher data rates to be used (e.g., up to 11 Mbps in 802.11b [2] and 54 Mbps in 802.11a [1]), compared with the 1 Mbps and 2 Mbps in the initial version. Higher data rates have paved the way for the incorporation of a larger variety of new applications including multimedia applications in a wireless LAN environment. The use of both multimedia applications in the same wireless LAN is likely to be common in many scenarios, such as in a home network or a cafe deploying a WLAN hotspot. However, without any traffic prioritization mechanism in MAC, high data rate alone may not be sufficient to meet the Quality of Service (QoS) requirements imposed by certain applications such as real time voice, audio and video.

Therefore, QoS for WLAN MAC has received much attention from researcher. Many simulations and research have been performed to support QoS at WLAN. One of them is proposed by the IEEE 802.11e task group defining the new Enhanced Distributed Coordination Function (EDCF) [1] MAC access method as a standard for QoS enhancement of 802.11 MAC. The main idea of EDCA is to apply different MAC parameters for each traffic. Therefore each traffic can be different based on its MAC parameter and will get different treatment. The objective of this paper is to evaluate the performance of IEEE 802.11e EDCA and support to QoS using ns 2.29 [4].

This paper is divided into five sections. Section 1 consists of introduction and background. Section 2 presents the theory concerning mechanism and concept from DCF and EDCA. Section 3 presents the result from the simulation of scenario 1 and scenario 2 and the result analysis from each simulation. The conclusion of this paper is presented in Section 4.

II. BASIC THEORY

II.1. IEEE 802.11 DCF

Distributed Coordination Function is the fundamental MAC method used in 802.11 and is based on a CSMA/CA mechanism. A mobile station (STA) is allowed to send packets after the medium is sensed idle for the duration greater than a Distributed Inter-Frame Space (DIFS). If during anytime in between the medium is sensed busy, a backoff procedure should be invoked. Specifically, a random variable uniformly distributed between zero and a Contention Window (CW) value should be chosen to set a Backoff Timer. This Backoff Timer will start to decrement in units of slot time, provided that no medium activity is indicated during that particular slot-time. The backoff procedure shall be suspended anytime the medium is determined to be busy and will be resumed after the medium is determined to be idle for another DIFS period. The STA is allowed to start transmission as soon as the Backoff Timer reaches zero. A mobile station (STA) shall wait for an ACK

when a frame is sent out. If the ACK is not successfully received within a specific ACK timeout period, the STA shall invoke backoff and retransmission procedure. The CW value shall be increased exponentially from a CWmin value until up to a CWmax value during each retransmission [1].

An additional Request To Send/Clear To Send (RTS/CTS) mechanism is defined to solve a hidden terminal problem inherent in Wireless LAN. The successful the exchange of RTS/CTS ensures that channel has been reserved for the transmission from the particular sender to the particular receiver. This is made possible by requiring all other STAs to set their Network Allocation Vector (NAV) properly after getting RTS/CTS and data frame. Therefore they will refrain from transmitting when the other STA is in transmission. The use of RTS/CTS is more helpful when the actual data size is larger compared with the size of RTS/CTS. When the data size is comparable with the size of RTS/CTS, the overhead caused by the RTS/CTS would compromise the overall performance.

II.2. IEEE 802.11e EDCA

It can be seen from the basic DCF mechanism above, that at least two parameters can be used to provide channel access differentiation: the defer time DIFS and CW, based on which the random backoff timer is generated. Lower DIFS and CW values provide higher priority for channel access. This is essentially how EDCF is developed [1]. Instead of treating all traffic with a single DIFS value and a single (CWmin, CWmax) set, EDCF defines that the channel access has up to four Access Categories (AC), each with its own Different Time called Arbitrary Distributed InterFrame Space (AIFS) and CWmin/CWmax values. According to the draft, one or more user priorities can be assigned to one AC and normally packets belonging to the same priority share one buffering queue [1].

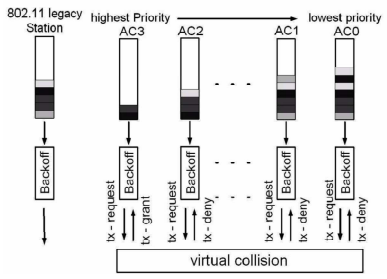

Figure 1. Access Categories at IEEE 802.11e [1]

Figure 1 shows the mechanism of EDCA at IEEE 802.11e which is a duplication mechanism of DCF from IEEE 802.11, but the queue buffer is different on each traffic categories in-group based on priority parameter from each traffic. Therefore, there exist two levels of channel access contention: internal contention among traffic of different priorities inside the same STA and external contention among traffic from different STAs. Collisions may happen at both levels and are resolved similarly such that higher priority traffic, will get more to access to channel, and low priority ones have to wait. In short, different value of time parameter (AIFS, [CWmin, CWmax]) and backoff timer can be used to set the priority in accessing channel from different traffic. Some parameter in determining the four Access Categories (AC) have been formulated in the IEEE draft as default parameters of QoS, as shown in Table 1.

Table. 1 Recommendation of AIFS and CW Value [1]

AC	*AIFS*	*Cwmin*	*Cwmax*
Priority_0	1	7	15
Priority_1	1	31	63
Priority_2	1	31	1023
Priority_3	2	31	1023

III. EXPERIMENTAL RESULTS

The purpose of this paper is to evaluate the performance of IEEE 802.11e EDCA mechanism. All simulation is conducted with ns 2.29 using patch EDCA from TKN Berlin [7]. Figure 2 shows the topology configuration used is our simulation. The topology consists of a WLAN which consists of 4 mobile node (MN), access point (AP) and 3 wired node (WS). In this simulation, traffic rate at wireless node is 1 Mbps, although for traffic rate of 11 Mbps or even 54 Mbps in wired link, the traffic rate is 10 Mbps. The performance of IEEE 802.11e EDCA can be evaluated from the receiving traffic through wired link connecting AP node and WS0 node.

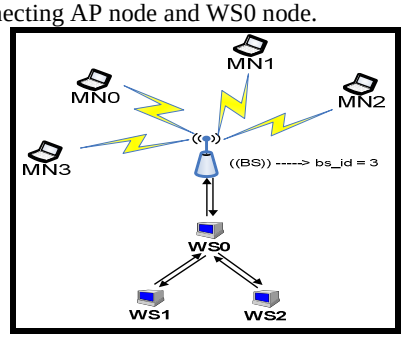

Figure 2. Topology Configuration

Several major performance metrics for evaluation EEE 802.11e EDCA are:

- Delay jitter: the variation delay in the receiving side due the different received for every packet [3].

$$J(i+1) = J(i) + |(R(i+1) - R(i)) - (R(i) - R(i-1)| \quad \text{.....[1]}$$

J(i+1) = delay jitter (ms)

R (i+1) = time when package arrive purpose

- *Throughput*: the traafic size through a link in a selected range of time [3].

$$Throughput = \frac{\sum packet}{\sum time} \times 8/1000 \text{ Kbps} \quad .....[2]$$

III.1 Scenario 1

There are four settings for the delivery process of traffic, and every setting consists of four applications. Therefore the total number of the application result is 16, which consists of four Access Categories (AC), which is traffic with priority of 0 (highest), priority 1, priority 2, and priority 3 (lowest). The application used is Constant Bit Rate (CBR) based on UDP protocol. The transfer rate of every application is 100 Kbps and the package CBR size of the traffic is 210 Bytes.

The first transmission is set for priority 3 applications (application with the lowest priority) at 20 second, and then followed with other applications with time interval of 10 to 50 Second, then the priority 0 (highest priority) starts transmitting. The next packet transmission is set at 150 Seconds. Then, at 220 to 250 seconds, the third packet transmission is conducted. Finally, at 320 to 350 seconds the fourth packet transmission is set. The transmission will continue to take place until 500 Second. The transfer rate will be added with 400 Kbps (100 Kbps per application) in stages, so that by the end of the simulation time the transfer rate will reach 1600 Kbps. It is important to remember that the transfer rate of the wireless LAN (wireless node) is equal to 1 Mbps.

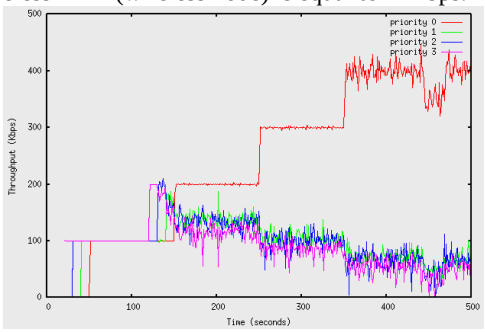

Figure 3. Troughput simulation_1 Based on Parameter at Table 1

Figure 3 shows that the traffic with high priority (priority 0) will get more resource than other traffic. The throughput of the traffic with priority 0 always reach or at least close to the transfer rate (100, 200, 300, 400 Kbps). The total transfer rate at that moment is 1600 Kbps, while the maximum transfer rate at the wireless link is 1 Mbps.

Figure 4 is the result of simulation conducted using the parameter at Table 2. Figure 4 shows that traffic with priority 1 has higher throughput compared with throughput at Figure 3. This is because of the existence of different parameter priorities to traffic priority 1. In Figure 3 [CWmin, CWmax] used is [31, 63], whereas in Figure 4, the value used is [15, 31]. The access CW is decreasing, hence the backoff timer selected is also smaller, so that it will improve the possibility of traffic to access the channel more compared with the ones with larger CW. Figure 4 shows the change of value CW at priority 1 traffic which will influence the throughput of priority 0 traffic.

Table 2. AIFS and CW Parameters from Simulation 2

AC	*AIFS*	*Cwmin*	*Cwmax*
Priority_0	2	7	15
Priority_1	2	15	31
Priority_2	3	31	1023
Priority_3	7	31	1023

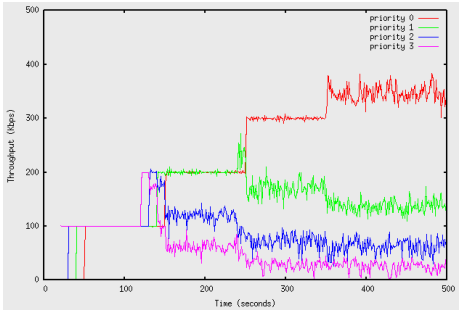

Figure 4. Troughput Simulation 2 Based on Parameter at Table 2

Table 3. AIFS and CW Parameter of simulation 3

AC	*AIFS*	*Cwmin*	*Cwmax*
Priority_0	1	7	15
Priority_1	2	15	31
Priority_2	3	31	1023
Priority_3	7	31	1023

Figure 5 shows the result and the impact of the change of AIFS parameter. The parameters in Table 3 is equal to those in Table 2, except for AIFS parameter. At the third simulation, AIFS priority 0 minimized to be 1 slot-time, of the priority 0 traffic only have to a wait for the channel in an empty state during AIFS (1 slot-time) before transmitting. The probability of priority 0 traffic to access the channel, progressively increased compared with simulation 2.

Figure 6 and 7 show that the traffic priority 0 and priority 1 have similar throughput value. This is because priority 1 parameter at simulation 4 become close to priority 0 ones, while at simulation 5, priorities parameter 1 set equal to priority 0. There is a few change of scenario at simulation 6. The priority 0 traffic transmission will only conducted by setting the first one, whereas for the second, third, and fourth, priority the traffic is deactivated. The other traffic remains the same as in scenario 1. The Priority 0 traffic consistently has the transfer rate of 100 Kbps. Figure 8 shows that the IEEE 802.11E EDCA can guarantee the traffic throughput.

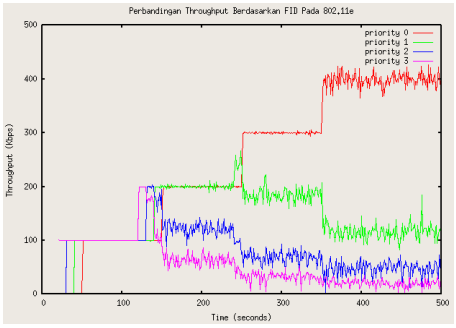

Figure 5. Throughput of simulation 3 based on Parameters from Table 3

Table 4. AIFS and CW Parameter of Simulation 4

AC	*AIFS*	*Cwmin*	*Cwmax*
Priority_0	2	7	15
Priority_1	2	12	20
Priority_2	3	31	1023
Priority_3	7	31	1023

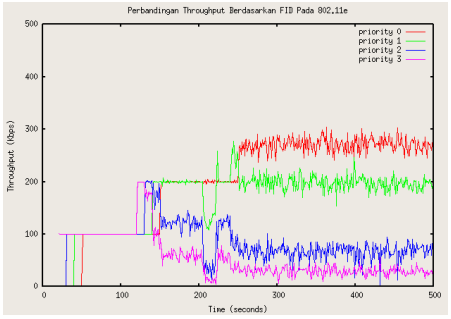

Figure 6. Throughput Simulation 4 based on Parameter at Table 4

Table 5. AIFS dan CW Parameter of Simulation 5

AC	*AIFS*	*Cwmin*	*Cwmax*
Priority_0	2	7	15
Priority_1	2	7	15
Priority_2	3	31	1023
Priority_3	7	31	1023

The EDCA mechanism cannot guarantee high priority traffic with high transfer rate. This is shown at the graph from the last simulation, in which the throughput of priority 0 traffic seldom reach 400 Kbps. This is due to the level of the transfer rate of the priority 0 applicationand other application, so that the throughput of priority 0 traffic will be lower.

Figure 9 shows that the delay jitter that happened in each priority traffic. It shows that traffic with high priority (priority 0) will have the lowest delay jitter. Delay jitter perceived is only at delay at the wired link between AP and WS0, and is not the end to end delay from sender to receiver nodes.

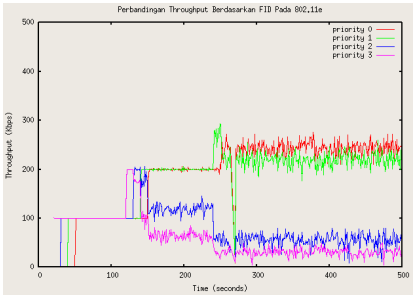

Figure 7. Throughput simulation 5 Based on Table 5

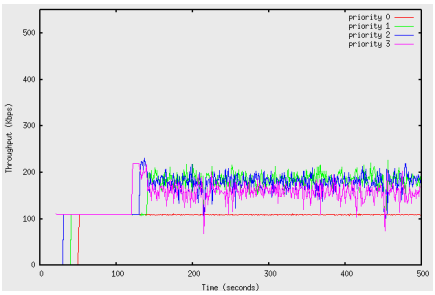

Figure 8. Throughput Simulation 6 based on Parameter at Tabel 1

III.2 Scenario 2

In this scenario, four applications with different priority parameters have been simulated. Each application transmits packets at 0-500 seconds. The application used is CBR, based on the UDP protocol, with transfer rate of 300 Kbps, for each applications. The total transfer rate from the four applications is 1200 Kbps. Figure 10 shows that only traffic with priority 0 which have throughput at range of 300 Kbps, while other traffic have smaller throughput of more than 300 Kbps.

Referring to Table 6, package (rcvdPkts) transmission during simulation will depend on the priority parameter of the traffic and also with throughtput mean (avgTput). The average jitter (avgJitter) will increase when the priority parameter is lower. At simulation 7 the total average throughput from the fourth traffic is 573,937 Kbps or only 57.4 % from the transfer rate of wireless (1 Mbps). Therefore the bandwidth utilization of IEEE 802.11e EDCA at scenario 2 is only 57% from the maximum transfer rate (which is equal to 1 Mbps).

II. CONCLUSIONS

The change of priorities parameter (AIFS, CWmin, CWmax) will influence throughput traffic. In other words, the smaller access AIFS, CWmin and CWmax probability of traffic will make the access channel to be greater.

The change of priority parameter value will affect the delay jitter at wired link between AP and WS0. Smaller access parameter means access delay jitter will also be smaller. In other words, the traffic with

high priority (priority 0) will have lower delay jitter compared with other traffic.

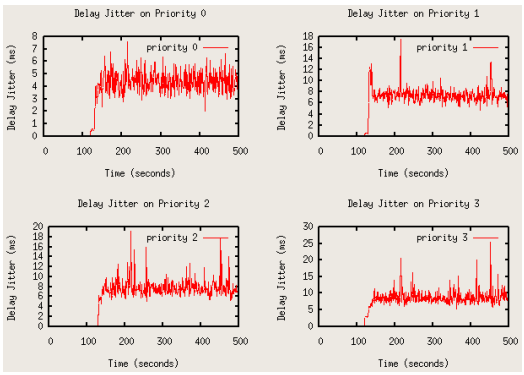

Figure 9. Delay jitter from Every traffic of Simulation 6

Table 6. Statistics from Simulation 7

Trafik	*rcvdPkts*	*avgTput (Kbps)*	*avgJitter (ms)*
Priority_0	87134	299.997	3.28733
Priority_1	50254	172.944	7.13043
Priority_2	20857	71.7634	21.0121
Priority_3	8498	29.2335	56.9367

IEEE 802.11E EDCA only guarantee QoS statistically, depends on the level of traffic selected. The QoS performance indicator (throughput and delay) is relative to the other priority traffic.

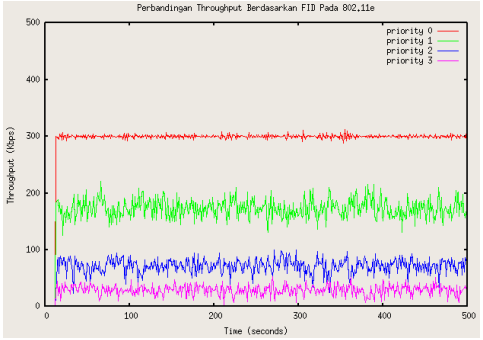

Figure 10. Throughput of Simulation 7 based on Parameter from Table 2

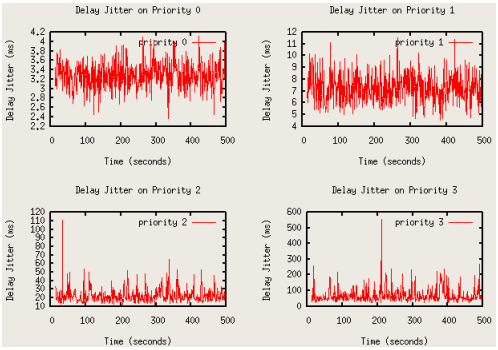

Figure 11. Delay Jitter Every Trafic at Simulation 7

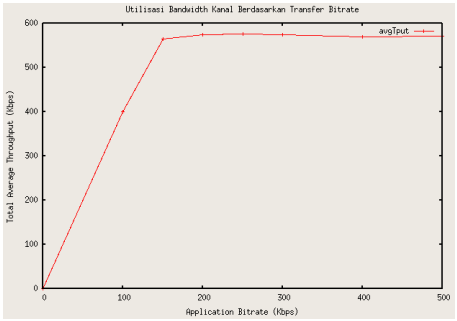

Figure 12. Statistical result of bandwidth utilisation at Scenario 2

REFERENCES

[1]. Dajiang He dan Charles Q. Shen, "Simulation Study of IEEE 802.11e EDCF", National University of Singapore,http://ieeexplore.ieee.org/iel5/8574/27174/01207630.pdf, 12 Mei 2007

[2]. Supplement to IEEE Standard for Information technology- Telecommunications and Information exchange between systems - Local and metropolitan area networks - Specific requirements - Part 11: Wireless LAN Medium Access Control (MAC) and Physical Layer (PHY) specifications: Higher-Speed Physical Layer Extension in the 2.4 GHz Band. IEEE Std 802.11b-1999.Edition, http://www.tehnicom.net/clanci/pdf/802.11b-1999_Cor1-2001.pdf, 31 May 2007

[3]. M. Barry, A. T. Campbell, and A. Veres, "Distributed Control Algorithms for Service Differentiation in Wireless Packet Networks", IEEE INFOCOM 2001, April 2001, pp. 582-590, www.ul.ie/mgbarry/Pubs/Infocom2001.pdf,

[4]. Ns-2, http://www.isi.edu/nsnam/ns/

[5]. NAM, http:// www.isi.edu/nsnam/ns/WWW.html/

[6]. Donghui Xie, "RPR MAC Delay Metric and SRP Phase One Simulation", Cisco Systems July 10, 2001, http://www.ieee802.org/17/documents/presentations/jul2001/dxie_phase1_01.pdf,

[7]. NS-2 Research, http://www.tkn.tu-berlin.de/research/802.11e_ns2/, last access 20 May 2007.

[8]. http://www.reti.polito.it/fiore/, last access 20 May 2007.

ISSN: 1411-1284

On Determination of Bio-Gasoline Octane Number Using Artificial Neural Network

Abdul Wahid, Bambang Heru Susanto, Hexi Trijati Rahayu, and Teguh Adilina

Chemical Process System Lab., Dept. of Chemical Engineering
Faculty of Engineering, University of Indonesia
Email: wahid@che.ui.edu

Abstract – **Artificial Neural Network (ANN) is used for determining octane number of bio-gasoline. The aim is to provide a solution for any alternative energy resources researcher of bio-gasoline in determining the bio-gasoline octane number more easily and accurately. The advantage of this method is it can recognize a relationship between input and output without knowing a mathematical equation of those input and output. ANN learns a relationship pattern of number of input and output data through training process, then predicts the output from a given new input. This research uses 43 data of bio-gasoline physical properties (density and 50% distillation temperature or TT50) as inputs and bio-gasoline octane numbers as outputs. Three ANN models of *multi-layer feed-forward* (MLFF), *generalized regression neural network* (GRNN), and *radial basis* (RB) are used in this research. The result shows RB is the best model with 0.07% average error. After that, the second is GRNN with 0.8% average error, and the last is MLFF with 1.6% average error. Except MLFF model, the other models can predict output very accurately (zero error). RB model has three points of five validation data and GRNN model in two points.**

I. INTRODUCTION

Consumption of gasoline in Indonesia is 39 thousands KL per day or more than 14 millions KL per year (2005) [1]. This is the huge numbers. Even, this will be 60 million KL if totalized with other fuel consumption. This causes Indonesia is a net importer country. Meanwhile, crude oil resources are limited that is shown by decreasing of the domestic oil production [2]. It is imperative to look for an alternative energy from a renewable material.

Indonesia is the second of the biggest producer country of CPO (crude palm oil) after Malaysia, that is 10 million tons/year. Even in 2010, Indonesia is predicted to the first of the biggest producer of CPO, producing 12 million tons/year [3]. Now, Indonesia's CPO is mostly (>90%) exported as a raw material without any advanced treatments. This is very different with Malaysia. The most production of Malaysia's CPO is treated in advance before exported to another country. This causes the increasing of an added value of the CPO.

There are many researches in bio-gasoline recently. They are according to encourage using of the alternative fuel and the design of automotive engine appropriate with bio-gasoline. The problem is how to determine octane number (ON) of bio-gasoline that is the important parameter of bio-gasoline quality. This is caused by the expensive of the ON testing cost and a little of ON testing tools. Using a model relating to physical properties of bio-gasoline and its ON is going to ease all of researchers developing bio-gasoline to determine bio-gasoline ON. In this research, we proposed *artificial neural networks* (ANN) to get an accurate result.

II. BASIC THEORY

There are four methods that is commonly used to determinate the bio-gasoline ON, those are:

1. Predicting it through cetane index (using temperature at 50% distillation or TT50 and then the cetane index is used to calculate bio-gasoline ON) [4].
2. Predicting it through FT-IR (Fourier Transform Infrared) method as proposed by Asfaha et.al. [5].
3. Using the ON-tester (by contacting directly with sensing device to bio-gasoline)
4. Using ASTM D 2699 method (using VCR (variable compression ratio) engine)

ANN can recognize the relationship between input and output without knowing the mathematical equation of the input and the output. This ability makes ANN can help the bio-gasoline researchers to determine bio-gasoline ON that has a complex relationship between its input and output (ON).

Figure 1 shows a simple ANN [6], where have 3 neurons of inputs (X_1, X_2, X_3), 1 neuron of output (Y) and relation weights of both inputs and outputs (W_1, W_2, W_3). Y receives inputs of X_1, X_2 and X_3 with the relation weights are W_1,W_2 and W_3, respectively. Three impulse of neurons are combined:

$$net = x_1 w_1 + x_2 w_2 + x_3 w_3 \quad (1)$$

Magnitude of impulse received by Y follows activation function:

$$y = f(net) \quad (2)$$

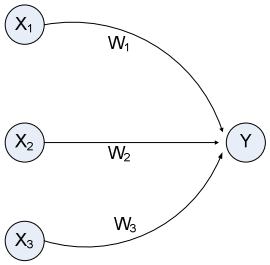

Figure 1. A simple artificial neural network

If value of activation function is strong enough, the signal will be continued. The value of activation function (output of network model) also can be used as basis to change the weights.

III. EXPERIMENT

In this research, the input data are physical properties data of bio-gasoline in the form of density and temperature of 50% distillation that is called TT50, meanwhile the output data are the bio-gasoline ON. Three ANN models are used in this research, they are *multi-layer feed-forward* (MLFF) that is a developing model from initial model of *back-propagation*; *radial basis* (RB) model, and *generalized regression neural network* (GRNN) model.

In the MLFF model, there is a training step to find number of an optimum layer and neuron. The optimum layer and neuron are used to predict the target (bio-gasoline ON). In the RB model, the network formation using two options: without (is called RB-WOGS) and with goal and spread parameters (is called RB-GS), while the GRNN model that is a developing model from RB model, uses the default function. All of models are processed using MATLAB® software.

IV. EXPERIMENTAL RESULTS

This research uses training data as shown by Figure 2, taken from the previous researches [7 – 10]. The data range are 0.73 – 0.8865 kg/m^3 for density, 249.8 - 320^{o}C for TT50, and 72.53 – 92 for ON.

The results of training process to build ANN in MLFF model show that more number of neurons in a layer, the number of iteration is smaller. So, the training process is faster. But, if the number of neuron is too many, it causes unstability in the algorithm and the number of iteration is more. In this research, the optimum numbers of neuron in one hidden layer are 4 neurons. But, the number of hidden layer has a little effect to the number of iteration in the training process. This may be caused by unstability in the algorithm when the hidden layer is added, then increasing in the number of iteration. Thereby, it is able to say that MLFF model with one hidden layer has been an optimum, although sometimes adding a hidden layer can make the training process is better. The structure of MLFF model is shown by Table 1.

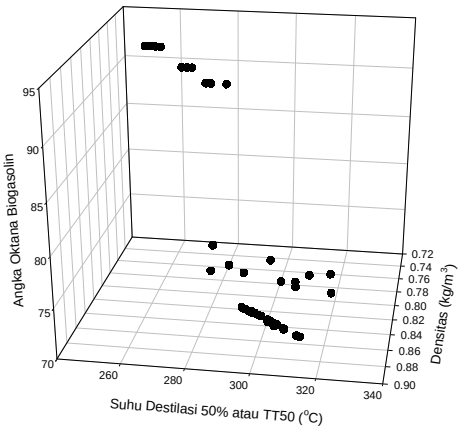

Figure 3. 43 data that is used in ANN training process

Table 1 The result of training process with MLFF model

Input : • Number of layer	1 (2 neurons)
Hidden layer : • Number of layer • Activation function	1 (4 neurons) Purelin
Output : • Number of layer • Activation function	1 (1 neuron) Purelin

A network model that is used in MLFF model is shown by Figure 3. MLFF network has one input layer with two neurons (X1 dan X2), one hidden layer with four neurons and one output layer (Y).

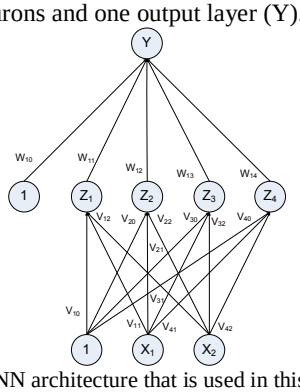

Figure 3 ANN architecture that is used in this research

The first test to validate the results of the three models uses the same data that is used in the training process. The purpose of this step is to ensure what the model can predict the target accurately. Figure 4 shows that RB model can predict the target accurately or the error is zero. This result can be achieved by RB-WOGS model as well as RB-GS model. GRNN model has 0.5% of average error, meanwhile MLFF model has 2.3% of average error.

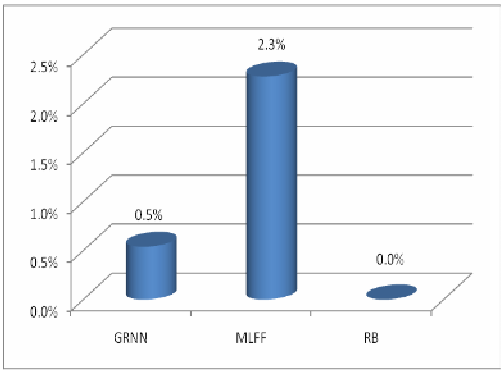

Figure 4. Average error of three ANN models using training data

How if the validation test uses new data, not the training data?

The test uses data that is not used in the training step is called validation step. The purpose of the validation step is to show the ability and stability of ANN performance in predicting the bio-gasoline ON. Table 2 shows the result of ON prediction uses the three ANN models.

Table 2 shows that the best model is RB with 0.07% of average error. GRNN model places the second with 0.8% of average error, and the end is MLFF model with 1.6% of average error. RB model can predict accurately in the three points of five validation data, GRNN model has two accurate point, and MLFF model has no any accurate point.

In addition, the results in the Table 2, for RB model uses RB-GS with goal parameter is 2 and spread value is 0.01 or called G1S.01. Those values are the optimum value as shown by Figure 5, because the average error is the smallest. If we use RB-WOGS the average error is huge (5702%). This is caused by the prediction result of the fifth point of validation data (density: 0.8298 and TT50: 330^{o}C) is far away from the target, that is -20,567.

Table 2 Validation data and ON calculation results using three ANN models

DATA VALIDASI			GRNN		MLFF		RB	
Density	TT 50 (^{o}C)	ON	ON	Error	ON	Error	ON	Error
0.7400	251	92.00	92	0.0%	90.8179	1.3%	92	0.0%
0.7300	269.6	88.00	88.0001	0.0%	87.3169	0.8%	88	0.0%
0.8278	313	74.68	73.661	1.4%	73.7902	1.2%	74.68	0.0%
0.8848	307	73.85	73.593	0.3%	72.7186	1.5%	73.68	0.02%
0.8298	330	72.39	74.065	2.3%	70.0063	3.3%	72.15	0.33%
Average Error				**0.8%**		**1.6%**		**0.07%**

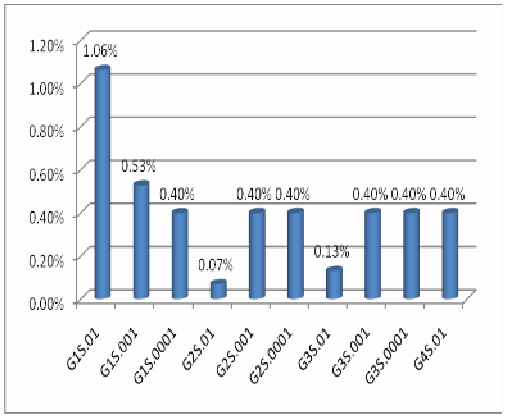

Figure 5. Average error of RB-GS model based on G and S values

V. CONCLUSIONS

ANN can be used to predict bio-gasoline octane number by using its physical properties (density and TT50). The validation results of three ANN models show that the ANN can predict the bio-gasoline ON better with the average error has range 0.07% - 1.6%. The result shows that RB model with G = 2 and S = 0.01 is the best model with 0.07% average error. After that, the second is GRNN with 0.8% average error, and the last is MLFF with 1.6% average error. Except MLFF model, the other models can predict output very accurately (zero error). RB model has three points of five validation data and GRNN model in two points.

REFERENCES

[1]http://members.bumn-ri.com/pertamina/news.html?news_id=11856 "Stok BBM Pertamina Melimpah - IMPOR BBM FEBRUARI DIPOTONG 55 PERSEN"

[2] Kurtubi, "Indonesia: Net Oil Importer", Center for Petroleum and Energy Economics Sudies (CPEES), Jakarta, 2004

[3] RISTEK, "Rencana Induk Kegiatan Rusnas Industri Kelapa Sawit", Jakarta 2004

[4] Nasikin M. et. al., "The effect of acidity to acid catalyst reaction that is occurred in trigliseride of palm oil", *Research Report of Dept. of Gas and Petrochemical Engineering Faculty of Engineering University of Indonesia* (Indonesian), 2004

[5] A.Iob, M.A.Ali, B.S.Tawabini, J.A.Anabtawi, S.A.Ali and A.A.Farayedhi, "Prediction of reformate RON by FT-IR", ***Fuel***, Vol.74, No.2, pp.227-231, 1995

[6] Jong Jek Siang, *Artificial Neural Network and Programming Using Matlab* – (Indonesian) Ed. I., Yogyakarta: Andi, 2005.

[7] J. E.Silalahi, "The increasing in bio-gasoline octane number through alkene hydration in palm oil bio-gasoline using HCl catalyst", (Indonesian), *Bachelor Thesis*, Dept. of Chemical Engineering University of Indonesia, 2007

[8] I. Onggo, "The increasing in bio-gasoline octane number through ester hydrolysis in palm oil bio-gasoline using zeolite catalyst", (Indonesia), *Bachelor Thesis*, Dept. of Chemical Engineering University of Indonesia, 2007

[9] Julius, "The increasing in bio-gasoline octane number through ester hydrolysis in palm oil bio-gasoline using HCl catalyst", (Indonesian), *Bachelor Thesis*, Dept. of Chemical Engineering University of Indonesia, 2007

[10] M. M. Dewayani, "Bio-gasoline production from methyl ester palm oil through cracking reaction using methyl cetone perocside and sulphate acid catalyst", (Indonesian), *Bachelor Thesis*, Dept. of Chemical Engineering University of Indonesia, 2005

ISSN: 1411-1284

Characteristics of Non Uniform FBG in C-band region Using Transfer Matrix Method

By: Qadriyyah[1)] Ary Syahriar [1,2)]

[1)] Center of Information Technology and Communication, Agency for the Assessment and Application of Technology of the Republic of Indonesia
[2)] Electrical Engineering Departement, University Al-Azhar Indonesia
Email: W_azzahra@yahoo.com)

Abstract - **Fiber Bragg Grating is one of the most important optical filter technology as a low cost and low loss component that has been used successfully in sensor and telecommunication application. In this paper we use couple mode theory for bragg gratings in observing the effect of the uniform and non uniform fiber bragg grating to the light wave propagating through fiber.**

The couple mode theory is integrated numerically using Transfer Matrix method. Reflectivity power in the uniform and non uniform fiber bragg grating are demonstrated, the demonstration will be limited to single-mode silica-based fiber operating at a wavelength of 1550 nm.

Keyword - FBG, Couple Mode Theory for FBG, Matrix Method, Reflectivity

I. INTRODUCTION

Fiber Bragg gratings (FBGs) are periodic perturbation of the refractive index along the length of the core of an optical fibre waveguide. The grating are induced by exposing the fiber core to a periodic pattern of ultra violet (UV) light over an extended time. The prolonged exposure result in a permanent refractive index change in the core of the fiber. The induced refractive index modulation, called a fibre bragg grating, depends on the pattern and properties of the exposure UV light. FBG is one of the most important optical filter technology as a low cost and low loss component that has been used successfully in sensor and telecommunication application such as Gain flattening for EDFA, temperature, strain and pressure sensor [2], true time delay (TTD) for microwave phased-array antennas system[3], photonic chrystal bandgap [4] and etc.

In this paper we will observing characteristic of the light wave propagating in the uniform and non uniform FBG and what different between them. Couple mode theory is a suitable tool to describe of light waves through a cylindrical waveguide with a slowly varying index. As numerically analysis for demonstrated reflectivity power in the uniform and non uniform grating we use *Transfer Matrix method* [1].

II. BASIC THEORY

The most suitable tool to describe the propagation of light waves through a cylindrical waveguide with a slowly varying index are couple mode theory. The theory provides a technique for obtaining quantitative information about the optical properties of the fibre Bragg grating. In this section we will follow the summarised derivation presented in the work of Erdogan[1]. The novelty behind couple-mode theory is the assumption that the transverse electric field of perturbed fibre can be expressed as a superposition of ideal guided modes of unperturbed fibre. As a result the transverse electric field can be expressed as a combination of forward and backward travelling waves as:

$$E_t(r,\theta,z,t)=\sum_m [A_m(z)e^{j\beta m^z} + B_m(z)\, e^{-j\beta m^z}].b_{mt}(r,\theta)\, e^{-j\omega t} \quad (1)$$

where $A_m(z)$ and $B_m(z)$ are the slowly varying amplitudes of the m th mode travelling in the forward and backward direction respectively. ω is the angular frequency of propagation and β is the propagation constant defined as $\beta = 2\pi neff/\lambda$, where n*eff* is the effective refractive index of a particular mode. b_m is the amplitude of the transverse electric field of the m th propagation constant.

In the presence of a slowly varying perturbation in the fibre core, the modes are forced to be coupled. As a result, the amplitudes of the *m* th mode will vary along *z* , due to the coupling with the *q* th mode. For coupling between the *m* th and the *q* th mode, the amplitudes A_m and B_m will vary according to:

$$dA_m/dz = j\sum_q A_q(K^t_{qm}+K^z_{qm})e^{j(\beta q-\beta m)z} + j\sum_q B_q(K^t_{qm}-K^z_{qm})e^{-j(\beta q+\beta m)z} \quad (2)$$

$$dB_m/dz = j\sum_q A_q(K^t_{qm}-K^z_{qm})e^{j(\beta q+\beta m)z} - j\sum_q B_q(K^t_{qm}+K^z_{qm})e^{-j(\beta q-\beta m)z} \quad (3)$$

where K^t_{qm} and K^z_{qm} are the respective transverse coupling coefficient and longitudinal coupling coefficient between the modes m and q.

$$K^t_{qm}(z)= \omega/4 \int_{2\pi,\infty} \Delta\varepsilon(r,\theta,z) b^t_q(r,\theta). b^{t*}_m(r,\theta) dr d\theta \quad (4)$$

where $\Delta\varepsilon$ (r,θ,z) is the permittivity perturbation and * represents the complex conjugate.

In common optical fibres, the UV-induced refractive index changes are uniform or non uniform inside the fibre core and negligible in the cladding. With this assumption, the index change can be expressed as:

$$\delta n_{eff}(r,\theta,z)=\delta n_{eff}(\overline{z})=\delta n_{eff}(z)\{1+s\cos[2\pi z/\Lambda+\varphi(z)]\} \quad (5)$$

$\delta n_{eff}(z)$ = "dc" index change spatially averaged over a grating period
s = fringe visibility of the index change
Λ = grating period
$\varphi(z)$ = phase describing the grating chirp

To complete the coupled-mode theory, there are two useful coefficients, the self coupling coefficient and the cross coupling coefficient defined as follows:

$$\sigma_{qm}(z)= \omega n_{co}/2 \int_{\Lambda} \delta n_{eff}(z) b^t_q(r,\theta).b^{t*}_m(r,\theta) dr d\theta \quad (6)$$

$$\kappa_{qm}(z)= s/2\ \sigma_{qm}(z) \quad (7)$$

where $\sigma_{qm}(z)$ is a "dc" coupling coefficient and $\kappa_{qm}(z)$ is an "ac" coupling coefficient.

The general coupling coefficient is defined as:

$$K^t_{qm}(z) = \sigma_{qm}(z) + 2\kappa_{qm}(z)\cos[2\pi/\Lambda\ z + \varphi(z)] \quad (8)$$

For fibre Bragg gratings, coupling occurs between two identical modes that propagate in opposite directions on the *z*-axis. The interaction between the two modes will be dominant near a fixed wavelength specified by the coupling coefficients. For a mode of amplitude A(z) and an identical counter-propagating mode of amplitude B(z) , the coupled-mode equations (2) and (3) can be simplified to:

$$dA^+/dz= j\sigma' A^+(z) + j\kappa B^+(z) \quad (9)$$

$$dB^+/dz= -j\sigma' B^+(z) - j\kappa^* A^+(z) \quad (10)$$

where
$A^+(z)$ = $A(z)e^{(j\delta dz-\varphi/2)}$
$B^+(z)$ = $B(z)e^{(-j\delta dz+\varphi/2)}$

σ' is the general "dc" self-coupling coefficient defined as:

$$\sigma' = \delta_d + \sigma - 1/2\ d\varphi/dz \quad (11)$$

The derivative 1/2 $d\varphi/dz$ describes the possible chirp in the grating. The detuning δ_d, that is always independent on the variable *z* is defined as:

$$\delta_d= \beta - \pi/\Lambda = \beta - \beta_D= 2\pi n_{eff}(1/\lambda - 1/\lambda_D) \quad (13)$$

where $\lambda_D=2n_{eff}\Lambda$ is the *design peak reflection wavelength* for a weak grating (δneff ~ 0) commonly known as the *Bragg wavelength*. For single-mode fibre (where the cutoff frequency $V \leq 2.405$) the "dc" coupling coefficient σ and the "ac"coupling coefficient κ defined in equations (6) and (7) can be simplified to:

$$\sigma = 2\overline{\pi/\lambda}\delta n_{eff} \quad (14)$$
$$\kappa = \kappa^* = \pi/\lambda\ \overline{s\delta n_{eff}} \quad (15)$$

The complex amplitude reflection coefficient under boundary conditions (A^+ (−L/2)=1) and (B^+ (L/2) =0) is:

$$\rho = B+(-L/2)/A+(-L/2)$$
$$= -\kappa\sinh(\gamma_B L)/\{\sigma'\sinh(\gamma_B L) + j\gamma_B \cosh(\gamma_B L)\} \quad (16)$$

where γ_B is the parameter relating the coupling coefficients as follows:
$\gamma_B = \sqrt{(\kappa^2 - \sigma'^2)}$

The power reflection coefficient of a fibre Bragg grating can be determined as:

$$R(\lambda)= |\rho|^2= \sinh^2(\gamma_B L)/\{\cosh^2(\gamma_B L) - \sigma'^2/\kappa^2\} \quad (17)$$

The power transmission coefficient is related to the reflection coefficient through the law of conservation of energy which states $R(\lambda) + T(\lambda) = 1$.

Other spectral properties of interest in fibre Bragg gratings are the group delay and the dispersion of the reflected light. These properties are obtained from the phase of the amplitude reflection coefficient ρ defined in equation (16). The group delay τ_ρ of the reflected light as defined by Erdogan[1] is

$$\tau_\rho = d\theta_\rho/d\omega = -\lambda^2/2\pi c\ d\theta_\rho/d\lambda \quad (18)$$

where θ_ρ is the phase of the amplitude reflection coefficient. The dispersion d_ρ is defined as the rate of change of the group delay with wavelength as follows:

$$d_\rho= d\tau_\rho/d\lambda= 2\tau_\rho/\lambda - (\lambda^2/2\pi c.d^2\theta_\rho/d\lambda^2)= -2\pi c/\lambda^2.d^2\theta_\rho/d\omega^2 \quad (19)$$

To solve the coupled-mode equations to calculate the reflection, transmission and the delay properties we use transfer matrix method. The principle behind the transfer matrix method is to subdivide the grating structure into multiple uniform or non uniform sections and then identify each section using a 2-by-2 matrix. The information

contained in each matrix is specific to the section. The individual matrices are then successively multiplied along the length of the grating to describe the behaviour of the entire grating. The greatest advantage of this technique lies in its flexibility to be used for both uniform and non-uniform gratings.

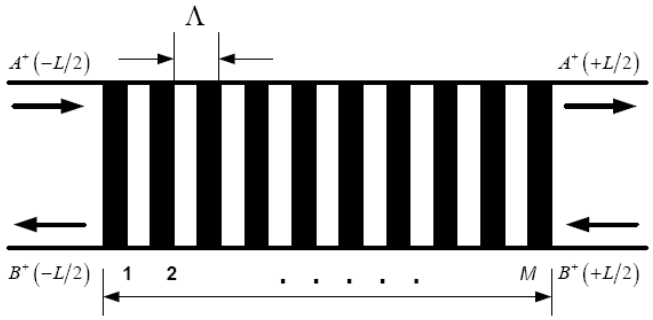

(a) Uniform grating

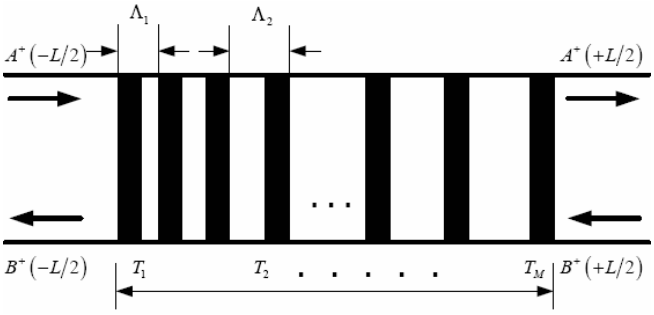

(b) Non-uniform grating

Figure 1 Illustration of grating simulation using the transfer matrix method

The first step in this approach is to divide the grating into M uniform or non-uniform matrix components with A_k^+ and B_k^+ being the field amplitudes after traversing section k . Here, the goal is to calculate the amplitude components of the final matrix $A_M^+=A^+(-L/2)$ and $B_M^+=B^+(-L/2)$. The propagation each of the sections k is described by a transfer matrix T_k expressed as follows:

$$(A_k^+/B_k^+) = T_k(A_{k-1}^+/B_{k-1}^+) \quad (20)$$

where the transfer matrix is T_k given by

$$T_k = \begin{vmatrix} \cosh(\gamma_B dz) - j(\sigma'/\gamma_B)\sinh(\gamma_B dz) & -j(\kappa/\gamma_B)\sinh(\gamma_B dz) \\ j(\kappa/\gamma_B)\sinh(\gamma_B dz) & \cosh(\gamma_B dz) + j(\sigma'/\gamma_B)\sinh(\gamma_B dz) \end{vmatrix} \quad (21)$$

Where $\gamma B = \sqrt{(\kappa^2 - \sigma'^2)}$ and dz is the length of *k* th uniform or non uniform section. Once the matrices of all the individual layers are known, the output amplitudes can be calculated from:

$$\begin{bmatrix} A_M^+ \\ B_M^+ \end{bmatrix} = T \begin{bmatrix} A_0^+ \\ B_0^+ \end{bmatrix}; \qquad T = T_M \cdot T_{M-1} \cdot \ldots \cdot T_k \cdot \ldots \cdot T_1 \quad (22)$$

The accuracy of the transfer matrix method depends on the number of uniform or non-uniform sections M used the analysis. A large value of M implies a higher accuracy. However M cannot be arbitrarily large. The choice of M must be such that the length of each uniform or non uniform section, dz is sufficiently larger than the grating period. By implication, M must satisfy:

$$M = 2n_{eff}L/\lambda_D \quad (23)$$

II. NUMERICAL SIMULATION RESULT

Based on couple mode equation above, we can makes numerical simulation by transfer matrix method to observe characteristics of light wave propagating in the uniform and non uniform FBG and what different between them with calculate the reflection, transmission, delay and dispersion properties.

We can simulate the reflectivity power over the length of uniform and non-uniform FBG, based on equation (17) using matrix method. The simulation will be executed with certain initial parameter:
λ_D=1.55e-6(design wavelength),λ_1=0.999λ_D and λ_1= 1.001λ_D as interval of wavelength in this simulation, R_{max}= 0.2 (required maximum reflectivity), c = 2.99793x10^8 (Speed of light), h = 25x10^{-9}, v = 1 (Fringe visibility), n*eff* = 1.47 (core index of photosensitive fibre), L = 1000x10^{-6} (length of grating in micrometers), M = 100, dz = L/M, □ = - L + (10.69x^{-3}) (Distance between gratings). All parameter above we use to simulate characteristic of uniform FBG, for non-uniform FBG we must design different dz and dzo for each grating section.

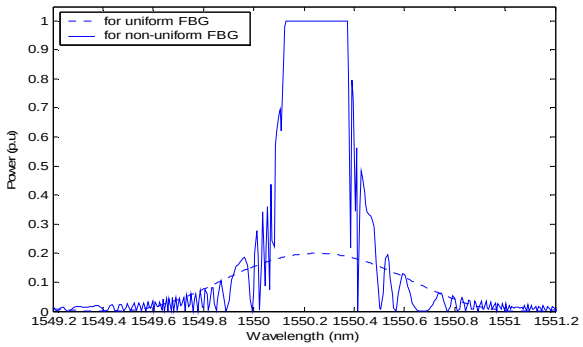

Figure 2 Comparison of reflection spectrum in the uniform and non-uniform Fiber Bragg Grating with same initial parameters.

Based on equation (17) and integrated numerically using transfer matrix method, Figure 2 show the maximum reflection spectrum in the uniform fiber bragg grating is 0.2 p.u from total input power 1 p.u. The interesting result of the non-uniform fiber bragg grating simulation is the phenomena as can be seen around the design wavelength 1550 nm, there is region as a photonic bandgap is formed,

that is a region in which no light is transmitted but is completely reflected. Outside this bandgap the reflectivity returns toward zero. Actually there are oscillations in the reflectivity. These oscillations are due to the finite size of the Bragg grating: the ideal infinite grating will exhibit a square like response.

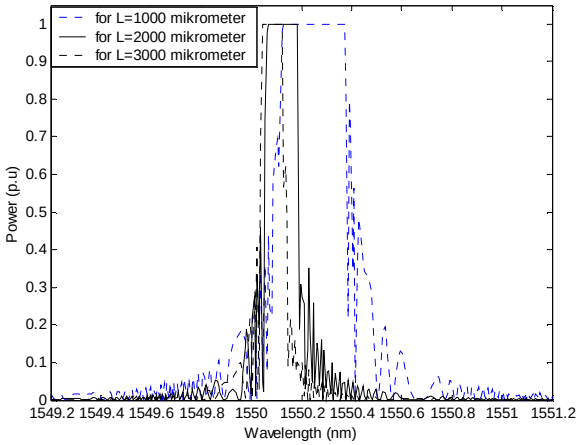

(a) Reflection spectra of non-uniform Bragg gratings of different lengths *L*, with reflectivity R = 0.2

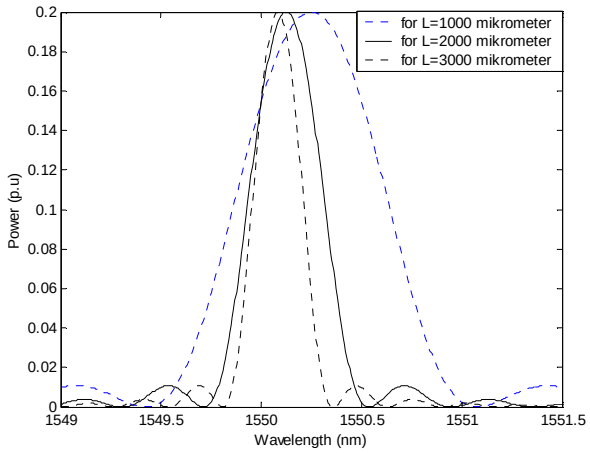

(b) Reflection spectra of uniform Bragg gratings of different lengths *L*, with reflectivity R = 0.2

Figure 3 Reflection spectra of non-uniform (a) and uniform (b) Bragg gratings with different length L.

The most significant feature of an fiber bragg gratings is the relatively narrow bandwidth of its reflection spectrum. In certain case where a wider bandwidth is needed, we need to modify the fiber bragg gratings. The best way to archieve this purpose is by using a short grating length in the design of the fiber bragg gratings. In figure 3 we can see the characteristic of non-uniform and uniform bragg gratings with different length where shorter length of the fiber bragg gratings will produce wider bandwidth, it mean that the bandwidth size is very sensitive to the grating length. Figure 3 also shows that for all the grating the peak reflectance is not equal in value to the design wavelength, there is a positive wavelength shift [1].

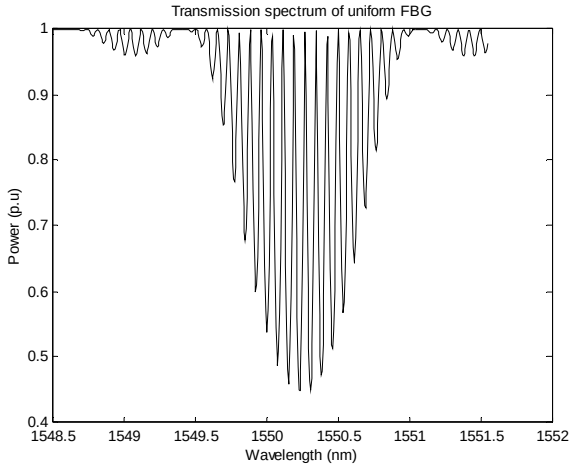

(a) Transmission spectra of uniform Bragg gratings

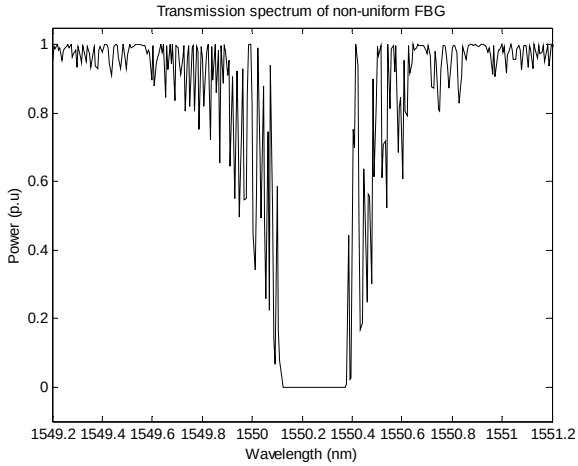

(b) Transmission spectra of non-uniform Bragg gratings

Figure 4 Transmission spectra of uniform (a) and non-uniform (b) Bragg gratings with length L= 1000 micrometer

We can see figure 4 to clarity the characteristic of uniform and non-uniform fiber bragg gratings. The transmission spectra show the minimum transmission spectrum in a region around the design wavelength for uniform bragg gratings is 0.2 p.u from total input power 1 p.u, and zero transmission in the same region for non-uniform bragg gratings simulation or completely reflected in this area.

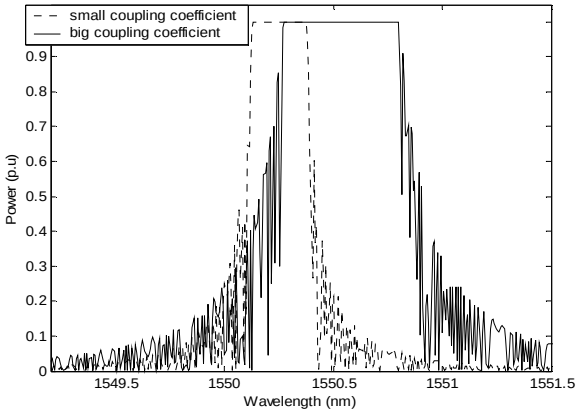

Figure 5 Reflection spectra of non-uniform Bragg gratings with length L= 1000 micrometer and different coupling coefisient

In figure 5 we look at what happens when changing the coupling coefficient, but keeping a length L such that the maximum reflectivity to be larger bandwidth.it men for small coupling coefficients the photonic bandgap is relatively narrow and for bigger coupling coefficient it is relatively wide.

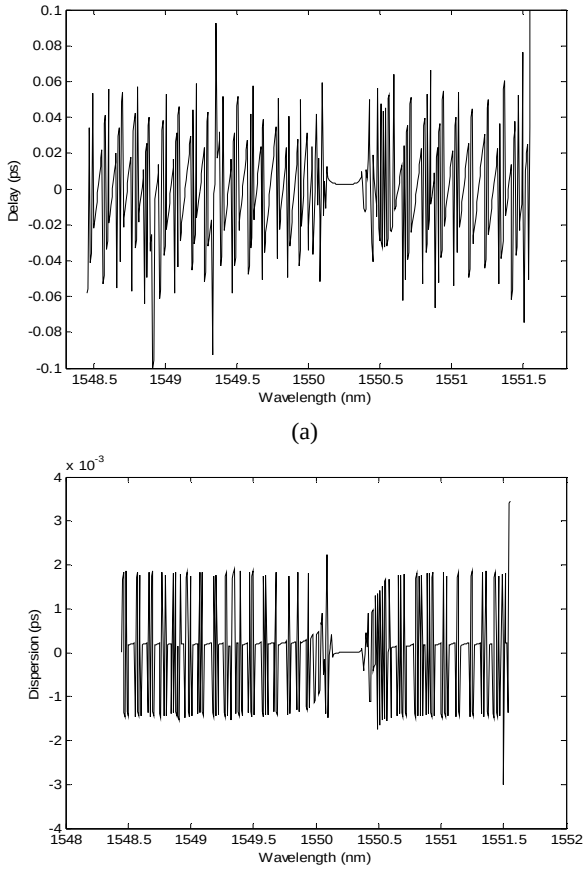

Figure 6 Delay (a) and dispersion (b) properties of non-uniform FBG with length L= 1000 micrometer

Based on equation (18) and (19) the delay and dispersion properties of reflected light in the non-uniform bragg gratings can we look at figure 6. The simulation show come about delay that almost same in every wavelength otherwise in the region of photonic bandgap or completely reflected area, where the delay in this area is zero. The dispersion (the rate of change of delay with wavelength) show that the light wave travel in the bragg gratings go through same mutation in every point otherwise in the photonic bandgap area. The delay and dispersion that happen in every point otherwise in the completely reflected area due to disparity of grating length along of the fiber bragg gratings.

IV. CONCLUSIONS

By couple mode theory and integrated numerically using Transfer Matrix method, we managed to show some characteristics of non-uniform fiber Bragg grating based on reflection, transmission, delay and dispersion properties. The interesting result of the non-uniform fiber bragg grating simulation is the phenomena as can be seen around the design wavelength 1550 nm, there is a region as a photonic bandgap is formed, that is a region in which no light is transmitted but is completely reflected, and the other characteristic of non-uniform bragg gratings is the sensitivity of bandwidth size to the grating length, where shorter length of the fiber bragg gratings will produce wider bandwidth. The other way to produce wider bandwidth but keeping a length L is by changing the coupling coefficient, where the bigger coupling oefficient will produce the wider bandwidth. The delay and dispersion was happen in every point otherwise in the completely reflected area due to disparity of grating length along of the fiber bragg gratings.

The transmission spectrum clarify establishment of photonic bandgap in the region around the design wavelength with zero transmission or completely reflected.

REFERENCES

[1] Erdogan T., "Fiber Grating Spectra", *Journal of Lightwave Technology*, vol. 15, no. 8, August 1997, pp. 1277 – 1294

[2] Kersey A.D., Davis M.A., Patrick H.J., Leblanc M., Koo K.P., Askins C.G., Putman M.A., Friebele E.J., "Fibre Bragg Grating Sensors", *Journal of Lightwave Technology*, vol. 15, no.8, 1997, pp. 1442 – 1463

[3] Ng W., Walston A.A., Tangonan G.L., Lee J.J., Newberg I.L. and Bernstein N., "The first demonstration of an optically steered microwave phased array antenna using true-time delay", *Journal of Lightwave Technology*, vol. 9, 1991, pp. 1124 – 1131

[4] Daniele Faccio, "A not very long introduction to Photonic Crystals", Chania, july 2006.

DNA-based Application Design for Secure-Mobile Network

Muhammad Suryanegara, *IEEE,* and Dadang Gunawan, *IEEE*

Wireless and Signal Processing Research Group (WASP)
Department of Electrical Engineering - Universitas Indonesia
Kampus UI Depok 16424, Depok – Indonesia
msurya@ee.ui.ac.id guna@eng.ui.ac.id

Abstract - **We propose DNA-based application design for secure-mobile network. The idea is to take benefit from user's DNA characteristic behave as unique identification. DNA-based application consists of 3 (three) main algorithm applied in mobile terminal, mobile network and database server. All DNA data will be formatted on IP-based information then might match 3G and B3G mobile wireless platform. Further analysis will be investigated to maintain noise immunity when DNA data passing through wireless channel. The development of DNA-based application will raise security level and user's trust when accessing any mobile application.**

Keywords : DNA, Security, Mobile network

I. INTRODUCTION

The needs of high level security platform has driven secure application to use *biometric characteristic* as main platform of validation and verification. Biometric characteristics are measurable physical or personal behavioral patterns used to recognize a human being [1]. The most common biometric characteristics used in major technical devices are, Fingerprint, Face, Iris, Voice and DNA. Compare with others, DNA biometric security platform is having the highest security performance, since its length of sequence guarantee personal uniqueness.

We propose design of DNA-based application for secure mobile network. The design consists of application stack, sequence diagram and proposed algorithm. It applies in 3 (three) main parts of wireless applications mainly : mobile terminal, mobile network, and database server of related application. Our work approaches 3G network platform then also can be developed toward B3G technology (all over IP).
The work is still on going research which has provided general design and pseudocodes of proposed algorithms.

II. SECURITY PLATFORM

A. Biometrics Platform

Biometric characters are measurable personal unique biological characters. They includes human *fingerprint, face, iris, voice, etc,* while the most promising biometric character is DNA (*Deoxyribonucleic Acid*).

Its uniqueness guarantee no character's duplications on earth. The replication possibility can be maintained to be zero, until thousands of human generation where duplications shall occur. Therefore, *biometric* character are commonly used for the basis of validity and verification of any secured application. In addition, many biometric researches are prominently developed, along with needs of high level security platform and significance growth of threat and fraud.

There are some advantages and disadvantages of *biometric characters.* For example, *fingerprint* is still the most popular *biometric character* used in digital devices. Its high level of trust and cheaper manufacturing cost are being main consideration. However, it has also disadvantage when taking into account *enrollment* process, which always requires clean user's finger.

In general, the increment of biometric reliability goes with complexity and manufacturing cost. In other side, needs of high level security platform not only required in complex system (such as in bank) but also in daily used application such as mobile cellular applications.

Based on reliability, *DNA* sequence is the most promising biometric character. The sequence guarantees no duplication because composed by around 3 billions series of (four) nucleotides characters. In addition, other *biometric character* are actually included in *DNA sequence,* since *DNA* is containing all data about the unique human (face pattern, ages, health condition, etc).

Most biometric's verfication procedure needs special user interface attached to application device. It is used to enroll user's biometric characteristic. DNA biometric platform also require special interface to read human's cell, such as from hair and nail. Therefore, utilization of DNA in secure applications face high barrier when touching technical aspect of user's interface. It needs high computation platform attached to application interface.

B. DNA-based application

A genome is the complete DNA complement of an organism, which contains the instructions controlling virtually everything about how the organism lives: development, metabolism, aging, sensitivity to infection, etc [2]. Advanced studies has also reveal the linkage between non-biological character (such as emotion) and DNA sequence pattern.

A DNA sequence is a string structure consisting of four nucleotide bases (A: *adenine*, C: *cytosine*, G: *guanine*, T: *tymine*). Every human cell contains 3,000,000,000 base pairs but only 6% can be used to synthesize protein, the rest 50% is a junk sequences . In DNA sequence, there are an estimated 20,000 - 25,000 human protein coding consists of *exon* which can be coded to protein, and *intron* which are not used in protein coding. Traditionally, identifying protein coding region can be done in biology laboratory. Because number of genes that must be identified is too large, developing protein coding is done by computer which saving time and reducing cost. Any method has been proposed to identifying coding region, e.g using HMM [3], filter and DFT.

In any digital application, genome potency is utilized by translating DNA-nucleotide series into digital format, called *DNA encoding*. Simple binary format can be used to represent 4 (four) nucleotides (A=00, T=01, G=10, C=11). Another recent methods is explained by Max H Garzon et al. Through simple binary format, a complete record of human DNA needs at least 6 Gigabit *storage* or c.a 750 MB. Hence, compression scheme is required, as proposed in [4]. Further process and modification to be done for matching general security purpose while advanced mathematic model shall be investigated in wireless platform.

III. DNA-BASED APPLICATION DESIGN

A. General Design

Figure 1 shows the DNA-based application stack in wireless environment. The principle of DNA-based is to be user's unique identification sign. DNA can be symbolized as DNA-print (image) or DNA-nucleotide sequence (series). In this paper, human's DNA uniqueness is measured based on nucleotide sequence, consists of 4 characters : A,T,G and C. The issue of wireless is on which *DNA* data (information) to be sent over channel. Design is taking into account wireless data format and error recovery performance considering noise channel. In proposed design we use 3G mobile as wireless platform.

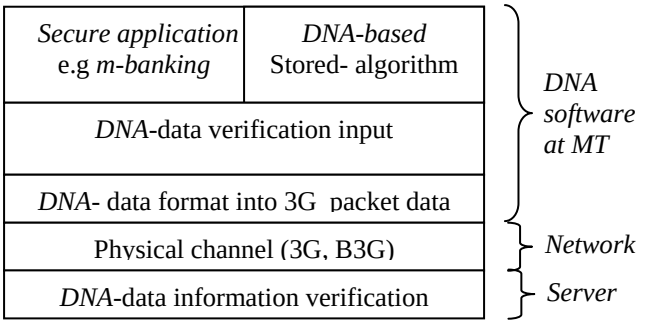

Figure 1. DNA-based application stack

The DNA-based application is developed in parallel with safety-required applications such *m-banking*. Both are embedded by using specific software development All *DNA* and information data (e.g transactions in *m-banking*) are formatted 3G packet data, as it will pass over wireless physical channel. Some modification is processed to match the data with 3G network platform.

B. Algorithms Development

As seen in Figure 1, application stacks are involving 3 main algorithms at *Mobile Terminal, Mobile Network* (channel), and *Database server*. Those are structured in Sequence diagram, depicted in Figure 2.

The scenarios are as following:

a. User input his/her DNA sequence through *Mobile Terminal* to be stored (recorded) in database server. In this case, server is on site of related applications, such as *bank* in m-banking service.
b. *DNA* sequence are formatted in 3G/B3G information data packet, sent through channel network. The analysis of *channel error* recovery will be investigated to guarantee DNA sequence correctness
c. Once data is stored, user's should verify him/herself by matching DNA-input (sample) to DNA-stored (template) in database, each time accessing the application. If verification succeed, user will be authenticated to do further access. In *m-banking* service, users will get access to start transaction after verified.

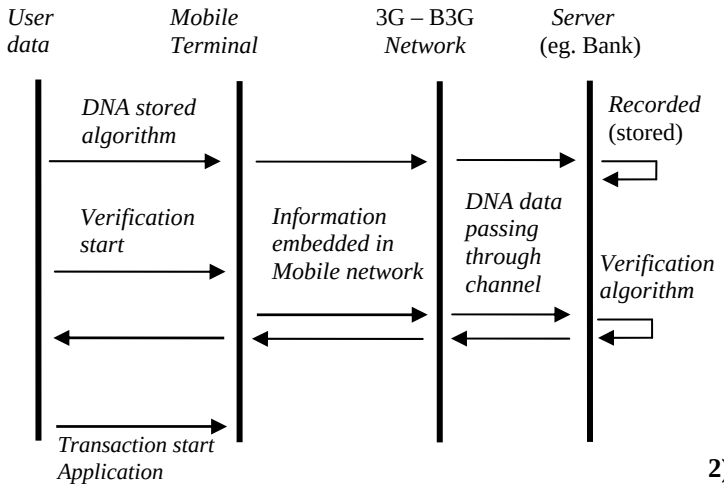

Figure 2. Sequence diagram of DNA-based application

The proposed algorithm are as follow :

1) DNA-stored algorithm at Mobile Terminal

DNA-stored algorithm is recording process of *DNA* sequence at *database Server*. The recorded data is used as *biometric* template data, primary used in verification. Following are proposed *pseudocodes* :

1. Declaring *DNA_stored* variable and initialization with user's DNA sequence at user's *Mobile Terminal.* The sequence can be image (*DNA-print*) or character string symbolizing nucleotides. In developing DNA-stored algorithm, we use simple DNA character string.

   DNA_stored (array) = *user_DNA_char* (series)
   example = [A T G G G C … C T A G A T C]

2. Translating *DNA_stored* to be digital format in 3G *Mobile Terminal*. Digitalization of DNA sequence are processed by encoding steps [5], transforming protein elements into binary digits.

   For example in simple DNA encoding, where
   A= [00] T= [01] G= [10] C= [11],

   the declaration and initialization variables are :
   DNA_digital(array) = *digitazing* (*DNA_stored*)
   DNA_digital(array) = *digitazing* (*A T G .. G C*)
   DNA_digital(array) = [00 01 10 ….. 10 11]

3. Compressing *DNA_digital* fitting database server capacity. Based on simple digitalization, DNA-sequence requires at least hundreds of Megabyte data. The compression purpose are also needed to reduce bandwidth transmission from *Mobile Terminal* to *database server*. Several methods [6] will be investigated to perform suitable compression of DNA. Grumbach et al, was the first who developed its compression. The declaration and initialization variables are :

   DNA_compress(array)=*compression*(*DNA_digital*)

   DNA_compress is final format of stored DNA sequence at database server.

2) Transmission over 3G/B3G networks

All *DNA* data will be formatted into IP-packet passing through mobile channel. As shown in Figure 2, application design stack is having 3G/B3G for its network platform. In physical layer, *DNA* sequence are regarded as digital data source encapsulated before passing through network. Error correction and detection scheme shall use applied method in 3G platform. Complete data encapsulation of 3G WCDMA Rel.99 and Rel.5 is presented in [7]. Figure 3 below showed DNA application running in 3G computer simulation.

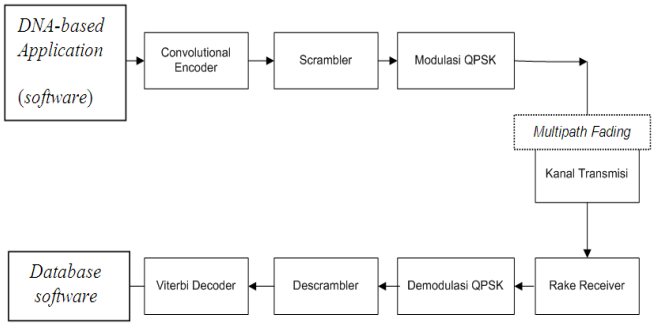

Figure 3. Block diagram of 3G and DNA application

Along with 3G, transmission are also set to match B3G scenarios, as some technologies has been recently developed. It includes IEEE 802.16 (WiMAX).

3) Verification algorithm at Database server

The verification aimed to verifying user as the right person who may access application in server. In biometric system, biometric template is the individual mathematic data set

calculated from user's biometric sample. For verifying, biometric systems need templates for comparison. [1]. Proposed design uses *DNA_compress* as template and *DNA_key* as user's biometric sample. Verification algorithm will result TRUE if *DNA_key* matched with *DNA_compress.*

However, for reducing complexity and increasing efficiency , we are developing CODIS-13-like algorithm to be used as the basis of verification algorithm. The algorithm will work by utilizing locus and genotype character, without using whole series of human DNA. At present, CODIS-13 is still efficient to determine human's uniqueness because doesn't require whole DNA series.

IV. PERSPECTIVE

We have proposed DNA-based application design, which status is on going research. Currently (up to September 2007) there is no conclusion at this stage, but our work will lead to a set of DNA-based algorithm for secure mobile applications. There is strong believe that DNA-based application will raise user's security trust when accessing mobile applications. Some limitations has been identified, primarily about access interface. For mapping human DNA, user needs to sample his/her biological DNA every time accessing application through additional biometric devices. At current technology stage, it will be very complex and won't be handy when embedded to mobile phone.

REFERENCES

[1] BITKOM, " German Biometric Strategic Platform Biometrics State of the Art, Industry Strategy Development, and Platform Conception : Study", Berlin, 2005.

[2] S. Saltzberg., "Gene Discovery in DNA Sequences", in IEEE Intelligent Systems, 1999, pp 44-48.

[3] C. Burge, Identification of Human Genes in Human Genomic DNA, Doctoral DisertationStanford, CA: Stanford University, 1997.

[4] Don Adjeroh, Yong Zhang, Amar Mukherjee, Matt Powell, Tim Bell, *DNA Sequence Compression Using the Burrows-Wheeler Transform*, West Virginia University, University of Central Florida, University of Canterbury

[5] Kamabe, H.; Seike, Y. "*On construction of codes for DNA computers*" Information Theory, 2003. Proceedings. IEEE Volume , Issue , 29 June-4 July 2003.

[6] Xin Chen; Kwong, S.; Ming Li "*A compression algorithm for DNA sequences*" IEEE Engineering in Medicine and Biology Magazine.

[7] Harri Holma, Antti Toskala, *WCDMA for UMTS: Radio Access for Third Generation Mobile Communications*, John Wiley and Sons, 2004.

ISSN: 1411-1284

A High Performance Wireless MIMO Communication System

Ahmad Taqwa[1,2], Soegijardjo Soegijoko[1], Sugihartono[1], and Suhartono Tjondronegoro[1].

[1]*Bandung Institute of Technology, Jalan Ganesa 10, Bandung 40132, Indonesia*
[2] *State Polytechnic of Sriwijaya, Jl. Srijayanegara, Palembang 30139, Indonesia*
Email: a_taqwa@yahoo.com

Abstract – **In this research we propose a closed-loop MIMO (Multiple-Input-Multiple-Output) system using transformation matrix in order to optimize capacity and to increase system performance. The grand scenario of this concept is the attained advantages of the transformation matrix, which is guaranteed by its derived analysis. First, transformation matrix can allocate transmitted signals power suit to the channel. Second, it can be manipulated in order to maximize the minimum-distance at the receiver. Finally, this transformation matrix can mitigate inter-channel correlation. Furthermore, computer simulations validates that our system at 0 dB SNR can reach optimal capacity up to 1 bps/Hz and SER up to 0,1 higher than opened-loop MIMO.**

Keywords– Capacity, CSI, fading, MIMO

I. INTRODUCTION

As known in wireless communication world, frequency bandwidth is limited and expensive. This is a challenge in providing broadband wireless communication services. In order to solve this problem we have to develop a bandwidth efficient system, which has high bit rate or capacity propagated through small enough frequency bandwidth. However, achieving higher bit rate and error-rate quality in the same time is sound impossible.

The main problem faced by wireless communication systems is channel-fading, which is in end-effect will decrease the system capacity and quality. There are several techniques proposed in order to mitigate this effect. One of the most significant technological developments of the last decade is MIMO using multiple antennas in input-output. With multiple antennas, diversity gain can be provided to counteract the destructive effect of fading and thus improve the performance significantly. What is especially exciting about the benefits offered by MIMO is that optimal capacity and high performance can be attained without additional frequency-spectral resource.

Deploying multiple antennas at the base station is an effective and promising solution to solve the challenge in providing broadband wireless communication services. Earlier studies in this area are focused on receive diversity since reverse-link capacity used to be considered as the bottleneck.

However, as highly asymmetrical services are ongoing to be introduced into wireless communication, improvement of forward-link performance is becoming the main challenge facing the effort toward next generation evolution. Transmit diversity is one of the key contributing technologies to address this problem. Common methods of transmit diversity employing spatially separated antennas reduce the impact of fading by offering multiple independent copies of the digitally modulated signals [13] and [17].

Depending on whether feedback information is utilized or not, transmit diversity schemes can be categorized as closed-loop or open-loop ones. Some open-loop transmit diversity techniques that are recently already introduced, include delay diversity [12], time switched transmit diversity [13], and orthogonal transmit diversity [16]. They can provide limited performance improvement but are practical to be implemented in current systems. In these schemes, the same information is transmitted through multiple antennas. Though partial or full spatial diversity can be achieved, either coherent receiver or additional resources (bandwidth, time or spreading codes) are required. Thus the overall efficiency of the system is very limited. Recently, a group of bandwidth effective transmits diversity schemes using open-loop methods in flat fading environments are proposed, which known as Bell lab layered space-time architecture (BLAST in [10] and [14]) and space-time trellis codes [15]. Compared with space-time trellis codes, BLAST has less complexity and higher spectral efficiency but poorer performance.

As abovementioned, both space-time trellis codes and BLAST operate in an open-loop, that is, without channel knowledge at the transmitter. Better performance can be expected provided when feedback information is utilized. In closed-loop schemes, CSI (channel state information) estimated by the receiver is fed back to the transmitter so that the base station can shape the transmission waveforms to maximize the SNR (signal-to-noise ratio) at the mobile. The well-known antenna beamforming [1], selective transmit diversity [11], and maximum ratio transmission [18] techniques are typical examples. Although their performance is usually considered as better than open-loop ones', higher system complexity

is needed and their success greatly depends on the quality of the channel estimates, the feedback delay, the dynamics of the signal and etc. Fortunately, in 3G standards, many of the proposed services are likely to be used in low-mobility environments under single-path conditions [17]. In such situation, precise CSI can be assumed to be available at the transmitter. Consequently it is necessary to investigate an effective closed-loop scheme in which both high spectral efficiency and best error performance can be achieved.

Motivated by this idea, we develop a closed-loop MIMO system using transformation matrix. The configuration of this system is similar to BLAST system. Design of linear transformation matrix is calculated based on water-pouring principle which is intended in order to maximize the channel capacity [2], [3], [7], and [9]. Furthermore, to achieve best performance of error probability, then maximum likelihood decision [4]-[5] with high minimum distance is adopted at the receiver. However, to fulfill this required performance we should assume that the channel is frequency non-selective (flat) and quasi-static.

In order to explore this new scheme deeper, so that the rest of the paper is organized as follow. In Section II, we introduce our channel model and the MIMO channel capacity. Moreover, the details of the capacity optimization and performance in several condition of channel will be described in Section III. After that, in Section IV we present simulation results of our proposed system compared to other MIMO systems. And finally, conclusion of this paper will be described in Section V.

II. BASIC THEORY OF MIMO CAPACITY

In figure 1, we consider single-user and point-to-point wireless communications system that consist of M_t antenna elements at the transmitter and M_r antenna elements at the receiver [8]. It is assumed that the channel has Rayleigh-, slow- or quasi-static-, and flat-fading. Then the input-output relation and other notations can be expressed as follow:

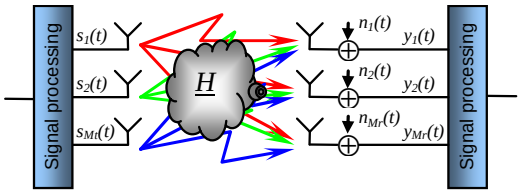

Fig. 1. MIMO configuration

- A modulated transmitted signal vector: $\underline{s} = [s_1, s_2, \ldots, s_{Mt}]^T$, and its covariance matrix is $\underline{R}_{ss}=E\{\underline{s}\,\underline{s}^H\}$.
- Received noise vector $\underline{n} = [n_1, n_2, \ldots, n_{Mr}]^T$ is a *Zero Mean Circularly Symmetric Complex Gaussian*[1] *(ZMCSCG)* with $\underline{R}_{nn}=E\{\underline{n}\ \underline{n}^H\}=N_o\ \underline{I}_{Mr}=\sigma^2\ \underline{I}_{Mr}$.
- A matrix of complex channel transfer is defined as $\underline{H}$.
- Received signal vector and input-output relation state:

$$\underline{y} = \sqrt{\frac{E_s}{M_t}}\,\underline{H}\cdot\underline{s}+\underline{n} = [y_1, y_2, \ldots, y_{Mr}]^T$$

- E_s is total average symbol energy.

In this MIMO system, maximum capacity is determined by *mutual information* between $\underline{s}$ and $\underline{y}$ vector, as $C = \underset{f(s)}{maks}\, I(\underline{s};\underline{y}) = H(\underline{y}) - H(\underline{y}|\underline{s})$. Wherein, $H(\bullet)$ is a notation for *differential entropy* of a vector, and $f(s)$ is probability distribution of $\underline{s}$. Because $\underline{s}$ and $\underline{n}$ vectors are independent, thus $H(\underline{y}|\underline{s})=H(\underline{n})$. Since differential entropy is defined as $H(\underline{y})=log_2(det(\pi e\underline{R}_{yy}))$ bps/Hz and $H(\underline{n}) = log_2(det(\pi e\underline{R}_{nn}))$ bps/Hz, thus we can form the general channel capacity as:

$$C = I(\underline{s};\underline{y}) = \max_{Tr(\underline{R}_{ss})=M_t} \log_2\left\{\det\left(\underline{I}_{M_r} + \frac{\rho}{M_t}\underline{H}\,\underline{R}_{ss}\,\underline{H}^H\right)\right\} \quad \ldots(1)$$

Wherein:

- C: Channel capacity [bps/Hz].
- $\underline{I}_{Mr}$: Identity matrix with size, M_r x M_r.
- $\underline{R}_{ss}$: Covariance matrix of transmitted symbol.
- ρ: Transmitted SNR.

It can be concluded from (1) that $\underline{R}_{ss}$ can be free arranged in order to optimize the capacity as long as it does not change the total transmitted power. On the other hand, the selected $\underline{R}_{ss}$ will yield optimal capacity if its chosen value can follow the channel condition such in closed-loop system in which the transmitter has knowledge of $\underline{H}$.

III. PROPOSED SYSTEM

A. Capacity Optimization

In order to optimize the capacity in (1) we propose to add transformation matrices in a closed-loop MIMO system as shown in fig. 2:

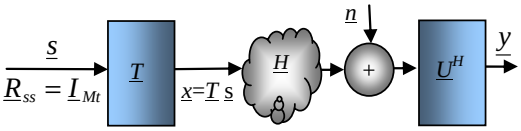

Fig. 2. MIMO with transformation matrix, $\underline{T}$

While $\underline{H}$ is known by transmitter, so the decomposition of a singular value of channel transfer matrix defined $\underline{H}=\underline{U}\ \underline{\Sigma}\ \underline{V}^H$ will result the capacity expression as in (2).

$$C = \log_2\left\{\det\left(\underline{I}_{M_r} + \frac{\rho}{M_t}\underline{\Sigma V}^H\,\underline{T}\,\underline{R}_{ss}\,\underline{T}^H\,\underline{V\Sigma}^H\right)\right\} \quad \ldots(2)$$

[1] A Gaussian random variable, Z=X+i*Y, is ZMCSCG if X and Y are i.i.d real Gaussian random variable with mean=0 and the same variance.

$$C = \log_2 \left\{ \det \left(\underline{I}_{M_r} + \frac{\rho}{M_t} \underline{\Sigma} \underline{K} \underline{\Sigma}^H \right) \right\}$$

Wherein matrix $\underline{U}$ with size of M_r x r and matrix $\underline{V}$ with size of Mt x r are unitary matrices, so that $\underline{U}^H\underline{U} = \underline{V}^H\underline{V} = \underline{I}_r$. While singular matrix expressed as $\underline{\Sigma} = diag\{\sigma_1, \sigma_{2,\ldots}, \sigma_r\}$, with $\sigma_i^2 = \lambda_i$ the-i^{th} eigen value of $\underline{H}\,\underline{H}^H$.

This result in (2) is the same as optimal formula introduced by Telatar [9]. In this case, capacity value is a function of γ_i that can be derived by *Lagrange* method, and follows with *water-pouring* algorithm [2]. After that, if we choose $\underline{V}^H\,\underline{T}\,\underline{R}_{ss}\,\underline{T}^H\,\underline{V} = diag(\gamma_1, \gamma_2, \ldots, \gamma_r) = \underline{K}$ and assume $\underline{R}_{ss} = \underline{I}_{Mt}$, so that the transformation matrix becomes $\underline{T} = \underline{V}\,\underline{K}^{1/2}$ following the power constraint $tr(\underline{R}_{xx}) = tr(\underline{R}_{ss}) = M_t$.

The grand scenario of this proposed method is that how this transformation matrix can also increase system performance, especially SNR and PEP. If $\underline{L}$ is unitary matrix that follows $\underline{L}\,\underline{L}^H = \underline{I}$, thus with a few manipulation matrix $\underline{T}$ becomes $\underline{T} = \underline{V}\,\underline{K}^{1/2}\underline{L}$. The addition of $\underline{L}$ is valid, because it still obeys the power constraint.

B. Received SNR

In [2] is described that this method can improve the received SNR of VBLAST. In view of the fact that $\Sigma_{Mr}\gamma_i\lambda_i > \Sigma_{Mr}\lambda_i$ so the received SNR:

$$SNR = \frac{E_s}{N_o Mt} \sum_{i=1}^{Mr} \lambda_i \gamma_i > SNR_{VBLAST} = \frac{E_s}{N_o Mt} \sum_{i=1}^{Mr} \lambda_i \quad \ldots(3)$$

Since higher SNR has superior signal power so that this can be the starting point to get a better error probability.

C. PEP (Pairwise Error Probability)

As defined by Tarokh [15] that probability, if $\underline{s}_1$ is sent and $\underline{s}_2$ is decided as received symbol, can be approximated with Chernoff bound as:

$$P(\underline{s}_1 \to \underline{s}_2 | \underline{H}') = Q\left(\sqrt{\frac{E_s}{2MtN_o} d^2(\underline{s}_1, \underline{s}_2)} \right) \le \exp\left(-\frac{E_s}{4M_t N_o} d^2(\underline{s}_1, \underline{s}_2) \right) \quad \ldots(4)$$

Where:

$$d^2(\underline{s}_1, \underline{s}_2) = \left\| \underline{H}'(\underline{s}_1 - \underline{s}_2) \right\|_F^2 = \left\| \underline{\Sigma} \underline{K}^{1/2} \underline{L}(\underline{s}_1 - \underline{s}_2) \right\|_F^2 \quad \ldots(5)$$

is the minimum distance of used signal code. From this equation we can conclude that optimal PEP can be achieved by setting the best value of $\underline{L}$ in order maximizing the minimum distance.

D. Maximizing the Minimum Distance

There are various values of unitary matrix $\underline{L}$ that can maximize the minimum distance. One grand scenario is through decomposition of transmitted signal-pair, $\underline{s}_1$-$\underline{s}_2 = \underline{U}_{ss}\,\underline{\Sigma}_{ss}\,\underline{V}_{ss}^H$. Where $\underline{U}_{ss}$ and $\underline{V}_{ss}$ are unitary matrices and have the relation $\underline{U}_{ss}^H\underline{U}_{ss} = \underline{V}_{ss}^H\underline{V}_{ss} = \underline{I}_M$. In view of the fact that singular value $\underline{\Sigma}_{ss}$ is real-positive, and $\underline{L}$ is chosen equal $\underline{U}_{ss}^H$, then the minimum distance in (5) becomes $d^2(\underline{s}_1,\underline{s}_2) = \| \underline{\Sigma}\,\underline{K}^{1/2}\,\underline{\Sigma}_{ss}\,\underline{V}_{ss}^H \|_F^2 = tr(\underline{\Sigma}\,\underline{K}^{1/2}\,\underline{\Sigma}_{ss}\,\underline{\Sigma}_{ss}^H\,\underline{K}^{1/2H}\,\underline{\Sigma}^H)$.

IV. SIMULATION RESULTS

Figure 3 presents a visualization proof of (1) and (2) as the result of capacity simulation as a function of SNR. The illustrations show us that the MIMO systems with CSI at the transmitter always have higher capacity than the MIMO without CSI. Moreover, the 10% outage capacity of MIMO with CSI reaches up to 1 bps/Hz higher than without CSI at SNR 0 dB.

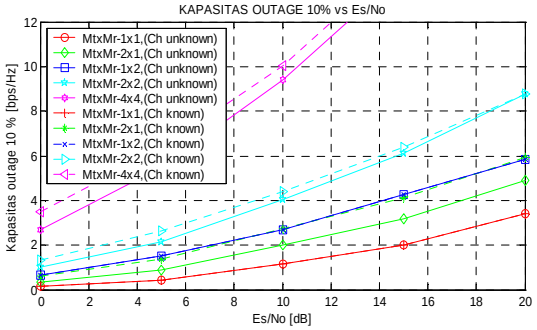

Fig. 3. Outage Capacity of several MIMO system

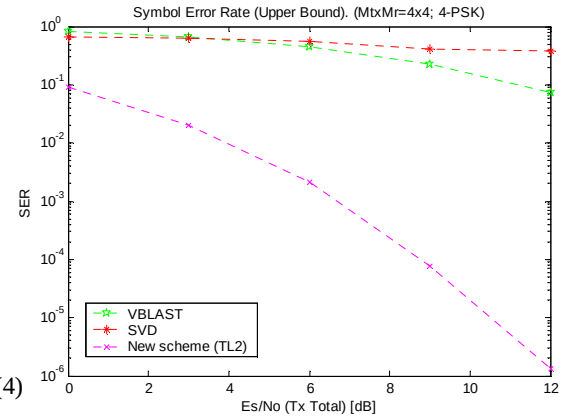

Fig. 4. SER upper bound of MIMO

On the other hand, Figure 4 illustrates SER upper bound of MIMO with CSI (for SVD and the new scheme) and MIMO without CSI (for VBLAST) versus SNR. Because this proposed method showed by (5) has higher value of minimum distance, so that SER becomes improved. Even at SNR of 0 dB our new scheme still superior than other scheme up to 1 symbol error in every 10 received symbols.

Unfortunately, the receiver of this new scheme is still complex and needs additional processing time in estimating the transmitted signal. Therefore, forthcoming we have to investigate a new simpler detector which has started in [4] and [5].

V. CONCLUSIONS

Using transformation matrix, our proposed system will achieve the same high capacity as the system developed by Telatar which is proved by (2). In addition, this system has enhanced average received SNR compared to open-loop MIMO such V-BLAST. This condition can be achieved because this system gives more transmission power effectively allocated into channel as stated in (3) according to water-pouring concept. Moreover, the covariance of $\underline{R}_{ss} = \underline{I}_{Mt}$ which is more natural and easier to realize at the transmitter makes this system able to be used with general signal code. But in selecting special code, we have to be careful in defining matrix $\underline{L}$, since each code has different value of $\underline{S}_1$-$\underline{S}_2$. However, if we can fit the value of $\underline{L}$ as stated in (5), our system will offer better SER.

Finally, its capability in order to maximize PEP declared in (4) as our grand scenario, will give this proposed system place in application for high speed wireless communication system. Nevertheless, the calculation of $\underline{L}$ via simulation currently still has high complexities at the receiver, especially for high M_t and M_r. Therefore our forthcoming research in order to develop a simple algorithm in finding $\underline{L}$ is offered to the reader.

Table. 1. MIMO Capacity and Performance Comparison.

Parameters	**VBLAST** Unknown CH	**SVD** Known CH	**New Scheme** Known CH
Capacity	*	*****	*****
SNR	*	*****	*****
SER	*	***	*****

REFERENCES

[1] A. F. Naguib, A. Paulraj and T. Kailath, “Capacity improvement with base-station antenna arrays in cellular CDMA”, IEE Trans. Veh. Technol., vol. 43, no. 3, pp. 691-698, Aug. 1994.

[2] A. Taqwa, Soegijardjo Soegijoko, Sugihartono, and Suhartono Tjondronegoro, "Capacity and Performance Optimization Techniques in Closed-loop MIMO Transmission Systems Using Transformation Matrix", in proc. of TSSA-WSSA, Bandung, 2006.

[3] A. Taqwa, Soegijardjo Soegijoko, Sugihartono, and Suhartono Tjondronegoro, "A High Speed Wireless MIMO Communication Systems Using Transformation Matrix", in proc. of ICEEI, Bandung, 2007.

[4] A. Taqwa, Soegijardjo Soegijoko, Sugihartono, and Suhartono Tjondronegoro, "Naturalization of Transmitted Signal Covariance of Wireless MIMO Systems for Capacity Optimization", in proc. of SITIA, Surabaya, 2007.

[5] A. Taqwa, Soegijardjo Soegijoko, Sugihartono, and Suhartono Tjondronegoro, "Simple ML Detector for Wireless Communication MIMO Systems with Singular Channel, in proc. of SITIA, Surabaya, 2007.

[6] A. Taqwa, Soegijardjo Soegijoko, Sugihartono, and Suhartono Tjondronegoro, "Ergodic and Outage Channel Capacity Comparison for Wireless Channel MIMO in Certain Condition of CSI", in proc. of EECCIS, Malang, 2006.

[7] C. Shen, L. Dai, S. Zhou, *and* Y. Yao, " A Novel Bandwidth Efficient Transmit Diversity Scheme Based on Water-filling ", State Key Lab on Microwave & Digital Communications Tsinghua University, Beijing, 100084

[8] D. Gesbert, H. Bolcskei, D. Gore, and A. Paulraj, "Outdoor MIMO Wireless Channels: Models and Performance Prediction", IEEE Trans. Commun., Dec. 2002.

[9] E. Telatar, "Capacity of multi-antenna Gaussian channels", AT&T Bell Labs Internal Tech. Memo, 1995.

[10] G. J. Foschini, “Layered space-time architecture for wireless communication in a fading environment when using multi-element antennas”, Bell Labs Tech. J., vol. 1, no. 2, pp. 41-59, Aut. 1996.

[11] H. Furukawa, K. Hamabe, and A. Ushirokawa, “SSDT--Site selection diversity transmission power control for CDMA forward link”, IEEE Journal on Selected Areas in Communications, vol. 18, no. 8, pp. 1546-1554, Aug. 2000.

[12] J. H. Winters, “The diversity gain of transmit diversity in wireless systems with Rayleigh fading”, IEEE Trans. Veh. Technol., vol. 47, no. 1, pp. 119-123, Feb. 1998.

[13] J. S. Thompson, P. M. Grant, and B. Mulgrew, “Downlink transmit diversity schemes for CDMA networks”, IEE Proceedings: Communications, vol. 147, no. 6, pp. 371-380, Dec. 2000.

[14] P. W. Wolniansky, G. J. Foschini, G. D. Golden and R. A. Valenzuela, “V-BLAST: an architecture for realizing very high data rates over the rich-scattering wireless channel”, in Proc. ISSSE’98, Pisa, Italy, pp. 295-300, 1998.

[15] V. Tarokh, N. Seshadri and A. R. Calderbank, “Space-time codes for high data rate wireless communication: Performance criterion and code construction”, IEEE Trans. Inf. Theory, vol. 44, no. 2, pp. 744-765, March 1998.

[16] V. Weerackody, “Diversity for the direct-sequence spectrum system using multiple transmit antennas”, in Proc. ICC’93, Geneva, Switzerland, pp. 1775-1779, 1993.

[17] R. T. Derryberry, S. D. Gray, D. M. Ionescu, G. Mandyam, and B. Raghothaman, “Transmit diversity in 3G CDMA systems”, Communication Magazine, vol. 40, no. 4, pp. 68-75, Apr. 2002.

[18] T. K. Y. Lo, “Maximum ratio transmission”, IEEE Trans. Commun., vol. 47, no. 10, pp. 1458-1461, Oct. 1999.

The Development of DSP Algorithm for *Virtual Surround Sound* using TMS320 C6713 DSK

Fajar Dwi Satyo, Muhammad Suryanegara, *IEEE,* Dadang Gunawan, *IEEE*

Wireless Signal Processing Research Group (WASP) – Department of Electrical Engineering
Universitas Indonesia - Kampus UI – Depok 16424 - Indonesia
Email : msurya@ee.ui.ac.id, guna@eng.ui.ac.id

Abstract - **This paper reviews a construction of DSP algorithm to implement virtual surround sound application. In analog system, its application was develop based on Head-Related Transfer Function (HRTF), while in digital design we used FIR and IIR digital filters. DSP algorithm is implemented in TMS320C6713 DSK programmed by CCS software. Our results are compared to HRTF characteristic generated by traditional computational method. The analysis shows that the virtual surround sound application can be implemented in DSP process. The applications works well in the frequency range from 0 to 4 kHz, and the characteristics of the results are similar to the traditional computational HRTF characteristics**

Keywords– Virtual Surroun Sound, HRTF, TMS320 C6713

I. INTRODUCTION

Digital Signal Processing (DSP) is today become the basis of any digital device [1]. Its premier ability to do fast computation behaves as primary advantages [1][2]. Inputs are processed by certain algorithm, producing output signals. DSP algorithm development is main key in order to fit in expected requirements. One of device to help building algorithm is DSP *Starter Kit* (DSK board) TMS320C6713. It may help developer or engineer to do real testing of the algorithm [2]

DSP technology includes worlds of audio and music, applied in its main processor [3]. One of the application in audio and music is the virtual surround sound application. *Virtual surround sound* is application to enhance sound quality of stereo speaker become as if a surround one. Traditionally, it was built by computing an algorithm called *Head-Related Transfer Function* (HRTF). This method is finding a numeric characteristic of output sound which is the same as *surround sound* character.

We review a construction of DSP algorithm to implement virtual surround sound application. Algorithm works on the basis of digital filters operations in 3 (three) sub-band frequency. It is implemented in DSP Starter Kit TMS320C6713, programmed with *Code Composer Studio* and working on frequency range 0 – 4 kHz.

Analysis shows that the virtual surround sound application can be digitally implemented using the TMS320C6713 DSK. The applications works well in the frequency range from 0 to 4 kHz, and the characteristics of the results are similar to the traditional computational HRTF characteristics in [4].

II. VIRTUAL SURROUND SOUND

A. Surround Sound

Principally, *surround sound* is scheme of speaker's position to produce a 3-D sound effect [5]. It is formed by several speakers working in certain frequency range, for example *surround sound* 5.1 means a structure of 5 (five) *speakers* working in high and middle frequency range, completed by by 1 (one) low frequency speaker.

Through analog and digital technology, *surround sound* can be attached to any home appliance, from PC to home theater. However, it make device coming with numbers of speakers. Speaker's requirements become a hinder when *surround sound* to be applied in small devices, such as *MP3 player* and *Handphone.* Device needs specific method in order to build surround sound effect through limited number of speakers, that is *Virtual surround sound*. The algorithm is applied in a *transfer function* called *Head-Related Transfer Function* (HRTF).

B. Head Related Transfer Function (HRTF)

The concept of HRTF is by analysing sound intensity which is heared by right and left human ears. [6]. Algorithm is developed by constructing a *transfer function* representing the values of those intensities. Spectrum of ear-receiving sound depends on factors of distance, angle, and transfer medium from source to ear [6]. On the other hand, human's ear perception also related to head-diameter, ear-surface, and shoulder factors. Those are formed into transfer functions for *left* ear and *right* ear. Equations (1) and (2) showing transfer functions for *HR* (right head) and *HL* (*left head*) :

$$H_R(\omega,\theta) = \frac{1 + j2\alpha\omega\tau}{1 + j\omega\tau} e^{-j\omega T_R} \quad (1)$$

$$H_L(\omega,\theta) = \frac{1 + j2(1-\alpha)\omega\tau}{1 + j\omega\tau} e^{-j\omega T_L} \quad (2)$$

$$\alpha = \frac{1}{2}(1 + \sin\theta) \quad (3)$$

$$\tau = \frac{1}{2}(a/c) \quad (4)$$

Where a is distance from source of sound to human's ears and c is sounds' velocity.

$$T_R = (1-\alpha)\tau \quad (5)$$

$$T_L = (\alpha\tau) \quad (6)$$

From (1) and (2), we obtained intensities in dB :

$$A_R = 20 \log |H_R| \quad (7)$$

$$A_L = 20 \log |H_L| \quad (8)$$

HRTF implementatios is mostly popular in analog devices. In this paper, we designed virtual surround sound through DSP approach. The basic idea is to build a DSP algorithm which produces sound characteristic that is the same as HRTF one. DSP algorithm is working based on 3 (three) divisions of *high, middle,* and *low frequency,* and constructed by FIR and IIR filters [6]. For doing implementation and measurement in Digital Signal Processor, we used TMS320C6713 DSP Starter Kit produced by Texas Instrument.

The HRTF characteristic is taken from [4], which computed a comparison between input and output signal power in conventional surround sound. Figure 1 showed HRTF characteristic in a frequency range between 100 – 4000 Hz [4]. The data were measured in *left* and *right* ears. Since HRTF was conventionally produced in analog system, its characteristics can be generated by numbers of digital filers. By dividing frequency range into 3 (three) sub-*band,* low and middle frequency have flat intensity while high band has fluctuative change.

III. DSP ALGORITHM FOR VIRTUAL SURROUND SOUND

A. Band Frequency design

In order to match HRTF characteristic, DSP algorithm is working on 3 (three) sub-band frequency (*low, high* and *middle*) which are functions of HRTF determined-factors : head-diameter, ear-surface, etc. Low frequency received in human's ear is determined by head's diameter (typically *d1*=150-1200 mm) and sound velocity (v=340m/s), where fc_1 = v/2(d1)= 850-1100 Hz. In this work, we used low frequency band fc_1 = 1100 Hz.

High frequency received in human's ear is determined by ear surface area (typically *d2*=3.5-5.5 cm) and sound velocity (v=340m/s), where fc_1 = v/2(d2)= 3000-5000 Hz. Since human's voice is always less than 4000 Hz, we used high frequency band fc_2 = 3000 Hz. The last division is middle frequency which is a value between low (fc_{31} = 1100 Hz) and high band (fc_{32} = 3000 Hz).

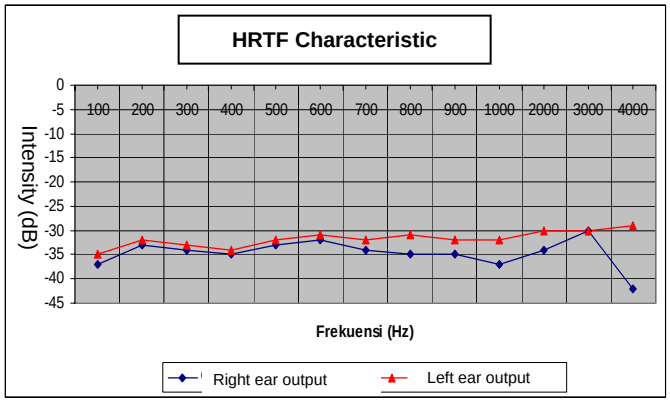

Figure 1. HRTF Characteristic [4]

Based on 3 (three) frequency divisions, we built a DSP design (algorithm) constructed in Figure 2. The algorithm is programmed in TMS320C6713 DSK using *Code composer studio*.

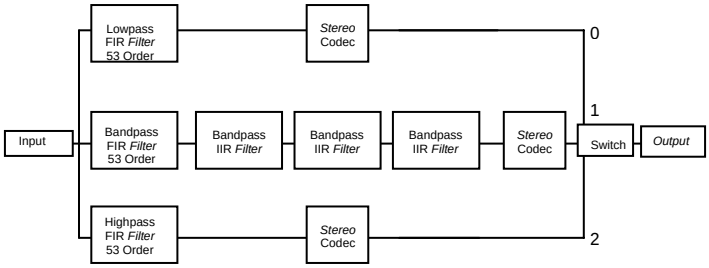

Figure 2. Construction of DSP algorithm

As seen in Figure 2, middle frequency band used 3 (three) *bandpass* IIR *filter*. This is to make our design matching conventional design in [4] which used 3 (three) *Parametric Equalizer* (PEQ). For minimizing DSK memory usage, our design doesn't install IIR filter in low and high frequency band.

Numbers of IIR filter has purpose to represent PEQ (as used in [4]) in middle frequency-band. This is preferred to maintain

efficiency because this band contains most human sounds, especially vocal voice.

B. Digital Filter Design

The filters parameters are designed using *FDA Tool* in MATLAB. Numbers of coefficients (*N*) affects performance of DSK TMS320C6713, therefore we prefers digital filters *FIR window-Hamming* and *IIR Chebyshec Type II*. Table 1 showed filter specification after computation.

TABLE 1
FILTER SPECIFICATION

Filter	***fs* (*Hz*)**	***Transition width***	***Cutoff***	***N***
FIR Lowpass	8000	500 Hz	*fc1* = 1100 Hz	53
FIR highpass	8000	500 Hz	*fc2*= 3000 Hz	53
FIR bandpass	8000	500 Hz	*fc*31 = 1100 Hz *fc*32 = 3000 Hz	53
IIR bandpass	8000	500 Hz	*fstop1* = 600 *fpass1* = 1100 *fpass2* = 3000 *fstop2* = 3500 *Astop1* = 60 dB *Apass1=1 dB* *Astop2=80 dB*	16

Figure 3, 4, 5 and 6 show filter's spectrums as specified in Table 1.

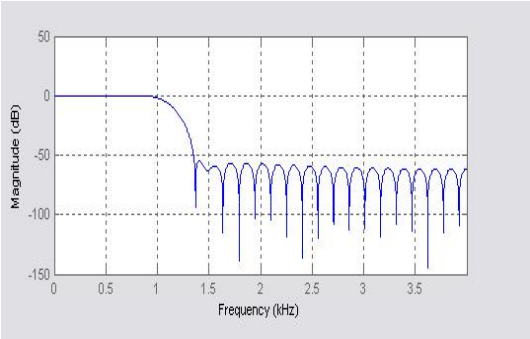

Figure 3. FIR *Lowpass Filter* spectrum

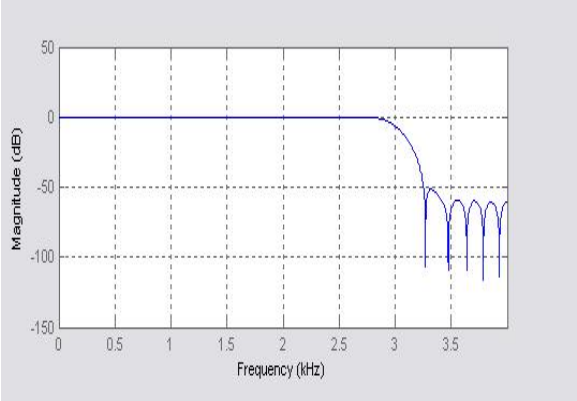

Figure 4. *FIR Highpass filter*

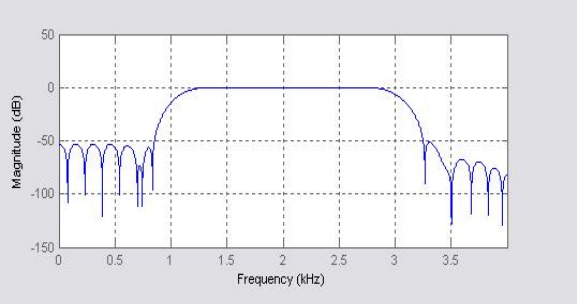

Figure 5. FIR *Bandpass Filter*

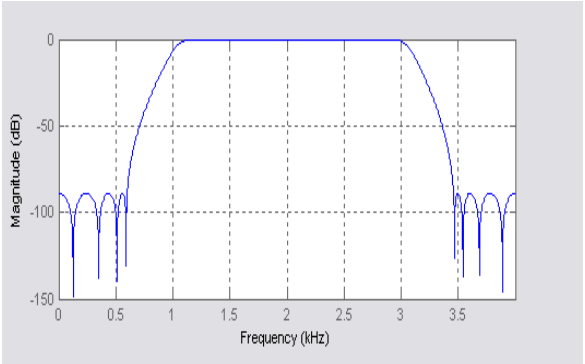

Figure 6. IIR *Bandpass Filter*

IV. RESULTS

DSP algorithm is computed using TMS320C6713 DSK where measurement specifications are set similar to [4]. In order to identify its *Virtual Surround Sound* performance, DSP output results are compared to HRTF characteristic in Figure 1. Output data are taken from measurement in right and left ears measurement of which $\theta = 45^0$. Figure 7 and Figure 8 show output characteristic for both measurements.

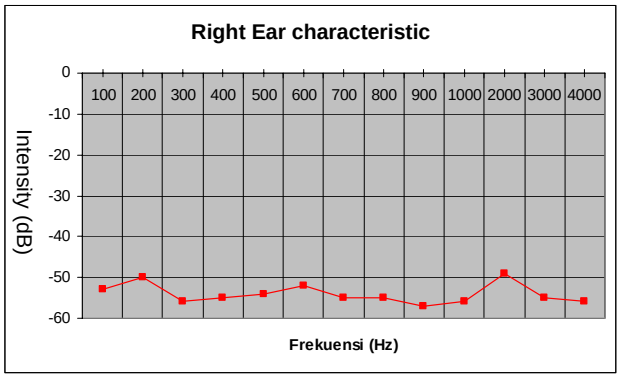

Figure 7. DSP output characteristic in right ear measurement

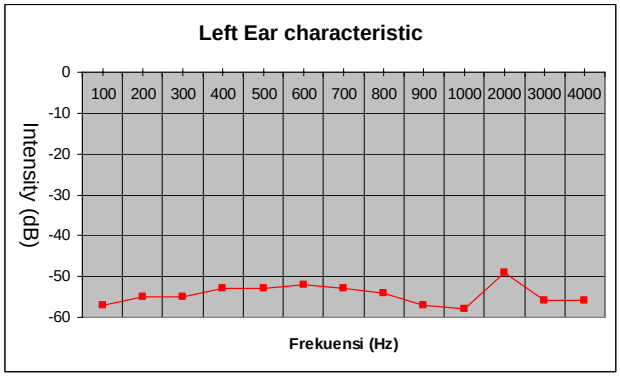

Figure 8. DSP output characteristic in left ear measurement

By comparing Figure 7, Figure 8 and Figure 1, we evaluated general tendency that DSP output are matching to HRTF characteristic computed in [4]. The climbing and decaying of both lines are more-less similar. There are significant differences of sound intensity between *DSP output* and *HRTF characteristic*. They are due to gain factors of sound devices, hence not affecting primary performance of its virtual surround sound. It can be concluded that graphs similarity means virtual surround sound application can be digitally implemented using TMS320C6713 DSK. Furthermore, it may be developed into any DSP appliances.

Data are measured in frequency range between 0 – 4000 Hz. In ideal computation, sampling frequency can be set to be 128 KHz. Our measurements use sampling frequency 8 kHz, due to noise occurance in TMS320C6713 DSK as limited by buffer memory condition.

V. CONCLUSION

We have reviewed construction of *Virtual Surround Sound* using DSP Starter Kit TMS320C6713. The analysis shows that application can be implemented in DSP process and works well in frequency range 0- 4000 Hz. The output results are similar to the traditional computational HRTF characteristics

VI. REFERENCES

[1] Ifeachor, E.C. and Jervis, B.K., ”Digital Signal Processing”, Prentice Hall Second Edition, 2001

[2] Chassaing, R. “Digital Signal Processing and Applications with the C6713 and C6416 DSK”, Wiley and Sons,New Jersey, 2005

[3] Hyoun-Suk Kim, Poong-Min Kim, and Hyun Bin Kim.” Cross-talk Cancellation Algorithm for 3D Sound Reproduction”, ETRI Journal, Volume 22, Number 2,June 2000

[4] Sakamoto, N., Kobayashi, T., Onoyettt, T. and Shirakawat, I.”DSP Implementation of Low Localization Algorithm Computational 3D Sound”, Dept. Information Systems Engineering, Osaka University, 2001.

[5] Tonnesen, C. and Steinmetz, J “3D Sound Synthesis”, Human Interface Technology Laboratory, 2001

[6] Dude. R.O “Modeling Head Related Transfer Functions”, Department of Electrical Engineering, San Jose University, 1993

Evaluation of Indoor HSDPA Performance Applying FEC Turbo Code

Muhammad Suryanegara and Moh. Harry Prabowo

Wireless and Signal Processing Research Group (WASP)
Department of Electrical Engineering - Universitas Indonesia
Kampus UI Depok 16424, Depok – Indonesia

***Abstract* - There are several factors determining throughput in HSDPA (High Speed Downlink Packet Access) measured in mobile terminal side. Those primary ones are terminal's capability, propagation and error code performance. Starting from 3rd generation mobile technology, Turbo Code is chosen as ideal FEC (Forward Error Correction) scheme offering minimum error rate at wireless environment. This paper evaluates HSDPA performance in indoor propagation model (office building) by varying prominent turbo code parameters. Evaluation was also running on simulation on several HSDPA basic parameters scenarios.**

Keywords : HSDPA, Turbo Code

I. INTRODUCTION

3G-WCDMA cellular system has not given satisfaction performance when accessing data application, expecially for video streaming, web browsing, and downloading music/game. In order to solve that limitations, 3GPP has released UMTS Rel 5 HSDPA (*High Speed Dowlink Packet Access*) has known as 3.5 Generation [1]. In parallel, by several years ahead, indoor multimedia demands will increases. Some technologies, such as WiFi offered high bitrate but not very high mobility. It is believed that by improving performance of HSDPA could be optimum solution for indoor mobile access.

HSDPA applies Turbo Code as FEC component. Turbo Code gives significant influence that may increase transfer rate without increasing the power. However, some weaknesses are high latency and complexity of decoder. This paper evaluates HSDPA performance in indoor propagation model (office building) by varying prominent turbo code parameters. Evaluation was also running on simulation on several HSDPA basic parameters scenarios.

By varying HSDPA basic parameters, the results show that HSDPA throughput was linear to number of information bits in block transport, number of allocated HS-DSCH code and inter-TTI interval value. By varying turbo code parameters, HSDPA gives lower error rate on numbers of iteration. It gives minimum HARQ transmission which leads to higher bit rate. However it gives another consequence that time-delay is increased which is not good for advance real-time applications.

II. HIGH SPEED DOWNLINK PACKET ACCESS

A. HSDPA

Basically there are 3 (three) main features in HSDPA which gives higher transmission rate. They are :

1. Fast Link Adaptation
In HSDPA, Adaptive Modulation Coding (AMC) uses 16-QAM and QPSK with *coding rate* ¼ - ¾. Because of AMC, *Spreading Factor* (SF) won't be varied and fast control power is not used. The formation AMC depends on *Channel Quality Indicator* (CQI)

2. Fast Retransmission
This scheme is done by *Hybrid Automatic Repeat reQuest* (HARQ) and soft combining. Through this feature, User Equipment (UE) will save the data to *soft memory*. When decoding fails, retransmission data will be combined with data in *soft memory* before decoding process. This method can improve diversity gain and decoding efficiency.

3. Fast Scheduling
Scheduling package was done in the basis of 2 ms. Therefore, HSDPA has *Transmission Time Interval* (TTI) or *interleaving* shorter than WCDMA (10,20,40, atau 80 ms).

For supporting those features, HSDPA was developed by adding some new channels, they are:

1.High Speed Downlink Shared Channel(HS-DSCH)
This channel was used by UEs for transmitting their data packages. Different to DSCH in WCDMA, HSDPA set constant *SF* to be 16. Features of AMC, HARQ, TTI 2ms, and maximum of 15 multicodes are used in parallel by HS-DSCH. Since they are

applied parallel, user's throughput depends on numbers and application accessed by another user.

2. High Speed Shared Control Channel (HS-SCCH)
This channel has fuction for signalling between Node B and UE. It carries key information needed for HS-DSCH demodulation process.

3.High Speed Dedicated Physical Control Channel (HS-DPCCH)
HS-DPCCH works on *uplink channel*. This channel has function for carriying ACK/NACK information on physical layer and delivers CQI information transmitted to Node B [1].

B. Indoor Propagation Model

This model estimates path loss in a room or closed area which is limited by various forms of the wall. Suitable for designing indoor, this model estimate all path loss in a room. Equation (1) was used to count pathloss on ITU propagation model

$$L = 20 \log f + \mathrm{N} \log d + Pf(n) - 28 \qquad (1)$$

Where :
L : *Path loss* (dB)
f : transmission frequency (MHz)
d : distance (m)
N : *distance power loss* coefficient
n : Amount of floor between transmitter antenna and receiver
$Pf(n)$: factor of *floor loss penetration*

Several values of N were determined based on frequency band, showing in Table 1.

Table 1 *Distance power loss coefficient* [2]

Frequency Band	Residential Area	Office Area	Commercial Area
900 MHz	N/A	33	20
1.2 GHz	N/A	32	22
1.3 GHz	N/A	32	22
1.8 GHz	28	30	22
4 GHz	N/A	28	22

Floor loss penetration factor depends on numbers of floor and transmission frequency. Those values are listed in Table 2.

C.Turbo Code

Turbo code improves transfer rate without increasing transmission power [3]. A weakness turbo code are high latency and complexity of decoder. If numbers of turbo code iteration is increases, performance will increase, but time delay also will be longer. The performance key of turbo code scheme is its decoding process. An analogy of its process is finding solution in puzzle. First decoder operates on vertical line (bit parity), and second decoder operates on horizontal line. In first iteration, both decoders are cutting off the answers then exchanging them to know the differences. This process are iterated until both decoder get a complete answer. The implementation of max* operators are significant in turbo decoding scheme. There are four MAP algorithm version, log-MAP, max-log-MAP, constan-log-MAP, and linier-log-MAP [4].

Table 2 Floor penetration loss factor [2]

Frequency Band	Number of Floors	Residential Area	Office Area	Commercial Area
900 MHz	1	N/A	9	N/A
900 MHz	2	N/A	19	N/A
900 MHz	3	N/A	24	N/A
1.8 GHz	n	4n	15+4(n-1)	6 + 3(n-1)
2.0 GHz	n	4n	15+4(n-1)	6 + 3(n-1)
5.2 GHz	1	N/A	16	N/A

III. SCENARIOS

In common HSDPA testing models, 3GPP Rel 5 has 5 (five) set *Fixed Reference Channel* (*FRC)* defining HS-DSCH configuration. *FRC H-Set* 1, 2, 3, and 6 apply 2 (two) modulation configurations: QPSK and 16-QAM, but *FRC H-Set* 4 and 5 only apply QPSK.

Simulation was improved from [5]. Our scenarios simulated *Fixed Reference Channel* (FRC) *H-Set* 1 to 6. The HSDPA performance is determined by its troughput value. Troughput is a sum of receiving data (kilobit) devided by time testing (second). It serves efective data rate for fixed channel. The throughput is indicated by reported-ACK and NACK showing either success or failure transmission.

IV. RESULTS

Figure 1 shows graphic of troughput vs Es/No on AWGN channel. We obtained Es/No as the function of *indoor propagation loss.* Graphic showed that when Es/No raised, troughput shall increased. We evaluated that throughput also depends on ACK, numbers of bit information, and testing time. Testing time is determined by inter-TTI interval value and the number of sending HARQ. Our experiment used constant inter-TTI interval value. Maximum of HARQ sending in the this simulation is 4. By increasing HARQ, the throughput would be smaller.

We evaluated results depicted in Figure 2 that numbers of itteration is affecting BER value. The more numbers of itteration in turbo decoding, its performance would increase. Consequently, error of sending block can be minimized and number of sending HARQ would also being reduced. As a result troughput value would increase. It results graph showed in Figure 3.

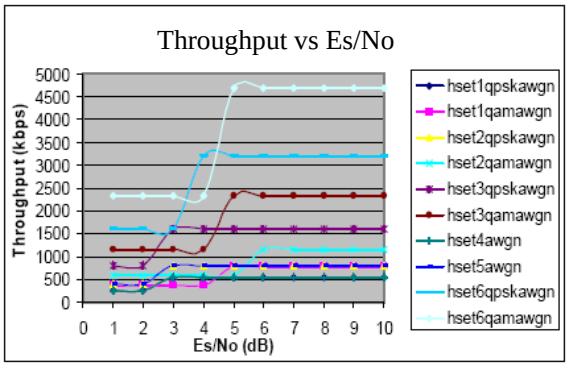

Figure 1. Troughput vs Es/No on AWGN channel

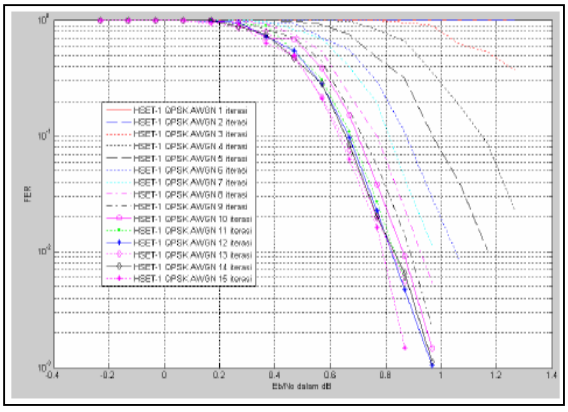

Figure 2. Graphic BER vs Eb/No(H-Set 1 QPSK AWGN) on numbers of iteration

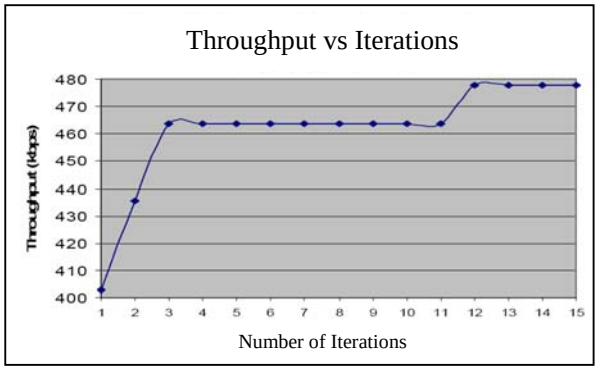

Figure 3. Graphic Throughput vs Number of Iterations

We tested 4 (four) turbo decode algorithms in *H-set 1* (QPSK). Figure 4 showed results that Max-log-MAP algorithm is the simplest one because it gives the smallest time delay. However, this algorithm delivers the worst BER value. BER performance of constant-log-MAP algorithm appeared to be in between max-log-MAP and log-MAP. It is faster than linear-log-MAP algorithm but more influenced by Rayleigh fading than linear-log-MAP algorithm.

The linear-log-MAP offer performance and complexity between log-MAP and constant-log-MAP. BER performance of this algorithm almost achieved BER performance of log-MAP. As a result, log-MAP is the most complex algorithm but gives the best BER performance than the other.

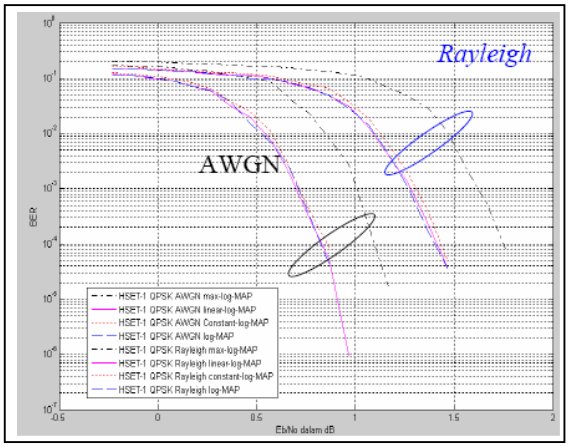

Figure 4. Graphic BER vs Eb/No (H-Set 1 QPSK)

Because of trade off between performance and time delay, turbo code choose types of decoding algorithm based on SNR (Signal to Noise Ratio) value. For example, linear-log-MAP algorithm is used in lower SNR, while max-log-MAP in higher one.

We simulated 5 (five) floors indoor office building model. The transmission power will decrease on every penetrated floors. Minimal pathloss was 49 dB whereas maximum pathloss is 99 dB. This pathloss is smaller than models on radio outdoor propagation [6]. Consequently, average throughput level of indoor would be larger than outdoor. From the value of pathloss, we may estimate power needed for indoor HSDPA system. In addition, placement of transmitter antenna in the floors is important to reduce pathloss. Figure 5 showed relationship between pathloss and throughput in varied iterations numbers. It can be observed that turbo code by more itterations (12 in our maximum simulation) gives the best performance.

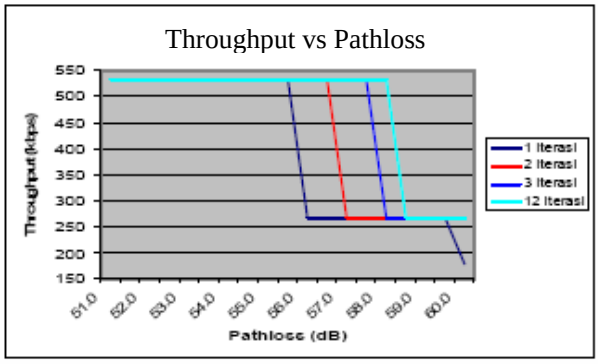

Figure 5. Graphic of Troughput vs Pathloss

V. CONCLUSIONS

We have evaluated HSDPA performance in indoor propagation models. The turbo code parameters that influenced to throughput are the number turbo code itteration and types of turbo decoding algorithm. The more numbers of itteration, BER value will be smaller and HARQ transmission becomes fewer. It gives consequence that throughput is increased. The turbo decoding log-MAP algorithm has the best performance among others, but it double time delay.

REFERENCES

[1] Yusuf Setiawan, *Study of HSDPA implementation in Operator X* , Master Thesis, Management of Telecommunications, Depok, 2006.

[2] ITU-R, *Propagation data and prediction methods for the planning of indoor radio communication systens and the radio local area networks in the frequency range 900 MHz to 100 GHz*, ITU-R Recommendations, Geneva, 2001. Accessed in 10th June 2007 from www.cict.inatel.br/nova2/

[3] A.Burr, *Turbo-codes: the ultimate error control codes?*, Jurnal Electronics & Communication Engineering, August 2001.

[4] M. C. Valenti dan J. Sun, *The UMTS Turbo Code and an Efficient Decoder Implementation Suitable for Software-Defined Radios*, International Journal of Wireless Information Networks (8)4 2001.

[5] Matthew C. Valenti, *Iterative Solutions Coded Modulation Library*, West Virginia University. Accessed in 6 March2007 from http://www.csee.wvu.edu/

[6] QUALCOMM, *HSDPA for Improved Downlink Data Transfer*, Accessed in 12 July 2006, from www.umtschips.com

ISSN: 1411-1284

Performance Analysis of Spiht Compressed Image Tranmission With Diversity Selction Combining on Radio Frequency

Baharuddin

Faculty of Engineering, University of Andalas, Kampus Limau Manis, Padang 25163
Tel. 075172497, fax. 075172566 email : baharuddin@ft.unand.ac.id

Abstract– **This paper describes a simulation of the image transmission system with diversity selection combining method on radio frequency. The SPIHT algorithm is used for image compression transmission on wireless channel. Diversity selection combining methods is used to combat errors during image transmission on wireless channels. The use of Reed Solomon channel coding is to recover errors from transsmitted image. The result shown that diversity selection combining method can be improved significantly the performance of image transmission**.

Keywords– Diversity Selection Combining, SPIHT, Reed-Solomon, Radio Frequency, Image Transmission.

I. INTRODUCTION

On transmission over wireless channel, there are cases that can cause the degrade quality of information: noise and fading(5). The disturbance can cause the wrong in receiving information on receiver. The occurrence of disturbances is random and unpredictable. It needs a technique to improve the quality of signal on receiver.

Beside that, the transmission over wireless channel has limitation bandwidth, while image tends to have big capacity. It can cause the ineffective use of bandwidth (8). To overcome the problem, it needs a technique to reduce number of data in image without loosing the important data that appropriate with human visual characteristic.

Technology in telecommunication is growing rapidly specially on wireless communication (11). It supported by the growing of portable communication technology that make it possible to exchange the multimedia information (data, voice image and video) where it becomes more popular and more desire. Among the multimedia information, the use of image become one of the important features and has been widely use in various applications such as internet, medical image, distance security camera, MMS (Multimedia Messaging Service) and other applications (2). It indicates that the use of image transmission system wirelessly is more desire and keeps growing.

In 1996, A Said and W A Pearlman purposed an compressed image technique wavelet based published in journal *A New, Fast, and Efficient Image Codec Based on Set Partitioning In Hierarchical Trees* (1). That technique called SPIHT that has fast algorithm and it is not so difficult. In 2004, Hafeth Hourani did a research about techniques in overcoming the phenomena of fading and noise on wireless channel publised in journal *An Overview of Diversity Techniques in Wireless Communication Systems* (5). He purposed diversity techniques as one of the way to overcome fading and noise in wireless communication systems..

The research proposed here referred to compression technique (1). For selection combining techniques referred to method proposed (6), but channel model used in this research is fading distribution rayleigh and noise which has normal distribution gaussian (9).

In this paper, image information with size 8 bpp was compressed with rate 0.6 bpp. SPIHT algorithm were used to get the image transmission system to maximize the use of bandwidth and diversity selection combining technique were used to improve image quality on receiver and Reed Solomon channel coding (31.15) were used to protect data during transmission process. So the title of this research is "Performance Analysis Of SPIHT Compressed Image Transmission With Diversity Selection Combining On Radio Frequency"

Several methods for image transmission over wireless channels had been done such as Liane C Ramac and Pramod K Varshney proposed *A Wavelet Domain Diversity Method for Transmission of Images over Wireless Channels*(6) that used diversity techniques on domain wavelet to get the good reconstruction image. In this image transmission, two-state Gilbert-Elliott channel (3),(4) was used. P G

Sherwood and K Zeger in their journal *Error Protection for Progressive Images Transmission over Memoryless and Fading Channels (*7) used data protection technique during transmission, and also Nikolaos Thomos, Nikolaos V Boulgouris, and Michael G Strinzis in their journal *Wireless Image Transmission Using Turbo Codes and Optimal Unequal Error Protection* (10) used *Turbo Codes* to protect image during transmission

II. BASIC THEORY

On this diversity selection technique, receiver chose the best signal that had biggest SNR. [6] Diagram block from this method is shown on figure 1, there is M diversity branch for signal that gets into chosen circuit, and y is the chosen of strongest signal and the output of this circuit. On fading channel, with M branch of Rayleigh channel on the receiver and assumed on every branch has the same average value of SNR, it formulated as follows: [21]

$$SNR = \Gamma = \frac{E_b}{N_0}\overline{\alpha^2} \qquad \text{.....(1)}$$

where $\overline{\alpha^2}$ is mean from the random variabel in this case the random variable is the envelope from fading Rayleigh. If each brances has instant SNR γ_i, the power of spectral density (PDF) from γ_i is :[12]

$$p(\gamma_i) = \frac{1}{\Gamma} e^{\frac{-\gamma_i}{\Gamma}} \qquad \gamma_i \geq 0 \qquad \text{.....(2)}$$

where Γ is average SNR from every branches. Probability that a branch has SNR less than the value of threshold γ is:[12]
]

$$P_r[\gamma_i \leq \gamma] = \int_0^{\infty} p(\gamma_i)d\gamma_i = \int_0^{\infty} \frac{1}{\Gamma} e^{\frac{-\gamma_i}{\Gamma}} d\gamma_i \text{ .....(3)}$$

Probability that every branches recieved simultanous signal less than SNR threshod γ is :[12]

$$P_r[\gamma_1,...,\gamma_M \leq \gamma] = (1 - e^{\frac{-\gamma}{\Gamma}})^M = P_M(\gamma) \text{ .....(4)}$$

$P_M(\gamma)$ is probability for all branches that fail to get the value of SNR = γ. If the only branch reached SNR > γ , the probability become :[12]

$$P_r[\gamma_i > \gamma] = 1 - P_M(\gamma) = 1 - (1 - e^{\frac{-\gamma}{\Gamma}})^M \qquad \text{.....(5)}$$

From the above equation, for the probability of SNR more than threshold γ when selection diversity is used. To indentify average of signal to noise ratio from received signal when using diversity, it needs pdf from signal fading. For selection diversity, the average SNR is gained from the first $P_M(\gamma)$.[12]

$$P_M(\gamma) = \frac{d}{d\gamma} P_M(\gamma) = \frac{M}{\Gamma}(1 - e^{\frac{-\gamma}{\Gamma}})^{M-1} e^{\frac{-\gamma}{\Gamma}} \text{ .....(6)}$$

So, the average SNR ($\bar{\gamma}$) is formulated as follows :[12]

$$\bar{\gamma} = \int_0^{\infty} \gamma P_M(\gamma) d\gamma = \Gamma \int_0^{\infty} Mx(1 - e^{-x})^{M-1} e^{-x} dx \text{ .....(7)}$$

where x is the comparison between γ and Γ.

The above equation is used to evaluate the increase of the average SNR given by selection diversity. Diversity selaction techniques offers the improvement on link margin without needing the added power on transmiter. This methods is easy to be implemented, but it did not result the optimum result since it did not use all possible branches.

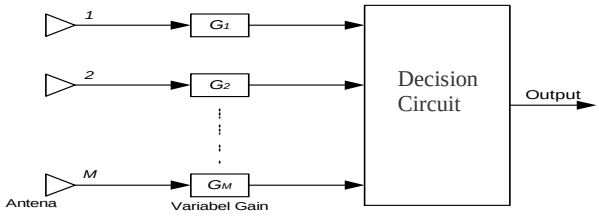

Figure 1. Selection Diversity Combining[12]

The generator envelope signal fading is the process of gaussian complex that has independent real part with imaginer part. On mobile radio channel, the distribution of *Rayleigh* is used to describe the statistic of different time from the recieved envelope for a signal *flat fading.* Fast fading is *Rayleigh fading* since this *fading* is distributed following the distribution of the *Rayleigh.* The method used to generate fading is illustrated as follows: [12]

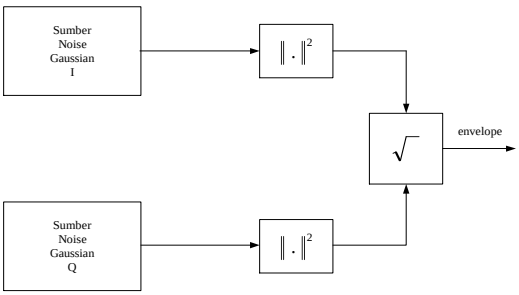

Figure 2. fading Rayleigh Generator [12]

Simulation model for the simulation system is:

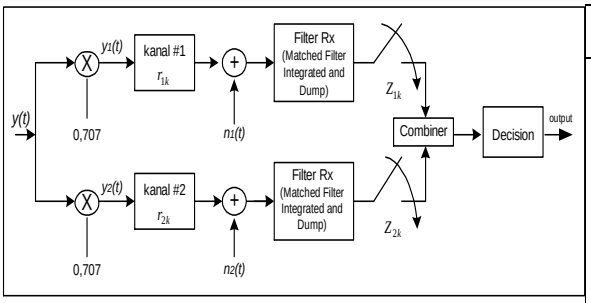

Figure 3. sytem model with *diversity combining*[12].

Decision Circuit

On decision circuit, there was docoding process that use to detect bit on the reciever. This process is done by applying a rule. The rule gives the optimum performance, so it could reduce the error. [12]

$$b'_k = \begin{cases} 1, & \text{if } A'_k \geq 0 \\ 0, & \text{if } A'_k < 0 \end{cases} \quad \text{.....(8)}$$

where :

b'_k = detected Bit on reciver

A'_k = output from combining circuit

III. EXPERIMENTAL RESULTS

The Result of Compressed Image Transmission SPIHT

Table 1. Compressed Image Transmission over fading channel + Noise with rate 0.8 bpp

SNR (dB)	BER	PSNR Diversity (dB)	PSNR without Diversity (dB)
10	0.0204	14.7464	14.6946
12	0.0175	19.5597	19.3743
14	0.0153	24.5918	21.2786
16	0.014	26.2011	24.6029
18	0.0134	30.2538	27.166
20	0.0126	33.7379	32.09

Table 1 and figure 4 and 5 represent the comparison of performance between using diversity and without diversity over compressed image transmission SPIHT with rate 0.8 bpp for fading channel distribution rayleigh and noise distribution normal Gaussian. For SNR 10 dB the value of BER 0.0204. For system that uses diversity, the value of PSNR is 14.7464 dB while the value PSNR without using diversity is 14.6946 dB. The improvement of performance diversity system is about 0.0518 dB if it compares to system without diversity. The improvement continues up to SNR 20 dB, for BER value 0.0126. The subjective result for SNR 14 dB on rate 0.8 bpp for the condition of fading and noise are given in figure 2.

Figure 4. Comparison result of image reconstruction between using diversity and without diversity for SNR 14 dB

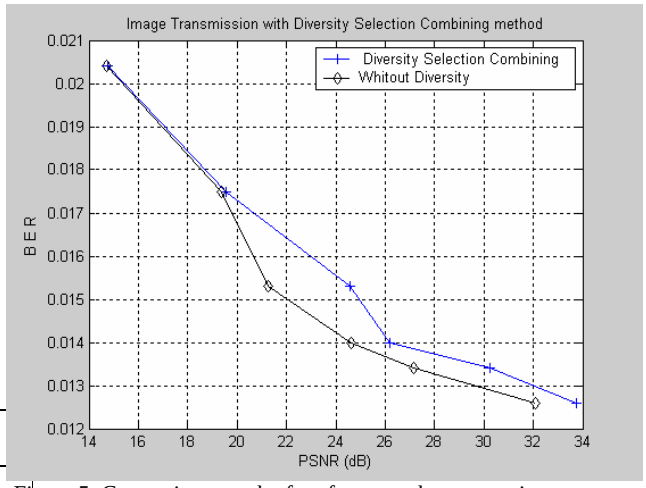

Figure 5. Comparison graph of performance between using diversity and without diversity system. On compressed image transmission with rate 0.8 bpp for channel fading + noise

IV. CONCLUSIONS

The used of diversity combing for compressed image improved the performance of system when it compared to compressed image without using diversity. The tests of this pattern were done with compressed ratio 0.8 bpp. Compressed ratios were tested on the condition of channel fading and noise. The simulation result showed that the used of diversity combining on compressed image transmission system were getting improve 1.6479 dB when it compared to compressed image without diversity.

REFERENCES

[1]. A. Said and W. A. Pearlman, **"A New, Fast, and Efficient Image Codec Based on Set Partitioning In**

Hierarchical Trees", *IEEE Trans. Circuits Syst Video Technol., vol. 6 pp. 243-250,(June 1996).*

[2]. Baharuddin**, "Transmisi Citra dengan Teknik Diversity pada Kanal Wireless"**, Thesis, *Insitut Teknologi Sepuluh November, (Januari 2005).*

[3] E. N. Gilbert, "Capacity of a burst-noise channel," *Bell Syst. Tech. J.*, pp. 1253–1265, (Sept. 1960)

.[4] E. O. Elliott, "Estimates of error rates for codes on burst error channels," *Bell Syst. Tech. J.*, vol. 42, p. 1977, (Sept. 1963).

[5] Hourani, Hafeth, **" An Overview of Diversity Techniques in Wireless Communication System"**, *Helsinki University of Technology Communication Lab 2005*

[6] Liane C. Ramac and Pramod K. Varshney, **"A Wavelet Domain Diversity Method for Transmission of Images over Wireless Channels"**, *IEEE Journal on Selected Areas in Communication, Vol. 18*, pp. 891–898 *No. 6, (June 2000).*

[7] P.G. Sherwood and K. Zeger,"**Error Protection for Progressive Image Transmission over Memoryless and Fading Channels"**, *IEEE Trans. Commun., vol.46, pp. 1555-1559, December 1998.*

[8]. Sudhakar, R, Karthiga Ms R, and Jayaraman , **"Image Compression using Coding of Wavelet Coefficients – A Survey"**, *Department of Electronic and Communication Engineering, PSG College of Technology*. 2002.

[9]. Theodore. S. Rappaport, "Wireless Communication Principles & Practice", Prentice-Hall Communications Engineering and Emerging Technologies Series, 1996

[10]. Thomos Nikolaos, Boulgouris Nikolaos V, and Strinzis Michael G, **"Wireless Image Transmission Using Turbo Codes and Optimal Unequal Error Protection"**, *IEEE Trans. On Image Processing Vol. 14* pp. 643–650 *No.11 (November 2005).*

[11]. Tuka, Veronika dan HS, Djati ,**"Peran Jaringan Seluler untuk Komunikasi Data"**, *Artikel Telekomunikasi Elektro Indonesia No.24,* pp. 24–31, *Tahun V (January 1999).*

[12]. Vijaya Chandran Ramasami, "BER Performance Over Fading Channels and Diversity Combining", EECS 862 Project, 2001.

ISSN: 1411-1284

Simulation and Analysis of IPTV Video Transmission and Video Quality Assessment with MPQM Method

Dwi Susanto, F., and Asvial. M., IEEE and AIAA member

Center for Information and Communication Engineering Research (CICER)
Electrical Engineering Department, Faculty of Engineering
University of Indonesia, Depok, Indonesia
febri.dst@gmail.com , asvial@ee.ui.ac.id

Abstract **- In internet protocol television (IPTV) system, during video signal transmission process, the different quality of the received signal compared to the source signal could be appeared as the quality impairments of signal video. The purpose of this research is to make a simulation and analysis of end-to-end video transmission over simplified IPTV network. The transmission process over IP network is simulated using one characteristic of IP network and has the direct impact to the video quality, such as packet loss, and ignorence some parameters. The simulation is developed using Simulink model in Matlab 7.0.4. and the quality assessment is proposed using moving picture quality metric (MPQM) method. Based on the determination of the video quality scoring, the requierment condition of the video transmission for the IPTV systen can be determined.**

Keywords - IPTV, Video Transmission, Video Quality, MPQM

I. INTRODUCTION

By compounding computer network and television broadcasting technology, the internet protocol television (IPTV) is released as a new service in the television industries. IPTV uses network technologies based on internet protocol where audio and video stream is converted to IP packets and transmitted over IP network. Various services such as email, searching, online game, teleconference, video call, video on demand (VoD), personal video recording (PVR) , etc could be applied in the IPTV system [1]. Here, the quality of video received by end user is once important parameter that direcly correlated to Quality of Services (QoS) of IPTV.

The 3 (three) main process for the video transmission is encoding, transmission and decoding. The encoding process is proposed at the transmitter site and is used to compress the video size and to arrange the video format; so that it can be optimally transmitted over IP network. In the video transmission process, jitter, delay, packet loss and other processes can be appeared and disturbed the transmission. The decoding is a reverse process of encoding and proposed at the receiver site. All that process can cause the quality impairment of the received video signal. The impairment has to be assessed and to be known in order to make it as small as possible. Beside that, we need to know the score of the received video signal quality to determine the minimum limit where the QoS is still assured.

One of the video signal quality measurement methods is moving picture quality metric (MPQM). MPQM is a measurement method based on single-end mode. It is mean that the quality measurement is proposed based on some parameters of the received signal video without using the reference video [2]. This method can be applied on user terminal, i.e. set-top box (STB). Using this method, the quality score of the received signal video can be assessed to evaluate the quality of signal video and to make decisin model to improved the quality of signal video.

In this paper, the transmission process of IPTV is simulated using an IP network characteristic that directly impact to the signal video quality, such as packet loss. Meanwhile other parameters are ignored and IP network can be pretended as the black box process. Some parameters of the received signal video are measured in order to get video quality score using MPQM method.

II. SYSTEM MODEL

The video transmission process is proposed in simplified IPTV network for end-to-end video streaming transmission, from video source transmission to the destination using one channel, as shown in Fig. 1.

A. Video Source Block

In the simulation process, the function of video source block is to determine the video input. This block supports all video format with type Windows Media Files, i.e. *.wmf, *.asf, *.wma, *.avi, etc. Video used in the simulation is a color video, so that it can be divided into three planes, red (R), green (G) and blue (B). R, G and B are a matrix model that represent the plane from input of RGB video stream. Video source block is also used to determine the

dimension of R, G and B matrix that is used in simulation. The dimension of the matrix must to be fit with the resolution of video input.

B. Encoder Block

The function of the encoder block is to execute encoding process of video input. The input of this block is the output of video source block. The circuit of encoder and decoder block in this simulation is based on Matlab Demos with some adjustments.

The first process in encoder block is data collection from video source block. The data is R, G, B matrix that is collected using outport and inport block. The next process is color space conversion. This process converts R, G, and B matrix to the Y, Cb, and Cr matrix. The purpose of this process is to make chroma sub sampling process possible since this process uses color information from YCbCr color space. Y is a matrix that represents luma (brightness) from a picture. Luma is a brightness level of a picture that has no correlation with its color. Cb and Cr are matrix that represent chrominance component of a picture. Chrominance is a color composition in a color signal. Usually luma component or brightness (Y) is paired with chroma components (Cb and Cr) [8].

The down sampling process is achieved at chroma sub sampling process. This process will reduce the resolution of picture in digital format by reducing frequency of the sampling rate. During the down sampling process, antialiasing filter is usually used in order to prevent aliasing process. The aliasing is a fault of frequency during the sampling process at lower sampling rate. Only chroma components (Cb and Cr) is used in the process, because human eyes is more sensitive to the brightness than color components [8].

For the next process, the data type needs to be matched with the process. Thus, the data type of the output of the chroma sub sampling process will be changed to the data type needed. This process is called data type conversion. And then, the output matrixes will be sent to the two channels, one is sent to the output matrixes directly to the block processing, and the other one is sent the output matrixes to the block processing after their undergo delay and padding process. In the delay and padding process, the input matrix will be delayed and padded. Padding is the process to expand the matrix dimension using special technique. Both Y'CbCr delayed and padded matrix and the raw one is to be input of the block processing, where both of them is to be compared.

The block processing extracts sub matrix from input matrix. Each sub matrix is to be send to the sub system. We can construct the circuit in the sub system, and the process is to be done base on that circuit. Each output of the sub matrix from the sub system is to be assembled to become the output matrix.

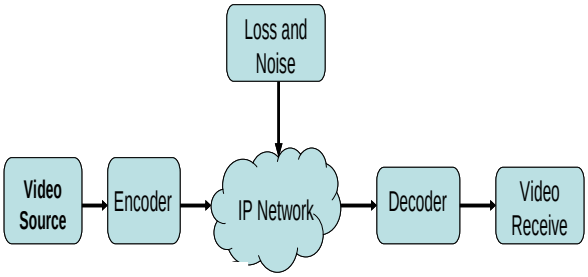

Figure 1. Blok diagram of IPTV video transmission simulation

The input of the block processing is sub matrix extracted from original chroma matrix and chroma matrix at the delay and the padding block. Contoller signal is used to control motion compensation encoder. The output of the sub matrix from motion compensation encoder is to be switched using controller signal. If the controller signal indicatr is positive, the sub matrix from motion compensation encoder is to be passed. Both of them is to be sent to the transform coder in order to get the output of sub matrix and bit value. The bit value is achieved from each sub matrix and then to summed. All of the output sub matrixes from whole processes in block processing is to be assembled to become output matrix, as the output of the encoder.

C. Channel Block

In the channel block, the data of the output chroma matrix from encoder block is to be collected. This data is needed to simulate packet loss. This matrix will receive some disturbances during it trip in the channel. In order to make it easier to be processed, the chroma matrix form is to be changed to the column vector with same amount of elements. This column vector then multiplied with constant between zero to one to make it smaller and is used to minus the previous column vector. The new column vector is changed back as a new column vector of chroma matrix. This new chroma matrix is to be an output of the channel block.

D. DecoderBlock

Decoder block is used to decode the input video so that the video could be displayed in the receiver site. Actually, the processes in the decoding have similarity with the processes in the encoding, but in the reverse sequence. Input of the decoder block is chroma matrix (Y', Cb and Cr) from the channel block. The decoder block uses MV from encoder and controller signal as its input. All inputs is to be processed in block processing.

After being processed in block processing, the chrominance matrix (Cb and Cr) is to be sampled. This process is called as the chroma sub sampling and

is used to increase the pixel resolution of the chrominance matrix. The last process is colour space conversion that converts Y'CbCr colour space to the RGB colour space, so that it can be RGB video and could be displayed at the receiver site.

E. Receiver Block

The receiver block represents the consumer site. This block receives RGB signal from the decoder block. The RGB signal is converted to the video and is displayed in order to be compared with the video source. This block is also used to save the video file to the hard drive for further analyze of its parameters. The video parameters are used to assess the video quality using MPQM method.

F. Assessment Procedure

The video quality assessment has some procedures as following explanation. The first step, the bit rate is checked for both video source and received video. Then these bit rates is used as the parameter to get packet loss rate (PLR) value that is needed in the video quality assessment using MPQM method. The formula to find PLR value using bit rate is as follows [11]:

$$PLR = \frac{original.bitrate - received.bitrate}{original.bitrate} x100\% \quad (1)$$

In order to assess quality value with MPQM method, we need to define the quality scale of the codec used and the value of parameter of calibration (R). In this simulation, the codec used has quality scale (Qe) 4 (in the range 3 – 5) since encoding process is proposed only for a simple simulation. The parameter of calibration is assumed to be equal 2 since the video bit rate is low and the complexity of the video is also low. Finally, all those parameters are used in the assessment process using equation (1).

III. SIMULATION AND QUALITY ASSESSMENT

Here, the simulink circuit used in the simulation process for each block is explained, started from the video source block, the encoder block, the channel block, the decoder block and the receiver block. And then, the result of simulations and assessment is analyzed. The simulink circuit of the simulation is ilustrated in Figure 2.

A. Video Source Block

In the video source block, the video input is arranged both its format and dimension. In the Figure 3 the simulink of the circuit in the video source block is shown. The circuit consists of the multimedia file block, the selector block and the out port block. From the multimedia file block, the video frame from multimedia file is read and is sent to the simulink model. The video used in the simulation is in the *.avi format. The output of the multimedia file block is RGB matrixes. These matrixes are sent to the selector block.

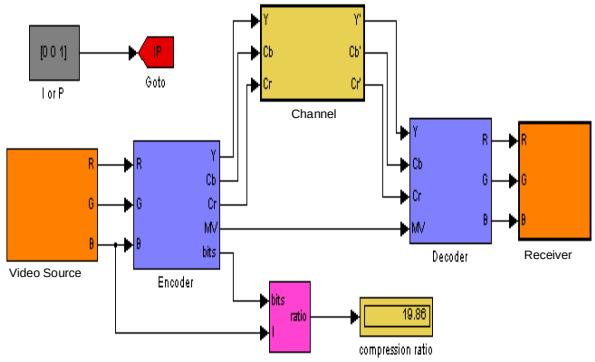

Figure 2. Complete circuit of the simulink used in the simulation.

B. Video Source Block

In the video source block, the video input is arranged both its format and dimension. The video source circuit consists of the multimedia file block, the selector block and the out port block. From the multimedia file block, the video frame from multimedia file is read and is sent to the simulink model. The video used in the simulation is in the *.avi format. The output of the multimedia file block is the RGB matrixes. These matrixes are sent to the selector block. The function of the selector block is to select or determine which element of that input could be passed to the next block. The choosing of the elements are based on the index value of the column and row of the matrix. The index value must be matched with the video input resolution. The out port block is a link from a system or sub system to the outside system or sub system. The video source is to be displayed using the video viewer block.

C. Encoder Block

The input video is encoded by encoder block. The encoder circuits consist of Inport block, Color Space Conversion block, Chroma Resampling block, Data Type Conversion block, Delay and Pad block, From block, Block Processing, dan Outport block.

The color space conversion block is used to convert color information from RGB color space to the YCbCr color space or vice versa. At the encoder block, the chroma sub sampling process is used to reduce the bandwidth needed for signal transmission process and to decrease the resolution of the picture or voice in digital format by reducing the frequency of the sampling rate. In the chroma sub sampling process, only chroma components are used since human eyes are more sensitive to the brightness (luma) than color component (chroma). Down sampling format used in the simulation is 4:4:4 to the 4:4:0 (MPEG2). YCbCr is compounded by format of 4:n:n. Number 4 represent a sampling rate of 13.5 MHz which is standard frequency (ITU-R BT.601)

for NTSC, PAL and SECAM. The next two digits represent the rate of component Cb and Cr.

The data type conversion is used to convert the data type of the input signal. The Delay block proposed the delay to the discrete-time input by using some sample or frame that depends on the delay parameter. The value of delay parameter must be integer and bigger than zero (zero value has no effect). The function of Pad block is to expand the dimension of the matrix by adding its row or column.

D. Channel Block

This block simulates the channel in the IP network, where there are disturbances happen to the packet data. One of the disturbances is the packet loss. The simulink circuit of the channel block is illustrated in Figure 3. The reshape block in this circuit is used to convert the input matrix to the column vector. In addition, this circuit is also used to multiply the components of the vector with constant. And sum block is used for subtraction process. After subtraction process, the column vector is converted again to the matrix form and then, is sent to the decoder block.

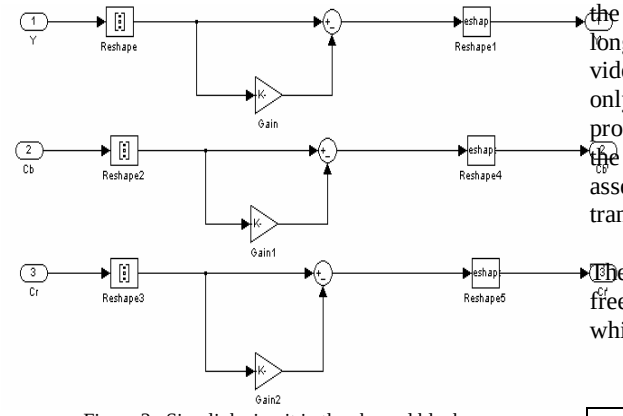

Figure 3. Simulink circuit in the channel block

E. Decoder Block

The decoder block receives the input signal from the channel block that are Y, Cb and Cr matrixes whose elements have changed as losses effect in the channel. The decoder block also receives MV index value from encoder block and controller signal from Goto and From block.

There are some subsystem block in the decoder block such as Block Processing block, Delay and Pad block, Data Type Conversion block, Chroma Resampling block, and Color Space Conversion block. The Block Processing block is used for repetition process to each sub matrix which is extracted from the input matrix. The Delay and Pad block is used to generate the delay and padding to the matrix or sub matrix input. Padding is a process that is used to increase the dimension of the matrix. The Data Type Conversion is used to convert data type of the input to the other kinds of data type.

In the Chroma Resampling block, upsampling process is proposed to change the format from 4: 2: 0 (MPEG2) format to the 4: 4: 4. This process is a reverse process of downsampling process in the encoder block. The Color Space Conversion block is used to convert Y'CbCr color space to the RGB color space so that they can be displayed at the receiver site.

F. Receiver Block

The Receiver block simulates the consumer site in the IPTV system. In this block, the output of the deocder block in the form of RGB signal is to be displayed and then be assessed. The receiver block uses Video Viewer block to display the RGB signal input to the form of video, and To Multimedia File block to save received video file to the hard drive.

G. Quality Assessment

Video used in the simulation is a simple video with minimum complexity, short duration, and small dimension. The purpose is to suit the performance of the simulation system. If we use complex video with long duration and big resolution, the frame rate of the video simulation could be smaller. In this assessment, only one video used and focused in the simulation process. The assessment process is proposed to know the example of the process of video quality assessment to the received video in the video transmission process.

The video specifications are shown in the Table 1. The specification of video used is collected using freeware Gspot Codec Information v2.60 RC01 which is one tool in the Cole2k Media – Codec Pack.

Table 2. The specification of video used in the simulation

Parameter	Hotel.avi
Size	**16,5 MB 16.940 KB 17.347.072 byte**
Duration	**10 second**
Frame	**300 frames**
Bitrate	**13.824 kbps**
Picture/s	**30 pics/ s**
Frame/s	**30 fps**
Dimension (Resolution)	**160 x 120**

Figure 4 ilustrates the process of video simulation. The video used in the simulation is in the *.avi format. Two displays of video are shown, the transmitted video at the left side and the received video at the right side. We can see that the display of transmitted video is brighter than the received one.

This mean the quality of received video is lower than the quality of transmitted video and as long transmission process, the quality degradations are appeared

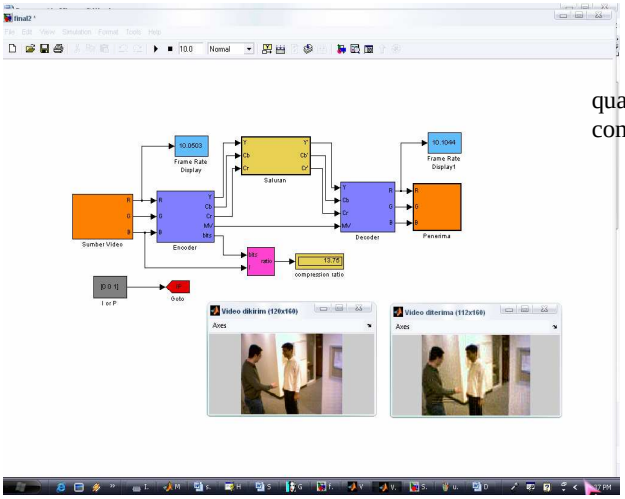

Figure 4. Simulation process to the video hotel.avi

From the simulation, the specification of received video is compared to the specification of transmitted video, as shown in Table 2.

Table 2. Comparation of transmitted and received video specification

Parameter	Transmitted Video	Received Video
Size	16,5 MB 16.940 KB 17.347.072 byte	15,6 MB 16.021 KB 16.406.016 byte
Duration	10 second	10 second
Frame	300 frames	300 frames
Bitrate	13.824 kbps	12.902 kbps
Picture/s	30 pics/ s	30 pics/s
Frame/s	30 fps	30 fps
Resolution	160 x 120	160 x 120

From the table between transmitted and received video, the changed parameters are only for the size and the bit rate of the video. These parameter is used to assess PLR using equation (1). Based on the data, the video quality is calculated and the result for this qulaity is 3.18. It is mean the video quality is in the range between 3 and 4 or in the range between fair and good level. This video quality value has sufficient rated since the minimum requirement of the IPTV video quality is in the scale of 3 to 5 [10]. In this simulation, the precision is not sufficient enough to assess the real video quality because in this simulation only bit rate parameter of the video is used. In the future works, some parameters based on the video complexity and high coded performance to asses the quality of the system is to proposed.

IV. CONCLUSION

Based on simulation results and IPTV video quality analysis using MPQM method, could be concluded:

A. The performance of the simulation circuit is still not sufficient enough to simulate video with high complexity since video will be displayed with high delay (small frame rate).
B. To simulate video with specified resolution or dimension, some adjustments of the dimension of RGB input matrix in the video source block is needed. Beside that some parameters value need to be changed if the video dimension is changed.
C. From the simulation, the quality value assessment using MPQM method is 3.18 and is still in recommendation value.

REFERENCES

[1] _____, "IPTV Service Requirement", *1st FG IPTV meeting*: *Geneva 10-14 July 2006*, ITU Union.

[2] Yves Cognet, "Measuring IPTV QoS Performance at the Box", Network Systems Designline, 2006. Accessed in December 2006. http://www.networksystemsdesignline.com/

[3] _____, "IPTV". Accessed on 28th November 2006 dari wikipedia. http://en.wikipedia.org/wiki/IPTV

[4] _____, "The IPTV Revolution: New Opportunities, New Challenges for Satellite Communications Systems". Accessed on 28th November 2006. www.globecommsystems.com/

[5] _____, "Delivering IPTV with the Windows Media Platform", *Microsoft Corporation*, 2003. Accessed on 28th November 2006. http://www.microsoft.com/

[6] _____, "Video Compression". Accesed 9th May 2007 from answers.com http://www.answers.com/topic/video-compression

[7] _____, "Performance Analysis for Video Streams Across Network", *White Paper*, NetPredict, Inc., 2003.

[8] _____, "Chroma Subsampling". Accesed 9th May 2007 from answers.com http://www.answers.com/topic/ycbcr-sampling

[9] _____, "Discrete Cosine Transform". Accesed 9th May 2007 from answers.com

http://www.answers.com/topic/dicrete-cosine-transform

[10] _____, "Delivering Optimal Quality of Experience (QoE) for IPTV Success", White Paper, Spirent Communications. 2006.

[11] ____ , "Packet Loss". Accesed 9th May 2007 from answers.com http://www.answers.com/topic/packet-loss

ISSN: 1411-1284

Intrusion Detection of Mobile Ad-Hoc Network (MANET): A Literature review

Satria Mandala[*], Md. Asri Ngadi[**], Abd Samad bin Haji Ismail[***], and A. Hanan Abdullah[****]

[*]Fakultas Sains dan Teknologi, Universitas Islam Negeri Malang, Jl. Gajayana 50 Malang, Indonesia
Tel. (0341) 551354, fax(0341) 558882 email : satriamandala@hotmail.com
[**], [***], [****] Fakulti. Sains Komputer & Sistem Maklumat
Universiti Teknologi Malaysia, 81310 UTM Skudai, Johor, Malaysia
Tel. + 607 5532001, fax. +607 5565044, email : dr.asri@utm.my, samad@utm.my, hanan@utm.my

Abstract– **In recent years, the security issues on MANET have become one of the primary concerns. The MANET is more vulnerable to attacks than wired network. These vulnerabilities are nature of the MANET structure that cannot be removed. As a result, attacks with malicious intent have been and will be devised to exploit these vulnerabilities and to cripple the MANET operation. Attack prevention measures, such as authentication and encryption, can be used as the first line of defense to reduce the possibilities of attacks. However, these techniques have a limitation to the effects of prevention techniques in general and they are designed for a set of known attacks. They are unlikely to prevent newer attacks that are designed to circumvent the existing security measures. For this reason, there is a need of second mechanism to detect and response these newer attacks, i.e. "intrusion detection". This paper aims to explore and classify current techniques of Intrusion Detection System (IDS) aware MANET. Moreover, attacks, IDS architectures, and researches achievement on MANET are discussed inclusively. Comparison on several researches achievement is also presented using various parameters. On last section, we provide conclusions and future research.**

Keywords– Intrusion Detection System (IDS), MANET, Literature review.

I. INTRODUCTION

In MANET, a set of interacting nodes should cooperatively implement routing functions to enable end-to-end communication along dynamic paths composed by multi-hop wireless links. Several multi-hop routing protocols have been proposed for MANET, and most popular ones include: DSR [1], OLSR [2], DSDV [3] and AODV [4]. A majority of these protocols relies on the assumption of a trustworthy cooperation among all participating devices; unfortunately, this may not be a realistic assumption in real systems. Malicious nodes could exploit characteristics of MANET to launch various kinds of attacks.

Node mobility on MANET cannot be restricted. As results, many IDS solutions have been proposed for wired network, which they are defined on strategic points such as switches, gateways, and routers, can not be implemented on the MANET. *Thus, the wired network IDS characteristics must be modified prior to be implemented in the MANET.*

The rest of this paper will be structured as follows. Section II describes background of IDS. Intrusion detection on MANET is presented on section III. In section IV, we give researches achievement summary based on the section III. Finally, the conclusions and future research are shown in section V.

II. IDS BACKGROUND

An intrusion-detection system (IDS) can be defined as the tools, methods, and resources to help identify, assess, and report unauthorized or unapproved network activity. Intrusion detection is typically one part of an overall protection system that is installed around a system or device—it is not a stand-alone protection measure.

Intrusion detection has a bit more history behind it. Endorf [5] stated that the intrusion detection was introduced as a formal research when James Anderson wrote a technical report [6] for the U.S. Air Force. Thus, it has been followed by Denning [7], Heberlein [8], and many researchers until todays.

Depending on the detection techniques used, IDS can be classified into three main categories [9] as follows: 1) signature or misuse based IDS), 2) anomaly based IDS, 3) specification based IDS, which it is a hybrid both of the signature and the anomaly based IDS. *The signature-based IDS* uses pre-known attack scenarios (or signatures) and compare them with incoming packets traffic. There are several approaches in the misuse detection, which they differ in representation and matching algorithm employed to detect the intrusion patterns. The detection approaches, such as expert system [10], pattern recognition [11], colored petri nets [12], and state transition analysis [13] are grouped on the

misuse. Meanwhile, *the anomaly-based IDS* attempts to detect activities that differ from the normal expected system behavior. This detection has several techniques, i.e.: statistics [14], neural networks [15], and other techniques such as immunology [16], data mining [[18], [19]], and Chi-square test utilization [17]. Moreover, a good taxonomy of wired IDSes was presented by Debar [20]. *The specification-based* IDS monitors current behavior of systems according to specifications that describe desired functionality for security-critical entities [48]. A mismatch between current behavior and the specifications will be reported as an attack.

III. MANET INTRUSION DETECTION

There are three focuses in this section: attacks, IDS architectures grouping, and researches achievement. The "researches achievement review" uses several parameters such as the IDS architectures, the detection techniques (see section II), the resistance to several attacks type, and the routing protocols (see section I).

III.A. ATTACKS

The MANET is susceptible to passive and active attacks [21]. The Passive attacks typically involve only eavesdropping of data, whereas the active attacks involve actions performed by adversaries such as replication, modification and deletion of exchanged data. In particular, attacks in MANET can cause congestion, propagate incorrect routing information, prevent services from working properly or shutdown them completely [[22],[25],[26],[23],[24],[27]].

Nodes that perform the active attacks are considered to be malicious, and referred to as *compromised*, while nodes that just drop the packets they receive with the aim of saving battery life are considered to be *selfish* [[28],[26]]. A selfish node affects the normal operation of the network by not participating in the routing protocols or by not forwarding packets.

In addition, a compromised node may use *the routing protocol* to advertise itself as having the shortest path to the node whose packets it wants to intercept as in the so called *black hole* attack [29], [30].

Spoofing is a special case of integrity attacks whereby a compromised node impersonates a legitimate one due to the lack of authentication in the current ad hoc routing protocols [[35],[36]]. The main result of the spoofing attack is the misrepresentation of the network topology that may cause network loops or partitioning. Lack of integrity and authentication in routing protocols creates *fabrication attacks* [[37],[4],[38]] that result in erroneous and bogus routing messages.

Denial of service (DoS) is another type of attack, where the attacker injects a large amount of junk packets into the network. These packets overspend a significant portion of network resources, and introduce wireless channel contention and network contention in the MANET [[39],[40]]. In addition, the routing table *overflow attack*, where an attacker attempts to create routes to non-existent nodes and the sleep deprivation attack, where an attacker tries to consume the batteries of a node, are two other types of the DoS attacks [41].

There are also more sophisticated routing attacks. Compared to the simple attacks described above, these sophisticated attacks are much harder to detect and to prevent, i.e.: *wormhole attacks* (two compromised nodes create a tunnel that is linked through a private connection and thus they by-pass the network [[31],[32]]), *rushing attacks* [33] and *sybil attacks* [34].

III.B. IDS ARCHITECTURES

Based on the network infrastructures, the MANET can be configured to either flat or multi-layer. The optimal IDS architecture for the MANET may depend on the network infrastructure itself. There are four main architectures on the network [43] , as follows: 1) Standalone IDS, 2) Distributed and Collaborative IDS, 3) Hierarchical IDS, and 4) Mobile Agent for Intrusion Detection Systems.

In the standalone architecture, the IDS runs on each node to determine intrusions independently. There is no cooperation and no data exchanged among the IDSes on the network. This architecture is also more suitable for flat network infrastructure than for multi-layered network infrastructure

The distributed and collaborative architecture has a rule that every node in the MANET must participate in intrusion detection and response by having an IDS agent running on them. The IDS agent is responsible for detecting and collecting local events and data to identify possible intrusions, as well as initiating a response independently.

The hierarchical architecture is an extended version of the distributed and collaborative IDS architecture. This architecture proposes using multi-layered network infrastructures where the network is divided into clusters. The architecture has cluster heads, in some sense, act as control points which are similar to switches, routers, or gate ways in wired networks.

The mobile agent for IDS architecture uses mobile agents to perform specific task on a nodes behalf the owner of the agents. This architecture allows the distribution of the intrusion detection tasks. There are several advantages using mobile agents [22], [42] , for intrusion detection.

III.C. RESEARCHES ACHIEVEMENT

Many researchers have proposed several IDS especially for the MANET, some of them will be reviewed in the following paragraph.

Since the nature of MANET node is distributed and requires cooperation to other nodes, ***Zhang, Lee, and Huang [30], [24]*** proposed "intrusion detection

(ID) and response system" should follow both the natures. In this proposed architecture model, each node is responsible for detecting signs of intrusion locally and independently, but neighboring nodes can collaboratively investigate in a broader range. Individual IDS agents are placed on each and every node. Each the IDS agent runs independently and monitors local activities (user and systems activities, and communication activities within the radio range). The agent detects intrusion from local traces and initiates response. If anomaly is detected in the local data, or if the evidence is inconclusive and a broader search is warranted, neighboring IDS agents will cooperatively participate in global intrusion detection actions. These individual IDS agents collectively form the IDS system to defend the wireless ad-hoc network.

Albers et al. [44] proposed a distributed and collaborative architecture of IDS by *using mobile agents*. A Local Intrusion Detection System (LIDS) is implemented on every node for local concern, which can be extended for global concern by cooperating with other LIDS. Two types of data are exchanged among LIDS: security data (to obtain complementary information from collaborating nodes) and intrusion alerts (to inform others of locally detected intrusion). In order to analyze the possible intrusion, data must be obtained from what the LIDS detects on, along with additional information from other nodes. Other LIDS might be run on different operating systems or use data from different activities such as system, application, or network activities; therefore, the format of this raw data might be different, which makes it hard for LIDS to analyze. However, such difficulties can be solved by using Simple Network Management Protocol (SNMP) data located in Management Information Base (MIBs) as an audit data source. Such a data source not only eliminates those difficulties, but also reduces the increase in using additional resources to collect audit data if an SNMP agent is already run on each node. For the methodology of detection, Local IDS Agent can use either anomaly or misuse detection. However, the combination of two mechanisms will offer the better model. Once the local intrusion is detected, the LIDS initiates a response and informs the other nodes in the network. Upon receiving an alert, the LIDS can protect itself against the intrusion.

Kachirski and Guha [45]**Error! Reference source not found.** proposed a multi-sensor intrusion detection system based on mobile agent technology. The system can be divided into three main modules, each of which represents a mobile agent with certain functionality, i.e.: monitoring, decision-making and initiating a response.

- Monitoring agent: Two functions are carried out at this class of agent: network monitoring and host monitoring.
- Action agent: Every node also hosts this action agent. The action agent can initiate a response, such as terminating the process or blocking the node from the network, if it meets intrusion activities where it lives.
- Decision agent: The decision agent is run only on certain nodes, mostly at the nodes that run network monitoring agents. If the local detection agent cannot make a decision on its own due to insufficient evidence of an intrusion, it will report to this decision agent in order to investigate deeply on the suspected node

Since nodes move arbitrarily across the network, a static hierarchy is not suitable for such dynamic network topology.

Sterne et al. [46] proposed a dynamic intrusion detection hierarchy that is potentially scalable to large networks use clustering. This method is similar with Kachirski and Guha [45], but it can be structured in more than two levels. Thus, nodes on first level are cluster heads, while nodes on the second level are *leaf nodes*. In this model, every node has the task to monitor, log, analyze, respond, and alert or report to cluster heads. The Cluster heads, in addition, must also perform: 1) Data fusion/integration and data filtering, 2) Computations of intrusion, and 3) Security Management.

B.Sun [47] proposed Zone Based IDS (ZBIDS). In the system, the MANET is spitted into non-overlapping zones (zone A to zone I). The nodes can be categorized into two types: the intra-zone node and the inter-zone node (or a gateway node). Each node has an IDS agent run on it. This agent is similar to the IDS agent proposed by Zhang and Lee. Others components on the system are data collection module and detection engine, local aggregation and correlation (LACE) and global aggregation and correlation (GACE). The data collection and the detection engine are responsible for collecting local audit data (for instance, system call activities, and system log files) and analyzing collected data for any sign of intrusion respectively. The remainder, LACE module is responsible for combining the results of these local detection engines and generating alerts if any abnormal behavior is detected. These alerts are broadcasted to other nodes within the same zone. However, for the GACE, its functionality depends on the type of the node. If the node is an intra-zone node, it only sends the generated alerts to the inter-zone nodes. Thus, if the node is an inter-zone node, it receives alerts from other intra-zone nodes, aggregates and correlates those alerts with its own alerts, and then generates alarms. The intrusion response module is responsible for handling the alarms generated from the GACE

IV. SUMMARY

Table 1. Comparison researches achievement on the MANET IDS

Author(s)	Name Specific	Architec-ture	Addressed Attacks type				Tech-nique detection	Routing protocol	Contribution
			Authen-tication	Routing (black hole, etc)	Selfish	Others (If any)			
Zhang and Lee, Y. Huang [30], [24]	None	Distributed and collabora-tive	No	Yes	No	No	Anomaly	AODV, DSR, DSDV	IDS agent for collaboration detection
P. Albers, O. Camp [44]	LIDS	Distributed and collabora-tive	No	Not implemented yet	No	No	Misuse, anomaly	Not implemented yet	Local IDS mobile agent for intrusion detection model
Kachirski and Guha [45]	None	Hierarchical architecture	No	No	No	Audit all system adhoc	Anomaly	Nothing	Hierarchical IDS using mobile agent
Sterne et al. [46]	None	Hierarchical architecture	No	Not implemented yet	No	Audit all system adhoc	Misuse, Anomaly	Not implemented yet	Dynamic intrusion detection hierarchy model
B. Sun, K.Wu, and U. W. Pooch [47]	ZBIDS	Distributed and collabora-tive	No	Yes (Disruption attacks)	No	No	Anomaly	DSR	Routing protocol protection from disruption

V. CONCLUSIONS AND FUTURE RESEARCH

With the nature of mobile ad hoc networks, almost all of the intrusion detection systems (IDSs) are structured to be distributed and have a cooperative architecture (see table 1). Refer to the table 1, mostly the proposed research prefers using anomaly detection approach. An intrusion detection system aims to detect attacks on mobile nodes or intrusions into the networks. However, attackers may try to attack the IDS system itself. Accordingly, the study of the defense to such attacks should be explored as well.

REFERENCES

[1] D.B. Johnson, D.A. Maltz, et.al. "The dynamic Source Routing Protocol for Mobile Ad hoc Networks (DSR)". Internet Draft, draft-ietf-manet-dsr-07.txt, work in progress, 2002

[2] T. Clausen, P. Jaquet, et.al. "Optimized link state routing protocol". Internet Draft, draft-ietf-manet-olsr-06.txt, work in progress, 2001

[3] C.E. Perkins, P. Bhagwat. "Highly dynamic destination-sequenced distance-vector routing (DSDV) for mobile computers". SIGCOMM 94 Conference on Communications Architectures, Protocols and Applications, 1994

[4] C.E Perkins, E. Belding-Royer. "Ad hoc On-demand Distance Vector (AODV)", Request For Comments (RFC) 3561, 2003

[5] C. Endorf, E. Schultz and J. Mellander, "Intrusion Detection & Prevention", McGraw-Hill, ISBN: 0072229543, 2004.

[6] J. P. Anderson. "Computer Security Threat Monitoring and Surveillance". Technical Report, James P. Anderson Co., Fort Washington, PA, 1980

[7] D.E. Denning, "An Intrusion-Detection Model". IEEE Transactions on Software Engineering, pp. 222- 231, 1987

[8] L. Heberlein, G. Dias, et.al. "A network security monitor". Proceedings of the IEEE Symposium on Security and Privacy, pp. 296-304, 1990

[9] A. Hijazi and N. Nasser. "Using Mobile Agents for Intrusion Detection in Wireless Ad Hoc Networks" in Wireless and Optical Communications Networks (WOCN), 2005

[10] T. F. Lunt, R. Jagannathan, et al. "IDES: The Enhanced Prototype C a Realtime Intrusion-Detection Expert System". Technical Report SRI-CSL-88-12, SRI International, Menlo Park, CA, 1988

[11] M. Esposito, C. Mazzariello, et.al. "Evaluating Pattern Recognition Techniques in Intrusion Detection Systems". The 7th International Workshop on Pattern Recognition in Information Systems, pp. 144-153, 2005

[12] S. Kumar and E. Spafford, "A Pattern Matching Model for Misuse Intrusion Detection". The 17th National Computer Security Conference, pp. 11-21, 1994

[13] P.A. Porras and R. Kemmerer, "Penetration State Transition Analysis C a Rule-Based Intrusion Detection Approach". The 8th Annual Computer Security Application Conference, pp. 220-229, 1992

[14] P. Porras and A. Valdes, "Live Traffic Analysis of TCP/IP Gateways". ISOC Symposium on Network and Distributed System Security, San Diego, CA, 1998

[15] H. Debar, M. Becker and D. Siboni. "A Neural Network Component for an Intrusion Detection System". Proceedings of IEEE Symposium on Research in Security and Privacy, Oakland, CA, pp. 240-250, 1992

[16] S. Forrest, S.A. Hofmeyr, and A. Somayaji. "Computer Immunology". Communications of the ACM, pp. 88-96, 1997

[17]N. Ye, X. Li, et.al. "Probabilistic Techniques for Intrusion Detection Based on Computer Audit Data". IEEE Transactions on Systems, Man, and Cybernetics, pp. 266-274, 2001
[18]W. Lee, S.J. Stolfo, K.W. Mok. "A Data Mining Framework for Building Intrusion Detection Models". IEEE Symposium on Security and Privacy (Oakland, California), 1999
[19]G. Florez, S.M. Bridges, and R.B. Vaughn, "An Improved Algorithm for Fuzzy Data Mining for Intrusion Detection". The North American Fuzzy Information Processing Society Conference, New Orleans, LA, 2002
[20]H. Debar, M. Dacier, and A.Wespi, "A Revised Taxonomy for Intrusion-Detection Systems". Annales des Telecommunications, pp. 361-378, 2000
[21]A.J. Menezes, S.A. Vanstone, P.C. Van Oorschot, "Handbook of Applied Cryptography", CRC Press, Inc., USA, 2001
[22]A. Mishra, K. Nadkarni, and A. Patcha. "Intrusion Detection in Wireless Ad Hoc Networks". IEEE Wireless Communications, Vol. 11, Issue 1, pp. 48-60, 2004
[23]L. Zhou and Z. J. Haas. "Securing ad hoc networks". IEEE Network Magazine , 1999
[24]Y. Zhang, W. Lee, and Y. Huang. "Intrusion Detection Techniques for Mobile Wireless Networks". ACM/Kluwer Wireless Networks Journal (ACM WINET), Vol. 9, No. 5, 2003.
[25]E.C.H. Ngai, M.R. Lyu, R.T. Chin. "An authentication service against dishonest users in mobile ad hoc networks, IEEE Proceedings on Aerospace Conference, vol. 2, pp. 1275–1285 2004.
[26]L. Blazevic et al. "Self-organization in mobile ad-hoc networks: the approach of terminodes, IEEE Communications Magazine , pp. 166–173, 2001
[27]W. Zhang, R. Rao, et. al. "Secure routing in ad hoc networks and a related intrusion detection problem", IEEE Military Communications Conference (MILCOM), vol. 2, 13–16 p. 735– 740, 2003
[28]J. Kong et al. "Adaptive security for multi-layer ad-hoc networks", Special Issue of Wireless Communications and Mobile Computing, John Wiley Inter Science Press , 2002
[29]P. Kyasanur, N. Vaidya. "Detection and handling of MAC layer misbehavior in wireless networks". International Conference on Dependable Systems and Networks. pp. 173–182, 2003
[30]Y. Zhang, W. Lee, Intrusion detection in wireless ad-hoc networks, The 6th Annual International Conference on Mobile Computing and Networking, pp. 275–283, 2000
[31]Y. Hu, A. Perrig, and D. Johnson. "Packet leashes: A defense against wormhole attacks in wireless ad hoc networks". Proceedings of IEEE INFOCOM'03, 2003
[32]Y. Hu, A. Perrig, D. Johnson, "Ariadne: a secure on-demand routing protocol for ad hoc networks". ACM MOBICOM, 2002
[33]Y. Hu, A. Perrig, and D. Johnson. "Rushing attacks and defense in wireless ad hoc network routing protocols". In Proceedings of ACM MobiCom Workshop - WiSe'03, 2003
[34]J. R. Douceur. "The sybil attack". The 1st International Workshop on Peer-to-Peer Systems pp. 251–260, 2002.
[35]J. Hubaux, L. Buttya´n, S. Capkun, "The quest for security in mobile ad hoc networks." The 2nd ACM International Symposium on Mobile Ad Hoc Networking and Computing, 2001
[36]P. Papadimitratos, Z.J. Haas, E.G. Sirer, "Path set selection in mobile ad hoc networks", The Proceedings of the 3rd ACM International Symposium on Mobile Ad Hoc Networking and Computing, pp. 1–11, 2002
[37]B. DeCleene et al. "Secure group communications for wireless networks". IEEE Military Communications Conference, 2001.
[38]S. Bo, W. Kui, U.W. Pooch. "Towards adaptive intrusion detection in mobile ad hoc networks". IEEE Global Telecommunications Conference, pp. 3551–3555, 2004
[39]C. Douligeris, A. Mitrokosta, "DDoS attacks and defense mechanisms: classification and state-of-the-art". Computer Networks: The International Journal of Computer and Telecommunications Networking 44 (5), pp. 643–666, 2004
[40]C.M. Chlamtac, J.J.-N. Liu, Mobile ad hoc networking: imperatives and challenges, Ad Hoc Networks 1, 2003
[41]H. Yang, H.Y. Luo, et.al. "Security in Mobile Ad Hoc networks: challenges and solutions". IEEE Wireless Communications, pp.38–47 , 2004.
[42]C. Krugel and T. Toth. "Applying mobile agent technology to intrusion detection". In ICSE Workshop on Software Engineering and Mobility, 2001.
[43]T. Anantvalee and J. Wu. "A Survey on Intrusion Detection in Mobile Ad Hoc Networks", Book Series Wireless Network Security, pp. 170 – 196, ISBN: 978-0-387-28040-0, 2007
[44]P. Albers, O. Camp, et al. "Security in Ad Hoc Networks: a General Intrusion Detection Architecture Enhancing Trust Based Approaches". Proceedings of the 1st International Workshop on Wireless Information Systems (WIS-2002), pp. 1-12, April 2002
[45]O. Kachirski, R. Guha. "Effective Intrusion Detection Using Multiple Sensors in Wireless Ad Hoc Networks." Proceedings of the 36th Hawaii International Conference on System Sciences (HICSS'03), IEEE, 2003
[46]D. Sterne, P. Balasubramanyam, et al. "A General Cooperative Intrusion Detection Architecture for MANETs". Proceedings of the 3rd IEEE International Workshop on Information Assurance (IWIA'05), pp. 57-70, 2005
[47]B. Sun, K.Wu, and U. W. Pooch. "Alert Aggregation in Mobile Ad Hoc Networks". The 2003 ACM Workshop on Wireless Security in conjuction with the 9th Annual International Conference on Mobile Computing and Networking (MobiCom'03), pp. 69-78, 2003
[48]C. Ko, J. Rowe, P. Brutch, K. Levitt, "System Health and Intrusion Monitoring Using a hierarchy of Constraints," Proceeding of 4th International Symposium, RAID, 2001

ISSN: 1411-1284

Planning of Digital Television System with DVB-T Technology In Indonesia

Denny Setiawan, Adis Alifiawan

Directorate of Frequency Spectrum and Satellite Orbit
Directorate General of Posts and Telecommunications
Sapta Pesona Building, 7th floor
Jl. Medan Merdeka Barat 17 Jakarta 10110
Telp. +62 21 3834983, Fax: +62 21 3522915
E-mail: denny.setiawan71@ui.edu, adis_alifiawan@yahoo.com

Abstract This paper will explain the method that is being used to allocate channels for digital television system in Indonesia. The system uses DVB-T as the underlying technology. The various types of Indonesian land surfaces need special treatment because it is related to radio wave propagation modeling. The special treatment is implemented by software simulation using CHIR Plus BC by LS Telecom. The main aspect to be seen from the simulation is interference, both from the same channel (co-channel) or from the adjacent channel. As an example, there will be showed the plan for several regions in Indonesia. Those are Banten, Jakarta, and West Java.

Keywords: DVB-T, interference, co-channel interference, adjacent-channel interference, Protection Ratio (PR).

I. INTRODUCTION

As the television business grows, the demand for channel availability is increasing too. The rapid development of broadcasting technology also creates better broadcasting system. From these two factors, several broadcasting system for digital television has been invented, those are DVB (Digital Video Broadcasting) from Europe, ATSC (Advanced Television Systems Committee) from United States, and ISDB (Integrated Services Digital Broadcasting) from Japan. However, the Indonesian government chooses the DVB standard to be implemented in Indonesia eventually.

DVB technology is actually a family of digital television broadcasting systems. It includes several variants [1]. Each of them relates to the transmission media that is used; those are DVB-T, DVB-S, and DVB-C. The extension T, S, and C stand for Terrestrial, Satellite, and Cable.

Terrestrial reception is divided into two parts, fixed reception and mobile reception. For the mobile reception, there is a technology called DVB-H. The extension H stands for Handheld.

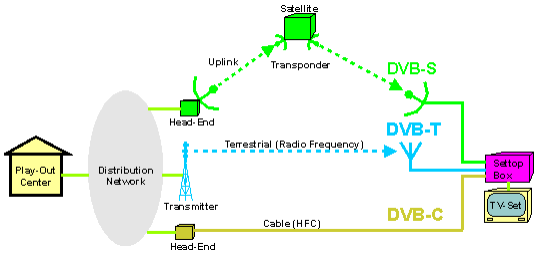

Figure 1. DVB Variants

DVB-T standard which will be implemented in Indonesia has technical parameters including system variant and designator that is adopted from M3 ITU-R. System variant that has been chosen is C2. Whereas the designator mode used is G type with 8000 carriers. The channel itself is assumed to be Ricean.

			Required C/N for BER=2. 10-4 after Viterbi (quasi error-free after Reed-Solomon, *)				
System variant	Modulation	Code Rate	Gaussian channel	Ricean channel (F1)	Rayleigh channel (P1)	Guard Interval	Bit Rate Mb/s
C2	64-QAM (M3)	2/3	16.5	17.1	19.3	1/8	22.12

Table 1. DVB-T system variant specifications used in Indonesia

In [2], there is an explanation about the equations used to determine Minimum Field Strength (MFS) for DVB-T system. MFS defines the technical threshold for field strength that still gives good quality reception in the receiver side. With the specification of 8 MHz bandwidth and lower UHF band allocation, that is channel 25 to 42, the MFS that is recommended is 42,6 dBµV/m.

II. PROTECTION RATIO (PR)

Protection ratio is a minimum field strength ratio between wanted signal and unwanted signals

in a certain service area that must be fulfilled to ensure good quality reception of the wanted signal. In other words, this is the threshold for interferences to be allowed.

PR values used in this planning process are taken from tables in [2]. PR values dedicated for co-channel and adjacent-channel interferences in DVB/DVB viewpoint (wanted: DVB; interfering: DVB) are as follows.

Modulasi	Code Rate	Gaussian Channel	Rice Channel	Rayleigh Channel
64-QAM	2/3	19	20	22

Table 2. PR for co-channel DVB/DVB

Channel	N-1	N+1
Protection Ratio	-30	-30

Table 3. PR for adjacent-channel DVB/DVB

Because of the planned allocation of DVB-T is in the UHF band which has been occupied by analog TV technology, it is necessary to see the interference between these two technologies. Based on the PAL standard of UHF TV implemented in Indonesia, the PR values for co-channel and adjacent-channel in DVB/TV viewpoint (wanted: DVB; interfering: TV) and in TV/DVB viewpoint (wanted: TV; interfering: DVB) are as follows.

Modulasi	Code Rate	Protection Ratio
64-QAM	2/3	3

Table 4. PR for co-channel DVB/TV

Modulasi	Code Rate	Protection Ratio	
		N-1	N+1
64-QAM	2/3	-35	-38

Table 5. PR for adjacent-channel DVB/TV

Sistem Analog	Unwanted Signal : DVB-T, 8 MHz	
	Trop. Interference	Cont. Interference
PAL B/G	34	40

Table 6. PR for co-channel TV/DVB

Sistem Analog	Unwanted Signal : DVB-T, 8 MHz	
	Trop. Interference	Cont. Interference
PAL B/G	-9	-5

Table 7. PR for adjacent-channel TV/DVB

III. DVB-T FREQUENCY ALLOCATION

DVB-T technology in Indonesia will be allocated in UHF band IV and V with most of the service areas and test points are already defined in [3]. In UHF band IV there are 16 channels (channel 22 – 37) and in UHF band V there are 27 channels (channel 38 – 62). However, not all of those channels are allocated for DVB-T, only channel 25 to 42 that are planned to be occupied (18 channels).

These 18 channels divided into 3 groups, those are group A, B, and C as can be seen in table 8. Each frequency group is allocated in each service area. The allocation process of the frequency groups must be very careful so that all of service areas can fulfill the PR requirement.

Group	1	2	3	4	5	6
A	25	28	31	34	37	40
B	26	29	32	35	38	41
C	27	30	33	36	39	42

Table 8. DVB-T frequency groups

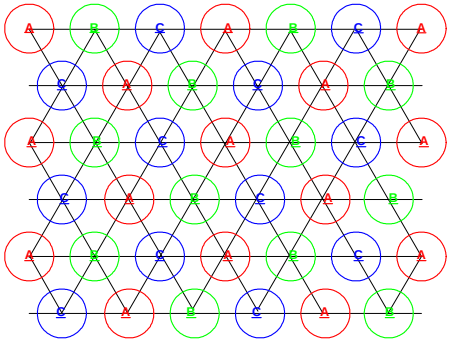

Figure 2. Configuration of group implementation

IV. THE SIMULATION OF DVB-T IMPLEMENTATION

In the planning of DVB-T implementation, DG Postel uses software simulation for modeling the radio wave propagation from transmitter in each service area. The software that is used is CHIR Plus BC by LS Telecom. This software has the data of Indonesian land surfaces.

To determine the transmitter location in simulation, it is decided to use one of the existing analog TV transmitters in the area after some considerations. However, if there is no existing transmitter yet, then it is decided to put new transmitter under some feasibility considerations. First, it is prioritized to allocate in urban environment. This is under the practical considerations of energy supply and transmitter maintenance. If the urban sited of transmitter still can't reach all the service area being planned, then it will be moved to another point so the service area is covered fully. The full coverage is defined when all of the test points' field strength reception are equal or greater than the MFS which is 42,6 dBµV/m.

In figure 3 below, it can be seen that the field strength contour is created follows the test points'

location. It is because test points defined as the outer points of service area.

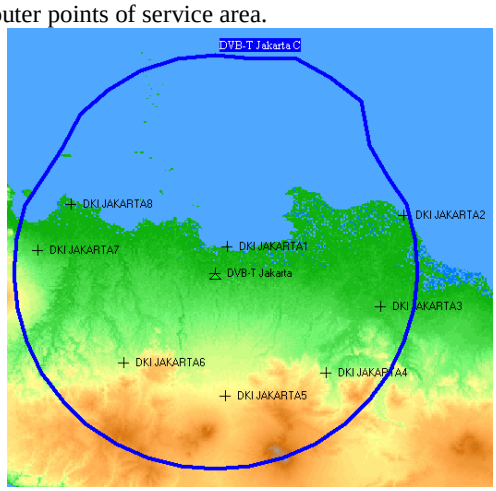

Figure 3. Contour is created follows the test points' location

It can be seen in attachment (figure 4) the simulation result for service areas in the region of Banten, Jakarta, and West Java. Each service area is characterized with one field strength contour. At the points on the contour the wanted field strength and the minimum field strength are equal. Each contour is colored red, green, and blue represent the group allocated for the area. Red represents group A, green represents group B, and blue represents group C. To ensure that all of the group allocation has been appropriate, then test points evaluation should be done. If the entire test points in a certain service area have difference between the wanted signal and unwanted signals equal or greater than PR, then the allocation has been proven to be appropriate. As an example, chose DVB-T Jakarta which has service area covers Jabodetabek (Jakarta, Bogor, Tangerang, and Bekasi).

In table 9 column 2 can be seen that field strength in Jakarta's test points is greater than MFS. It means service area Jakarta has been fully covered. Whereas next columns from table 9 shows the values of received field strength in Jakarta's test points from other transmitters around it.

Field strength from other transmitters need to be considered because it is useful to analyze the interferences that suffer service area Jakarta. It is seen in table 10 the calculated field strength differences in Jakarta's test points between the field strength received from Jakarta transmitter and one that received from surrounding transmitters. No value in table 10 is less than ITU recommended PR values as stated above. Those are 20 dB for co-channel and -30 dB for adjacent-channel interferences.

From figure 4, it can be seen that service area Cirebon and Majalengka use the same frequency group, group B. It is also happened in service area Sumedang and Kuningan which use the same frequency group, group C. These 4 service areas are using SFN (Single Frequency Network) technique. Service area Cirebon and Majalengka merged into SFN ID 18. Service area Sumedang and Kuningan merged into SFN ID 19. The merger has to be done because there is no other way to allocate different frequency group for these areas. There is too crowded in there. If it is still forced to have different group, it will interfere the surrounding areas.

Interference with analog TV is not the main concern in this planning simulation because it relates with the policy from Indonesian frequency regulator, which is DG Postel, as described bellow.

V. POLICY TOWARD ANALOG TV

DVB-T allocation in UHF band will absolutely clash with analog TV which has occupied the band first. The policy from DG Postel related to this issue is to give the analog TV stations a transition period. The transition period must be used by them to migrate to digital television technology. While in the transition period, the clashed channel will be prioritized for analog TV. It means that every DVB-T station which clash with occupied analog TV station in a certain channel will be allocated in another feasible UHF channel.

To allocate clashed DVB-T station to another UHF channel, there are few things to consider. First of all, the new channel must be ensured that no one occupy it. Then, this new channel must also be evaluated for interference to the surroundings. Third, if the allocations take place in the border to another country, it must be held coordination with that country. The countries have to be considered for coordination in Indonesia are Malaysia and Singapore.

VI. CONCLUSION

The most important thing in DVB-T frequency group allocation planning is to consider interferences so it still under the PR threshold. Interferences have to be seen from two viewpoints, from DVB-T as the wanted side and DVB-T as the unwanted side to another technology. Two conditions have to be concerned for each of them, co-channel and adjacent-channel interferences. Beside of that, the frequency group allocations have to be as efficient as possible.

REFERENCES

[1] A . Shanmugam, " Terestrial Data Broadcasting ", UNESCO – ITU – ABU Regional Workshop : Enabling Implementation of ICTs.

[2] International Telecommunication Union (ITU). "Rec. ITU-R BT.1368-3, Planning criteria for digital terrestrial television services in the VHF/UHF bands"
[3] Keputusan Menteri Perhubungan Nomor 76 Tahun 2003, Rencana Induk (*Master Plan*) Frekuensi Radio Penyelenggaraan Telekomunikasi Khusus Untuk Keperluan Televisi Siaran Analog Pada Pita *Ultra High Frequency* (UHF).

BIBLIOGRAPHIES

[1] Dr. Lars-Göran Larsson. Introduction of Digital Terrestrial TV Broadcasting in Indonesia. 2006.
[2] International Telecommunication Union (ITU). 2006. "Final Acts of the Regional Radiocommunication Conference for planning of the digital terrestrial broadcasting service in parts of Regions 1 and 3, in the frequency bands 174-230 MHz and 470-862 MHz (RRC-06)". Geneva, 15 Mei – 16 Juni 2006.

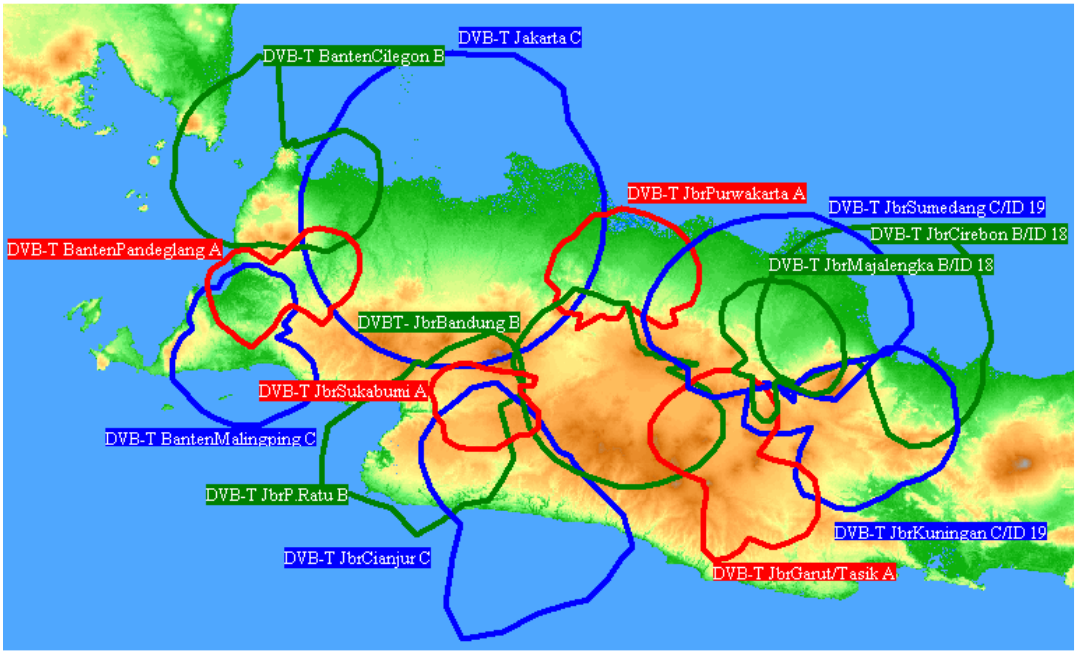

Figure 4. Simulation result for DVB-T service areas in the region of Banten, Jakarta, and West Java.

	Field Strength (dBuV/m)									
Test Points	JAKARTA	SUMEDANG	MALINGPING	CIANJUR	BANDUNG	CILEGON	P. RATU	PURWAKARTA	SUKABUMI	PANDEGLANG
	Group C	Group C	Group C	Group C	Group B	Group B	Group B	Group A	Group A	Group A
JAKARTA1	86.5	14.4	11.3	-10.1	12.1	25.9	-2.3	19.3	-35.8	17.8
JAKARTA2	43.3	23.2	1.3	-18.7	11.7	7.9	-7.8	31.5	-40.4	4.1
JAKARTA3	48.3	26.3	3.6	-13.3	25.7	12.3	14.2	45.4	-33.9	6.4
JAKARTA4	52	23.3	7.2	-7.4	36.6	14.2	26.4	35.6	-29.2	9.6
JAKARTA5	57.4	15.5	12.7	21.3	25.5	19.9	7.3	20.8	-16.8	17.8
JAKARTA6	56.7	9.7	19.4	17.4	12.2	29.5	-0.3	11.5	-9.1	33.7
JAKARTA7	46.6	5.1	24.1	7	1.3	59.9	-12.7	6	-22.9	32.4
JAKARTA8	50.3	5.8	18.5	4.4	0.9	54.9	-10.9	6.9	-29.5	24.3

Table 9. Received field strength in Jakarta's test points

	Field Strength Difference (dBuV/m)								
Test Points	SUMEDANG	MALINGPING	CIANJUR	BANDUNG	CILEGON	P. RATU	PURWAKARTA	SUKABUMI	PANDEGLANG
	Group C	Group C	Group C	Group B	Group B	Group B	Group A	Group A	Group A
JAKARTA1	72.1	75.2	96.6	74.4	60.6	88.8	67.2	122.3	68.7
JAKARTA2	20.1	42	62	31.6	35.4	51.1	11.8	83.7	39.2
JAKARTA3	22	44.7	61.6	22.6	36	34.1	2.9	82.2	41.9
JAKARTA4	28.7	44.8	59.4	15.4	37.8	25.6	16.4	81.2	42.4
JAKARTA5	41.9	44.7	36.1	31.9	37.5	50.1	36.6	74.2	39.6
JAKARTA6	47	37.3	39.3	44.5	27.2	57	45.2	65.8	23
JAKARTA7	41.5	22.5	39.6	45.3	-13.3	59.3	40.6	69.5	14.2
JAKARTA8	44.5	31.8	45.9	49.4	-4.6	61.2	43.4	79.8	26

Table 10. Received field strength differences in Jakarta's test points

ISSN: 1411-1284

Spiht Compressed Image Transmission With Diversity Equal Gain Combining Method On Wavelet Domain

Baharuddin

Faculty of Engineering, University of Andalas, Kampus Limau Manis, Padang 25163
Tel. 075172497, fax. 075172566 email : baharuddin@ft.unand.ac.id

Abstract– **This paper describes a simulation of the image transmission system with diversity equal gain combining method on wavelet domain. The SPIHT algorithm is used for image compression transmission on wireless channel. Diversity equal gain combining methods is used to combat errors during image transmission on wireless channels. The use of Reed Solomon channel coding is to recover errors from transsmitted image. The result shown that diversity equal gain combining method can be improved significantly the performance of image transmission**.

Keywords– Diversity Selection Combining, SPIHT, Reed-Solomon, Wavelet, Image Transmission.

I. INTRODUCTION

Among the multimedia information, the use of image become one of the important features and has been widely use in various applications such as internet, medical image, distance security camera, MMS (Multimedia Messaging Service) and other applications (2). It indicates that the use of image transmission system wirelessly is more desire and keeps growing. Technology in telecommunication is growing rapidly specially on wireless communication (11). It supported by the growing of portable communication technology that make it possible to exchange the multimedia information (data, voice image and video) where it becomes more popular and more desire.

On transmission over wireless channel, there are cases that can cause the degrade quality of information: noise and fading(5). The disturbance can cause the wrong in receiving information on receiver. The occurrence of disturbances is random and unpredictable. It needs a technique to improve the quality of signal on receiver.

Beside that, the transmission over wireless channel has limitation bandwidth, while image tends to have big capacity. It can cause the ineffective use of bandwidth (8). To overcome the problem, it needs a technique to reduce number of data in image without loosing the important data that appropriate with human visual characteristic.

The research proposed here referred to compression technique (1). For selection combining techniques referred to method proposed (6), but channel model used in this research is fading distribution rayleigh and noise which has normal distribution gaussian (9).

In 1996, A Said and W A Pearlman purposed an compressed image technique wavelet based published in journal *A New, Fast, and Efficient Image Codec Based on Set Partitioning In Hierarchical Trees* (1). That technique called SPIHT that has fast algorithm and it is not so difficult. In 2004, Hafeth Hourani did a research about techniques in overcoming the phenomena of fading and noise on wireless channel published in journal *An Overview of Diversity Techniques in Wireless Communication Systems* (5). He purposed diversity techniques as one of the way to overcome fading and noise in wireless communication systems..

Several methods for image transmission over wireless channels had been done such as Liane C Ramac and Pramod K Varshney proposed *A Wavelet Domain Diversity Method for Transmission of Images over Wireless Channels*(6) that used diversity techniques on domain wavelet to get the good reconstruction image. In this image transmission, two-state Gilbert-Elliott channel (3),(4) was used. P G Sherwood and K Zeger in their journal *Error Protection for Progressive Images Transmission over Memoryless and Fading Channels (*7) used data protection technique during transmission, and also Nikolaos Thomos, Nikolaos V Boulgouris, and Michael G Strinzis in their journal *Wireless Image Transmission Using Turbo Codes and Optimal Unequal Error Protection* (10) used *Turbo Codes* to protect image during transmission

In this paper, image information with size 8 bpp was compressed with rate 0.7 bpp. SPIHT algorithm were used to get the image transmission system to maximize the use of bandwidth and diversity selection combining technique were used to improve image quality on receiver and Reed Solomon channel coding

(31.15) were used to protect data during transmission process. So the title of this research is "SPIHT Compressed Image Transmission With Diversity Equal Gain Combining Method On Wavelet Domain"

II. BASIC THEORY

2.1 Diversity Equal Gain Combining Method for Compressed Images

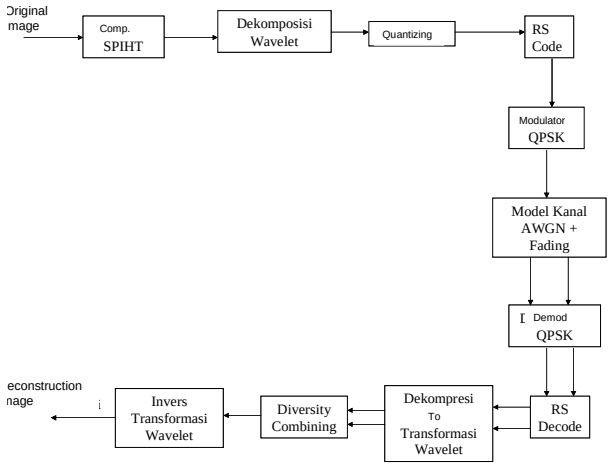

Figure 1. Diagram block of compressed image transmission SPIHT with *Diversity Equal Gain Combining method* on Wavelet Domain

The process of diversity combining use two diversity channels, by implementing error correction with interleave bit stream binary 100 bit in row and grouped bit stream to blocks. Figure 2 showed coding method with interleaving and RS channel coding for a given data block. Blocks are transmitted by rows and then interleaving the blocks by coloum. Diversity combining method uses the basic of combination block on wavelet domain. The received bit stream from diversity channel that uncorrelated are divided to L blocks and compare to block by block. The diversity rule used on compressed image transmission system SPIHT is based on the dividing block. (6)

2.2 Diversity Equal Gain Combining Algorithm

Algorithm of this diversity is based on block choosing of bit *b(l)*, from one bit stream, it is based on the characteristic of wavelet transformation, and this rule can be defined as follow:

One of the main characteristics of a SPIHT compression code technique is the process of sequencing the transmissitted data. Algorithm of sequncing coefisient is based on the choosing of significant coeficient with $2^n \le |c_{i,j}| < 2^{n+1}$ where *n* lessen on every pass. If $|c_{i,j}| \ge 2^n$ the coefisient is significant, other than that, the coeficient is not sicnificant. SPIHT compression will be done with the ratio of compression 0.7 bit per pixel. The bit stream of SPIHT compression output will be protected with Reed Solomon channel coding (31.15) that has ability in correcting 8 bit in one code word data from 31 symbols of transmitted data. Symbols that resulted by Reed Solomon channel coding will rechange to be bit stream to become QPSK modulator input. On QPSK modulator, simulation will done with baseband model. The output of QPSK modulator input will transmit lessly with Rayleigh Fading channel model and GN (Additive White Gaussian Noise) to model error that possible happen on transmission lessly.

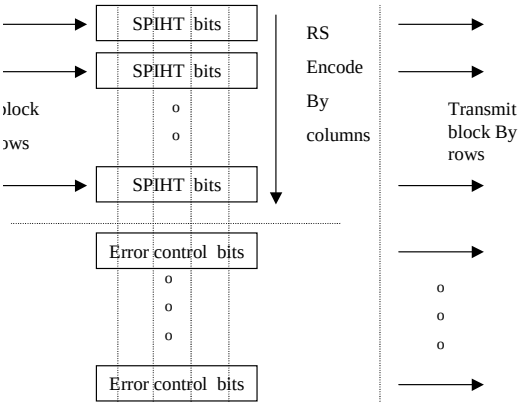

Figure 2. Interleaving scheme with coding for a given data block.

On the receiver, this system is designed with the algorithm of diversity equal gain combining technique by using 2 diversity antennas to correct the error of information signal during transmission. Algorithm from Diversity Equal Gain Combining technique is explained as follows:

Signals that passed on AWGN channel and Rayleigh Fading will get error. It caused error of received information on receiver. Diversity equal gain combining technique is used to reduce the error. Two diversity antennas on receiver are used to receive signal from two channels of multipath fading + AWGN that uncorrelated each other. Two uncorrelated signals from two diversity antennas become the input for the block of diversity EGC (*Equal Gain Combining*). Both signals will co-phase to be added up without using the weight. The output from block of diversity Equal Gain Combining is determined by (Baharuddin, 2005). :

$$y(t) = \sum_{i=1}^{M} e^{-j\theta_i} r_i(t) \quad (3)$$

where $r_i(t)$ is the received of equivalent signal lowpass, it formulated as follows (Baharuddin, 2005):

$$r_i(t) = A_i e^{j\theta_i} s(t) + z_i(t) \quad (4)$$

with $s_i(t)$ is the equivalent signal lowpass that send by transmitter and $z_i(t)$ is AWGN. So, resulted signal of *diversity equal gain combining* is formulated as follows (Baharuddin, 2005). :

$$y(t) = \left(\sum_{i=0}^{M} A_i \right) s(t) + \sum_{i=0}^{M} e^{-j\theta_i} z_i(t) \quad (5)$$

with : M = total of path

With diversity combing technique, it will result an output information signal that undergone the improvement of the performance. The signal of the resulting output of diversity combing block will undergone the demodulation QPSK to become the input of decoder Reed-Solomon. The bit stream of demodulation QPSK output will be regrouped to symbols and then put to decoder Reed-Solomon to correct the error data as well as eliminate parity from the received data. The result of this block will compare to the output of SPIHT compression block on the transmitter to calculate the value of BER (Bit Error Rate). Then, the bit stream will be processed on SPIHT decompressed. The result of SPIHT decompressed will be passed on wavelet reconstruction and it can be reconstructed. To measure the quality of the design system, the reconstructed image will compare to the input original image in order to measure the PSNR (*Peak Signal to Noise Ratio*).

Two parameters which use to measure the quality of system are BER (Bit Error Rate) and PSNR (*Peak Signal to Noise Ratio*). The measure of BER is done by comparing the resulted output of SPIHT compression on transmitter and bit will be processed on SPIHT decompression on the receiver. By measuring BER (Bit Error Rate), the influence of diversity equal gain combining technique on this system can be shown. By looking at the difference of BER value between system that use diversity equal gain combining and the system without using diversity equal gain combining, we can see the influence of diversity EGC (Equal Gain Combining) techniques on the received of fix bit stream SPIHT. The smaller of BER mean the better of the system. The second parameter to measure the quality of the system is by measuring PSNR (Peak Signal to Noise Ratio). It is done by comparing between input image and resulted image (image reconstructed)

III. EXPERIMENTAL RESULTS

The Simulation of the performance of image transmission compression system SPIHT use Diversity Equal Gain Combining technique and it based on diagram block on figure 1. The analysis based on the result of symulation. The ratio compression given is 0.7 bpp. The following table is the comparison of the value of SNR, BER, and PSNR of Barbara image on ratio compression 0.7 bpp.

Tabel 1 The comparison of value between BER and PSNR of image transmission compression SPIHT with Diversity EGC technique and without Diversity EGC technique of Barbara image 0,7 bpp

SNR (dB)	Without Diversity Equal Gain Combining		With Diversity Equal Gain Combining	
	BER	PSNR (dB)	BER	PSNR (dB)
10	0,0651	7,6276	0,0133	14,779
12	0,0323	10,3681	0,0014	16,289
14	0,0114	13,0076	0,0001	18,688
16	0,0073	15,2432	$3,5342 \times 10^{-5}$	21,229
18	0,0003	17,1749	$1,2622 \times 10^{-4}$	25,846
20	$3,3266 \times 10^{-4}$	19,5359	0	31,643

Without Diversity EGC	With Diversity EGC
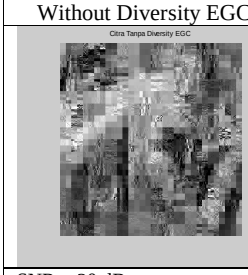	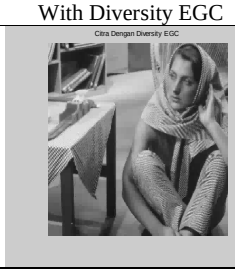
SNR = 20 dB Total of error bit received = 65 BER = $3,3226 \times 10^{-4}$ PSNR = 19,5359 dB	SNR = 20 dB Total of error bit received = 0 BER = 0 PSNR = 31,6439 dB

Figure 3. The comparison of reconstructed image Barbara between system with *Diversity* EGC and system without *Diversity* EGC and system without *Diversity* EGC with compression ratio 0.7 bpp and SNR 20 dB

From the above table, it can be seen that on SNR 10 dB on system with diversity Equal Gain Combining will get the value of BER 0,0274 and the value of PSNR 12,7754 dB, while system without diversity Equal Gain Combining will get the value of BER BER 0,0857 and the value of PSNR 5,6231 dB. From the result, it can be seen that the improvement of the system with diversity Equal Gain Combining if compare to system without diversity Equal Gain Combining. For the value of PSNR, there is an improvement 7,1523 dB and for the value of BER there is a decrease 0.0583. The improvement of PSNR value happened on every SNR value from 10 dB to 20 dB for the system without diversity Equal Gain Combining, while for system with diversity Equal Gain Combining, the improvement of PSNR value done from SNR 10 dB to 20 dB. The decrease of BER value happened on every SNR value to the value of BER zero, it happened to SNR 20 dB for system with diversity Equal Gain Combining. One of the subjective value for SNR 20 dB can be seen on figure 3

For Barbara image on ratio compression 0.7 bpp, the increase of PSNR average value is 6.9396 dB for the value of SNR from 10 dB to 20 dB. For the value BER will result the decrease of average 0.0214.

.

IV. CONCLUSIONS

Base on the experimental, it can be concluded that the increase of SNR value resulted on the decrease BER, but it does not always increase the value of PSNR of image reconstruction. It resulted that the value of PSNR does not depend on the total of bit error, but it depends on the placement of bit error on bit circuit. The increase of bit per pixel does not impact on BER value but it impact to the PSNR value of image reconstruction. The bigger of bit per pixel, means the bigger of PSNR value. On Barbara image 0.7 bpp there is the increase of PSNR on the average of 6.9296 dB and the decrease of BER on the average of 0.0214

REFERENCES

[1]. A. Said and W. A. Pearlman, **"A New, Fast, and Efficient Image Codec Based on Set Partitioning In Hierarchical Trees"**, *IEEE Trans. Circuits Syst Video Technol., vol. 6 pp. 243-250,(June 1996).*

[2]. Baharuddin**, "Transmisi Citra dengan Teknik Diversity pada Kanal Wireless"**, Thesis, *Insitut Teknologi Sepuluh November, (Januari 2005).*

[3] E. N. Gilbert, "Capacity of a burst-noise channel," *Bell Syst. Tech. J.*, pp. 1253–1265, (Sept. 1960)

.[4] E. O. Elliott, "Estimates of error rates for codes on burst error channels," *Bell Syst. Tech. J.*, vol. 42, p. 1977, (Sept. 1963).

[5] Hourani, Hafeth, **" An Overview of Diversity Techniques in Wireless Communication System"**, *Helsinki University of Technology Communication Lab 2005*

[6] Liane C. Ramac and Pramod K. Varshney, **"A Wavelet Domain Diversity Method for Transmission of Images over Wireless Channels"**, *IEEE Journal on Selected Areas in Communication, Vol. 18*, pp. 891–898 *No. 6, (June 2000).*

[7] P.G. Sherwood and K. Zeger,"**Error Protection for Progressive Image Transmission over Memoryless and Fading Channels"**, *IEEE Trans. Commun., vol.46, pp. 1555-1559, December 1998.*

[8]. Sudhakar, R, Karthiga Ms R, and Jayaraman , **"Image Compression using Coding of Wavelet Coefficients – A Survey"**, *Department of Electronic and Communication Engineering, PSG College of Technology*. 2002.

[9]. Theodore. S. Rappaport, "Wireless Communication Principles & Practice", Prentice-Hall Communications Engineering and Emerging Technologies Series, 1996

[10]. Thomos Nikolaos, Boulgouris Nikolaos V, and Strinzis Michael G, **"Wireless Image Transmission Using Turbo Codes and Optimal Unequal Error Protection"**, *IEEE Trans. On Image Processing Vol. 14* pp. 643–650 *No.11 (November 2005).*

[11]. Tuka, Veronika dan HS, Djati ,**"Peran Jaringan Seluler untuk Komunikasi Data"**, *Artikel Telekomunikasi Elektro Indonesia No.24,* pp. 24–31, *Tahun V (January 1999).*

[12]. Vijaya Chandran Ramasami, "BER Performance Over Fading Channels and Diversity Combining", EECS 862 Project, 2001.

ISSN: 1411-1284

On the Design, Implementation and Evaluation of Networking System for Context Sensitive Classroom

Kalamullah Ramli

Electrical Engineering Department, Faculty of Engineering, Universitas Indonesia
Kampus UI - Depok 16424 – INDONESIA
Tel. +62-21-7270077, Fax: +62-21-7270077, e-mail: k.ramli@eng.ui.ac.id

Abstract-***We are developing classroom with network-based context sensitive presentation media. Once the classroom's sensor detects and authenticates lecturer's mobile computer its embedded system automatically retrieves respective presentation files, runs related software, turns on the LCD and starts presentation show. The system implements method enabling identification of course that takes place at a certain time. Names of lecturer are paired with the mobile computer's MAC address for identification purpose. Therefore the abovementioned automatic process is applied to the designated lecture's mobile device. The performance of the sytem is measured on functional and file transfer mechanism. In addition to system's reliability in file transfer, results show as well linear correlation between file size and transfer time. But transferring file for the first time takes longer time than transferring the file on next occasions.***

Keywords: *Context sensitive classrom,, networking system, MAC Address, mobile device*

1. INTRODUCTION

Ubiquitous [1][2] or Pervasive technology [3] is a concept where technology is invisible to and interacts with the environment. Pervasive system interacts with the user proactively. Among the characteristics of such system are mobile [4], embedded and invisible.

We are developing and implementing smart class with pervasive approach. The system automatizes routine processes usually conducted by lecturers during their class delivery. These proceses are:

1. identification and authentification
2. file transfer (from mobile computer to class server)
3. sequence of presentation preparation, which includes activating and communicating with hardware such as LCD projector

Identification is conducted through the acknowledgment of mobile computer's MAC address. File transfer mechanism is performed through Java networking. Java methods are also used to activate presentation software, whereas communication between server and presentation hardware is achieved through serial cable RS-232.

2. CONTEXT SENSITIVE CLASS DESIGN

Smart class can be defined as a classroom whereby the environment supports the notion of context sensitive system. Context is a situation that exists in the environment. Context gives information to the system, to take proactive action. To develop context sensitive system network of hidden sensors and hidden processors are required.

In line with smart class attributes, pervasive concept requires a system to fulfil characteristics, such as:

1. Proactive to adapt with changing situation
2. Requires minimum user involvement
3. Accommodate mobile users
4. Automated processes

Unified modeling language (UML) is used first in the design cycle. Next, use case diagram, class diagram and sequence diagram are used in this process. Use case diagram explains function and features of the system from the viewpoint of actors outside the system itself. Figure 1 depicts use diagram of the system. As can be seen in Figure 1, there are four functions in the system, namely login, file transfer, system editing, and LCD projector's activation.

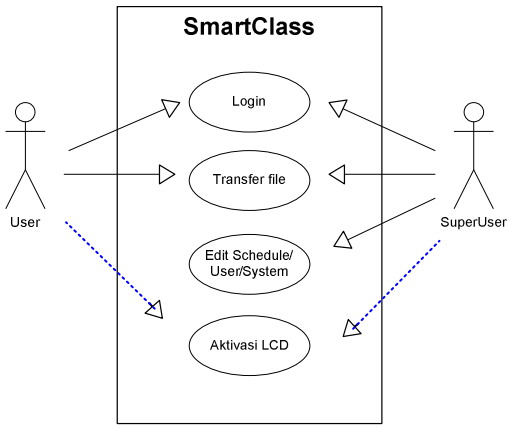

Figure 1. Use Diagram of the System

The first actor in our scenario is a lecturer. The other actor is student and system administrator or super user. System administrator has additional and

unique functions such as updating MAC address list, add/delete clients and observing log file.

Class diagram represents classes or containers of objects that build the overall system. In this diagram interrelation between classes is also shown. Due to limited space class diagram of the system could not be depicted here.

Sequence diagram is used to explain interrelation between objects to perform overall system functionalities on the basis of its sequence of occurence. Process is started when the clients entering the wireless coverage and send their MAC address to register into the class environment to get access to the smart class. The final process accomplishes when lecturer leaves the wireless coverage, presumably when the class is finished.

Figure 2 depicts one of the sequence diagrams derived in the system usage scenario.

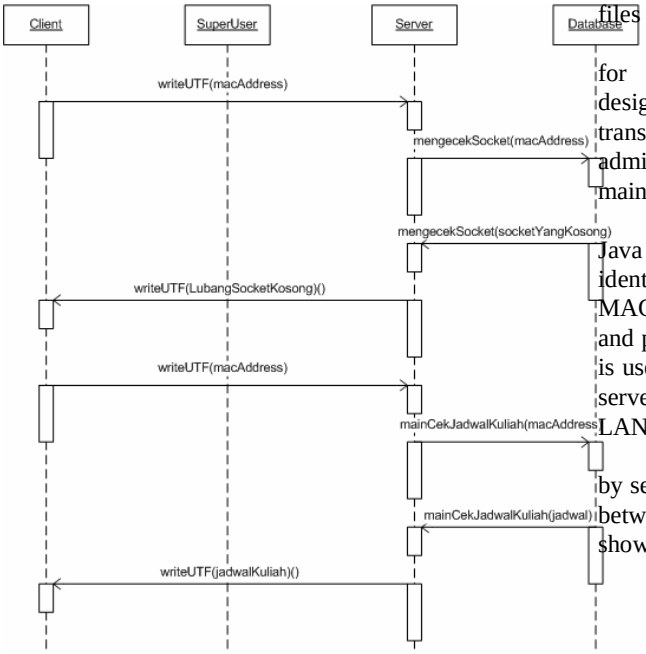

Figure 2. A Sequence Diagram of the System

3. CONTEXT-SENSITIVE CLASS ARCHITECTURE

Smart Class consists of six main parts, namely server, client, super user, wireless network, set of controlled hardware, and software application. The architecture is depicted in Figure 2.

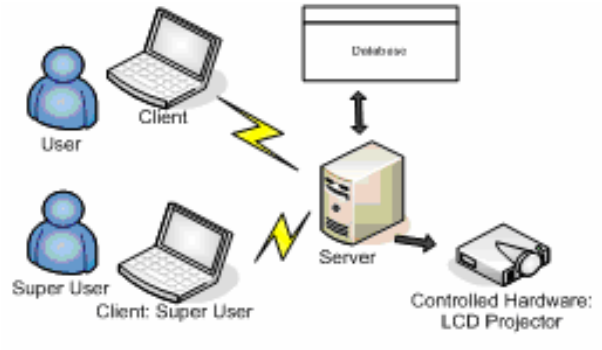

Figure 2 Smart Class Architecture

Server manages processes in the system. These include databases of lecture schedule and MAC address of lecturer's mobile computers or laptops. It is also the functions of server to switch presentation projector on and off, and transferring presentation files from laptops.

Client is user's mobile computers or laptop. File for presentation is put on a certain location designated by smart class protocol, for automatic transfer. Super user is special user who owns administrative right, such as database update and maintenance.

Software part is the main driver for the system. Java is used for both client and server. Client identification is performed through validation of MAC address and authentication through user name and password pair. Java database connection (JDBC) is used for database access. Communication between server and client is performed wirelessly. Wireless LAN is used for this purpose.

Hardware, in this case is projector, is managed by server. A control cable to manage communication between server computer and LCD projector is shown in Figure 3

Figure 3. Control Cable

Our LCD projector receives two kinds of input from the server, namely input data display and input data control. Input data display accepts picture signal. For this purpose a VGA port with 15 male pin as depicted in Figure 4 is used.

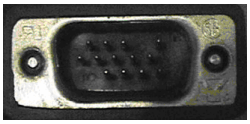

Figure 4. Male Port with 15 Pin

Input data control organizes LCD Projector operation. Controlling is performed by sending serial data using RS-232C through control cable. Control cable has two different ports at its end. Interface cable to the computer is a serial port DB-9. At the LCD end is a serial port Mini DIN-8. Figure 5 depicts both of these ports.

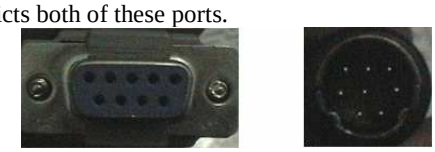

Figure 5. Female Port DB-9 and Male Port Mini DIN-8

The pin configuration between DB-9 and Mini DIN-8 ports is shown in Table 1.

Table 1. DB-9 and Mini DIN-8 Ports Configuration

Signal	Mini DIN 8	DB-9
Common Ground	8,4	5
Transmitted Data (TD)	1	3
Received Data (RD)	7	2
Data Terminal Ready (DTR)	3	4
Data Set Ready (DSR)	-	6
Request To Send (RTS)	2	7
Clear To Send (CTS)	5	8
Carrier Detect (DCD)	6	1

To control the LCD server sends serial data according to RS-232C communication method with 9600 bps, no parity, 8-bit data, 1 stop bit. Control data is set to a format shown in in Figure 6

STX (02h)	Command (3 Byte)	ETX (03h)

Figure 6. Data Control Format for LCD Projector

Character command is a special code sent by server to order LCD projector to be in a certain state. Possible states include power on and off which are used in our system. List of command codes is shown in Table 2.

Table 2. List of Command Codes for LCD Projector Control

Function	Command
Power on	PON
Power off	POF
Icon display on	MO0
Icon display off	MO1
Auto setting (RGB Input)	PAT
Status display on	DON
Status display off	DOF

4. CONTEXT-SENSITIVE CLASS EVALUATION

Our pervasive class is evaluated using two types of tests. That is, functional test and performance test. Functional test is aimed at proofing the all the functionalities of the system work properly. Performance test is targeted to verify the perceive usefulness of the sytem to the users. Usefulness of the system is obtained if system responsiveness is within the tolerance limit of user's satisfaction.

4.1 User Identification

Identification process is started when client looks for server. As wireless adapter signal of a client detects wireless access point signal, it generates and sends its MAC address to server. Server, through a look-up table database, verifies the MAC address and positively confirms if it is owned by registered lecturer. If MAC address is not a registered one server refuses connection. Figure 7 depicts this condition.

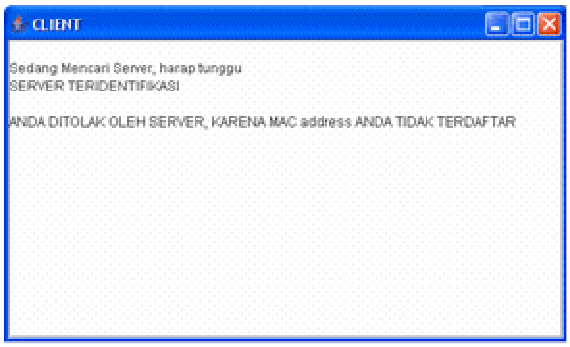

Figure 7. Server Detected, Connection Refused

Next identification phase is intended to ensure that only lecturer attending proper class at the right time is granted further access dan system services. Hence acknowledgment for initial connection does not mean acceptance for automated file transfer to the server and LCD projector activation. Figure 8 shows the lecture schedule and MAC address pair in a database table.

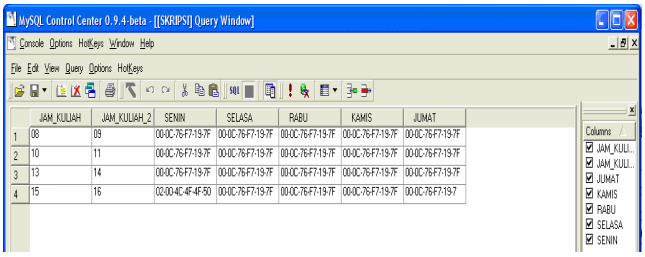

Figure 8. Lecture Schedule and MAC Address Pair

4.2 File Transfer

Lecturer clients identified entering the pervasive class zone at their lecture time have their presentation

file automatically transferred into the server. No user involvement is necessary during the process. User interface as shown in Figure 9 is emerged at client terminal as the transfer process is performed.

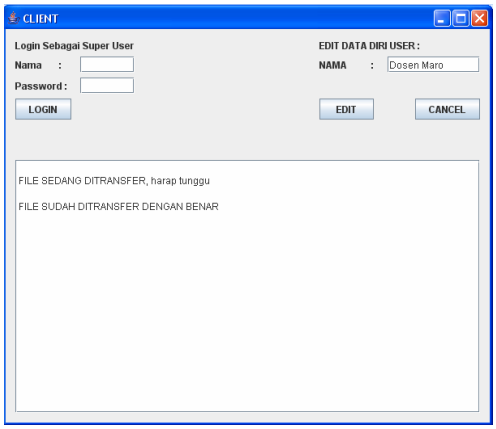

Figure 9. File is transferred to the Class Server

4.3 LCD Projector Activation

Activation is performed after the file transfer process is finished. PON and POF commands are sent to activate and deactivate the projector, respectively. LCD sends response to inform its counterpart hardware whether the command is correct and, hence, understood or not.

A sequence of ASCII carriage return code, i.e ASCII 13 or 0DH, and new lince code, i.e 10 or 0AH, is appended in each data set transfer. If LCD is ordered to standy, for example, sequence of code 02H, 50H, 4FH, 4EH, 03H, 0DH and 0AH are sent in sequence. That is, 50H for P, 4FH for O and 4EH for N. Header and tail for this data set is 02H and 03H respectively.

4.3 Performance Measurement

Performance measurement is performed for two purposes. That is, to measure reliablity the system in transferring the file and to assess the time required to accomplish this task.

Performance tests show that the system is reliable in transferring the file. The size of files transferred between client and server is maintained properly for all tests performed. In terms of measurement file transfer time we use files of different size. Measurement is performed with excellent wireless signal, using 11 Mbps access point and within the distance of 2 metres. It is found that the size of files has positive and linier correlation with the time required to transfer. The result is depicted in Figure 10.

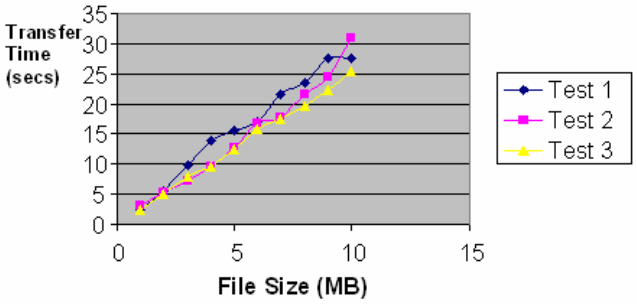

Figure 10. File Transfer Time

5. CONCLUSION

The paper describes design, implementation and evaluation of context-sensitive class room. Wireless access points, room server, mobile clients and programmable control are components of the classroom. As pervasive characteristices requires, factors such as adaptiveness, minimum user involvement, automated process, and support for mobile users have been imposed to the system.

Our functional and performance evaluation shows that the system works appropriately and fulfill perceived of usefulness. Minimum delay and minimum packet loss, though, are mainly due to light load of the network traffic during the test.

6. ACKNOWLEDGEMENT

Thanks to Robby Marolop and David Januar Tambunan for their contributions on the development and laboratory works.

7. REFERENCES

[1] Weiser, Mark. *"Creating the Invisible Interface" Symposium on User Interface Software and Technology New York, NY: ACM Press, 1994.*

[2] Wiser, Mark. *"The World Is Not a Desktop." ACM Interactions 1, no. 1 (1994): 7-8.*

[3] Satyanarayanan, M., "Pervasive Computing: Vision and Challenges**"**, IEEE Personal Communications 1070- 9916/01, August 2001

[4] Ramli, Kalamullah, "On the Developing and Evaluating the Performance of Mobile Video and e-Learning Space", the International Journal of Learning, ISSN: 1447-9494, Vol. 13, 2006

XML Transformation for Adaptive M-Learning

Sri Wahjuni[1], **Kalamullah Ramli**[2]
[1]Computer Science Department, Institut Pertanian Bogor, Kampus IPB- Bogor, Indonesia, my_juni04@ipb.ac.id
[2]Electrical Engineering Department, Universitas Indonesia, Kampus UI – Depok, Indonesia, k.ramli@eng.ui.ac.id

Abstract – ***The significant improvement of m-learning to e-learning is the capability of the first one in allowing learning materials to be accessed through mobile devices. This paper describes design and implementation of mobile adaptor in the adaptive m-learning environment, using adaptation technique through format transcoding. This technique uses eXtensible Markup Language (XML) technology. The presentation that is suitable to the device's computing capability is produced by a device specific stylesheet or known as single pipeline. PHP as an open source server scripting language is employed to implement XML transformation through XSLT due to its lightweight characteristic. Our experiment shows that the response time is still in tolerable range, i.e., less than one second.***

Keywords- m-learning, web, adaptive, single pipeline, open source.

I. INTRODUCTION

Learning is a lifelong activity [1]. The increasing requirement of mobility as well as communication and Internet technology improvement has moved the educational needs from e-learning which is based on the desktop browsers to m-learning which is based on mobile browsers. Different device characteristics between the desktop computer e.g., notebook, and the handheld devices e.g, smartphone and PDA, need different treatment.

II. BASIC THEORY

In the previous research, a web based m-learning is implemented by developing a specific mobile devices portal known as multichannel [2]. This method impacts significant disadvantages in the content compatibility and maintenance complexity. A mobile adaptor framework is proposed by Trifonova for the first time [3]. This adaptor is needed to perform presentation format adaptation among the heterogeneous computer/communication devices. However she did not mentioned how to implement this adaptor in a web based environment.

There are three locations suitable to perform Web application adaptation process, namely server, proxy, and client side [4]. In case of server, an adaptation technique is required to convert one markup language to others or known as transformation method [5].

eXtensible Markup Language (XML) is a description language that distinguishes and detaches data from its presentation. This technology supports multiplatform interoperability as well as enables the system to perform an on-the-fly adaptation via transformation. XML offers advantages such as more efficient Web management since only one data format is needed for each of its content. This, in turn, ensures the data compatibility. XML is composed by some modules that build an XML Family as pictured in Figure 1. eXtensible Stylesheet Language (XSL) is one of XML module which is used to perform an XML document presentation.

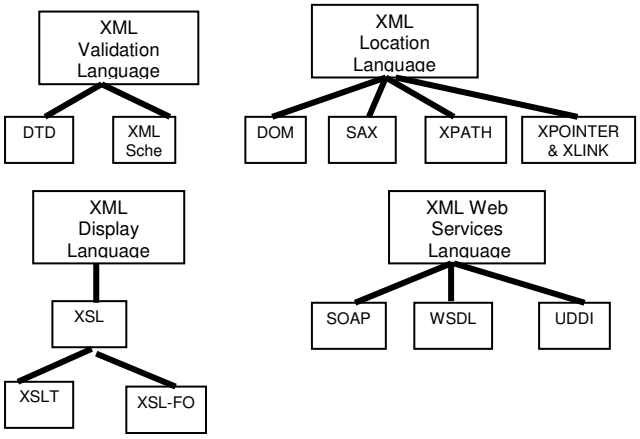

Fig. 1. XML Family

The adaptation process involves eXtensible Stylesheet Language Transformation (XSLT) and Document Object Modeling (DOM) for markup transcoding, as well as transformation processor. The XML document is the input which is applied to a device specific template (XSL) to produce a suitable markup language.

There are three transformation methods suitable to perform an XML transformation, namely single pipeline, multiple pipeline, or combination of the two. In case of single pipeline, the server page needs to identify the client device first, before chooses a suitable stylesheet to apply to the XML document. Each device needs a specific stylesheet, however a device-specific stylesheet allows to apply to different web page.

Evaluation testing is performed based on the technical quality requirements of the m-learning [6]. Those requirements are reliability (this will define the media formats), screen size and resolution (to define how a web page is presented in the client's device screen), and standard tools and metadata (to ensure the content consistency).

III. EXPERIMENTAL RESULT

In this paper we proposed a web based mobile adaptor which has an automatic client device recognition function (see Fig.2). The Context Discovery is the module to catch the client profiles which is needed by the Mobile Content Management and Adaptation module. The Packaging and Synchronization module is accessed if the client requires an off line materials.

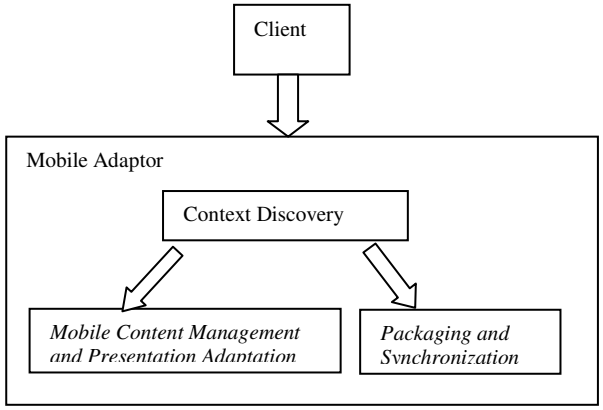

Fig. 2 Mobile Adaptor

This research implements single pipeline transformation method due to its presentation consistency and storage usage efficiency. The transformation machine is developed using PHP as a server scripting language. PHP is selected due to its lightweight characteristic and its status as open source software. Based on client recognition delivers by Context Discovery module the suitable presentation is produced by device-specific stylesheet that is obtained from the repository (see Fig. 3). Due to design simplification this research uses the same machine for web server, content server, and adaptation server.

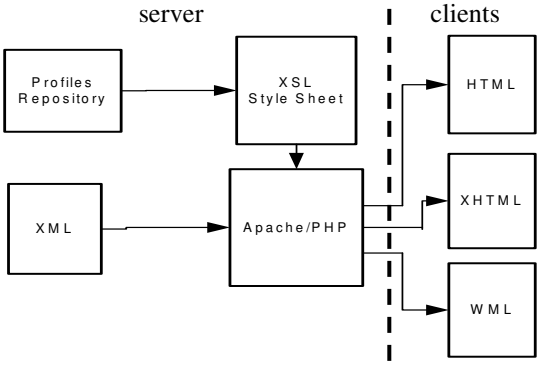

Fig. 3 Single Pipeline Transformation

XML and XSL document conversion to DOM document is needed before entering the transformation processor (see Fig. 4). This conversion will restructure the XML/XSL document to the tree structure before retrieving

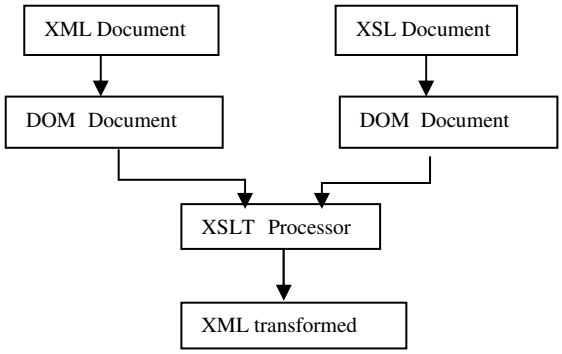

Fig. 4 Document Conversion

by the transformation processor. The output of the processor is a markup language suitable to the client browser

Figure 5 and 6 show the sample presentation of two pages which is accessed using different devices. The client just need to click or request one URL and the system will delivers the suitable presentation web page automatically.

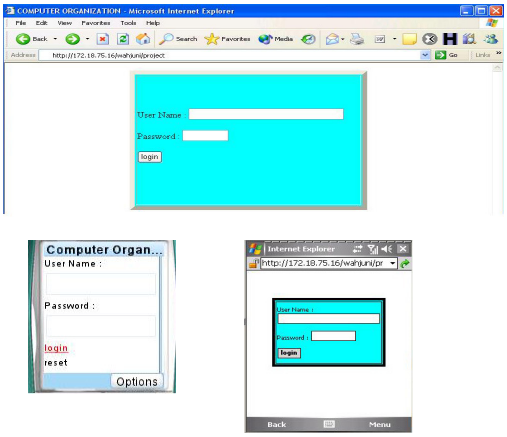

Fig.5 Sample User validation page

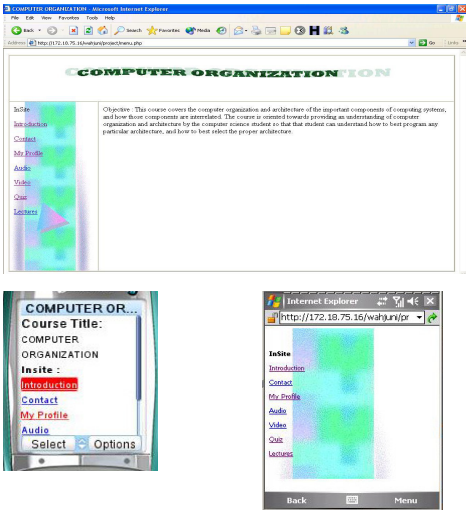

Fig. 6. Sample Front Page

The response time of four use case being tested is captured in Figure 7. The X axis is the elapsed time of the 2 second testing while the Y axis is the given response time of the validate user, access document, access quiz1, and access quiz2. The experiment shows that the average response time of the interactive use case i.e. Quiz, is 0.25 second. This duration is within the tolerable range of web accessing response time.

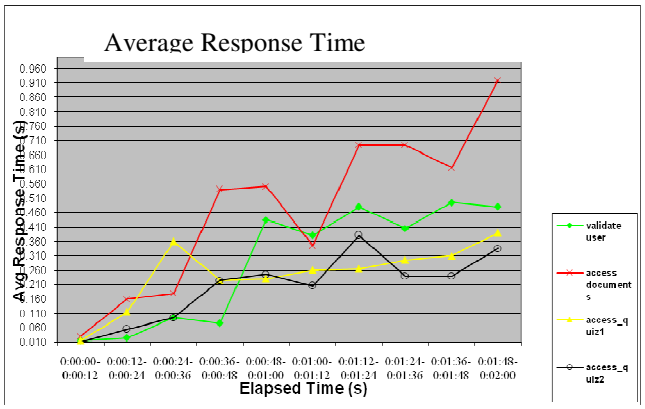

Fig. 7 Average Response Time

Conclusion

Our research work shows that XML transformation technology using XSLT can be implemented to perform on-the-fly or dynamic adaptation. This dynamic adaptation is a significant component in the adaptive m-learning development. PHP is a potential server scripting language to implement an adaptation processor as part of this XML transformation technology. Its *lightweight* characteristic, as well as its open source software status, are significant advantages. The experiment shows that the response time is still within the Web application accessing time tolerance, which is less than one second.

References

[1] Mike Sharples, "The Design of Personal Mobile Technologies for Lifelong Learning", *Computers and Education, 34*, 2000 : pp. 177-193.

[2] Jueming Chen, Kinshuk," Mobile Technology in Educational Services", *Journal of Educational Multimedia and Hypermedia*, 14 (1) 2005 : pp. 91-109.

[3] Anna Trifonova, Marco Ronchetti, **"**A General Architecture to Support Mobility in Learning", *Proceedings of the IEEE International Conference on Advanced Learning Technologies (ICALT'04)*, 2004.

[4] Mark H. Butler, "Current Technologies for Device Independence", Publishing System and Solution Laboratory HP Laboratory Bristol, Bristol, 2001.

[5] W3C.*Authoring Techniques for Device Independence*, 2004. http://www.w3.org/TR/di-atdi/ [May 21, 2007].

[6] David P., Hokyoung R. *A Framework for Assessing the Quality of Mobile Learning,* 2006. www.massey.ac.nz/~hryu [May 21, 2007].

ISSN: 1411-1284

Performance Evaluation of Weighted Round Robin based Scheduler over Wimax

Riri Fitri Sari, I Gde D, Nur Mukhayaroh, Dewi Laksmiati

Department of Electrical Engineering, University of Indonesia
Kampus Baru Baru U,I Depok, 16424, Indonesia
e-mail: riri@eng.ui.ac.id, i.gde@ui.edu , nur.mukhayaroh@ui.edu , dewi.laksmiati@ui.edu

Abstract– **Wimax is a wireless network that was designed to serve all kind of traffic. Therefore, Wimax is required to fulfill QoS requirements of any applications and information passing over the network. Appropriate scheduler implementation for packets carried on Wimax network can increase QoS achievement possibility.**

Wimax module used in our simulation was developed by Networks & Distributed Systems Laboratory (NDSL), Taiwan, as an extension to NS-2 simulator. This module uses the Weighted Round Robin (WRR) based scheduler to deal with packets transmission. This paper is aimed at evaluating WRR based scheduler in relation to Wimax network performance. Performance metrics reported in this work are packet loss, throughput, and average delay.

Keywords– Wimax, ns-2, Weighted Round Robin

I. INTRODUCTION

IEEE 802.16 standard defines specification of MAC layer and PHY layer in Wimax wireless network technology. MAC management message, i.e. request-response ranging (RNG-REQ/RNG-RSP), the downlink/uplink channel descriptor (DCD/UCD), downlink/uplink map (DL-MAP/UL-MAP), and other control messages are implemented to operate on Wimax network.

Network Simulator 2 (NS-2) has been the de-facto standard for simulating packet switched network. There are a lot of network research published works that use NS-2 to evaluate and verify the research. Although a few researchers have developed IEEE 802.16 simulator over NS-2, the tools are not for public usage.

NS-2 can quickly combine various models from traffic, network layer protocol, and MAC layer protocol. These components enable NS to simulate different types of network along with its topologies.

In our work, we install a Wimax module on NS-2.29 simulator. The Wimax module is developed by Networks & Distributed Systems Laboratory (NDSL), Taiwan. This module is focused to improve MAC protocol which inherits from original MAC protocol in NS-2. The MAC protocol implements scheduler based on WRR to manage packets transmission.

Traffic over Wimax network are classified into five classes of service, which are Unsolicit Grant Service (UGS) for traffic with constant bit rate (for example Voice Over IP without silence suppression), enhanced real time polling service (ertPS) for traffic with variable bit rate but guaranteed delay and data rate, real time polling service (rtPS)for application that generate data at variable rate periodically, non real time Polling service (nrtPS) traffic with flexible delay and guaranteed minimum data rate, and Best Effort (BE) which does not have any QoS requirement.

In this page, we review the basic theory which underlies this work and present the result analysis of the simulation on WRR scheduler over Wimax.

II. BASIC THEORY

II.1. Wimax Architecture

MAC layer in IEEE 802.16 can be divided into three sublayers, which are:

- *convergence sublayer*. This sublayer maps specific traffic in transport layer with MAC common part sublayer. The main function of this sublayer is to change IP address from upper layer to several Service Flow Identifier (SFID) or reverse process (from SFID to IP address) and record the mappings between SFID and Transport Connection Identifier (TCID). This function enables MAC layer to record important information on QoS parameters and their destination address.
- *common part sublayer*. This sublayer independent of transport layer mechanism. This sublayer responsible for fragmentation and segmentation packets received from MAC upper layer, Service Data Unit (SDU), controlling QoS, scheduling, and MAC PDU retransmission.
- *Security sublayer*, handles the security of the network, which are authentication, secure key exchange, and encryption.

Convergence sublayer classifies incoming SDU based on traffic type (voice traffic and web browser) and allocate SDU into service flow using SFID 32 bit.

When service flow is admitted or activated, the service flow is mapped into a MAP connection which will handle QoS requirement using 16 bit CID. A service flow contains a collection of several QoS parameters. Using adaptive burst profile, each service allocated to a certain physical layer configuration (for instance, modulation scheme, FEC, and more) to run the service.

After service flow is given a CID, service flow will be forwarded to the correct queue. Uplink packet handling is managed by Base Station (BS) through signaling process to Subscriber Station (SS). In SS, packet scheduler will pick the packet from the queue and transmit it to the network with suitable time slot as defined in Uplink Map Message (UL-MAP) sent by BS.

Packet header suppression is used to avoid redundant information transmission through the air. It helps decreasing the packet delay, which is required by applications such as VoIP. After service flow has been classified and has been given CID, unchanged information header (such as ATM cell ehader or IP header) will be suppressed.

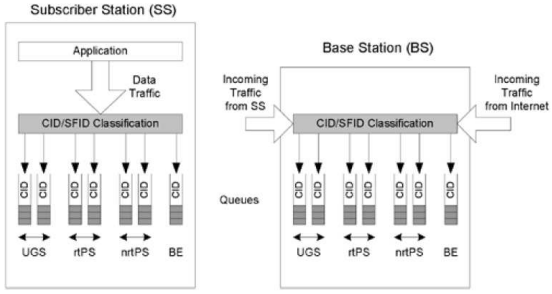

Figure 1. Traffic mapping to the correct QoS queue [3]

Protocol Data Unit (PDU) from the upper layer is inserted into different level of queue after SFID-CID mapping. Data packet in this queue is treated as MSDU and fragmented or packed into various size, depend on the scheduling operation occurs in MAC layer. Those packets are then processed using selective block Automatic Repeat Request (ARQ) if the ARQ capability is enabled.

II.2. Wimax Module

Some Wimax module components have been used in this simulation:

1. CS sublayer
2. CPCS MAC sublayer

II.3. Weighted Round Robin

WRR is a scheduling algorithm that can be implemented in many fields, for instance resource sharing in a computer or network. In network, WRR serves a number of packets from non-empty connection queue. Number of packet can be computed by normalizing weight divided by the average of packet size. The following pseudo-code presents the general WRR mechanism [2]:

```
//calculate the number of packets to be
served in each round by the connections

for each connection c
   c.normalized_weight = c.weight /
c.mean_packet_size

min = findSmallestNormalizedWeight

for each connection c
   c.packets_to_be_served =
c.normalized_weight / min

// main loop
loop
   for each non-empty connection c
      min(c.packets_to_be_served,
c.packets_waiting).times do
         servePacket c.getPacket
```

Scheduler is responsible in managing general uplink bandwidth such as in distributing resources in keeping the quality. Scheduler standard is not defined in IEEE 802.16 standard. Thus, it is an open area for academia or industry to implement scheduler which is suitable for their own purposes.

III. EXPERIMENTAL RESULTS

Based on the referenced Wimax module, our simulation uses the topology shown in Figure 2.

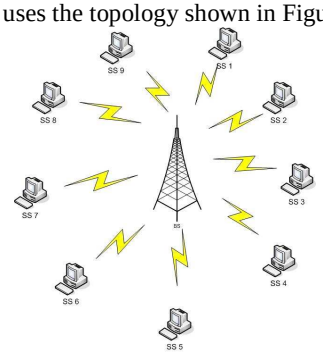

Figure 2. Simulation Topology

In this scenario, we varied the number of Subscriber Station (SS) using a particular class of service. First, simulation is executed with 5 SS that belong to UGS class. Other classes only have one SS. Subsequently, we built a topology with 5 nodes using ertPS traffic attached to the nodes The complete simulation scenario is provided in Table 1.

	UGS	rtPS	nrtPS	ertPS	BE
1	5	1	1	1	1
2	1	5	1	1	1
3	1	1	5	1	1
4	1	1	1	5	1
5	1	1	1	1	5

Table 1. Variation of SS for a certain QoS class

For SS with Unsolicited Grant Service (UGS), enhanced real time Polling Service (ertPS) and real time Polling Service (rtPS) class, Constant Bit Rate (CBR) data is generated from UDP agent. Meanwhile, for the non real time Polling Service (nrtPS) class and Best Effort (BE), we use FTP agent. This condition is created since CBR traffic requires minimum throughput guarantee, and FTP traffic generates variable flow size. In addition, FTP is more tolerant to delay.

Subsequently to compute the Wimax network performance, we computed the packet loss, throughput, and average delay calculation. Analysis is made per schenario and per class, in a certain node. In this simulation, node 0 (BS) is the node being analyzed, because all traffic from all SS are sent to BS, and BS also sent traffics to SS.

Throughput is computed base on the Equation 1:

$$\text{Throughput} = \sum_{i=t_n}^{i=t_{n+1}} \text{packetSize}; 0 \le n \le t \quad \ldots\ldots\ldots (1)$$

Packet loss is also computed using Equation 2:

$$\text{Loss} = \left(\frac{\sum_{i=t_n}^{i=t_{n+1}} \text{dropPacket}}{\sum_{i=t_n}^{i=t_{n+1}} \text{sendPacket}} \right) * 100 ; \; 0 \le n \le t \quad \ldots\ldots\ldots\ldots (2)$$

The computed delay is the average delay, not delay per packet, because this module produces trace file which is in "receive" records, packet sequence numbers are reset to 0.

Formula for calculating average delay per second is:

$$\text{Delay} = \left(\frac{\sum_{i=t_n}^{i=t_{n+1}} \text{receivedTime} - \sum_{i=t_n}^{i=t_{n+1}} \text{sendTime}}{\sum_{i=t_n}^{i=t_{n+1}} \text{receivedPacket}} \right) ; \; 0 \le n \le t \quad \ldots\ldots\ldots (3)$$

Figure 3 shows the simulation result executed in Network Animator (NAM):

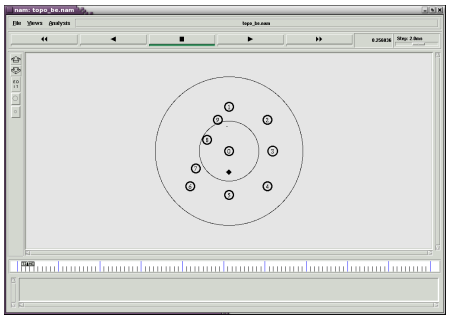

Figure 3. Simulation result in NAM

After the calculation is completed, graphs are generated using Gnuplot. Figure 4, 5, 6, 7, and 8 show the result for UGS, rtPS, ertPS, nrtPS, and BE transmission.

III.1 Throughput

Figure 4. Throughput for Topology 1.

Figure 5. Throughput for Topology 2.

From the throughput graphs above, it can be seen that the number of SS using a certain QoS class, affects the throughput from the QoS class. The more SS using that class, the higher the class's throughput. From the graphs, it also can be observed that WRR based scheduler performance have the same outcome for all classes. Therefore, throughput from all QoS classes are relatively stable, and each class obtains throughput value as it should be.

Throughput for rtPS class it relatively higher than from other classes. This is because of variable packet size generated by traffic generator while rtPS also has a medium priority (3) among other classes.

Figure 6. Throughput for Topology 3.

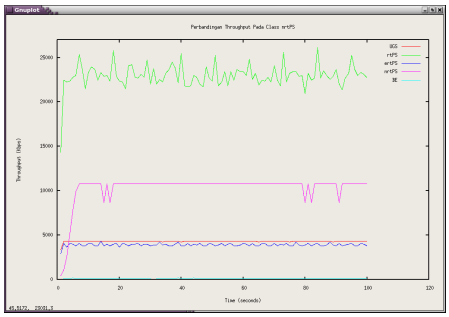

Figure 7. Throughput for Topology 4.

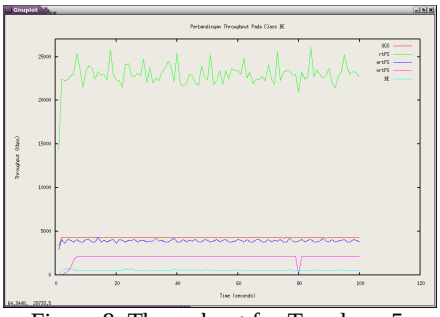

Figure 8. Throughput for Topology 5.

III.2. Average delay

From delay graphs above, it can be observed that the number of SS using a certain QoS class, does not significantly affecting the average delay. The graphs also show that WRR based scheduler cannot suppressed delay of ertPS class. Delay of ertPS class increases along with the increase in time. Generally, WRR does not support average delay which is suitable for multimedia application QoS requirement. It is shown by the average delay of all QoS classes which values exceed delay limitation for multimedia application.

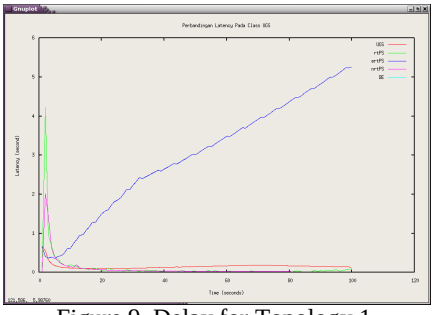

Figure 9. Delay for Topology 1.

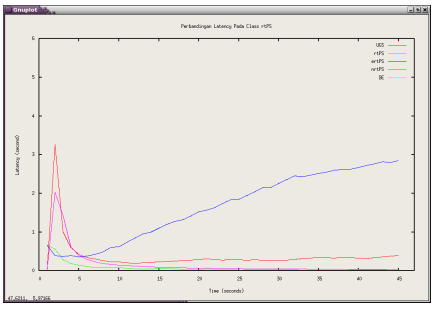

Figure 10. Delay for Topology 2.

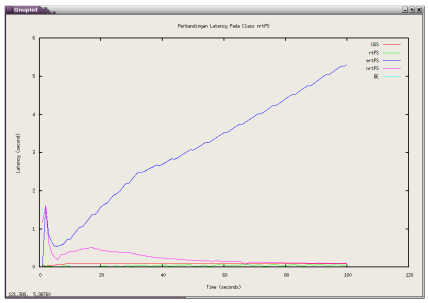

Figure 11. Delay for Topology 3.

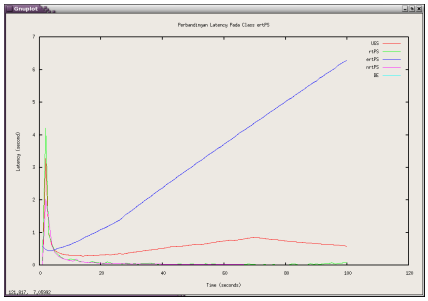

Figure 12. Delay for Topology 4.

From the graphs in Figure 9 to 18, it can be seen that there are increasing packet loss in the beginning of simulation. It is because in the beginning of simulation, all SS and BS are busy doing the process of ranging to enter the network.

After a period, the packet loss is almost zero. It is shown that WRR based scheduler have positive effect to suppress packet loss.

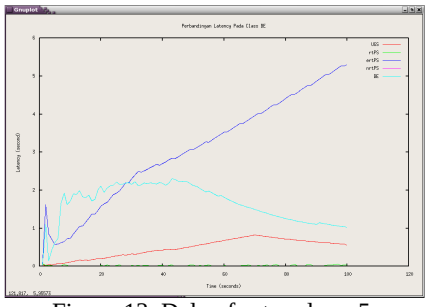

Figure 13. Delay for topology 5.

III.3. Packet loss

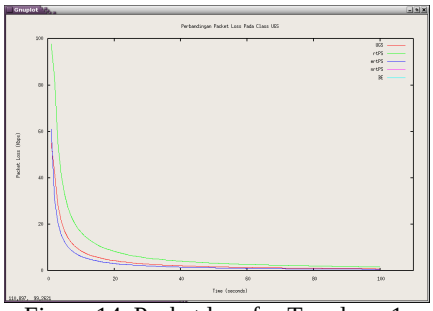

Figure 14. Packet loss for Topology 1.

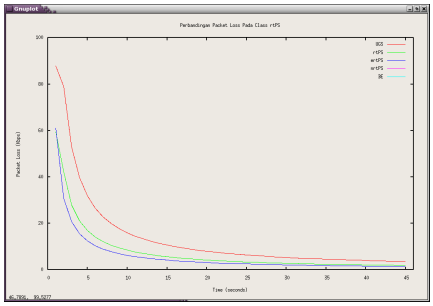

Figure 15. Packet loss for Topology 2.

IV. CONCLUSIONS

It can be concluded that WRR based scheduler implementation in Wimax has supported Wimax QoS by suppressing packet loss and providing each QoS classes throughput value as they should be. However, WRR has not been able to reduce average delay from each QoS classes. Therefore QoS classes cannot obtain delay value as they should. Implemented WRR scheduler is not suitable for ertPS, especially to lessen the delay of ertPS traffic.

Implementation of improved WRR algorithm or other algorithm for Wimax scheduler should be done for future improvement, so that Wimax can fully support the advanced requirement of multimedia application.

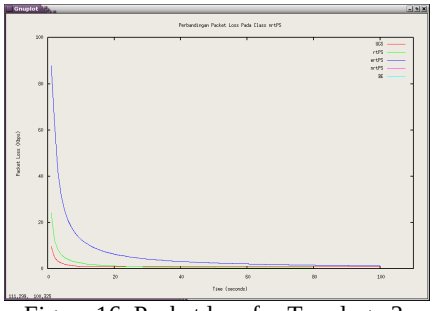

Figure 16. Packet loss for Topology 3.

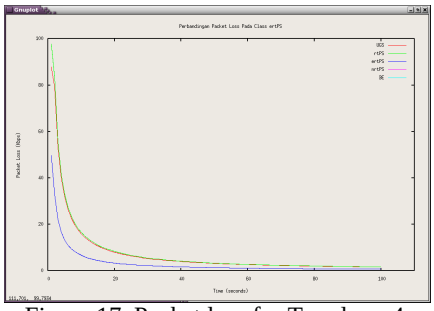

Figure 17. Packet loss for Topology 4.

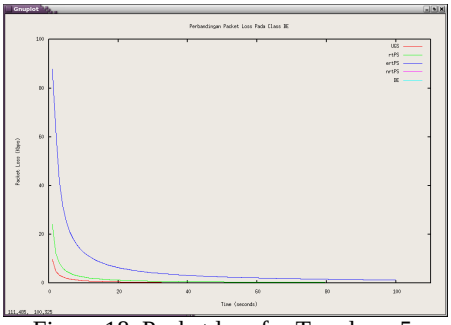

Figure 18. Packet loss for Topology 5.

REFERENCES

[1] Jenhui Chen, Chih-Chieh Wang, *"The Design and Implementation of WIMAX Module for ns-2 Simulator"*, October l0, 2006, Pisa, Italy

[2] Weighted Round Robin. http://en.wikipedia. org/wiki/Weighted_round_robin, Last accessed 20 March 2007.

[3] *"IEEE 802.16 Standard"*, IEEE 802.16 Working Group, 2004

[4] Mark C. Wood, An Analysis of the Design and Implementation of QoS over Wimax. Last accessed 23 March 2007, http://www.rajjain.com/cse574-06/wimax_ qos.htm

ISSN: 1411-1284

SIMPLE-O: Web Based Automated Essay Grading System Using Latent Semantic Analysis method for Indonesian Language considering weighted word and word synonym

Anak Agung Putri Ratna, Adhe W Astato, Bagio Budiardjo, Djoko Hartanto
Electrical Engineering Department Faculty of Engineering, University of Indonesia
ratna@eng.ui.ac.id, adhe@ee.ui.ac.id, bbudi@eng.ui.ac.id, djoko@eng.ui.ac.id

Abstract :

Examination in essay form is an indicator to determine student's capability where choices are not provided. Methods used in automated essay grading system nowadays are still under research because they need to follow some specific rules. One of the grading methods, i.e. Latent Semantic Analysis (LSA), which uses matrix algebra to compare between expected answer and student's essay answer [1].

This paper describes an effort to developed LSA, enhanced with word weighting and the word synonym to improve the accuracy of grading. This system is called SIMPLE-O, which is used to grade answers using bahasa Indonesia. The exam is carried out on-line examination through the Web. From the experiments conducted, for medium size classes (with 30 participants) the conformity lies between 85.87 – 94.11% agreement with the human rater.

Keyword : online assessment, Latent Semantic Analysis Method, SIMPLE-O, grading system, human raters, essay grading, E-learning.

1. BACKGROUND

Advance in computer technology and telecommunication has effecting changes in every area, including on education area, where the learning systems is advancing from conventional way to a future technology way such as E-learning. E-learning is a system where all the delivery of learning information, training, and software is by mean of electronic devices such as computer, or mobile electronic (e.g. mobile phone) as tools to deliver the content of a training, education and learning [2]. E –learning is expanding at all level of education, basic education level, middle education and also higher education, college environment.

E-learning concept means everything is electronically done, assessment can be done by online, from answering the quizzes, and scoring. This thing will give benefit to the trainer and students because the time consumed for the assessment will be much more shorter, efective and efficien. Another benefit from this systems, by help of computer device, scoring will be much faster and accurate [1,3]. And of course this system can handle more bigger class with more students.

Evaluation form whether by conventional or E-learning, based on two main format [4], an objective format and essay format. Objective test questions consists of a selection from a list of answers that already prepared (multiple choice). Commercial product of an objective format is broadly used for non essay like WebCT[5] and Cisco online Assessment System. Online format that have been developed by Electrical Engineering Department, Faculty of Engineering, University of Indonesia is also a non essay format, like Yes/No , Multiple choice, matching answer of fill in the blank with one word [6-9].

Essay questions is a format where answer is not provided, students have to answer with a sentences, thats make the answer vary , different answer comes up from every participant of the test.

Up until today, a lot of essay scoring systems being introduced, like PEG (Project Essay Grading) [3, 10], E-rater [3,10,11,12], Bayesian Scoring System [1,3,10,13] and IEA (Intelligent Essay Assessor) [3,10,13].

Applying automatic essay scoring as mentioned above, all have been done in English. Language base that used here is very reflecting on the process and result from a scoring process to the participant's answer because of the diversity of language characteristic.

One of the method that can be use to do scoring essay answer automatically is a method called Latent Semantic Analysis. This method is the one that used by (intelligent essay assessor) who has agreement rate with human raters 85% – 91%, is a method that extract and represent sentence with mathematical calculation or statistic on text in large number [10]. Mathematic calculation is done by mapping match or not with word from word list on matrix. My previous researches on Essay Grading System had been accomplished and published. [14, 15]

This research, will build a system called SIMPLE – O, using LSA method, bahasa Indonesia basis and add a weighted on words that considered important from chosen keyword. Weight value will be given by multiplying value by 2. Aside, on this system, similar words will be carefully watched, where in a system that using bahasa Indonesia, this thing become significant.

2. SIMPLE-O ALGORITHM

SIMPLE-O consist of several modules, those are:

1. Login Module
2. Lecturer Module
3. Student Module

This research will build web based simple algorithm. It will work like: first we select the keyword. If there are keywords chosen that also a weight word, then it will be given double weight as the usual keyword. Then keyword and weight word mapped into matrix and going through SVD process, and create 3 matrixes, 2 orthogonal matrixes and 1 diagonal matrix.

After doing a simplification on the diagonal matrix, calculate Frobenius normalization for each matrix, matrix from reference answer or students answer. Student's value is a comparison normalization value from student answer with normalization from reference answer.

Figure 1 shown an activity diagram for weighted word and matrix conversion from reference answer. Figure 1 also describe how conversion process to a matrix is formed, including weighted process. From sentences answer, select which is the keyword and weigthed word. Then search keyword and weigthed word from every sentence on the answer to form a matrix coloumn. For keyword, given value 1 for each time it showed on the sentences and for weigthed word will be multiplied by two. This process will be done after all the sentences have been checked and convert to matrixes coloumn.

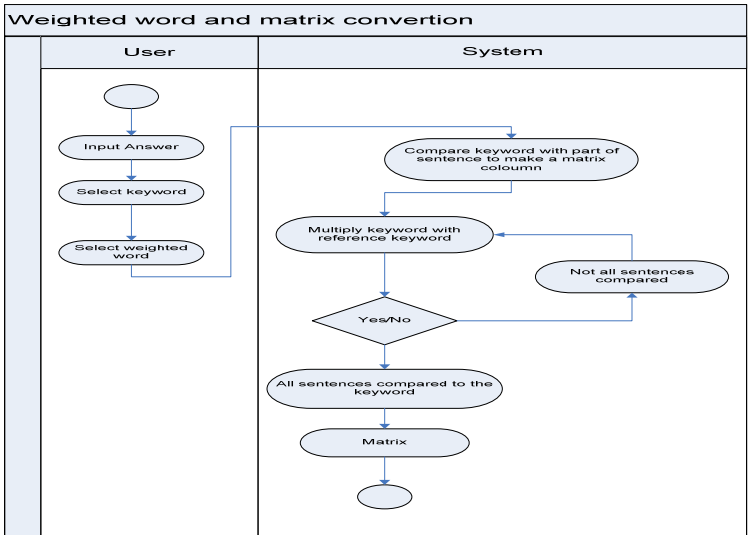

Figure 1. Activity diagram weigthed word and matrix convertion Indonesian language is a unique language, to deliver a message, is can use more than one word, more than one sentences, a lot of word has synonym. Indonesian has diversity in culture; every culture has their language and also foreign language is adopted and use for daily language.

On Online assessment, cause of limited time and stress of the environment, a lot of students use word that different from the references words, but still have a similar meaning.

For those reason, a database of synonym words have to be built, and also alternative words that might be used by students, where if it was examine by lecturer, the answer is right, even though the answer is not using words from the references answer.

3. TRIAL METHOD

This application requires hardware and software support. Hardware for this application is a personal computer with Pentium M Centrino base as server. Clients using another spec of computer that connected to the Local Area Network from Electrical Engineering Departement, University of Indonesia, and some using wireless LAN.

Server using software like Apache HTTP server 2.0.49 for the HTTP application, MySQL Server Clients 4.0.20d as the center of database processing and Mathlab 5.3 for calculating mathematical algebra. For programming, PHP is used. Client need to have a common web browser like Microsoft Internet Explorer, or Opera, Mozilla, Netscape.

The trial is done by using answer that filled by students. In this case students take the assessments by online using following terms :

a. Middle size class with 30 participants
b. Keyword and weigthed word that selected and agreed minimun by 3 competent human raters (the amount can be vary), where answer was also agreed by 5 human raters
c. Questions taken from 10 essay questions for each of the assessment participants

4. RESULTS AND ANALYSIS

Trial for middle class

Trial for middle class is with 30 participants online with 10 questions. Two of the graphic shows comparation between system value and human raters value, as shown on figure 2 and figure 3.The figures shows that the system is acurate for high human raters value. For middle human raters value, which is 60 to 80, human raters value compared to the system value has some significant. The results on middle class can be shown at Table 1, where we can see that the value range between 85.87 % to 94.11 %.

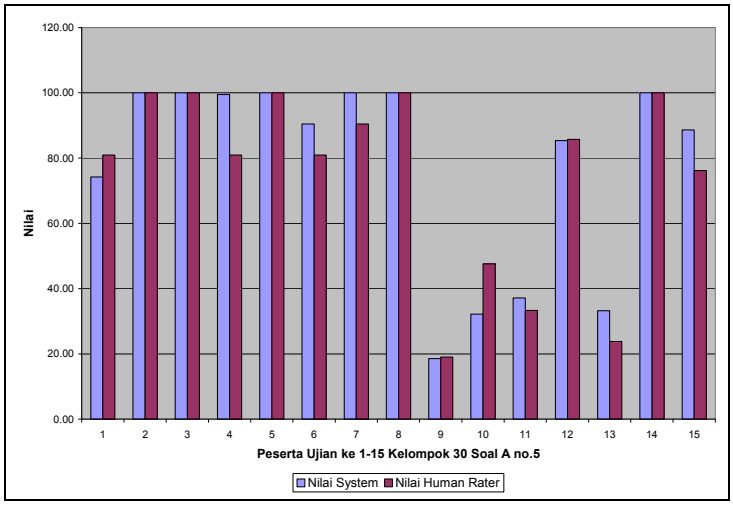

Figure 2. Graphic comparation between SIMPLE-O and human raters for middle class.

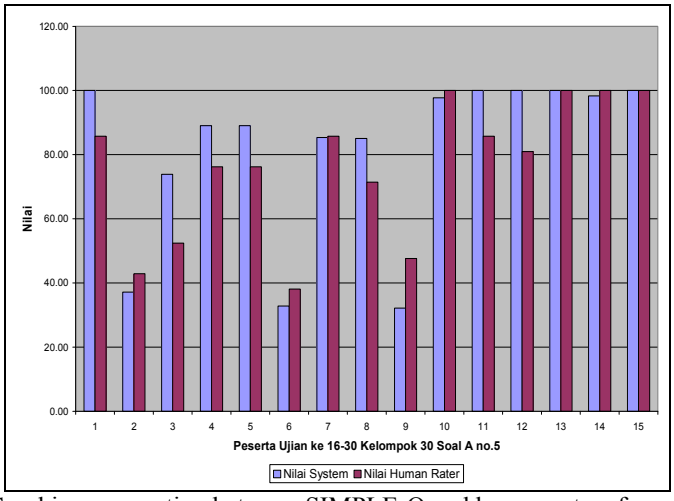

Figure 3. Graphic comparation between SIMPLE-O and human raters for middle class.

Tab1e 1. Agreement value with human raters for middle class

No	*Question number*	*Agreement*
1	A7	85.87
2	A9	88.59
3	A4	89.58
4	A6	89.67
5	A1	90.49
6	A3	90.77
7	A8	90.77
8	A2	92.14
9	A5	92.49
10	A10	94.11

The table shows that agreement value to human raters range between 85.87 % to 94.11 %

From the results, we can be summarized that SIMPLE-O has more advantage and disadvantage that can be solved for future reference. One of the possibilities is on selecting keyword. And word placement and similar word can be used to improve SIMPLE-O value to be more accurate.

5. SUMMARY

1. SIMPLE-O system can works well using bahasa Indonesia.
2. From SIMPLE-O trial, we get the agreement level 85.87 % to 94.11 % for middle size class.
3. For lower level, result of the SIMPLE trial is lower than pure LSA for small class and middle class, but
   for upper limit, SIMPLE-O is higher than trial result of pure LSA.

For future development, this research can be continue by watching the keyword selection, listing all the equal keyword and weighted to the keyword position in sentence.

Reference

[1] Lawrence M Rudner, Tahung Liang, " Automated Essay Scoring Using Bayes' Theorem", The Journal of Technology, Learning and Assessment, volume 1, Number 2, June 2002

[2] Derek Stokley, "E-learning Definition and Explanation (Elearning, Online Training, Online Learning", http://derekstockley.com.au/elearning-definition.html, Australia, last up date : 26 February 2006

[3] Laurence Rudner, Phill Gagne, "an Overview of Three Approaches to Scoring Written Essays by Computer", Practical Assessment, Research & Evaluation, A peer-reviewed electronic Journal, 2001 from: http://ericae.net/pare/getvn.asp?v=7&n=26

[4] Asmawi Zainul, Noebi Nasution, "Penilaian Hasil Belajar", PAU untuk peningkatan dan Pengembangan Aktivitas Instruksional Direktorat Jendral Pendidikan Tinggi Departemen Pendidikan Nasional, Jakarta, 2001

[5] Linlin Irene Chen, Ruth Robbins, "On Line Testing for Business Programming Class", Proceeding of 8th Annual International Distance Education Conference January 23-26, 2001

[6] Anak Agung Putri Ratna, Luhur Bayuaji and Muhammad Salman, "Design And Implementation of Distance Learning in Basic Computer Course", *IMSA'01 IASTED Proceeding*, pp. 51-55, Hawaii, 2001

[7] Anak Agung Putri Ratna, Adjie Pamungkas, Natalia Evianti and Muhammad Salman, "Daskom On-Line: User Management Implementation on Web Based Learning Application", *Web Net Proceedings*, pp 1041-1042, Orlando 2001

[8] Anak Agung Putri Ratna, Astha Ekadiyanto, Djoko Hartanto, Seinosuke Narita, "Daskom On-Line: Implementation Distance Learning On Basic of Computer Course" , *Web Net Proceedings*, pp 1600-1602, Denver 2002

[9] Anak Agung Putri Ratna, Patar P Raymont, Natalia Evianti, Djoko Hartanto, Seinosuke Narita, "Distance E-Learning Implementation and Analysis on Jarkom On-line Evaluation Sistem", *IMSA'03 IASTED Proceeding*, Hawaii, 2003

[10] Salvatore Valenti, Francesca Neri, Alessandro Cucchiarelli, "An Overview of Current Research on Automated Essay Grading", Journal of Information Technology Education, Volume 2, 2003.

[11] Jill Burstein, Magdalena Wolska, "Toward Evaluation of Writing Style: Finding Overley Repetitive Word Use in Student Essays", 10th Conference of the European Chapter of Association for Computational Linguistics, April 12- 17, 2003, Budapest, Hungary.

[12] Burstein, J., Leacock, C. Chodorow, M. , *"Criterion^{SM} : Online essay evaluation : An Application for automated evaluation of student essays"* Proceedings of the Fifteenth Annual Conference on Innovative Applications of Artificial Intelligence, Acapulco, Mexico, August 2003. (This paper has recieved a AAAI Deployed Application Award.)

[13] Peter W Foltz, Darrel Laham, Thomas K Landauer, "The Intelligent Essay Assessor Application to Educational Technology", Interactive Multimedia Electronic Journal of Computer Enhanced Learning, Wake Forest University, 1999.

[14] Anak Agung Putri Ratna, Adhe Widi A, Siti Andella, Bagio Budiardjo, Seinosuke Narita, "Web Based Automated Essay Grading System Using Latent Semantic Analysis Method for Indonesian Language with Most Important Words", *ED-Media Proceedings*, Orlando, June, 2006

[15] Anak Agung Putri Ratna, M. Salman, Bagio Budiardjo, Djoko Hartanto, Seinosuke Narita, "SIMPLE: Sistem Penilaian Essay Otomatis Berbasis WEB Dengan Methoda Latent Semantic Analysis Yang Digunakan pada Bahasa Indonesia Dengan Penambahan Kata Bobot", Journal of Technology, Faculty of Engineering, University of Indonesia, No. 3 Thn XX, September 2006, ISSN: 0215-1685.

ISSN: 1411-1284

On the Development of Mobile User Interface for *VeRAS*: Programmable Universal Remote Access System with Context-Sensitive Approach

Kalamullah Ramli

Study Program on Computer Engineering, EE Department, Faculty of Engineering, Universitas Indonesia
Kampus UI - Depok 16424 – INDONESIA, t. +62-21-7270077, f. +62-21-7270077, k.ramli@eng.ui.ac.id

ABSTRACT-**We are implementing uniVersal Remote Access System –termed as VeRAS- that connects all related and independent information from controller devices to give services such as computing, sensing, or transparent communication services to a group of users. This interaction usually can be managed personally to keep the privacy of its users. User interfaces of this system are installed on user's handhelds. The programming language used in creating this user interface is Java 2 Micro Edition (J2ME), which is a development of JAVA programming language that has been adjusted to cope with the resource limitation of handheld devices. The handhelds are smart phones with Bluetooth connection. VeRAS meets the minimum requirements of a context-sensitive system which demands minimum user interaction to the system, but maintain its maximum benefit for the user while holds the principal of good user interface. This is verified through a series of tests that VeRAS accomplishes user tasks on specific time, given the user is within the server's Bluetooth area. The simple yet intuitive VeRAS user interface is capable of controlling temperature, lamps and TV channels easily. The system performance analysis shows that the system requires around 15 seconds to detect user's present and establishes connection. However, once the connection established, the system performs in real time manner.**

Keywords: *remote controller, context-sensitive approach, smart phones, user interface, pervasive system*

1. INTRODUCTION

Research and development of pervasive computing technology and its applications has been performed by many universities and industries. Samples of research and development work are Aura project by Carnegie Mellon University [1], Oxygen of Massachusett Institute of Technology (MIT) [2], and Portalano of University of Washington [3] [4]. AT&T research [5] at Cambridge and IBM TJ Watson [6] research centre have also invested quite significant funding on this research field.

One of the main characteristics of pervasive system is context sensivity. That is, a system that understands context on which the interaction among users and between users and system take place. This helps minimizing user involvement in the proecess. The system understands who the user is and everything in system that relates to the user preferences, and confindentiality.

In our research we try to implement context sensitiveness nature of a pervasive system into a room. This is a system that sets the environment automatically according to the user preferences. Controlled devices to be managed proactively include television channels, lamps and room temperatur.

VeRAS stands for Universal Remote Access System. This is a programmable system that allows user to control many devices through a smart phone.

Although pervasive system requires minimal user involvement an interaction device is considered necessary for preferences setting, and also for presence detection and authentication purpose. Smart phone is used as interaction device to the system. The phone communicate to the system through its bluetooth feature. A micorocontroller and TV remote controller completes the overall VeRAS system.

This paper is focused on the explanation of the development of user interface for Universal Remote Access System (VeRAS). Section Two outlines the architecture of the system. Design considerations are described in Section Three. Section four explains VeRAS implementation and evaluation. Section Six concludes the paper.

2. *VeRAS* ARCHITECTURE

VeRAS is an implementation of context-sensitive concept of pervasive technology into an intelligent room where, among other functionalities, users can

personalized the condition in the room based on their preferences. The system consists of smart phone as accessing device, modified TV remote control, smart processor represented by a room server and controlled devices such as TV, air-conditions and lamps. VeRAS architecture is shown in Figure 1.

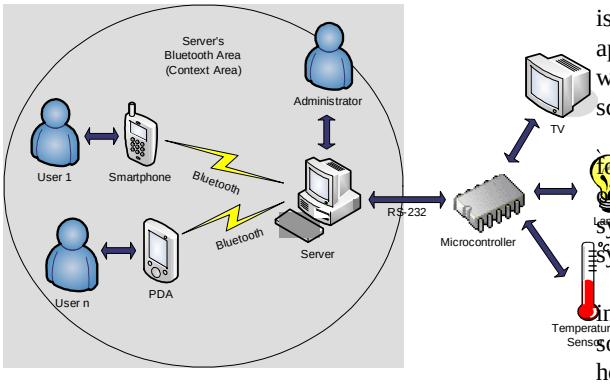

Figure 1. Architecture of VeRAS

VeRAS server application is the main part of the system. This application controls and coordinates the whole work process of the system. The processes which is performed by VeRAS and being controlled and coordinated by the server application are: user identification, user registration, user profile update, user detection, task scheduling, lamp controlling, TV controlling, and room temperature monitoring.

VeRAS uses two types of communications namely bluetooth serial communication which is used on communication between handheld and computer, and UART serial communication, which is used on communication between computer and microcontroller. In establishing this communication, VeRAS uses certain communication protocol. With this protocol, information exchange and translation process can be performed quickly. Therefore VeRAS works in real-time and act responsively to user's tasks.

VeRAS hardware interface connects microcontroler to control home appliances. This hardware interface uses microcontroler ports as a communication line between the microcontroler and the hardware interface itself.

3. *VeRAS* UI DESIGN CONSIDERATIONS

The development of VeRAS user interface on client side, i.e.smart phone, is based on the user interface design considerations outlined in [7]. Related considerations are descibed in the following paragraphs.

Navigation between major user interface items is important. If users feel it is difficult to get from one screen to another, then they become frustrated and give up. The flow between screens should match the flow of the work the users want to accomplish. It is important that the user interface is flexible enough to support their various approaches, because different users might work in different ways

Word messages and labels effectively. The text displayed on smart phone screen is a primary source of information for users. If the text is worded poorly, then the interface will be perceived poorly by users. Text should be worded positively, imply that the user is in control, and provide insight into how to use the application properly. Text should also be consistently worded and displayed in a consistent place on the screen.

Understand the UI widgets. Use the right widget for the right task, helping to increase the consistency of the application. Use of icons and well-known symbols helps users to quickly understand what system software they deal with.

Design should be simple and intuitable. Simple indicates that users feel easy to use the system software. Intuitable means that if users do not know how to use the system software, they should be able to determine how to use it by making educated guesses. And if the guesses are wrong, system should provide reasonable results from which users can understand and learn.

Avoid excessive user interfaces. Crowded screens are difficult to navigate, understand and, hence, are hard to use. Experimental results [7] confirm that the overall density of the screen should not exceed 40 percent, whereas local density within groupings should not exceed 62 percent.

VeRAS user interface on smart phone is developed with several goals: simple, secure, support authentication, user friendly, real-time application and smart. Smart means requires minimum user involvement in setting up the room condition, lamps and TV channels proactively.

Usage scenario is required to appropriately develop the user interface. The scenario are as follows:

1. Users activate the application on smart phone
2. Password is required and paired with MAC address in the VeRASsystem database
3. System verifies and authenticates password
4. Application verify whether users is already within the room wireless range. This triggers searching process
5. Within the area, users could first update their profiles and preferences in system database, otherwise the room will be set to the state that has already assigned by latest profile
6. Users could perform some controlling actions such as:
    - RemoteTVs
    - Remote lamps
    - Time and room temperatur set
    - Profile editing
    - Change pasword and username

Software engineering priciples then guide us to plot the scenario in sequence diagram. This is shown in Figure 2.

4. VeRAS IMPLEMENTATION AND EVALUATION

Smart phone is considered a universal device that is comonly and widely used now. Important factor is that many people understand how to use and utilize smart phone and its feature.

The smart phone employs symbian OS, which is very common to any handphone, and supports Java MIDP 2.0 as well as JSR 82. Additional consideration is that smart phone has been equipped with bluetooth and more computing power than ordinary handphone.

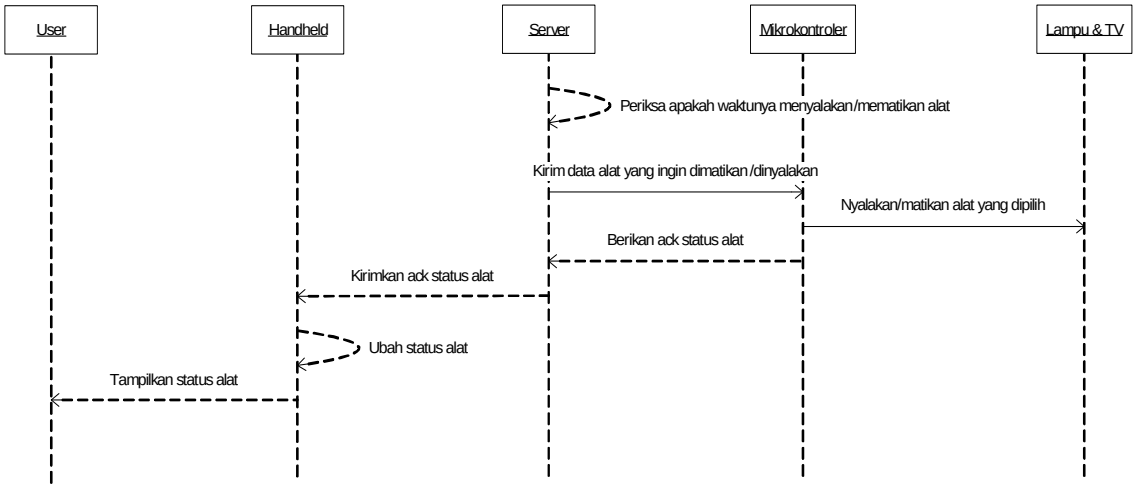

Figure 2. VeRAS Sequence Diagram

Further standard programming steps such as the development of use-case diagram and class diagram has also been performed. The pictures are not included in this paper.

VeRAS user interface is developed using J2ME application and its Wireless Tool Kit (WTK). WTK is very helpful in emulating the real VeRAS system software. The resulting emulation of VeRAS is depicted in Figure 3.

Figure 3. VeRAS Emulation on WTK (Default Colour Phone)

In programming the user interface on smart phone we use high-level API to maintain system software compatibility with a wide range of smart phones. In addtion, high-level API is easier to

handle. Classes used for our system are inherited from *javax.mocroedition.lcdui.Screen*. In displaying something on smart phone screen such as text, graphics, form classes inherited from *javax.mocroedition.lcdui.Display* are used.

Resulted user interface can be seen at Figure 4 for TV remote control and room controller functions. Figure 5 shows room map and lamp controller.

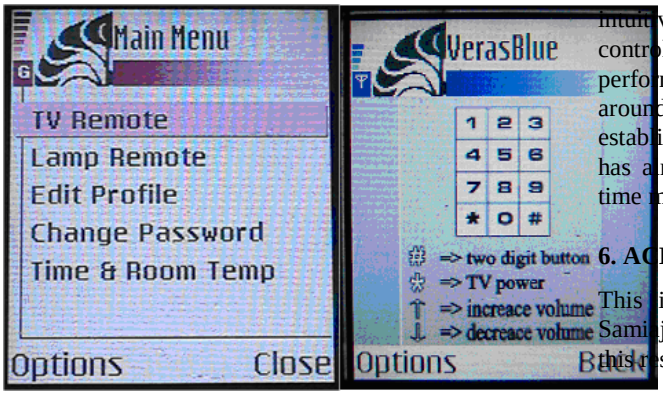

Figure 4. VeRAS: TV Remote (r.) & Room Controller (l.)

VeRAS Evaluation is conducted for functional and performance tests. Functional test is performed to verify necessary tasks such as user identification, user profile update, lamp controlling, and TV controlling can be accomplished. All functions have been tested and works very well.

Figure 5. VeRAS: Room Map and Lamp Controler

Performance tests show that user identification process takes quite a long time, that is about 15 seconds. Meanwhile the result of user profile update, lamp controlling, and TV controlling processes are quick enough, that is about 0.6 sec, 0.5 sec, and 0.04 sec respectively. The tests are performed further to both types of the serial communications. The tests show that system takes less than 200 ms for exchanging data. To conlude, VeRAS communication system workS within the limit of a real-time system.

5. CONCLUSION

VeRAS meets the minimum requirements of a context-sensitive system which demands minimum user interaction to the system, but maintain its maximum benefit for user. VeRAS holds the principal of good user interface. This is verified through a series of tests that VeRAS accomplish user tasks on specifically short time. The simple yet intuitive VeRAS user interface is capable of controlling lamps and TV easily. The system performance analysis shows that the system requires around 15 seconds to detect user's present and establishes connection. However, if the whole system has already connected, the system performs in real time manner

6. ACKNOWLEDGMENT

This is to acknowledge the involvement of Mr. Samiaji, Mr. Putra, Mr. Sonjaya in several pieces of this research puzzle.

7. REFERENCES

[1] Polandian, V., et al. "Task-based Adaptation for Ubiquitous Computing", In *IEEE Trans. on Systems, Man, and Cybernetics, Part C: Applications and Reviews, Special Issue on Engineering Autonomic Systems*, Vol. 36(3), May 2006

[2] Brown, E. S., "Project Oxygen's New Wind", *Technology Review*, December 2001

[3] Grimm, R., et all, "Systems Directions for Pervasive Computing", University of Washington

[4] Partridge, K., Arnstein, L., Borriello, G., and Whitted, T. *Fast Intrabody Signaling* " Demonstration at Wireless and Mobile Computer Systems and Applications (WMCSA), Monterey, CA, December 2000 http://portolano.cs.washington.edu/papers/ (on Nov. 5th, 2007)

[5] Harter, A., Hopper, A. ,"A Distributed Location System for the Active Office", IEEE Network, Vol. 8, No. 1, January 1994

[6] Selker, T., Burleson, W., "Context-aware Design and interaction in Computer Systems," *IBM Syst Journal*, v. 39, 880-891, 2000.

[7] Ambler, S. W., "User Interface Design Tips, Techniques and Principles", http://www.ambysoft.com/essays/userInterfaceDesign.html, (on December 12th, 2005)

ISSN: 1411-1284

Design of Ultra Wideband Antennas using Genetic Algorithm

Sofian Hamid*

* Fac. of Engineering, University of Al Azhar Indonesia, Jl. Sisingamangaraja, Jakarta 12110
Tel. 021-72792753, fax. 021-7244767, HP 081381937722, email : sofian@uai.ac.id

Abstract– **A novel approach on synthesizing and optimizing ultra wideband planar dipole radiating-element is presented. The approach is based on the integration of genetic algorithm (GA) and method of moments (MoM) on a planar surface, meshed by triangular elements. A vector basis function suitable for triangular mesh, called Rao-Wilton-Glisson (RWG) basis function, is applied. The shapes of the radiating elements are optimized using GA with the goal to find the best shape that has the widest impedance-bandwidth. The impedance-bandwidth ratio resulted from this optimization is above 8:1, where the return loss values in that band is below -10 dB.**

Keywords– ultra wideband, method of moments, genetic algorithm, microstrip antennas

I. INTRODUCTION

There are several issues in designing UWB systems, such as antenna design, source pulses, interference, propagation and channel effects, and modulation methods. One of the most challenging topics is designing the UWB radiating element. In this work, the antenna itself is expected to work from 3.1 GHz to above 10.6 GHz (upper limit of UWB band.

The antenna is preferably small, having a non-dispersive characteristics, frequency independent radiation pattern, and wide impedance bandwidth through the 3 - 30 GHz band. Another important requirement is its capability for compact array application. To the author knowledge, popular broadband antennas nowadays like bow-tie, vivaldi, TEM horn, etc., could not fulfill all those preferences.

The small size constraint leads the investigation to the use of planar microstrip antennas. Up to now, many microstrip antennas radiator are designed by using popular shapes like rectangle, circle, or triangle. In the last few years, researchers proposed modification of tear-drop shapes in the design of planar dipole antenna [1]. It was reported that the antenna worked well in terms of impedance bandwidth from 1 - 10 GHz. Unfortunately, analytical model and systematical design process were not reported or included. It seems that the antenna was designed by empirical experiment.

In this work, the challenge on designing the UWB radiating element is dealt by using genetic algorithm (GA) in connection with method of moments (MoM) and available commercial tools. GA has been used in electromagnetic community since a decade ago. It is used as an optimization tool in many electromagnetic problems such as, optimization of linear antenna array, microwave absorbers, broadband patch antenna, layered electromagnetic devices, etc.

II. BASIC THEORY

GA belongs to global techniques optimization methods. Compared to random-walk, GA is more efficient and provides much faster convergence [2]. GA is able to optimize discontinuous and non-differentiable functions with many local minima, which is usually a challenging task for gradient-based optimization techniques. GA uses a model based on the process of natural selection using survival fittest procedure. Terminologies that are used to describe how the GA works are taken from this natural process [2]-[4].

Method of moments (MoM) is one of the most popular tools in the field of numerical electromagnetic, especially in antenna analysis and design [5]-[8]. This method is based on the integral equation technique since it deals with the sources and is performed in the frequency domain [8]. MoM transforms the integral or partial differential equations into algebraic equations by expanding the unknown quantity into a set of linearly independent known functions.

The use of MoM to find the field response on an antenna surface *S* accurately, requires that the surface antenna should be discretized properly. Discretizing the surface of an antenna into triangular mesh has a benefit due to its capability to follow the conformity of the antenna geometry.
To model the patch structure with triangle meshes, boundaries of the structure should be specified. For example, to create an arbitrary planar dipole, one approach is to divide the structure into number of

cells. Each cell consists of a pair triangle. Then, the maximum number of cells in *x* and *y*-direction are specified. The arbitrary shape of the patch is obtained by randomly generating the number of cells in *x*-direction for every *y*-interval. The number of cells generated in *x*-direction should be below than the specified maximum value of cells in that direction. After that, the *Delaunay* triangulation is performed. An example of the result from this process can be seen in Figure 1.

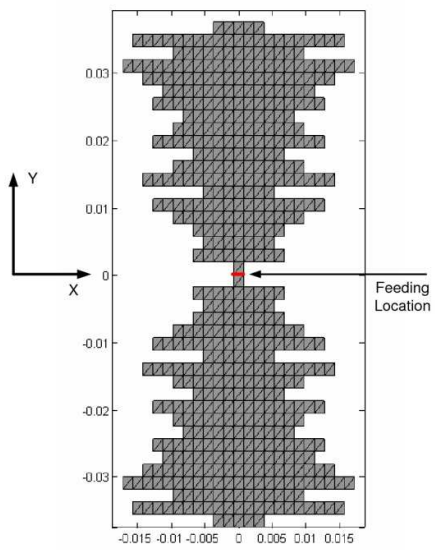

Figure 1: Example of a random planar dipole

In this case, *x* and *y*-axis symmetric condition is imposed. The triangulation process gives information about the mesh in two arrays

- array of Cartesian coordinates in 3 Dimension (x,y,z),
- array of node numbers for every triangle.

By this information, the number and location of all triangles and edges are known.

In this work, RWG basis function is chosen. It is a set of vector basis functions suitable for use with the EFIE and triangular patch modeling [9]. To synthesize and optimize arbitrary patched antenna, we combine the advantages of genetic algorithm and method of moments, using Rao-Wilton-Glisson (RWG) basis function defined on the triangle mesh. Their relation can be seen in the flowchart of figure 2. Each arbitrary radiating element is composed of random series of cells, row-by-row. One cell is composed of a pair of two triangular patches which form a rectangular patch. We map the number of cells in each row into bits representation, which is the gene. Combining all genes will result in the chromosome creation, which is the bits representation for all rows. Chromosome represents the structure to be optimized.

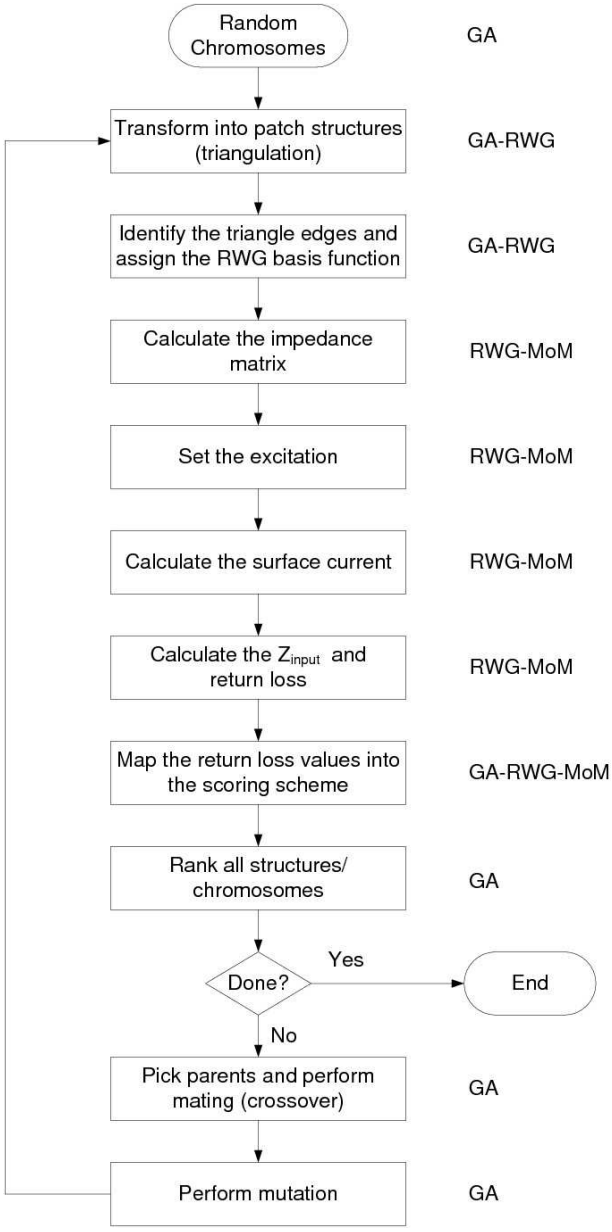

Figure 2: GA-MoM-RWG integration

The process begins by initializing random chromosomes. If, for example, the number of cells in every row (gene) is the same, then a planar rectangle dipole is obtained. Genetic algorithm will change the number of cells in every row to obtain the optimized shape of the radiating element that fulfills the goal. The size of the cell should be below $\lambda/10$ of the highest frequency simulation. The higher the number of cells, the smoother the shape of the radiating element constructed. After the structure is constructed based on the chromosome information, triangulation by using built in Matlab function, delaunay.m, is performed. Identification of boundary edges and inners, or common edges is needed before the assignment of basis functions.

Following this step, impedance matrix calculation, which takes the most of the computation time, is performed in all pre-defined frequency points. Feeding edge excitation 1*V* is set at the edge closest to the origin. Based on this setting and the result from the impedance matrix calculation, the surface current can be found by using a matrix inversion method. The input impedance is calculated based on the ratio of voltage and current on the gap, or at the feeding edge. Then, the return loss is calculated by using formula

$$RL = 10\log|\Gamma_{in}| \quad (1)$$

where Γ_{in} is the input reflection coefficient, obtained from

$$\Gamma_{in} = \frac{Z_A - Z_O}{Z_A + Z_O} \quad (2)$$

where Z_A and Z_O are the input impedance of antenna and reference impedance, respectively.

The goal of this process is to minimize the return loss at every defined frequency point, at least below -10 dB. A scoring scheme is developed to evaluate every structure generated randomly (at the beginning), or genetically (for the following generation). The next step is to rank all structures to determine the goodness of the structure. Decision should be made by considering the result from ranking step, either to continue the process or simply to end it.

If the decision is to continue the process, then the next step is to select parents and perform mating to obtain new chromosomes (children). A new generation is created that has a chromosome combination from the parents. To open new possibilities and enrich diversity, mutation is performed. In this way, the solution is prevented to reach the goal too fast or stuck in the local minima. Following those processes, a loop is created for the new generation to calculate the impedance matrix, impedance input and the return loss. Now, the current and following generation is obtained genetically, not random anymore.

III. SIMULATION SETUP

The number of cells used in this simulation is $N = R \times C = 44 \times C$ cells, where R is the fixed number of row while C is the variable number of cells in every row, ranging from 1 to 23. Two rows which intersect the feeding edge location are set to have only one cell. Since the structure to be optimized are arbitrary planar symmetric dipoles (to have symmetric radiation pattern), the task of optimization is reduced by a half. The number of parameters (cells in each row) to be optimized by using genetic algorithm are reduced to 42=2 = 21 parameters. The symmetric condition normal to the feeding axis, leads to the consequence that *C* should be odd. If a pure random search is used, then there will be 12^{21} or 4.6×10^{22} structures need to be examined.

In this simulation, the number of population *Npop* is chosen to be 16 while the iteration or generation number is 40. Mutation is set to 10% of the total bits in all chromosomes (population). Random single point crossover is used here to mate the picked parents. Selection strategy for parents is based on proportionate selection (roulette-wheel selection) so that every chromosome has a chance to be picked as a parent, proportional to the goodness of its score value. The scoring scheme will map the interval value of return loss at every frequency point into some positive numbers.

The number of frequency point is proportional to the length of the computation time. In this simulation, the structure is first optimized at the range 1.5 GHz to 11.5 GHz using 21 frequency points, or 500 MHz spacing. After achieving the results, by using the scaling properties of antennas, the optimized result will be scaled two times smaller and examined for the range 3 GHz to 30 GHz.

IV. SIMULATION RESULTS

We obtain at least 15 structures which their return loss values are below -10 dB in the frequency optimization range and the best six structures are given in figure 3. All six structures have smooth shapes and have only some variations in the far-end curvature, or the boundary parts which are far from the feeding edge. These structures are optimized to have a very wide impedance bandwidth (return loss). To achieve the wide impedance bandwidth requirement, the structures should have a frequency independent or a non resonating behavior. Resonant structures generally have sharp edges or abrupt changes (discontinuity) in their curvature. Typical examples of resonating structures are wire antennas and square or circular microstrip antennas.

The structures in figure 3 are likely non-resonating ones due to their smooth and curved contour. They have monotony increasing number of cells in the consecutive row until they reach the maximum number of cells in a row, approximately in the middle of the structure. After that, their contours are constant and tend to get narrow again.

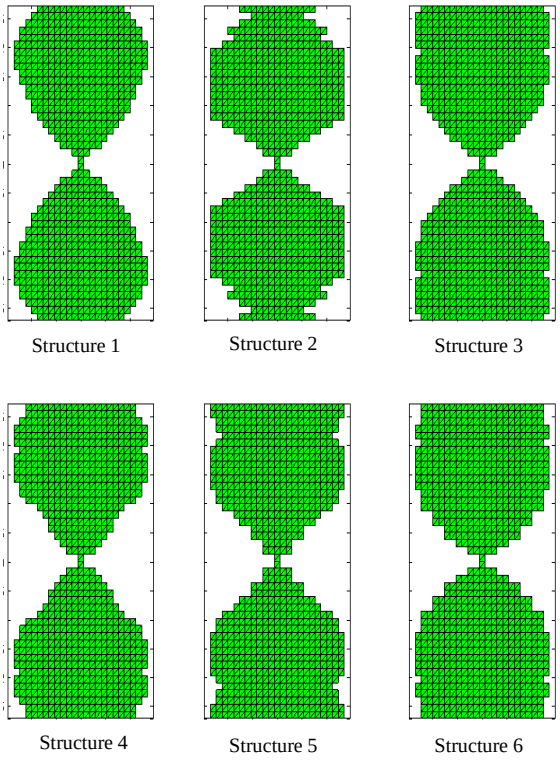

Figure 3: The best six structures

We plot the return loss values for every structure. Figure 4 and 5 show that all structures have quite similar performance (below -10 dB from 3 GHz to 30 GHz), where the structure #6 in average, has the smallest return loss. Those plots are referenced to the impedance of 200 Ohm.

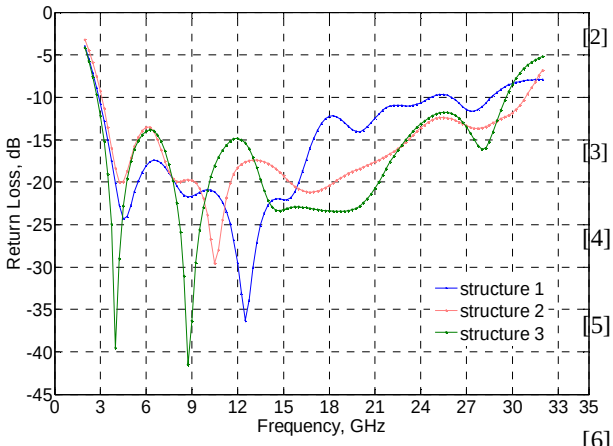

Figure 4: Return loss from structure 1 – 3

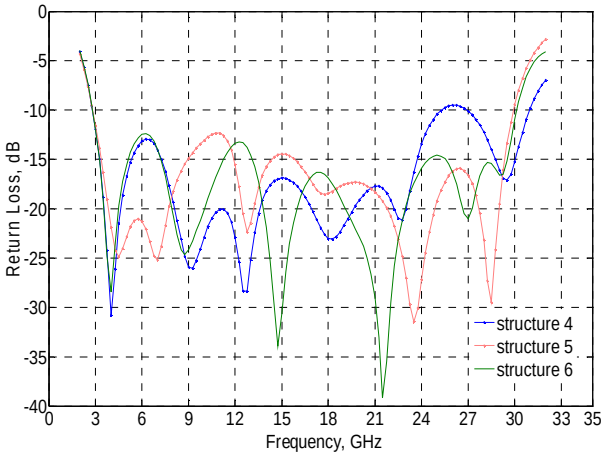

Figure 5: Return loss from structure 4 – 6

V. CONCLUSIONS

A novel approach on synthesizing ultra wideband antennas using genetic algorithm has been presented. The optimized structures, which could work from 3 to 30 GHz, have similar curvature behavior along the boundary edge. They are narrow and smooth, especially near the feeding location. Their geometries show an increasing width until around the middle of the structure and tend to decrease until the far-end of the structure.

REFERENCES

[1] SY. Suh, "A comprehensive investigation of new planar wideband antennas," *dissertation*, Virginia Polytechnic Institute and State University, 2002.

[2] J. M. Johnson and Y. Rahmat-Samii, "Genetic algorithms in engineering electromagnetics," *IEEE Antennas Propagat. Mag.*, vol. 39, pp. 7-25, Aug. 1997.

[3] R. L. Haupt, "An introduction to genetic algorithm for electromagnetics," *IEEE Antennas Propagat. Mag.*, vol. 37, pp. 7-15, Apr. 1995.

[4] R. L. Haupt and S. E. Haupt, *Practical Genetic Algorithm*, 2*end* edition, ISBN: 0-471-45565-2, John Wiley & Sons, Inc., New Jersey, 2004.

[5] P. Russer, *Electromagnetics, Microwave Circuit, and Antennas Design for Communication Engineering*, ISBN 1-58053-532-1, Artech House, 2003.

[6] C. A. Balanis, *Antenna Theory: Analysis and Design*, 2*end* edition, ISBN 0-471-59268-4, John Wiley & Sons, Inc., New York, 1997.

[7] W. L. Stutzman and G. A. Thiele, *Antenna Theory and Design*, ISBN: 0-471-02590-9, 2nd edition, John Wiley & Sons, New York, 1998.

[8] T. K. Sarkar, A. R. Djordjevic, and B. M. Kolundzija, "Method of moments applied to antennas," in *Handbook of Antennas in Wireless Communications*, L. C. Godara, Ed. Boca Raton: CRC Press, 2002.

[9] S. M. Rao, D. R. Wilton, and A. W. Glisson, "Electromagnetic scattering by surfaces of arbitrary shape," *IEEE Trans. Antennas Propagat.*, vol.AP-30, pp. 409-418, May 1982.

ISSN: 1411-1824

Studi on Selection of Technical Solution and Tariff Model for Implementation of Mobile Number Portability

Djamhari Sirat[1], Zuhad Kurniawan[2], Gunawan Wibisono[3]
Departemen Teknik Elektro, Fakultas Teknik, Universitas Indonesia
Kampus UI Depok 16424, Indonesia
E-mail : djsirat@ee.ui.ac.id[1], gunawan@ee.ui.ac.id[3]

Astract-**Mobile Number Portability (MNP) service is one of method which can be applied to increase the fair competition among operators is to implement. This concept offers the ability to retain their MSISDN number when porting from one service provider to others. One of the technical solution to support the implementation of this service is : Intelligent Network based Solution which has more benefits than others such as SRF based Solution and Call Divert Solution. This solution has been chosen supported by decision making method based Analytic Hierarchy Process (AHP) and eight criteria which most influence to choose this method as suitable solution to be implement.**

1. Introduction

The growing of cellular telecommunication in Indonesia is very fast. In this condition, it is possible for someone has more than one cellular number, even from different operator. Because each operator has its own benefit specification. *Mobile Number Portability* (MNP) makes user could retain their existing cellular number when changing mobile service provider (operator). By implementation MNP, prefix number is not reflected the specified operator but could own by another operator. It has been stated in the decree No. 36/1999, that numbering is limited resource, so the numbering have to manage by government [1].

Main objective of developing MNP is to provide fair competition among the existing cellular operators in order to reduce tariff telecommunication. By decreasing tariff, so the number of sumbscriber will increase. The most important problem in global roaming is that the MNP is not implemented yet in the most country in the world [2]. This condition cuase that the competition is not happened yet and the position of user is very weak in those country.

2. Selection of Technical Solution for MNP Services

Analytic Hierarchy Process (AHP) is used in order to decide the best technical solution in implementing of MNP service in Indonesia. The AHP method is used to select the best alternative solution among IN based solution, *Signaling Relay Function* based solution, and Divert call solution. Each solution will be evaluated and ranked the degree of priority based on eight factors that influence and become reason in order to select technical solution in MNP service. These eight factors are as follow

- *Timing* (**TM**); whether that the selected solution is suitable with the exissting GSM network and the possibility implementation
- *Cost Effectiveness* (**CE**); the selected solution is concerning in the investation fund that has been spend.
- *Compatibility with International Standards* (**CS**); The selected solution have to comply with international standard in order to make easy for the future developing and cooperation between vendors
- *Portability Within and Across Mobile Technologies* (**PM**); the selected

solution have to accommodate another cellular technology that will be joined

- *Impact on Other Solutions* (**IO**); the selected solution has the capability to use another application
- *Operational Support System* (**OS**); the selected solution have to concern in administration customer porting and to control distribution information porting number
- *Routing Arrangements* (**RA**); whether that the selected solution has impact to the existing routing call.
- *Interconnection of Networks* (**IN**); whether that the selected solution has impact to interconnection

3. Analyze MNP Service based on AHP creteria

a. MNP Solution based on IN

In solution based on IN, the originating network will make query to number portability database in order to identify the operator of the called party, by getting the prefix-network which show the identity the operator. The calling is transmitted to resipient network and then proceed as normal GSM call.

b. MNP Solution based on Signalling Relay Function (SRF)

MNP solution based on SRF is one method that has adopted in Britain, so popular to call as UK solution. This solution is used the capability of CCS No. 7. CCS No. 7 has capability to capture *Mobile Application Part* (MAP) in GSM system and manipulate so can be transmitted to destination network. By using this capability, MNP service can be implemented in GSM system.

c. MNP Solution Based on Call Diversion (CD)

According to the switching network capability, MNP solution based on call diversion can be implemented in short time because there are not need to make any changing.

4. Supporting System Analytic Hierarchy Process (AHP) Decision

In here, two technical solution will be compared by introducing the value that shown the priority of each solution. This value is shown at Table 2.

Table 2
Scale Value of Qualitative Comparison

Value	Desciption
1	Alternative A is as equal importance as alternatif B
3	Alternative A is moderate importance than alternatifive B
5	Alternative A is strong importance than alternative B
7	Alternative A is very strong importance than alternative B
9	Alternative A is the extreme importance than alternative B
2,4,6,8	If both alternatives have closed value

By observing into the operator GSM condition, we find the value of eight criteria for selection process technical solution as given in Table 3.

Table 3
The Value of Criteria Comparison

	TM	CE	CS	PM	IO	OS	RA	IN
TM	**1**	**1/3**	**5**	**5**	**7**	**7**	**3**	**3**
CE	**3**	**1**	**7**	**7**	**7**	**7**	**5**	**5**
CS	**1/5**	**1/7**	**1**	**1**	**3**	**3**	**1/3**	**1/3**
PM	**1/5**	**1/7**	**1**	**1**	**3**	**3**	**1/3**	**1/3**
IO	**1/7**	**1/3**	**1/3**	**1/3**	**1**	**1**	**1/5**	**1/5**
OS	**1/7**	**1/7**	**1/3**	**1/3**	**1**	**1**	**1/3**	**1/3**
RA	**1/3**	**1/5**	**3**	**3**	**5**	**3**	**1**	**1**
IN	**1/3**	**1/5**	**3**	**3**	**5**	**5**	**1**	**1**

Between criteria is then compared for pairwise of technical solution, the results are given in Table 4.

Table 4
Weighted Value of Technical Solution Comparison

CRITERIA	SOLUTION A	SOLUTION B	Weighted Value
TM	IN	SRF	5
	IN	CD	3

	SRF	CD	3/5
CE	IN	SRF	5
	IN	CD	1/3
	SRF	CD	1/5
CS	IN	SRF	1
	IN	CD	1
	SRF	CD	1
PM	IN	SRF	5
	IN	CD	1
	SRF	CD	1/3
IO	IN	SRF	3
	IN	CD	1
	SRF	CD	1/3
OS	IN	SRF	5
	IN	CD	3
	SRF	CD	1/3
RA	IN	SRF	3
	IN	CD	3
	SRF	CD	1
IN	IN	SRF	5
	IN	CD	3
	SRF	CD	1/3

Table 2 is then normalized to find the real value of comparison criteria for each criteria (TM, CE, CS, PM, IO, OS, RA, IN). The normalized criteria for TM-TM criteria is given by

Normalized TM-TM is given by

$$= \frac{\text{(TM-TM objective)}}{\text{(Total weighted criteria value in one coloumn)}}$$

$$= \frac{1}{(1+3+0.20+0.20+0.14+0.14+0.33+0.33)}$$

$$= \mathbf{0.18683} \qquad (1)$$

By doing the same step for each column, the matrix normalization can be shown in Table 5. Weighted criteria is the average value of one criteria in one rom. By doing the same step to find weighted criteria, the normalized value for technical solution can be found. The wieghted priority is sum product each criteria in technical solution by weighted criteria which given as

Weighted priority
= ∑(weighted technical solution X weighted criteria)

The weighted priority for technical solution based on IN, SRF solution, and Call Divert solution can be shown in Table 6. It is shown from Table 6, that the best solution for implementing MNP service in Indonesia is technical solution based on IN.

6. Tariff Model For MNP Services

Cost recovery mechanisms in MNP should promote competition, and not weaken the benefits which number portability would bring in the mobile market. The costing principles are intended to form the basis for determining inter-service provider charges. It is important to show benefit of MNP service to porting customer, non-porting customer, and operator.

a. Effective Competition

This means that the charging structure should not distort competition or deter service providers from introducing MNP

b. Cost Minimization

Charging principles should encourage carriers to minimize their costs by ensuring that all service providers receive the appropriate incentives to adopt efficient technology and business practices.

c. Cost Causation

The principle of cost causality requires that a customer, whose decision to port this number causes costs to be incurred, pay for these costs. Thus, the principle of cost causality is important for ensuing efficient allocation of resources.

d. Distribution of Benefits

Cost recovery mechanisms should recognize that ported mobile customers are not the only beneficiaries of number portability. Benefits from MNP accrue both to customers porting their numbers and also to mobile customers in general through increased competition in the mobile market. The non-porting customers would also benefit from fewer misdialed calls.

e. Reciprocity dan Symmetry

Cost recovery mechanisms should, as far as possible, be symmetrical and reciprocal,

given that portability needs to be offered in both directions.

f. Relevant Cost

The relevant cost principle requires that only those costs that are incremental to providing MNP should be recovered through inter-service provider charges.

7. Cost for MNP

In general there are 3 types cost in MNP service as follows

a. System Setup Cost

System set-up costs are the costs incurred by the service provider in order to establish the technical and administrative capability to provide portability. In particular, costs of:-

- Establishing and maintaining the databases that contain information on ported numbers.
- Making network and system modifications, configurations or reconfigurations, operation, maintenance including adapting or replacing software and billing system.
- Testing functionality within the applicable systems and in conjunction with any other service provider's systems.

b. Additional Conveyance Costs

Additional conveyance costs are the additional costs for conveyance of an individual call to a ported number. Conveyance costs are associated with resources used in:-

- Effecting the switch-processing required to set up each ported call, and
- Providing the switch and transmission capacity for any part of the duration of each ported call additional to the costs of conveyance of non-ported calls from the donor service provider's network to the recipient service provider's network.

c. Administrative Costs

Administration Costs are the costs incurred in the porting of an individual number. The costs incurred by the service providers in changing the number records in its network and the administrative costs involved with respect to each number ported

8. Some Factors Influenced MNP Tariff

In MNP services, there are some factors that influence MNP service.

a. Call Scenarios

There are some call scenarios in MNP services:

- *originating call* form donor network and *terminating call* to *ported number* in resipent network
- originating call from donor network and call terminating to non-proted number at resipent network.
- Originating call from donor network and terminating call to ported number to resipent network from network of another operator

b. Relevant Costs

Some costs that relevant with each call scenarios, these costs are:

- Network Component Costs
- Operation and Maintenance Costs
- Other costs

c. Relevant Volume of Ported Customers

Relevant volume of ported customer should be predicted in determine MNP tariff.

9. Analyze Tariff of MNP Service

Refer to other country that had implemented MNP services, the following lesson learn can be adopted:

- Administration cost is paid by user who want change provider.
- Call scenario to ported number is different than that to non-ported number.
- Tariff for call ed made to ported number is based on interconnection scenario plus conveyance cost
- No fixed cost charges to porting number.

13. Conclusion

1. The technical solution based on IN is the best solution for implemtation MNP service in Indonesia at the moment.
2. Cost for MNP services includus
   - Administration cost is paid by user who want change provider.
   - Tariff for call ed made to ported number is based on interconnection scenario plus conveyance cost
   - No fixed cost charges to porting number.

14. Reference

[1] "_____", "Undang-Undang No 36 Tahun 1999 Tentang Telekomunikasi**",** 1999

[2] http://www.infodev.org, "Telecommunications Regulation Handbook" December, 2004

[3] "_____","Study on The Cost Allocation for Number Portability ", Europe Economics, October, 1999

[4] "_____", "3rd Generation Partnership Project,Technical Specification Group Core Network;Support of MNP (MNP), 3GPP TS23.066", Desember, 2003

[5]"_____","Estimation of Cost in United Kingdom", Oftel, 1999

[6]"_____","Report on IDA's Determination of Fixed and Mobile Inter-operator Number Portability Charges", Infocommunications Development Authority of Singapore, March, 2000

[7]"_____"," Implementation of MNP in CEPT Countries", October, 2005

Table 5. Normalized Value for Each Criteria Comparison

Normalisasi	TM	CE	CS	PM	IO	OS	RA	IN
TM	0.18683	0.13359	0.24194	0.24194	0.21875	0.23333	0.26786	0.26786
CE	0.56050	0.40076	0.33871	0.33871	0.21875	0.23333	0.44643	0.44643
CS	0.03737	0.05725	0.04839	0.04839	0.09375	0.10000	0.02976	0.02976
PM	0.03737	0.05725	0.04839	0.04839	0.09375	0.10000	0.02976	0.02976
IO	0.02669	0.13359	0.01613	0.01613	0.03125	0.03333	0.01786	0.01786
OS	0.02669	0.05725	0.01613	0.01613	0.03125	0.03333	0.02976	0.02976
RA	0.06228	0.08015	0.14516	0.14516	0.15625	0.10000	0.08929	0.08929
IN	0.06228	0.08015	0.14516	0.14516	0.15625	0.16667	0.08929	0.08929

Table 6. Weight Priority of Technical Solution

	TM	CE	CS	PM	IO	OS	RA	IN	Weight Priority
Weight Criteria	**0.22**	**0.37**	**0.06**	**0.06**	**0.04**	**0.03**	**0.11**	**0.12**	
IN Solution	0.65	0.22	0.33	0.48	0.43	0.63	0.60	0.63	**0.45**
SRF Solution	0.13	0.13	0.33	0.11	0.14	0.11	0.20	0.11	**0.15**
Call Divert	0.22	0.65	0.33	0.41	0.43	0.26	0.20	0.26	**0.41**

ISSN: 1411-1284

Wavelength Dependence in Three Waveguides Directional Coupler Using Method of Lines

Helmi Adam [1)], Ary Syahriar [1,2)]

[1)] Electrical Engineering Departement, University of Al-Azhar Indonesia
[2)] Information Technology and Electronic Center, Agency for the Assessment and Application of Technology Republic of Indonesia
[3)]

Abstract-- **The directional coupler is the important component in optical communication, it use in many application such as optical power splitting, wavelength multiplexing and other application. The basic principle in directional coupler is power transfer between two paralel waveguides via evanescent field. In the three waveguides directional coupler that are consist of three paralel waveguides, this can be analyse for case when the wave launched in the center of waveguide, or in one of two of the outer waveguides. In this paper, we perform the analysis of three waveguides directional coupler by using method of lines. By this method, the power transfer between waveguide and the wavelength caharacteristic can be analysed. The interesting caharacteristic is when multiple wavelength launched, the output power in each wavelength in all waveguide is not same and become sinusoidal.**

Keywords-- *Three paralel waveguides, directional coupler, method of lines.*

I. INTRODUCTION

Today, the directional coupler [1] become the most famous optical component. Many research have been carried out for this device. The basic principle in directional coupler is power transfer between two paralel waveguides via evanescent field. When two paralel waveguide placed closely together the evanescent field travelling from the throughput fiber reaches the coupled waveguide and excite a mode in it. The power will transfered between coupled waveguide periodicaly. The coupled propagation can stopped by choosing the length where the power divide as need.

The basic structure of three waveguides directional coupler consist of three paralel waveguides, so it can be analyse for two case. First case is when the input wave launched to the center of three waveguide, and the second case is the input wave launched to the one of two of the outer waveguides, both of two case will produce diffrent characteristic.

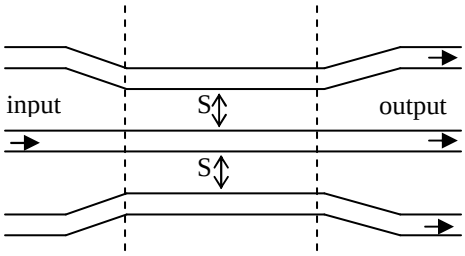

Figure 1. Three waveguides directional coupler sructure

The coupled mode theory [2], usually used to analysed the directional coupler structure, for three waveguide this theory is possible. But, because of the complex structure, it will complicated [3]. So, in this paper we try to analyse this component using one of the numerical method [4], the method of lines [5]. This method was proven very useful and accurate for design and analyse many optical component structure.

We can perform this method by divide the structure with several line in transversal direction, discritized the differential form in wave equation, and find the result by finding the eigen value. Then we can get the form of mode in waveguide.

In this paper we assume the three of waveguide is identical symmetrical, and equally spaced

II. THE METHOD OF LINES

To analyse three paralel waveguide with method of lines, we need to divide the structure with several line in transversal direction, so that become some part with distance between line is Δx [5], like shown in figure 2.

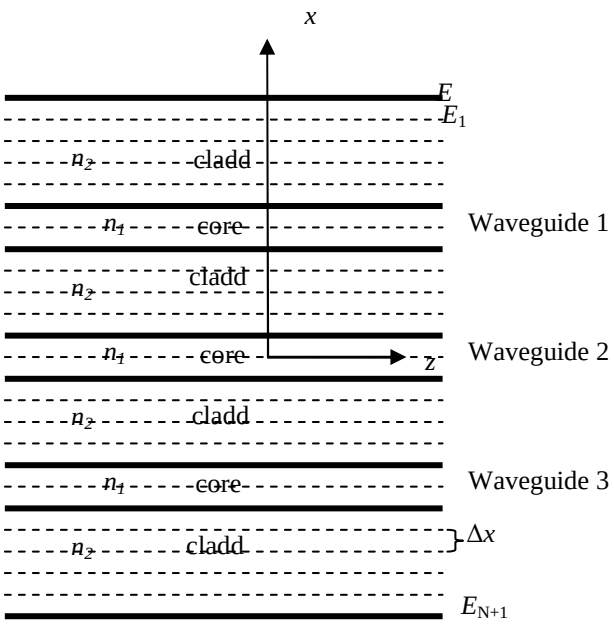

Figure 2. Discritization of three waveguides directional coupler sructure

First, we use Helmholtz equation for TE modes,

$$\frac{\partial^2 E_y}{\partial x^2} + \frac{\partial^2 E_y}{\partial z^2} + k^2 E_y = 0 \qquad (1)$$

For $\frac{\partial^2 E_y}{\partial x^2}$ we can use central difference,

$$\frac{\partial^2 E_y}{\partial x^2} = \frac{E_{i+1} + 2E_1 + E_{i\ 1}}{\Delta x^2} \qquad (2)$$

We subtitute equation (2) in to (1) :

$$\frac{\partial^2 E_y}{\partial z^2} + \frac{E_{i+1} - 2E_1 + E_{i\ 1}}{\Delta x^2} + k_o^2 n^2(x) E_y = 0 \qquad (3)$$

Equation (3) can be write in vectorial form :

$$\frac{\partial^2 \vec{E}_y}{\partial z^2} + \vec{Q}^2 \vec{E} = 0 \qquad (4)$$

Where $\vec{E}$ is transpose of column vector that consist $E(x)$ field in $x_1, x_2, \ldots x_n$ point.

And $\vec{Q}^2$ can be write as :

$$\vec{Q}^2 = \frac{1}{\Delta x^2}\begin{bmatrix} -2 & 1 & 0 & .. & 0 \\ 1 & -2 & .. & .. & .. \\ 0 & .. & .. & .. & 0 \\ .. & .. & .. & -2 & 1 \\ 0 & .. & 0 & 1 & -2 \end{bmatrix} + k_o^2 \begin{bmatrix} n_{x1} & 0 & .. & .. & 0 \\ 0 & n_{x2} & .. & .. & .. \\ .. & .. & .. & .. & .. \\ .. & .. & .. & .. & 0 \\ 0 & .. & .. & 0 & n_{xN} \end{bmatrix} \qquad (5)$$

$n_{x1}, n_{x2}, \ldots n_{xN}$ is refractice index in waveguide structure that round in $x_1, x_2, \ldots x_n$ point.

$\vec{Q}^2$ consist three diaginal matrix, to solve the equation we need diagonalization :

$$\vec{\beta} = \vec{T}\ \vec{Q}\ \vec{T}^{\ 1} \qquad (6)$$

Where $\vec{\beta}$ is diagonalization result from $\vec{Q}^2$ that consist eigen value, and $\vec{T}$ consist eigen vector from $\vec{Q}^2$.

Then, equation (4) can be rewrite as :

$$\frac{\partial^2 E_y}{\partial z^2} + \vec{\beta}^2 \vec{E} = 0 \qquad (7)$$

Equation (7) is wave equation that propagate in z direction. If we assume wave reflected to $-z$ direction is very small so can be neglect, the solution is :

$$\vec{E} = e^{-i\vec{B}z} \qquad (8)$$

To find solution of wave that propagate along z direction, we can use :

$$\vec{E} = \vec{T}\ e^{\ i\beta z}\ \vec{T}^{-1}\ \vec{E}_{inp} \qquad (9)$$

Power in each z point can be described as :

$$P(z) = \left| \int_{\infty}^{\infty} E(x,0) E(x,z) dx \right|^2 \qquad (10)$$

III. RESULTS

Figure 3 show wave propagation in three paralel waveguide. In this simulation we use core refractive index 1.457, cladd refractive index 1.463, wavelength 1.52 μm, core width is 5 μm, and distance between waveguide is 5 μm. This 3-dimension simulation can be obtain using beam propagation method (BPM) [4], the result from method of lines in equation (9) calculated in each *z* point in propagation direction.

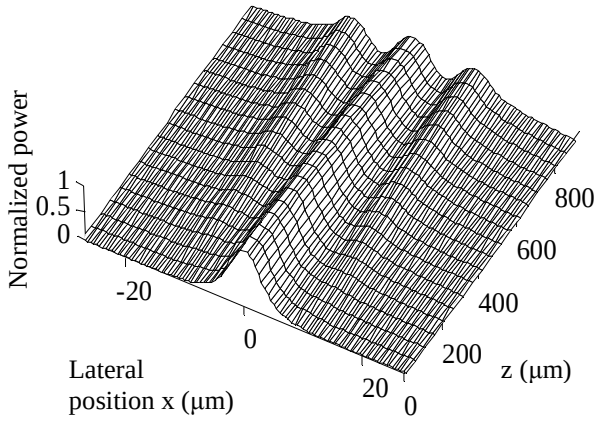

(a)

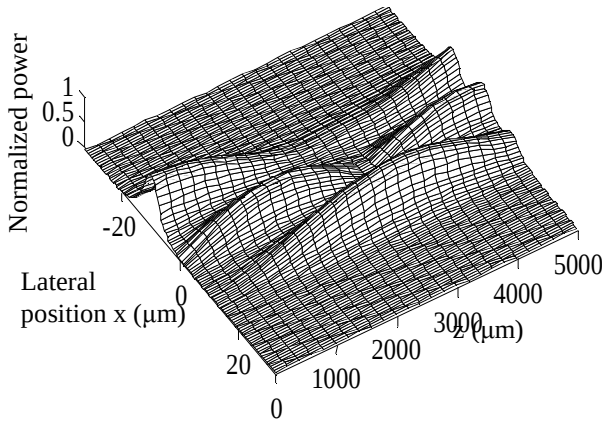

(b)

Figure 3. Wave propagation in three waveguide directional coupler
(a) Input launched into central waveguide
(b) Input launched into outer waveguide

If an input wave launched into the center waveguide, it will coupled to two of outer waveguide, and the power will trasfered. We see the power of each waveguide become equal at z = 940 μm. This can used to make directional coupler that divide output to the same part. But if an input launched into one of two outer waveguides, is hard to find equal power for each three waveguide.

Figure 4 show the mode profile of input and output. Input launched to center waveguide can divide to three output in equal size of power (33%). This input is get at z = 0 μm, and the output at z = 940 μm.

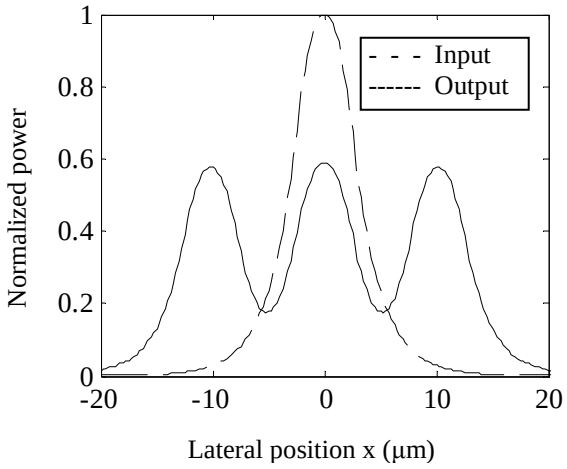

Figure 4. Power distribution in three waveguide directional coupler

Figure 5 show power along the propagation in three paralel waveguide. In this simulation we use two mwthod. The power in each waveguide can calculated by integrating field in each waveguide in each *z* point in figure 3.

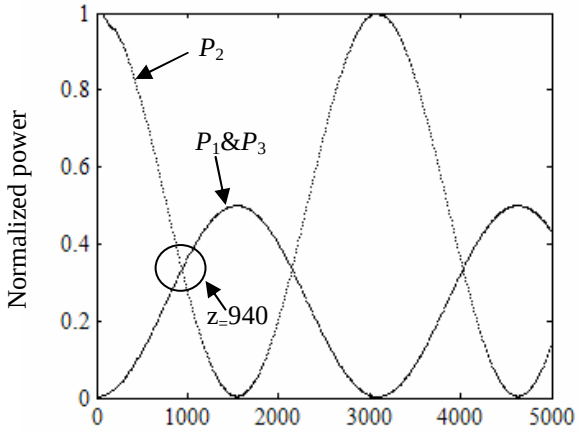

(a)

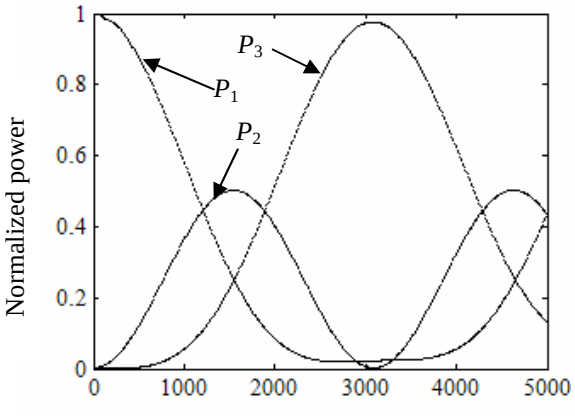

(b)

Figure 5. Power along the propagation
(a) Input launched into central waveguide
(b) Input launched into outer waveguide

In the figure 5(a) all power of three waveguide meet periodically, it mean each waveguide have equal power at a meeet point. In figure 5(b) we don't find any meet point between three waveguide, it mean the power is never equal each other along the propagation. In all of waveguide, the power travel in the propagation direction sinusoidally.

All previous simulations are using single wavelength at 1.52 μm. For WDM we use many wavelength as carrier, hence we will analyse this three waveguides directional coupler for their effect of wavelength.

Figure 6 show the power level of each wavelength value in each waveguide. This simulation using wavelength range between 1.31 μm - 1.55 μm. Figure 6(a) using z=940 μm as the meet point of simulation in figure 5(a). And for figure 2 we use z=1500 μm.

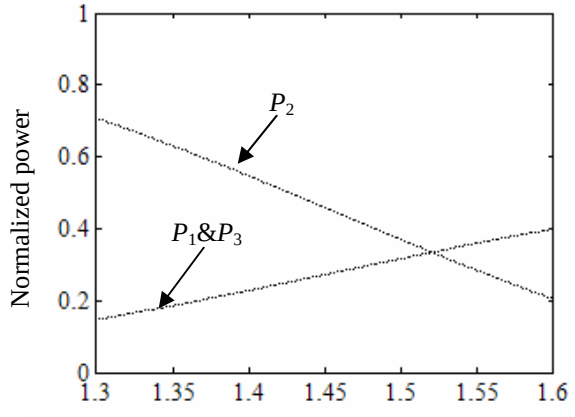

(a)

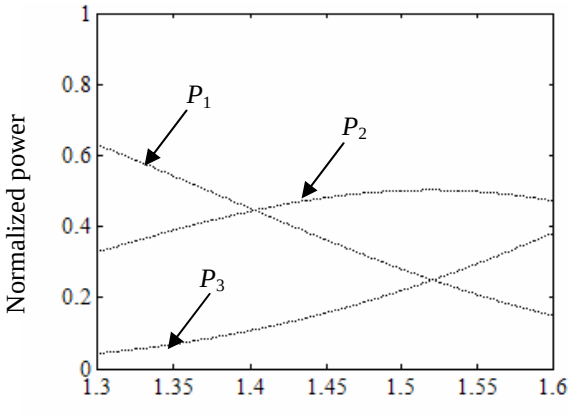

(b)

Figure 6. power level of each wavelength value in each waveguide.

As we see in the figure 6, the power distribution is not flat but sinusoidal, so it will be make three waveguides directional coupler difficult for used in multiple wavelength, because the power never have same level in each wavelength.

IV. CONCLUSIONS

The three waveguides directional coupler can be analyse for two case. If a wave launched into the center waveguide it will coupled to two of outer waveguide. At a point, power of each waveguide become equal. But, if we launched a wave to one of two outer waveguide it will hard to find a point that all of waveguide in equal size of power. In all of waveguide, the power travel in the propagation direction sinusoidally.

For multiple wavelength. the power distribution in each wavelength is not flat but sinusoidal, so power never have same level in each wavelength. That make the three waveguides directional coupler difficult for used in multiple wavelength

REFERENCES

[1] R. Syms, J. Cozens, "Optical guided waves and devices", McGraw Hill, London 1992.
[2] H.A Haus, W. Huang, "Coupled mode theory", Proceeding of the IEEE, vol. 79, 1505-1518, 1998.
[3] C.M. Kim and Y.J. Im, "Switching operations of three-waveguide optical switches," IEEE Journal of Quantum Electronics, vol 6, 170-174, 2000.
[4] Kiusalaas," Numerical methods in engineering with MATLAB". Cambridge University Press, New York, 2005.
[5] U. Rogge, R. Pregla, "Method of lines for the analysis of dielectric waveguides", IEEE journal of lightwave technology, vol. LT-11, 2015-2020, 1993.

ISSN: 1411-1284

Circularly Polarised Equilateral Triangular Patch Microstrip Antenna for Quasi Zenith Satellite

M. Darsono and Eko Tjipto Rahardjo.

Antenna Propagation and Microwave Research Group
Electrical Engineering Departement, Faculty Engineering of University of Indonesia
Depok 16424

Abstract : The equilateral triangular radiator patch microstrip antenna is developed to obtain circular polarization to support next generation of mobile satellite communication by using Quasi-Zenith satellite. The Quasi Zenith satellite is designed for Global Positioning Services (GPS) at the S- band frequency which will be launched year 2008 by Japan on position geosynchronous orbit. The Antenna is designed to use 50 Ω feed network of quadrature coupler hybrid 90^0 transmission line of microstrip with single element of radiator patch trilateral. The antenna is designed to operate at the resonance frequency 2.62 GHz. The simulation and experiment result showed good agreement for the operating frequency, the return loss and axial ratio.

1. Introduction

Recently satellite technology continue to expand for the application of global communications such as GPS. It is estimated in the year 2008 Japan will launch satellite technology that called Quasi-Zenith Satellite System (QZSS). Quasi-Zenith satellite to be launched to consist of three satellite occupied trajectory situation geosynchronous orbit[1]. Frequency allocation for the system of Quasi Zenith satellite at the frequency 2.6 GHz (2.605 GHz - 2.630 GHz) [2].

The equilateral triangular patch of single element is designed as receiving antenna with circular polarization characteristic[3]. The circularly polarized is generated designed by using fed coupler hybrid network as phase shifter [4]. Furthermore the antenna geometry is design by using cavity model[5]. The target is to obtain circular polarization axial ratio $\leq$ 3 dB and maximum gain 6 dB .

2. Design and Specification Antenna

Figure 1 is the microstrip antenna design form consists of transmission line and a patch. Geometry of the substrate antenna is W x L = 82 x 123 mm, where side length of patch (*a* and b), the line length (L_{1-7}) and the line width (W_{1-3}). And the substrate media specification is TLY-5-0310-CH / CH has thickness (h) 0.8 mm with dielectric constant (ε_r) 2.2.

Side footage of radiator patch uses the theory method cavity model of resonance frequency 2.62 GHz. Trough the usage of dominant mode for TM_{10} obtained the side length of a patch is 51.465 mm. Because of the fringing effect existence, so the effective (a_{eff}) length of a patch obtained equal to 50.925 mm [5,6].

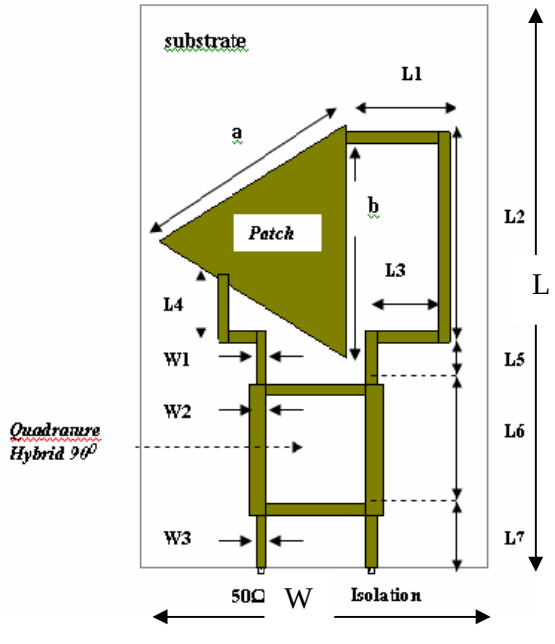

Figure 1 Design microstrip antenna.

From the above antenna design known the size dimension d.h : a = 51.0578 mm , b = 50.48 mm, L1 = 24.6 mm, L2 = 45.92 mm, L3 = 17.22 mm, L4 = 14.76 mm, L5 = 9.02 mm, L6 = 28.7 mm, L7 = 11.48 mm, W1 = 2.46 mm, W2 = 4.1 mm, W3 = 2.46 mm.

Input impedance 50 Ω of fed network at transmission line obtained fed line width (*w*) equal to 2.46 mm. For the network designed by using hybrid coupler $1/4\lambda_g$, for the effective relative permittivity constant (ε_{eff}) 1.87, andly obtained λ_g is 83.94 mm [4,7].

To obtain the maximum result from some antenna parameters, can be conducted with change of fed loci positions between two port output lines of hybrid coupler network to patch's side.

3. Result and Discussion

To result of antenna can be seen by parameter characteristic of return loss, Voltage Standing Wave Ratio (VSWR), axial ratio and of gain through simulation and measurement [7,8]. Simulation conducted by using Method of Moment (Mom) software and measurement conducted by in Laboratory Telecommunications, Faculty Engineering of University of Indonesia by using Spectrum Analyzer Anritsu type of MS68B3. At measurement of microstrip antenna of two port input line attached by SMA connector with impedance 50 Ω , where one port line which is isolation attached by a dummy load with impedance 50 Ω .

Figure 2(a) showing graph result of simulation at bandwidth frequency of return loss ≤ - 10 dB equal to 119.6 MHz (2.55 GHz – 2. 6696 GHz), where minimum of return loss equal to – 26.78 dB at resonance frequency 2.621 GHz. While picture 2(b) is graph result of measurement bandwidth frequency of return loss ≤ -10 dB equal to 53 MHz (2.596 GHz (marker 1) – 2.649 GHz (marker 2)), where minimum of return loss equal to – 32.684 dB at resonance frequency 2.624 GHz (marker 3). At parameter of return loss obtain shift the resonance frequency between of result simulation and measurement equal to 0.11 %.

Figure 3(a) is graph result of simulation at bandwidth frequency of VSWR ≤ 2 dB equal to 37.7 MHz (2.6011 GHz – 2.6388 GHz), where minimum VSWR is 0.796 dB at resonance frequency 2.621GHz.. Figure 3(b) is graph result of measurement at bandwidth frequency of VSWR ≤ 2 dB equal to 53 MHz (2.596 GHz (marker 1) – 2.649 GHz (marker 2)), where minimum VSWR is 1.09 dB at resonance frequency 2.624 GHz. Result of simulation and measurement obtained shift the resonance frequency equal to 0.11%.

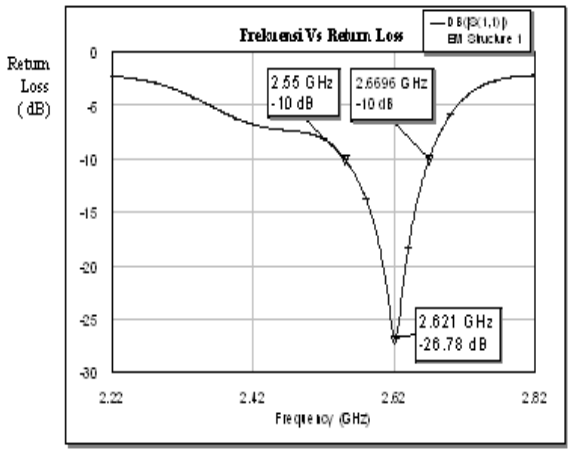

Figure 2.(a) Return loss Vs Frequency of simulation.

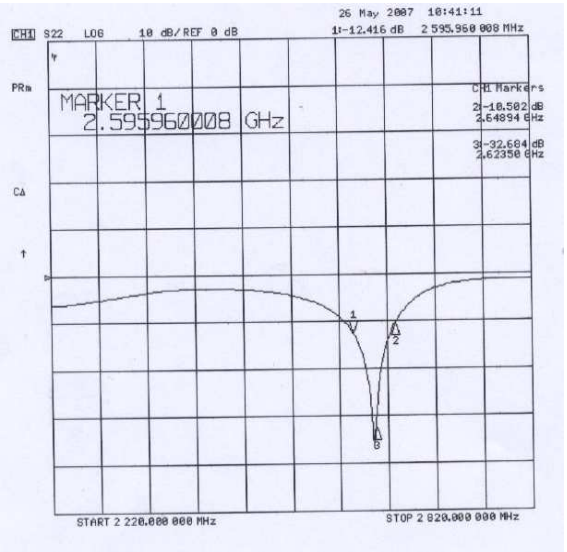

Figure 2.(b) Return loss Vs Frequency of measurement.

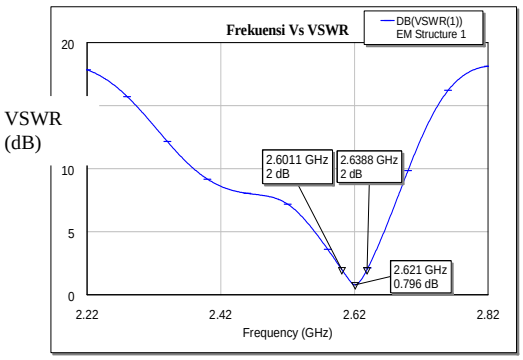

Figure 3(a) VSWR Vs Frequency of simulation.

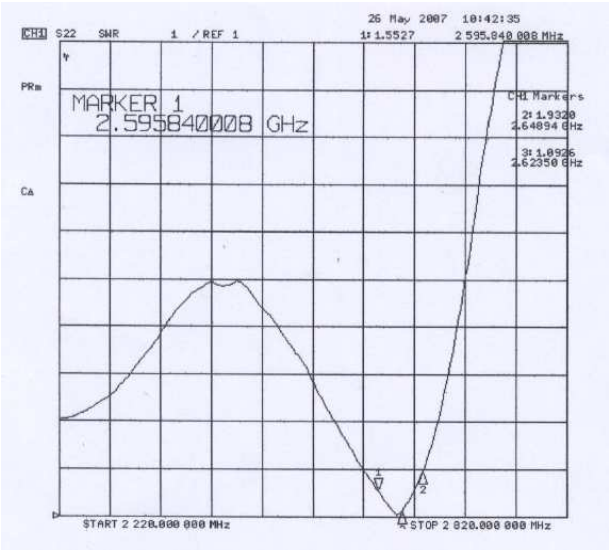

Figure 3(b) VSWR Vs Frequency of measurement.

For result is required by circular polarization of parameter axial ratio ≤ 3 dB[3]. Figure 4(a) is graph result of simulation at bandwidth frequency of axial ratio ≤ 3 dB equal to 47.7 MHz (2.58615 GHz – 2.63392 GHz), where minimum of axial ratio is 1.073 dB at resonance frequency 2.61GHz. Figure 4(b) is graph result of measurement at bandwidth frequency of axial ratio ≤ 3 dB equal to 40 MHz (2.61 GHz – 2.65 GHz), where minimum of axial ratio is 0.61 dB at resonance frequency 2.63 GHz.. Result of measurement and simulation obtain shift the resonance frequency 0.76 %.

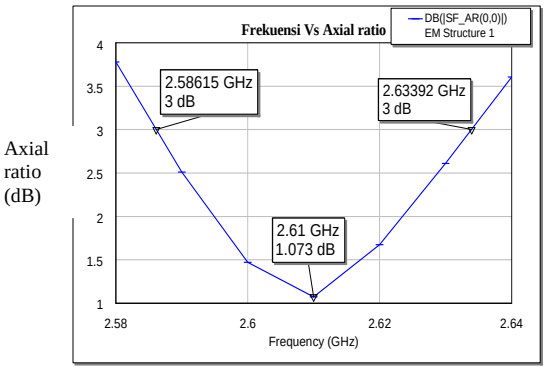

Figure 4 (a) Axial ratio Vs Frequency of simulation.

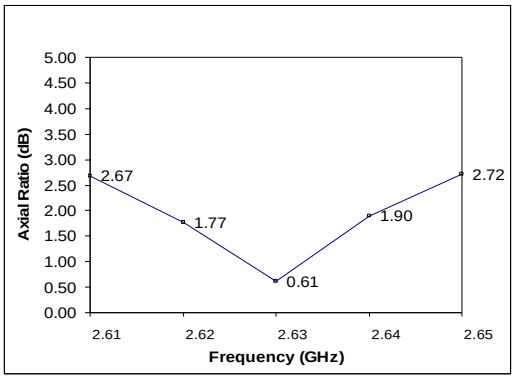

Figure 4(b) Axial Ratio Vs Frequency of measurement.

Figure 5 is graph of gain to frequency result of measurement. For the frequency 2.58 GHz up to frequency 2.7 GHz obtained by maximum gain is 6.07 dB at frequency 2.62 GHz . This result have showed from characteristic of antenna where the target of maximum gain which expected equal to 6 dB.

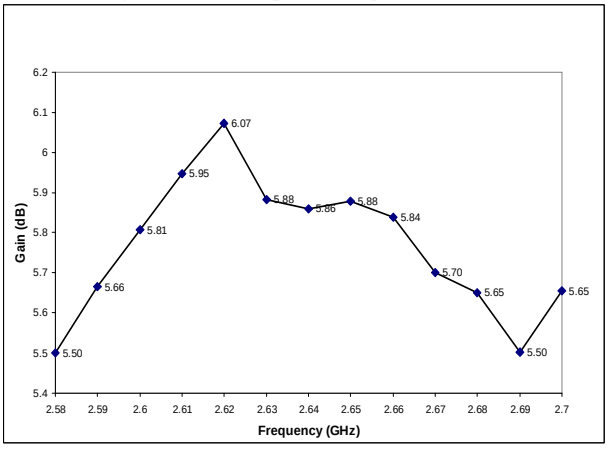

Figure 5 Gain Vs Frequency of measurement.

4. Conclusion

The equilateral triangular radiator patch microstrip antenna fed by quadrature 90^0 hybrid coupler yield resonant frequency Quasi Zenith satellite. The characteristic of antenna can be seen from measured parameter value to through measurement or simulations. The result of simulation and measurement bandwidth of VSWR $\leq$ 2 dB are 37.7 MHz and 53 MHz, respectively the axial ratio $\leq$ 3 dB where the minimum 1, 073 dB on simulation and 0.26 dB measurement at resonant frequency. The respectively maximum gain is 6.07 dB. Thus by implementation of antenna with those characteristic have a standard is such as expected at operating frequency of Quasi Zenith.

References

[1]. Yongcheol SUH, Yusuke KONISH, Tomohiro HAKAMATA, Ryosuke SHIBASAKI," The Effects of Quasi-Zenith Satellite System in Urban Enviroments ",Center for Spatial Information Science, University of Tokyo, http://www.chikatsu-lab.g.dendai.ac.jp/s_forum/pdf/2003/41_suh.pdf

[2]. ……., " Strategies for future spectrum management in Japan", Ministry of Internal Affairs and Communication, Japan, Oct 2005.

[3]. J.T .Sri Sumantyo and K.Ito,2006" Circularly Polarised Equilateral Triangular Patch Antenna for Mobile Satellite Communications " , *IEE Proc.Microw Antennas Propag.Vol 153,No 3 , Juni* .

[4]. Robert E.Collin , 1992 " Foundation For Microwave Engineering " , McGraw-Hill, 2nd ed,

[5]. Kazuhiro Hirasawa,Misao Haneishi, 1992 " Analysis,Design, and Measurment of Small and low-Profile Antenas " , Artech House.

[6]. Manostosh Biswas, Jawad Y Siddiqui and Debatosh Guha, " Computer Aided Design of Triangular Microstrip Patch Antenna in Multilayerd Media ", http://www.ursi.org/Proceedings/ProcGA05/pdf/B04P.13(0882).pdf.

[7]. JR James & PS Hall,1993 " Handbook of Microstrip Antennas", Peter Peregrinus Ltd, Volume 1 dan Volume 2.

[8]. John D. Kraus ,1988 " Antennas " , McGraw –Hill, 2nd ed,

ISSN: 1411-1284

V-Shaped Linear Tapered Slot Antenna with CPW Feed for Ultra Wideband Applications

Fitri Yuli Zulkifli[1], Bayu Aji[2] and Eko Tjipto Rahardjo[3]

[1,2,3]Antenna propagation and Microwave Research Group (AMRG)
Center for Information and Communication Engineering Research (CICER)
Department of Electrical Engineering, University of Indonesia
Kampus Baru UI Depok, West Java,16424, Indonesia
yuli@ee.ui.ac.id[1]
b_prasetyo@student.eng.ui.ac.id[2]
eko@ee.ui.ac.id[3]

Abstract - **In this paper, a modified and compact design of V-Shaped Linear Tapered Slot Antenna (VLTSA) with the Coplanar Waveguide (CPW) Feeding as an Ultra Wideband Antenna is proposed and studied by simulation and experiment. It is demonstrated that this antenna design has an impedance bandwidth of over 4 GHz, and the antenna gain varies within the impedance bandwidth.**

Keywords – V-Shaped Linear Tapered Slot Antenna, Coplanar Waveguide, Ultra Wideband, Microstrip Antenna.

I. INTRODUCTION

The needs for Ultra Wideband (UWB) Antenna for various applications such as telecommunications and ground penetrating radar have recently attracted many attentions. The antenna for future applications especially for telecommunication must be practical, lightweight and easy to be handled. Microstrip antenna has these characteristics except that it has narrow bandwidth. The narrow bandwidth characteristic of microstrip antenna can be enlarged by various methods. One of the methods that can be used is the slot technique.

The slot technique itself has several kinds of methods that can be used to make larger bandwidth for microstrip antenna; such as log periodic slot, spiral slot, or just a rectangular slot. In this paper, we use Tapered Slot technique, especially V-Shaped Linear Tapered Slot Antenna (V-LTSA) technique because it has many advantages mentioned in [1] and [2] such as wider bandwidth, very compact and low cross-polarization. V-LTSA is a variant of Tapered Slot Antenna.

The design of V- LTSA in this research is based on reference [2]. In reference [2], the V-LTSA is designed for Low Earth Orbit Satellites (LEOS), with the feeding technique uniplanar microstrip-to-coplanar strip line type feed. This feeding type is compact but more complex to design rather than with CPW feed. CPW feed has attracted many researchers because of its advantages such as little dispersion, low radiation loss, easy to adjust the impedance matching of antenna and easy to be integrated to Microwave Integrated Circuits (MMIC).These advantages of the CPW are the reason of this research to use CPW feed combined to V-LTSA.This antenna is designed for frequency around 1.5 GHz to 6 GHz because it's potential applications in telecommunication.

II. MICROSTRIP ANTENNA

Microstrip antenna is a simple configuration which consists of radiation patch on one side of a dielectric substrate (ε_r) and a ground plane on the other side of it. Fig.1 shows the simple configuration of a microstrip antenna with rectangular shape patch.

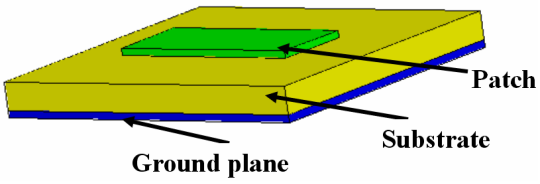

Fig. 1. Configuration of microstrip antenna

The patch conductors are normally of copper and can assume virtually any shape, but regular shapes are generally used to simplify analysis and performance prediction.

The substrates are flexible in nature which can also be suitable for conformal wrap-around antennas with usual dielectric constant of $2.2 \leq \varepsilon_r \leq 12$ for frequency 1 to 100 GHz.

III. ANTENNA DESIGN

A.V-Shaped Linear Tapered Slot Antenna

To design V-LTSA, there are some important variable parameters which influence the characteristic parameter of the antenna. They are as shown in Fig 2:

1. Inner Angle (θ_1)
2. Outer Angle (θ_2),
3. Length of tapered slot (L3).

Those three parameters are important in controlling the achievable bandwidth. For the inner and outer angle, reference [3] mentioned that the ratio between outer and inner angle should be around 10^o, and after several simulations, the best angle was for $\theta 1 = 1.82^o$ and $\theta 2 = 9.25^o$

B.CPW Feed line

The V-LTSA is fed by CPW. To design the CPW feed line, the dimension of parameters width of CPW (W) and CPW feed gap (G) must be determined to have the matching impedance of 50 ohm. The tuning slot (parameters L2, W2) and length of the feed line (L) are than used in controlling the matching of the feed.

After combining the design of V-LTSA with CPW feed line, the antenna design proposed is shown in Fig 2. The V-LTSA is simulated with εr = 2.2 and thickness of d = 1.57 mm.

The dimension of the proposed V-LTSA design is:

70 mm x 35 mm. With CPW feed line: W = 3.6 mm, G = 0.4 mm, L = 25.9 mm, L2 = 4.9 mm, W2 = 6.8 mm. And for the tapered slot part: L3 = 42.4 mm, a = 9.8 mm, b = 7 mm, c = 3.5 mm. For $\theta 1 = 1.82^o$, $\theta 2 = 9.25^o$.

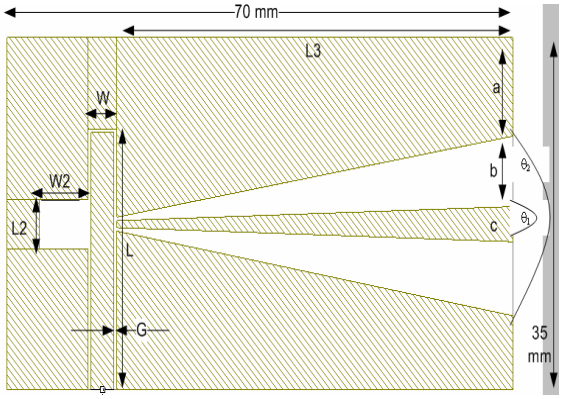

Fig. 2: Proposed V-LTSA Design

IV. RESULTS AND DISCUSSION

A. Simulation Results

Fig. 3 shows the simulation result of the VSWR = 2 impedance bandwidth. This impedance bandwidth is from the frequency 1.3583 GHz to 5.688 GHz. Therefore the impedance bandwidth result from simulation is around 4.3 GHz. This result has passed the UWB characteristic ruled from Federal Communication Commission (FCC). FCC rules that an UWB antenna has fractional bandwidth equal to or greater than 20% or has bandwidth equal to or greater than 500 MHz [4].

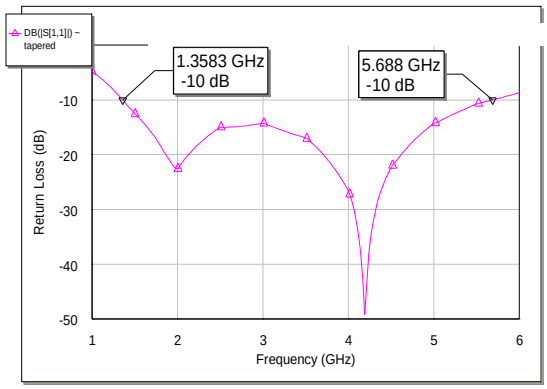

Fig. 3: Simulated Return Loss of Proposed Antenna

B. Experiment Result

After designing the proposed V-LTSA, which has passed the UWB characteristic, it has been fabricated on RT Duroid 5880 with εr= 2.2 and thickness of d = 1.57mm. The

antenna has also been measured in anechoic chamber, where the measurement results are shown in Fig. 4 and Fig. 5.

Fig. 4 shows the impedance bandwidth of the V-LTSA. The impedance bandwidth starts from the frequency 1.985 GHz to above 6 GHz. The precise upper frequency could not be measured because of the limitation of the measurement equipment provided in the anechoic chamber.

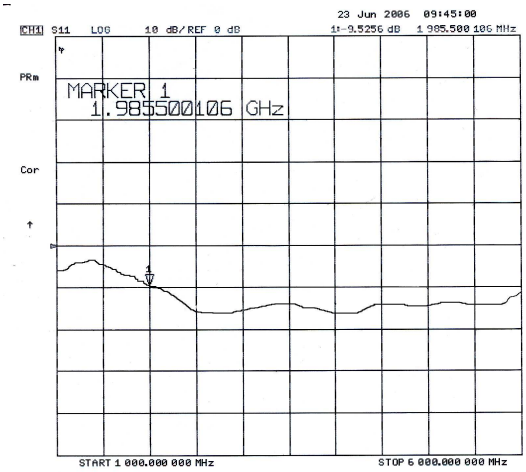

Fig.4: Measured Return Loss of Proposed Antenna

Fig. 5 shows the gain measurement of the proposed antenna from 3.6 GHz to 5.6 GHz due to the limitation of the measurement equipment. The gain of this proposed antenna is the absolute gain and varies from 1.76 dB to 5.36 dB within the impedance bandwidth. The gain as a function of frequency shows that the gain tends to increase as the frequency increases. This phenomenon is usual because based on Friis formula, the gain is proportionally related to frequency.

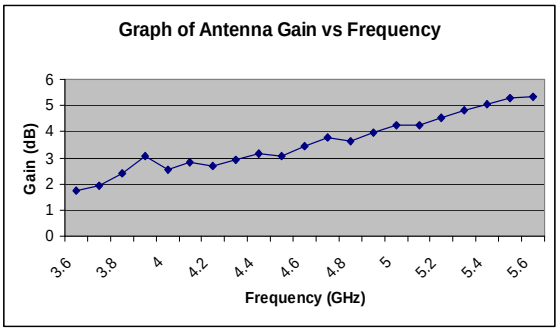

Fig. 5: Measured Antenna Gain of Proposed Antenna

The radiation pattern was also measured for frequency 3.3 GHz, 4.3 GHz and 5.3 GHz. At frequency 3.3 GHz, the E-plan shows that the main beam occurs at 100^o – 130^o. Figure 6 shows the radiation pattern at frequency 4.3 GHz. The radiation pattern shows the main beam occurs at 100^o – 110^o, whereas at frequency 5.3 GHz, the main beam also occurs at 100^o – 110^o.

For the H-plan, the main beam for frequency 3.3 GHz occurs at 100^o - 120^o, for frequency 4.3 GHz at 100^o -110^o and for frequency 5.3 GHz at 110^o – 130^o.

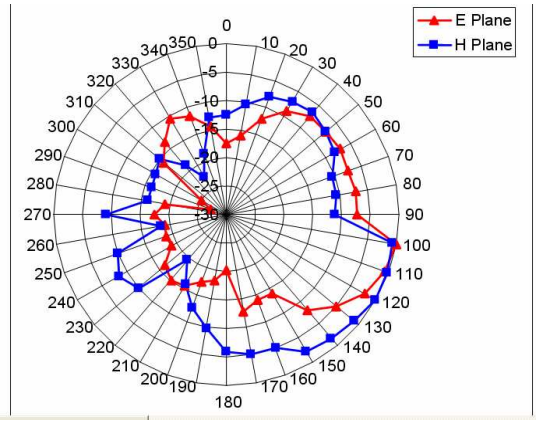

Fig. 6: Measured Radiation Pattern of Proposed Antenna at 4.3 GHz

Figure 7 shows the measurement result of input impedance of the antenna. The measurement shows that at frequency 1.98 GHz, the input impedance is 50.7 – 34.9j Ω. Therefore the antenna at this frequency is capacitive. The figure also shows that the input impedance of the antenna can not meet the ideal VSWR = 1 which is at 50 Ω.

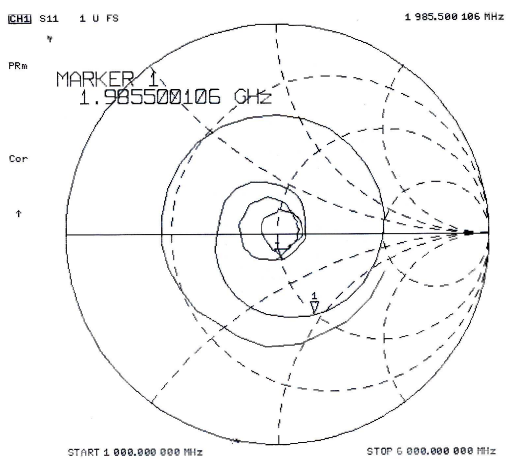

Figure 7. Measured Input Impedance (Zin) of proposed antenna

V. CONCLUSION

The V-LTSA with CPW feed line was designed fabricated and measured. This antenna can be considered for UWB Antenna. The simulation and measurement results show that the antenna is ultra wideband with impedance bandwidth from 1.985 GHz to above 6 GHz. The antenna gain varies from 1.76 dB to 5.36 dB within the impedance bandwidth.

REFERENCE

[1] Yngvesson, K.S., Korzeniowski, T.L., Young-Sik Kim, Kollberg, E.L., Johansson, J.F., "The Tapered Slot Antenna – A New Integrated Element for Millimeter-Wave Applications", *IEEE Trans. on Antennas and Propagat.*, vol. 37, no. 2, Februari 1989.

[2] Simons,R.N., Dib,N.I., Lee,R.Q., Katehi, L.P.B., "Integrated Uniplanar Transition for Linearly Tapered Slot Antenna", *IEEE Trans. On Antennas and Propagat.*, Vol. 43, No 9, September 1995.

[3] Wang, H. Y., Mirshekax-Syahkal, D., Dilworth, I. J., "Numerical Modeling of V-Shaped Linearly Tapered Slot Antennas" 1997 *IEEE Int. Antennas and Propagat. Symp. Dig.*, page 1118 – 1121, IEEE vol.2, 13 – 18 July 1997.

[4] Breed, G., "*A Summary of FCC Rules for Ultra Wideband Communications*", High Frequency Electronics, Summit Technical Media, January 2005.

ISSN: 1411-1284

Audio Video Processing on Tapeless On-Air Television System

Dodi Sudiana* and Mohamat Sudiantoro*

* Dept. of Electrical Engineering, Fac. of Engineering, University of Indonesia,
Kampus Baru UI, Depok 16424
Tel. +62-21-727-0078, fax. +62-21-727-0077 email : dodi@ee.ui.ac.id

Abstract-**Digital on-air television system has been rapidly developed in the digital-era nowadays. The analog TV system was broadcasted in 1941 for the first time (B/W, NTSC), followed by colour NTSC in 1953. PAL and SECAM were introduced in 1960 and in 1982 broadcast engineers developed the digital video for the first time. HDTV as a new television standard was initiated in 1990, MPEG1, JPEG, DBV and MPEG2 are launched in 1991, 1992 and 1994, respectively. Up to now these system are still in development and new technologies grow rapidly. In Indonesia, most of TV stations have recorded video in analog format and converted them to digital, however, the broadcasting system transmits the video in analog format again due to the receiving TV systems belong to the audiences. Since the video is recorded and edited on magnetic tapes, it could be damaged due to scratch, dirt, fungus, and other physical disturbances. Therefore, the quality of both video and audio will be degraded. To solve this problem, the analog audio and video signal could be converted to digital and compressed to MPEG2 format to save the allocation space. The whole editing system is performed using computers and no tapes are involved (tapeless system). This paper will discuss the conversion of analog audio and video signals into digital format and evaluate its performance in a real video production on a tapeless on-air television broadcasting system.**

Keyword: *video audio processing, tapeless on-air television system, MPEG2*

I. INTRODUCTION

The advanced technology of digital audio-video processing has been changed the television broadcasting industry. TV stations have to attract more audiences in very tight competition and TV programs have to be zero mistaken. One of the solution to have high quality in audio and video broadcasting is to convert the analog data to digital format, eventhough the broadcasting is still in analog due to the widely used analog TV receiving systems belong to the audience. Since all of recordings are converted to digital format, they are stored in computers storage, so the operation cost can be reduced because there are no video tapes needed. Previously, the magnetic tape in Betacam format is the major recording storage in many TV broadcasting companies. There is a major problem in using magnetic tapes, i.e. the tape player/recorder. Mechanical rotation in the tape and direct contact between the head and the tape could be resulted in scratches on the tape surfaces. Tropical high temperature and humidity could also introduced fungus in the tape. Stacks due to mechanical problem in the player/recorder could also cut the magnetic tape itself. Since all of these problems could be occured anytime, the production cost will rise and the risk of broadcasting failure, which is the most fatal problem, will be worst. More vulnerable digital audio/video format will solve these problems, although still has some weakness in storage system.

Digital on air and *tapeless TV production* have been developed as a new trend in the world TV broadcasting industries nowadays, including Indonesia. Several TV stations have applied this system in their production lines. Using digital communication, *broadband network* and *digital storage*, the efficiency in space, time, cost and high quality Audio/Video should be achieved in the production process. New broadcasting companies in TV industry could also be built with less initial cost.

This paper will analyze the digital audio/video conversion process and the performance of digital on-air and tapeless TV production system in term of quality of data and efficiency in time and storage space. The sample data was taken from one of TV broadcasting company in Jakarta.

II. BASIC THEORY

Image is a 2-dimensional data, which is formed from the light reflectance of an object captured by an imager. The imager could be human eyes, camera or scanners. The intensity of light in the image could be expressed as $f(x,y)$, where:.

(x,y)	: cartesian-coordinate in 2-dimension
$f(x,y)$	: light intensity at point (x,y)

The intensity function is a multiplication of the light received $i(x,y)$ and the reflectivity of the object $r(x,y)$. Light has color characteristic which is described as color

temperature. In a clear day, the sun gives light energy of 9000 fc (footcandle), 1000 fc in a cloudy day and 0,01 fc of a full moon in the night. The reflectivity r(x,y) depends on the capability of the object reflects the signal, which is 0 for a perfect absorbance objects and 1 for perfect reflective objects. The intensity *f(x,y)* of a black and white picture is stated as gray level.

$$i_{min} < f < i_{max} \quad (1)$$

Color images is spectral images, which consist of three basic color components per picture point (pixel). Color intensity at a pixel point is a composite of the three color intensities. In a TV system, color addition system is used to compose any color, which is red, green and blue. Other system is subtractive color mixing which is widely used in printing and drawing. The pigment colors are: yellow, red and blue. The digital imageries are converted from analog images through sampling and quantization. For example, an analog image in 3×3 cm size is sampled to 30×30 pixels which is stored as a matrix in the computer memory as shown in Fig. 1. The more detailed the sample is taken, the higher resolution of digital image is achieved. Nowadays, the sampling rate of analog imageries acquired using commercially available camera have reached 5 Mega pixel and still increasing for various size of images. Therefore, the quality of digital images almost the same as the analog ones.

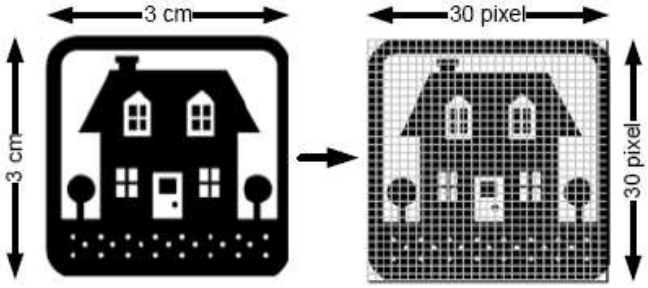

(a) (b)

Figure 1. a. Example of an analog image, b. Sampling process of an analog image with a matrix 30×30 size

TV cameras record moving objects through the lenses and a prism block to refract into red, green and blue, convert the light energy into electrical signals using the Charge Coupled Display (CCD) as shown in Fig. 2. The output of CCD signal is analog and modulated by an encoder.

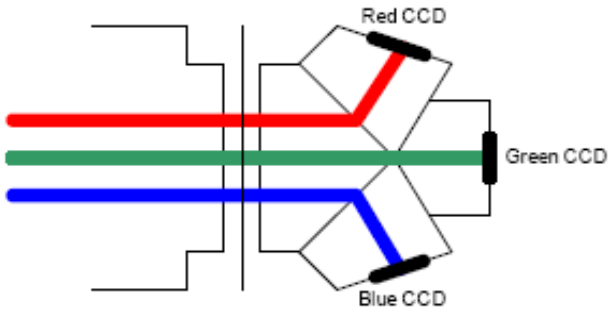

Fig. 2. Prism block and the CCD

There are 3 color systems that generally used in the world TV industry: Phase Alternating Line (PAL), National Television System cCommittee (NTSC) and SECAM (Séquentiel couleur à mémoire, French which means sequenced color with memory) as shown in Fig. 3. PAL has 625/50 Hz scanning line per frame, 25 frame per second and bandwidth 5,5 MHz, while NTSC has 525/60Hz scanning line per frame, 30 frame per second and 4,5 MHz bandwidth.

Indonesia, Australia and most of countries in Asia have adopted PAL system. NTSC is used in the US, while SECAM mostly used in the European Union. In the PAL coloring system, the red, green and blue signals from CCD are converted to YUV matrix. The block diagram of PAL encoder system is shown in Fig. 4. NTSC and SECAM signals are converted to Luminance-Chrominance and YdbDr matrices, respectively.

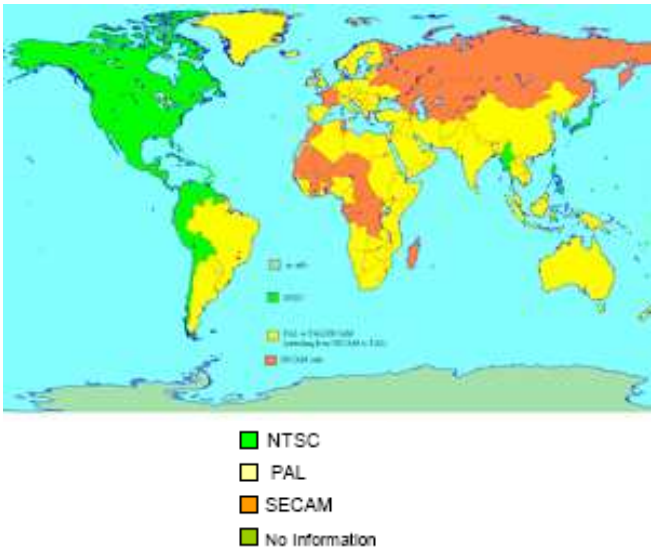

Figure 3. Color System used in the world TV system

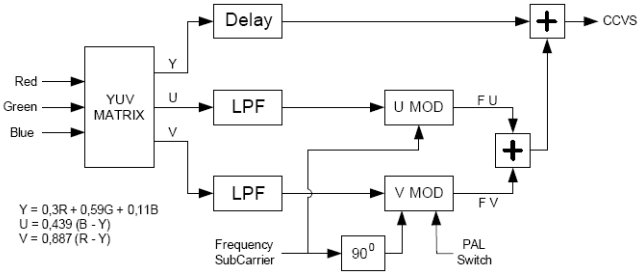

Figure 4. Block diagram of PAL encoder

Y signal is the Luminance or moving images without color (black and white), U and V are the color component of PAL system with a certain composition as shown in the Figure. The encoder uses the Quadrature Amplitude Modulated Subcarrier as modulation method which resulted in Color Composite Video Signal (CCVS) or simply called as video. This analog video is then converted into uncompressed digital video using ADC (Analog to Digital Converter). Video compression is used to reduce the digital video bitrate and get more efficiency in memory or storage space and resulted in the reliability in transmission both audio and video. There are several compression methods, such as AVI, WAV, MP3 and MPEG. In the case study at one of TV broadcasting company, MPEG compression is selected.

The video format is 4:2:0, PAL with 25 frame per second bit rate, so the 122 Mbps video could be compressed to only 12 Mbps.

III. VIDEO COMPRESSION METHOD

The compression of audio and video is performed by reducing the data redundancy in transmission process and recover the original data in the receiver side. Pair of transmiter and receiver is called the codec (coder and encoder). A video codec is a device or software that enables video compression and/or decompression for digital video. In the video signal there are two redundancies: (a) temporal and spatial redundancy and (b) psychovisual redundancy. Temporal redundancy could be defined as pixels in two video frames that have the same values in the same location. Exploiting temporal redundancy is one of the primary techniques in video compression, while spatial redundancy is the elements that are duplicated within a structure, such as pixels in a still image and bit patterns in a file.

Psychovisual redundancy deals with lossy compression, so the information could be lost to some extent. Since the human eye does not respond to all visual information with equal sensitivity, some information is simply of less relative importance. This information is referred to as psychovisual redundant and can be eliminated without introducing any significant difference to the human eye. The reduction of redundant visual information has some practical applications in image/video compression. Since the reduction of psychovisual redundancy results in quantitative loss of information, this type of reduction is referred to as quantization. The most common technique for quantization is the reduction of number of colors used in the image, thus color quantization. Since some information is lost, the color quantization is an irreversible process. Even if this method of compression is lossy, in situations where such compression technique is acceptable the compression can be very effective and reduce the size of the video considerably.

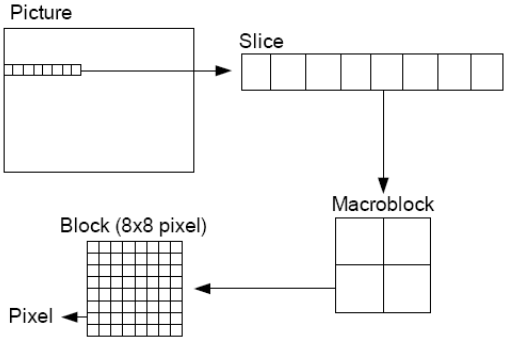

Figure 5. Hirarchy of digital frame

MPEG2 describes a combination of lossy video compression and lossy audio compression (audio data compression) methods which permit storage and transmission of movies using currently available storage media and transmission bandwidth. It is widely used as the format of digital television signals that are broadcast by terrestrial (over-the-air), cable, and direct broadcast satellite TV systems. It also specifies the format of movies and other programs that are distributed on DVD and similar disks. Basically the structure of the frame in MPEG2 is the same as digital frame shown in Fig. 5. Since there are redundancies in the video frames, several frames could be predicted from the previous or the next one. Therefore, not all of the frames are transmitted so the bandwidth becomes smaller. MPEG-2 specifies that the raw frames be compressed into three kinds of frames: intra-coded frames (I-frames), predictive-coded frames (P-frames), and bidirectionally-predictive-coded frames (B-frames). An I-frame is a compressed version of a single uncompressed (raw) frame. It takes advantage of spatial redundancy and of the inability of the eye to detect certain changes in the image. Unlike P-frames and B-frames, I-frames do not depend on data in the preceding or the following frames. Briefly, the raw frame is divided into 8 pixel by 8 pixel blocks as shown in Fig. 4. The data in each block is transformed by a discrete cosine transform. The result is an 8 by 8 matrix of coefficients. The transform converts spatial variations into frequency variations, but it does not change the information in the block; the original block can be recreated exactly by applying the inverse cosine transform. The advantage of doing this is that the image

can now be simplified by quantizing the coefficients. Many of the coefficients, usually the higher frequency components, will then be zero. The disadvantage of this step is the loss of some subtle distinctions in brightness and color. If the inverse transform is applied to the matrix after it is quantized, the output image looks very similar to the original image but that is not quite different. Next, the quantized coefficient matrix is compressed. Typically, one corner of the quantized matrix is filled with zeros. By starting in the opposite corner of the matrix, then zigzagging through the matrix to combine the coefficients into a string. Next step is substituting run-length codes for consecutive zeros in the string, and then applying Huffman coding to that result. The matrix will be reduced to a smaller array of numbers. This array is the information that is broadcast and in the receiver side, the whole process is reversed, enabling it to reconstruct, to a close approximation of the original frames of video. Typically, every 15th frame or so is made into an I-frame. P-frames and B-frames might follow an I-frame like IBBPBBPBBPBB(I), to form a Group Of Pictures (GOP).

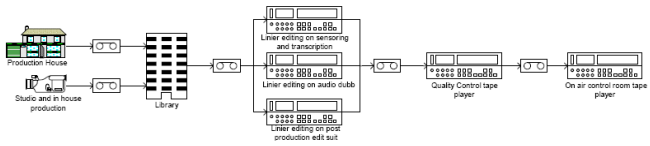

Figure 6. The production process of tapeless on-air system

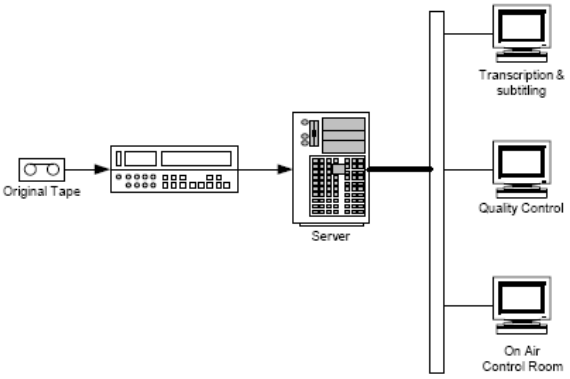

Figure 7. The production process of movie program: "Layar Emas" using tapeless on-air system

In the TV broadcasting company, digital video is stored, edited, and transmitted as a production process which is depicted in Fig. 6. For a movie production, "Layar Emas" for example, the tapeless on-air production involves 3 clusters of server node as shown in Fig. 7. Each node has 8 harddisks with capacity of 36 Gbyte (for cluster 1 and 3) and 146 Gbyte (for cluster 2). The total capacity of video server is then (2 nodes × 36 Gbyte × 8 × 3) + (1 node × 146 Gbyte × 8 × 3)= 5,232 Gbyte. The storage format used in these servers is RAID5, therefore 1/3 of the total capacity of the servers is used to store RAID5 data format. The advantage of this system is keeping the server up even there is an error in one of the disk. The memory allocation of the video server is 1.744 Gbyte (1/3 of the total system capacity) for system format RAID5, 1,152 Gbyte for commercials and 2,336 Gbyte for TV broadcast program. Audio and video data which has already broadcasted will be erased from the disk and replaced by a new program. Since November 2006, the station has been applied the tapeless on-air system comprehensively. All of programs such as dramas, movies, cartoons and news (in package) are broadcasted using a playlist which contains the audio and video stored in the server. Although magnetic tape player/recorder (VTR) is still prepared in the control room to handle any trouble on the servers. VTR is also used when there is a delay of program recordings delivery to the station, so there is no time to ingest (converting, editing, etc.) the video.

IV. ANALYSIS RESULTS

Since it was launched in November 2006, the tapeless on-air system is evaluated based on errors occur in the production process. The data is sampled from editing room, libray and master control before and after the new system is applied. The process monitoring is performed manually based on complaints from the editing operators or editors. Operational hours of editing room is 16 hours, while the library and master control rooms is 24 hours, respectively.

Based on the number of complaints, the errors are categorized as: VTR error (such as jammed), NLE & Server (hang, hardware error), mechanics (roller, tape cut-off), electronics (power line, synchronization), installation (driver corrupts), software, human (skill).In the period of 20003-3006, the total number of errors and monthly averaged errors occur in the production process is shown in Fig. 8 and Fig. 9, respectively.

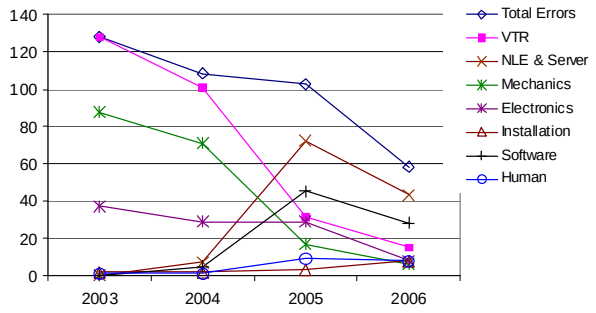

Figure 8. Total number of defects and errors in the production process

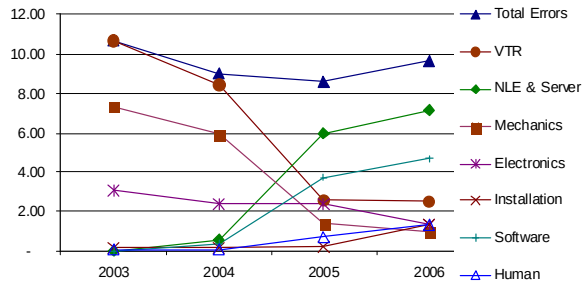

Figure 9. Monthly averaged number of defects and errors in the production process

For comparison, the total number of errors in tape-based and tapeless on-air system in the production process are also presented in Fig. 10 and 11, respectively. In these figures, the trend of tape-based errors is decreasing since the application of tapeless system since Nov. 2006. VTR is the most erroneous part in the system since it involves mechanical movement of magnetic tapes, however, these errors are decreasing as the tapeless on-air system is applied in 2006.

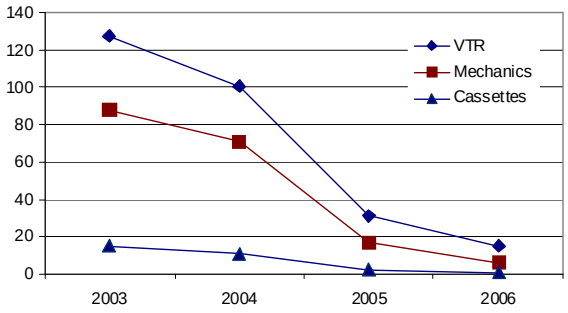

Figure 10. Total number of errors on tape-based on-air system

In the tapeless on-air system, the most erroneous part is the NLE-servers, since they had initial errors since the first intallation, followed by software due to the same reason. The installation error is increasing due to the new handling of software installation that needs skillful operator. As shown in Fig. 9, the lack of skillful operator increases the error caused by human factor.

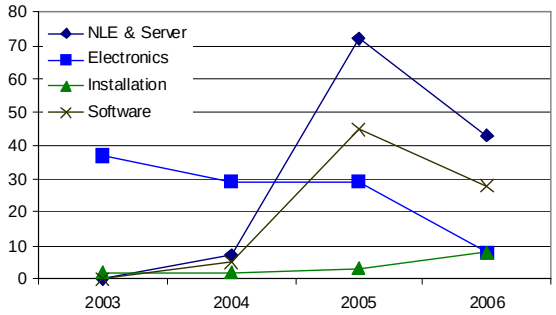

Figure 11. Total number of errors on tapeless on-air system

Table 1. Observation results of audio and video quality in one of the TV program

Date	Time	Program (Movie Title)	Error Type		Err. Frames
			Video	Audio	
14/11	22:24	Twin Effect 2	Boxes on moving object (BoMO)	-	2-3
	22:43		BoMO	-	2-3
	23:38		BoMO	-	2-3
15/11	22:15	Independence Day	Distributed crystal box (DCB)	-	2-3
16/11	22:45	Swordsman 2	BoMO	-	2-3
17/11	-	Setahun Samsons	-	-	-
18/11	22:49	Lovely Luna	DCB	-	2-3
	23:58		DCB	-	2-3
19/11	22:56	Ih Mama Capek Deh!	DCB	-	2-3
	23:08		DCB	-	2-3
	23:24		DCB	-	2-3
20/11	-	OB Spesial	-	-	-
	-	Delik	-	-	-
	-	Tracking	-	-	-
21/11	22:45	Armor of God	Freeze 1 frame	-	2
	23:00		DCB	-	2-3
22/11	-	The Peace Maker	-	-	-
23/11	22:45	Born to Defence	DCB	-	2-3
24/11	-	Jaka Tingkir	-	-	-
25/11	22:55	Tak Biasa	Lined Video	-	25
	23:40		DCB	-	2-3
	23:55		DCB	-	2-3

To evaluate the quality of video broadcasting, the observation is performed for a month on a program (layar emas) and other programs in the same time

segment (22:00-24:00). The program is observed using a TV unit (SHARP fineCrystal 21inch). The main observation is the quality of digital audio and video, not the strength of the signal received.. If the error occurs in the quality of audio/video, then the source of errors resulted from production process or computer storage. If the errors occur in the receiving unit, then the source may be from the broadcasting or TV receiving system. The observation result is shown in Table 1.

V. CONCLUSIONS

The implementation of tapeless on-air system has reduced the total errors in TV broadcasting system. From the data samples obtained, during 2003-2006, the decreasing of errors by implementing tapeless on-air TV system could reach 21% (2003-2004), 69% (2004-2005), and 17% (2005-2006), respectively. Human and installation error is increasing due to the lack of human resources. The quality of video observed mainly due to the production process and errors averaged at 2-3 frames, except a program with lined video which exceeds 20 frames.

REFERENCES:

1. P. N Tudor, MPEG-2 Video Compresion, Electronics & Communication Engineering Journal, December 1995.
2. The Free Encyclopedia, PAL, Wikipedia, May 2006.
3. The New Paradigm for Digital Video Storage & Delivery, SeaChange Broadcast MediaCluster.
4. Technical On Air Control Room Section dan Maintenance Section, Daily Report, RCTI, 2006.

ISSN: 1411-1284

DUAL FREQUENCY EQUILATERAL TRIANGULAR MICROSTRIP ANTENNA FOR INDOOR GSM APPLICATION

Fitri Yuli Zulkifli, Agus Rahmatullah, Eko Tjipto Rahardjo
Antenna Propagation and Microwave Research Group (AMRG)
Center for Information and Communication Engineering Research (CICER)
Department of Electrical Engineering, University of Indonesia
Kampus Baru UI Depok, West Java,16424, Indonesia
Email: yuli@ee.ui.ac.id, 4g00se@gmail.com, eko@ee.ui.ac.id

Abstract -**Indoor GSM network is needed to distribute GSM signal into high buildings. The network needs antenna to transmit signal into each levels in the building. Researches in microstrip antenna which operate in GSM band are used for outdoor base station and mobile station application. This paper proposes microstrip antenna for indoor GSM network.**

GSM network operates in both frequency band 890 MHz – 960 MHz (GSM 900) and 1710 MHz – 1880 MHz (GSM 1800). Microstrip antenna with equilateral triangular patch and fed by microstrip line is designed to produce the first frequency band GSM 1800. The second frequency band is produced by adding a stub which acts like a monopole antenna at the feed line.

The measurement shows the designed microstrip antenna works at GSM 900 and 1800 frequency band. The impedance bandwidth in 900 band is 272 MHz with gain approximately 1 dB. For the 1800 band, the impedance bandwidth is 380,31 MHz and gain is approximately 4 dB.

Keywords – Dual frequency, microstrip antenna, indoor GSM application

I. INTRODUCTION

GSM networks (Global System for Mobile Communication) have enormous growth over the last decade. The GSM users want more mobility, able to communicate indoor and outdoor. At first, GSM used only one frequency band at 890 – 960 MHz, but because this band is limited in its mobility and the need for capacity, then another frequency band is used 1710 -1880 MHz. [1]

The GSM network is basically planned for outdoor use, but now, GSM users in buildings increases. Therefore GSM must also plan indoor coverage. In order to cover customer in buildings with low receiving signal, it needs indoor network. Indoor GSM network use a BTS to connect to MSC, and also indoor antenna in each levels to transmit signal to the customer. There are two types of indoor GSM antenna, omni directional and panel directional [2]. Both of them are usually made from aluminum. There is another type of antenna which could also be used in indoor GSM network because of its low profile and easy to fabricate. This research proposes the use of microstrip antenna for indoor GSM antenna.

There has been an increase interest in microstrip antenna for GSM application such as [3] - [6]. Reference [3] designed microstrip antenna with conformal shape for 3G base station application. Reference [4] used microstrip antenna PIFA double patch rectangular stacked array and used shorting pins and slot. This antenna is applicable in GSM 1800 handset. In [5] the antenna is a compact dual band dual polarized antenna, applicable for GSM, DCS and UMTS base station. While in [6], a multilayer array microstrip antenna for dual band GSM is designed. From the references [2] – [6], the antennas are either for outdoor applications or they are not microstrip antenna designs for indoor GSM.

Therefore, this paper proposes a dual frequency equilateral triangular microstrip antenna for indoor GSM application.

II. ANTENNA DESIGN

The antenna design uses equilateral triangular patch due to minimize the dimension of the patch antenna. The substrate parameter which is shown in table 1 is used in designing and fabricating the antenna.

Table I
Substrate parameter for antenna

Parameter	Value
Substrate type	TLY 3 0310 CH/CH
Relative dielectric constant	2.33 ± 0.02
Loss tangent	0.0012
Dielectric thickness	0.7874 mm
Conductor thickness	0.01778 mm
Thermal conductivity (90^{o} C)	0.22 W/m/K

The designed antenna in this research is fed with microstrip line feed which operates in dual frequency band GSM 900 (890 MHz – 960 MHz) and GSM 1800 (1710 MHz – 1880 MHz).
The feeding technique used is micostrip line feed technique. By putting the impedance of the line to 50 ohm, substrate thickness 0,031 inch, and dielectric constant to 2,33, the feed width is 5,40 mm.

In order to produce the second frequency band 900 MHz, a reactive load was used. Dual characteristic of the bandwidth is cause by adding a stub on the feed line which acts like a monopole antenna.

The optimum length and the position of the stub were characterized by using simulator Microwave Office software. The designed antenna is shown in figure 1.

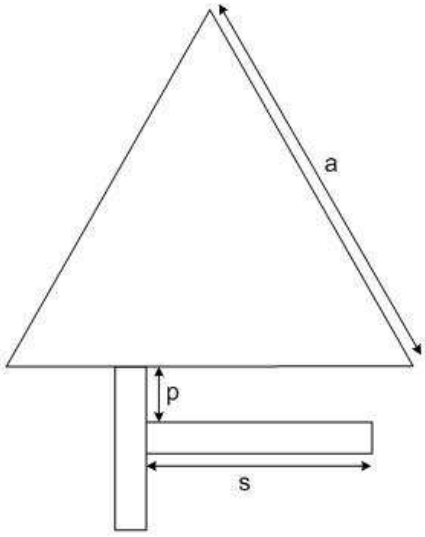

Fig 1 The configuration of proposed antenna design

By adjusting stub length s and stub position p, characteristics such as impedance bandwidth, return loss and VSWR changes. Both parameters play an important role to perform dual frequency antenna. Fig. 2 and 3 shows the characterization of the antenna.

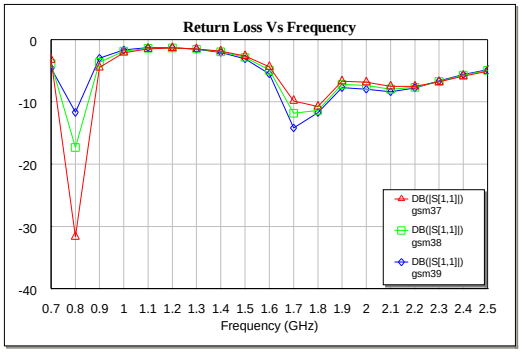

Fig 2 Monopole length characteristic

Figure 2 shows the characterization of the parameter monopole length (s). The monopole length was simulated from 37 mm to 39.5 mm. The result was a trade of between dual frequency impedance bandwidth or good impedance matching. The optimum result was at 38,5 mm stub length. This gives better impedance bandwidth at both frequency bands and better return loss.

Figure 3 shows the stub position (p) characteristic to produce the second frequency band. The figure shows that at 9 mm stub position, an optimum return loss in both frequency bands are achieved.

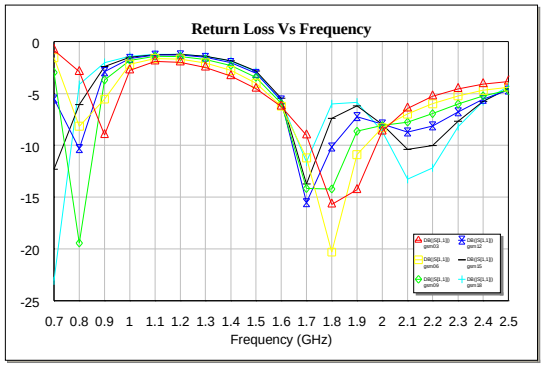

Fig 3 Monopole position characteristic to frequency

The optimum result of the antenna characterization is shown in in Fig. 4.

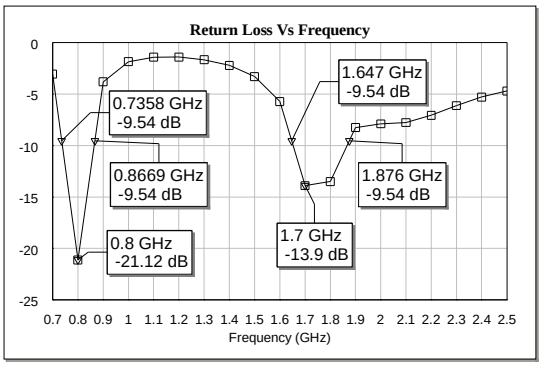

Fig 4. Simulation result of Return Loss VS Frequency

Fig 4 shows the impedance bandwidth of the antenna at VSWR = 2 is 131,1 MHz in 800 MHz frequency band (735,8 MHz - 866,9 MHz). While in 1800 MHz frequency band, the impedance bandwidth is 229 MHz (1647 MHz – 1876 MHz).

III. ANTENNA MEASUREMENT

The most important thing in the fabrication is accuracy of the antenna design which has to be very precise with the designed because at high frequency, a little difference in antenna dimension will change the antenna parameter. Antenna measurement is held in Anechoic Chamber, which can absorb electromagnetic wave to decrease reflection and interferences in measuring antenna.

A. Single Port Measurement

Figure 5 and 6 shows the measurement result of input impedance and return loss respectively. From fig 5, the input impedance for frequency resonance 902,98 MHz is 55,529 – j1,621 ohm.

Figure 6 shows the antenna impedance bandwidth with VSWR $\leq$ 2 is 272 MHz (708,42 – 980,47 MHz) or 30.12 % to resonance frequency (902,98 MHz) in 900 MHz frequency band. For 1800 MHz frequency band, the impedance bandwidth is 380.31 MHz (1541.37 – 1921.68 MHz) or 20.05 % to resonance frequency (1897 MHz). The return loss at 902,98 MHz is -23,198 dB and 1897 MHz is about -19 dB.

.

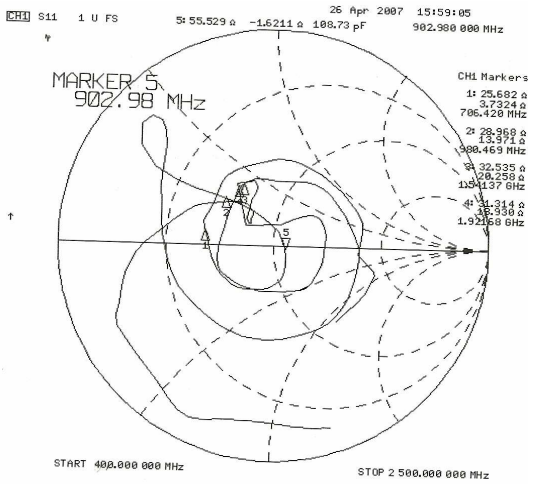

Figure 5. Input Impedance measurement of proposed antenna

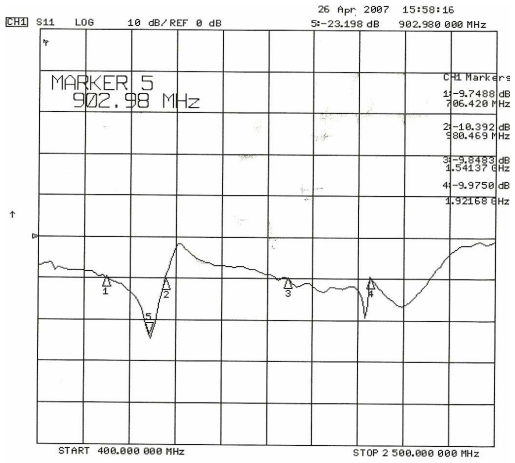

Figure 6. Return Loss measurement of proposed antenna

B. Radiation Pattern Measurement

Figure 7 and 8 shows the measured radiation pattern. Figure 7 shows the radiation pattern for 903 MHz resonance frequency. While Fig. 8 shows the radiation pattern for frequency 1800 MHz.

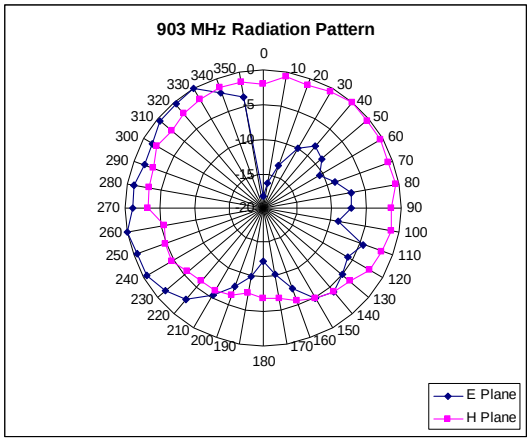

Fig 7. Radiation pattern of antenna at frequency 903 MHz

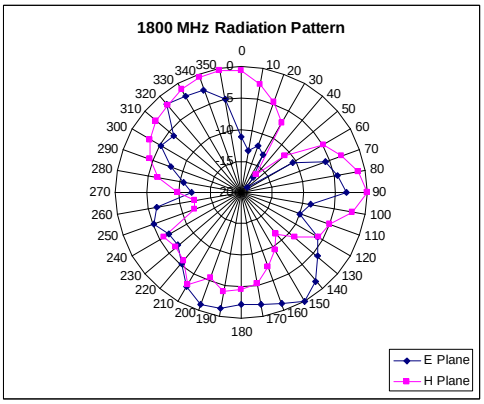

Fig 8. Radiation pattern of antenna at frequency 1800 MHz

C. Absolute Gain Measurement

The antenna gain is measured in operating frequency band at 890 – 960 MHz and 1710 – 1880 MHz. The gain measurements are shown in Fig. 9 and 10. From Fig.9 the antenna gain is ~1 dB in 900 MHz frequency band and ~4 dB in 1800 MHz frequency band.

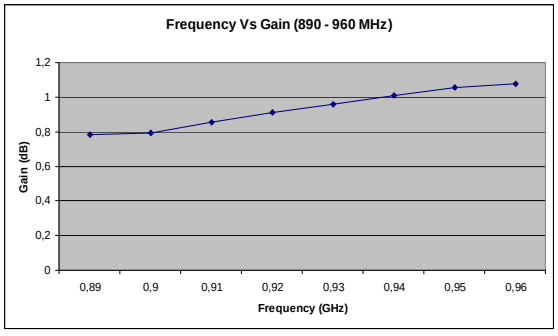

Fig 9. Gain antenna at frequency 890 – 960 MHz

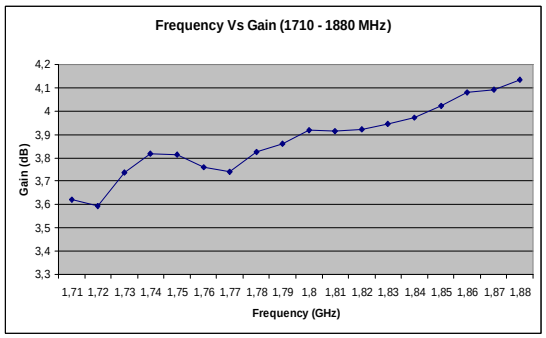

Fig 10. Gain antenna at frequency 1710 – 1880 MHz

CONCLUSION

This research has successfully designed, fabricated and measured dual frequency equilateral triangular microstrip antenna for indoor GSM application. The antenna can operate at both frequency band 900 MHz and 1800 MHz. The antenna operates from 708,42 MHz to 980,47 MHz in 900 MHz frequency band and 1541,37 MHz to 1921,68 MHz in 1800 MHz frequency band. The gain of the antenna is 1 dB for 900 MHz band and 4 dB for 1800 MHz.

REFERECE

[1] "Cell Planning Overview," Ericsson Radio System AB (October 2005), page 43

[2] "Installation of In Building Solutions," Ericsson Radio System AB, Ch 12

[3] Vedran Azman, *Conformal Antenna Arrays for 3G Cellular Base Stations* (Australia: University of Queensland, 2002), page 93 http://innovexpo.itee.uq.edu.au/2002/projects/s374365/

[4] Barreiros, Cameirao, Peixeiro , *Microstrip patch antenna for GSM 1800 handsets* (Lisbon : 1999) http://ieeexplore.ieee.org/Xplore/login.jsp?url=/iel5/6373/17053/00788370.pdf

[5] V. Deillon, J-F. Zürcher, A. K. Skrivervik, *A compact dual-band dual-polarized antenna element for GSM/DCS/UMTS base stations* (Lausanne: 2003) http://www3.interscience.wiley.com/

[6] V.B. Romodin and L.V. Shebalkova, *Dualband Microstrip Array for Wireless Communication* (Russia: 2005) http://www.actapress.com/PaperInfo.aspx?PaperID=20132

ISSN: 1411-1284

Synchronization Mechanism in Software for Optical Components Analyzer

Z. Akbar and B. Widiyatmoko

Research Center for Physics, Indonesian Institute of Sciences
Komplek PUSPITEK Serpong, Tanggerang, Banten, Telp. 7560570, Fax. 7560554
Email: zaenal.akbar@lipi.go.id

Abstract

An optical components analyzer has been developed and used by group for electronic and instrumentation, research center for physics, Indonesian institute of science since 2006. The system consists of several modules. I.e. broadband laser source, tunable filter, fiber coupler, photo detector and software. The software acting as a module to control, acquiring, and analyze data in real time scheme that is depending to a clock-constrained variable. Therefore we need a synchronization mechanism to synchronize all processes in software to gain an accurate result.

Previously, a manual timer implemanted as synchronization module on each process in software. Every process waiting for countdown timer reached before going forward. This mechanism is suitable for device under test that have similar characteristic. Top accommodatye various charateristic, we need to implement more promissing mechanism.

In this paper, we introduce our approach to synchronizing processes in software by implemanting a real-Time Communicating Sequential Processes (RTCSP) model. RTCSP is a language for modeling the communicating behavior of real-time systems. In applications of real-time CSP, each component of a system-hardware or software-is represented by a process indicating the point at which communication may take placde. These processes may then be combined to produce a description of the system in terms of its components.

As implementation, we identify every process that occurs in software and then from each process, we are looking for possible input and output, called event. All of these processes with their events then mapped in table to identify their possible events combinations. From this table, some rules generated with constraints that only one event could occurs in one time and some processes must be preceded by another process.

The result shows that by implementing RTCSP as synchronization mechanism, we argue that the system becoming more robust miss acquiring data.

Keywords: synchronization, real-time, optical components analyzer

ISSN: 1411-1284

A Preliminary Implementation Of Joint Source And Channel Coding In MIMO System

Lydia Sari†, Gunawan Wibisono‡, Dadang Gunawan‡‡

Electrical Engineering Dept. University of Indonesia, Kampus Baru UI Depok 16424
Tel. 7270078 Fax 7270050 E-mails: †lydiasari@cbn.net.id, ‡gunawan@eng.ui.ac.id, ‡‡guna@eng.ui.ac.id

Abstract – **The coding process in MIMO system is directly related to the effort of maximizing channel gain, namely diversity gain and multiplexing gain. In contrast to the channel coding extensively investigated in various research-literatures on MIMO system, the source-coding method for the system is typically not expressly covered. The justification for this common approach is the Shannon Separation Theory, which states that source and channel coding can be separately done without affecting the system performance. More recent researches show that the Shannon Separation Theory does not hold for certain conditions, which encourage researches on joint source and channel coding methods.**

In this paper a preliminary joint source and channel coding in the form of Rate Compatible Punctured Convolutional Code (RCPC Code) applied as an Unequal Error Protection (UEP) to the source stream is proposed. The RCPC code is achieved by puncturing a low rate 1/N code periodically with period P to obtain a family of codes with rate P/(P + ℓ) where ℓ can be varied between 1 and (N-1)P. Simulations are done to examine the performance of the code. Results show that the proposed RCPC code enables unequal error protection to the source information ordered with increasing importance. A further research is planned to implement RCPC on MIMO system.

Keywords – MIMO, Rate-Compatible Convolutional Code, Unequal Error Protection

I. INTRODUCTION

Current researches propose Multiple-Input Multiple-Output (MIMO) as the main technology to support digital wireless communications systems of the third generation and beyond. MIMO is an extension of smart-antenna technology, in which both the trasmitter and receiver sides of the system are equipped with multiple antennas. The technology is especially appealing due to its potential of linear-growing capacity as a function of antenna numbers, and its capability to exploit multipath fading which is a pitfall in conventional wireless communication system.

The coding process in MIMO system is directly related to the effort of maximizing channel gain, namely diversity gain and multiplexing gain. The diversity gain characterizes the system's robustness against errors, while multiplexing gain characterizes the system capacity. One of the theoretically suitable channel coding method for MIMO is Space-Time Code [1], which later extends into Space Time Trellis Code [2] and Space Time Block Code [3].

In contrast to the channel coding extensively investigated in various research-literatures on MIMO system, the source-coding method for the system is typically not expressly covered. The justification for this common approach is the Shannon Separation Theory, which states that source and channel coding can be separately done without affecting the system performance [4]. More recent researches show that the Shannon Separation Theory does not hold for certain conditions [5], which encourage still more researches on joint source and channel coding methods.

A recent approach of a joint source and channel coding method in MIMO is investigated in [6] mainly to obtain a performance parameter named expected distortion, while not specifying the code rate of the system.

One of the known concepts of joint source and channel coding is Unequal Error Protection (UEP) in which source information is given different level of protection according to its importance. A Rate-compatible Convolutional Code (RCPC) is a method which enables a system to have different code rates to match the source information requirements, and therefore can be applied in UEP. It is of our interest to examine the possibility of implementing RCPC codes on MIMO system.

The second section of the paper will cover the definition of RCPC code and its application to UEP is considered. The third section gives preliminary experimental result, and conclusion is given in the last section.

II. RCPC Code: Definition and Application on UEP

A family of RCPC codes is derived from a mother code of rate $R = 1/N$ and memory M with generator tap matrix [7]

$$g = \overset{\uparrow}{N}\underset{\downarrow}{\overset{\leftarrow M+l \rightarrow}{(g_{ik})}} \quad (1)$$

with tap connection (g_{ik}) $\in$ (0,1), where 1 denotes a connection from the *k*-th *shift register state* ke-*k* to the *i*-th output. *Puncturing period P* and *N* determine the code rate [7]

$$R = P/P+\ell \qquad \ell = 1,...,(N\text{-}1)P \tag{2}$$

from $P/(P+1)$ to $1/N$. RCPC codes are punctured codes from a mother code with puncturing matrices [7]

$$a(l) = \overset{\uparrow}{N}_{\downarrow}\left(a_{ij}^{\leftarrow P\rightarrow}(l)\right) \tag{3}$$

with $a_{ij}(l) \in (0,1)$ and 0 denotes puncturing. Puncturing ddecoder whilst using codes with different rates, instead of switching between an array of encoders and decoders. The puncturing of codes will provide a rate-compatibility with the following rules [7]

$$\text{if } a_{ij}(\ell_0)=1 \text{ then } a_{ij}(\ell)=1 \text{ for all } \ell \geq \ell_0 \geq 1 \tag{4a}$$

or equivalently

$$\text{if } a_{ij}(\ell_0)=0 \text{ then } a_{ij}(\ell)=0 \text{ for all } \ell \leq \ell_0 \leq 1 \tag{4b}$$

As RCPC codes are in the class of convolutional codes requiring Viterbi decoding in the receiver, the optimality criterion used follows Viterbi's upperbound error event probability [8]

$$P_E \leq \frac{1}{P}\sum_{d=d_{free}}^{\infty} a_d P_d \tag{5}$$

and error probability

$$P_b \leq \frac{1}{P}\sum_{d=d_{free}}^{\infty} c_d P_d \tag{6}$$

with P_d is th probability that the wrong path at distance *d* is selected. The distance spectra a_d and c_d should be as small as possible and depends on *N, M,P, g,* and $a(\ell)$. The transmission scheme for RCPC code over a nonfrequency-selective fading channel with multiplicative distortion a_F is shown in Fig. 1. The expectation value $E\{a_F^2\} = 1$ and [7]

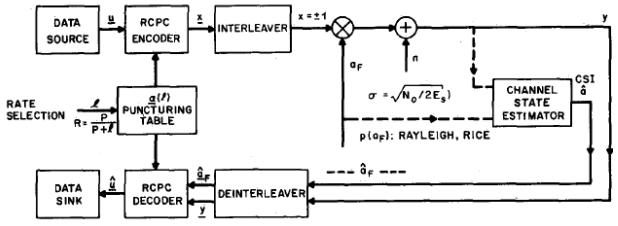

Fig. 1. Data transmission using RCPC [7]

$$p_{aF}(a_F) = 2\,a_F\,(1+C/M)\exp\left[-a_F^2(1+C/M)+(C/M)\right] \cdot I_0\left(2\,a_F\sqrt{(C/M(1+C/M))}\right) \tag{7}$$

For Ricean channel, *C/M* is the ratio of the direct to the diffusely reflected signal energy, while for *C/M* = 0 and *C/M* = ∞ a Rayleigh fading and a Gaussian channel is obtained, respectively. In the fading case a perfect interleaving is assumed, implying that the Channel State Information (CSI) values a_F and the received code values *y* are statistically independent with density function (7). The channel SNR is measured by E_s/N_0 where $E_s = E_b/R$ due to the varying rate of the code.

The Viterbi algorithm for decoding RCPC code uses the metric [7]

$$\lambda_j = \sum_{i=1}^{N} a_{ij} a_{ijF} x_{ij}^{(m)} y_{ij} \tag{8}$$

where x_{ij} denotes the transmitted binary information symbols, a_{ijF} denotes the fading factor with density $p(a_F)$, and y_{ij} denotes the received symbols.

The system performance in Rayleigh fading environment by soft decision on y_{ij} using the full CSI with perfect estimation is [7]

$$P_d \leq \frac{1}{2}\left(\frac{1}{1+E_s/N_0}\right)^d \tag{9}$$

Fig. 2 shows the RCPC performance for the Rayleigh channel. It is shown that BER 10^{-5} can be achieved with gains ranging from 7,9 dB and 20 dB, by changing the code rate from 1/3 to 4/5.

The application of joint source and coding is enabled by, among others, implementing unequal error protection on the transmitted binary information sequence. The protection given to more important bits is stronger compared to one given to the less important bits. This system requires the ability of the source coder to provide the information of this relative importance or vulnerability to errors of certain source bits. This type of information is called Source Significant Information (SSI).

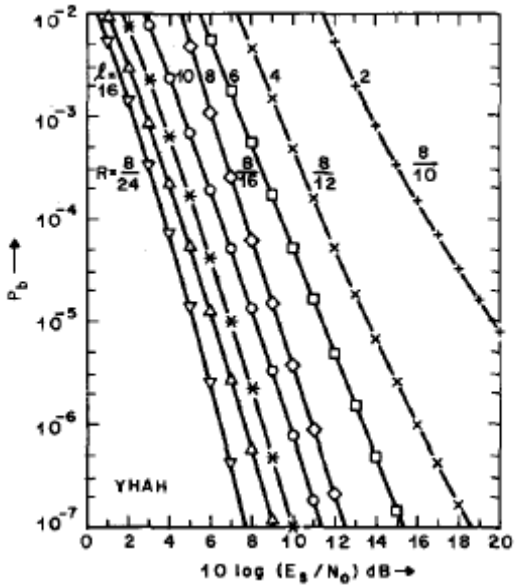

Fig. 2. BER performance of RCPC codes on interleaved Rayleigh channel, *N*=3, *P*=8, ℓ=2,4,...,16, *R*=8/(8+ ℓ), *M*=4 [7]

The required BER after decoding a group of information bits is one example of SSI. Assuming that in a block of *n* information bits there are *K* groups with n_k

information bits in the kth group requiring a BER of P_{bk} after decoding. P_{bk} would be the SSI and [7]

$$\sum_{k=1}^{K} n_k = n \tag{10}$$

Similar to [7], an example where source bits are ordered according to their relative importance and the required P_{bk} is given in Table 1. It is our interest to use only one encoder and one decoder for this purpose, instead of separately encoding K groups of information using K different encoders and K different decoders which might complicate the system.

Table 1. Data Frames Ordered According to the Required P_{bk}

		P_{b4} <	P_{b3} <	P_{b2} <	P_{b1}
	M	n_4	n_3	n_2	n_1
	"0"				
Code index ℓ_k		ℓ_4 >	ℓ_3 >	ℓ_2 >	ℓ_1
R_k		$P/P+\ell_4$	$P/P+\ell_3$	$P/P+\ell_2$	$P/P+\ell_1$
$a(\ell_k)$		$a(\ell_4)$	$a(\ell_3)$	$a(\ell_2)$	$a(\ell_1)$
Free distance		d_4	d_3	d_2	d_1

RCPC codes are well suited for this constraint. As shown in Table 1, the ordered information bits are shifted into the shift register of a 1/N, M stages RCPC coder. The first group consisting of n_1 information bits is coded using $a(\ell_1)$, and as the first bit of the second group enters the encoder, the system immediately switches to using puncturing table $a(\ell_2)$. The system will switch to puncturing table $a(\ell_3)$ as the first bit of the third group enters the decoder, and the process carries on until all information bits are transmitted. The process is terminated after the group n_k by shifting M "0" bits into the shift register. This implies transmitting M/R_k overhead bits to terminate the trellis, and the average code rate is then [7]

$$R = \frac{\sum_{k=1}^{K} n_k}{\sum_{k=1}^{K} n_k \cdot (P + l_k)/P + M(P + l_k)/P} \tag{11}$$

III. IMPLEMENTATION OF RCPC CODES ON MIMO SYSTEM

To be able to implement joint source and channel coding to MIMO system, it is proposed to implement unequal error protection (UEP) to the system. The information bits are ordered according to their relative importance as implied in Table 1, and the more important bits are given stronger protection. As the design of an ideal UEP which adapts channel coding to a multimedia source bits is very complex, in this preliminary work the source bits are modeled as discrete time continuous amplitude source, namely

$$\{s_k\}_{k=1}^{\infty}, s_k \in \Re \tag{12}$$

S different source information bits are transmitted using M_t transmit antennas in a Rayleigh fading environment, and M_r received antennas are employed in the receiver side. The transmission using multiple antennas result in a matrix channel. Fig. 3 shows the block diagram of a MIMO system.

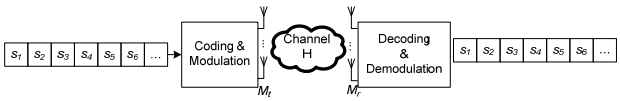

Fig. 3 Diagram of a MIMO wireless system

Assuming the channel undergoes flat fading and information signal s is transmitted by the t-th antenna, each of the receive antenna will see a complex-weighted version of the transmitted signal. A signal arriving at the r-th is denoted $h_{rt}s$, where h_{rt} stands for channel response between the t-th transmit antenna and the r-th receive antenna. The vector $[h_{1t}, h_{2t}, ..., h_{Mrt}]$ is the channel response between the t-th transmit antenna and all receive antennas.

The channel matrix for the MIMO system (**H**) can be written in a matrix notation, that is

$$\mathbf{H} = \begin{bmatrix} h_{11} & h_{12} & \cdots & h_{1M_T} \\ h_{21} & h_{22} & \cdots & h_{2M_T} \\ \vdots & \vdots & \vdots & \vdots \\ h_{M_R 1} & h_{M_R 2} & \cdots & h_{M_R M_T} \end{bmatrix}$$

If signal vector $\mathbf{x} = [x_1, x_2, ..., x_{Mt}]^T$ is transmitted consecutively by the 1st, 2nd, ..., up to the M_t-th transmit antenna, the arriving signals on the receive antennas can be written as:

$$\mathbf{y} = \mathbf{H}\mathbf{x} + \mathbf{z} \tag{13}$$

where **z** denotes the channel noise. The proposed MIMO system with UEP is shown in Fig. 4a and 4b.

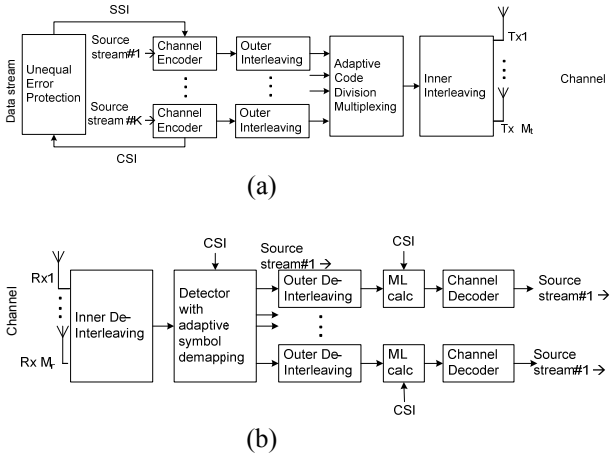

Fig. 4 Diagram of MIMO system with UEP, (a) transmitter, (b) receiver

The source significant information (SSI) is as explained in the previous section, while the channel state information (CSI) contains fading depth information. The adaptive modulation is proposed as it is theoretically possible to be implemented alongside RCPC codes whose rate varies with the source information bits, but will not be covered in this paper.

The code rate is punctured from a mother rate of ½, using an encoder with memory $M = 2$ and generator matrix

$$g = \begin{bmatrix} 1 & 1 & 1 \\ 1 & 0 & 1 \end{bmatrix}$$

Fig. 5 shows the rate-compatible puncturing scheme used in the simulation, where $P = 4$, and the puncturing table used is

$$a(1) = \begin{bmatrix} 1 & 1 & 1 & 0 \\ 1 & 1 & 0 & 0 \end{bmatrix}$$

implying a rate of 4/5.

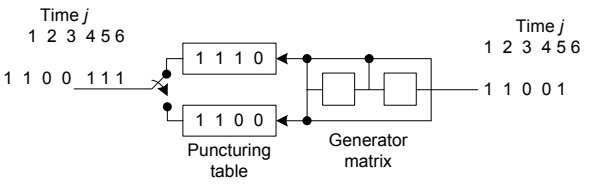

Fig. 5 Encoding scheme using RCPC codes

After a period of P=4, the group of bits use another puncturing table namely

$$a(2) = \begin{bmatrix} 1 & 1 & 1 & 0 \\ 1 & 1 & 1 & 0 \end{bmatrix}$$

which implies a rate of 4/6, and this rate can still be lowered further to 4/7, 4/8 using incremental redundancy. As the focus in this paper is the UEP using RCPC, interleaving, modulation as well as deinterleaving and demodulation are bypassed and the decoder performance is measured.

As the transmitted signal originate from multiple antennas, the rate is divided by the number of the transmit antenna M_t, resulting in

$$R = \frac{\sum_{k=1}^{K} n_k}{\sum_{k=1}^{K} n_k \cdot (P + l_k)/P + M(P + l_k)/P} \cdot \frac{1}{M_t} \qquad (14)$$

To ensure good performance, it has to be guaranteed that during the transitional phase between two matrices $a(\ell_k)$ and $a(\ell_{k+1})$, the distance properties of all paths originating in code ℓ_k do not suffer a loss of distance. The rate compatibility rule (4a) ensures that the ℓ_{k+1} code does not puncture any "1" in the path, that is, maintaining a certain maximal rate. Simulation result in Fig. 6 shows that the BER can be kept low at the transition between rates, and for 128 information bits BER can improve significantly between rates 4/5 to ½.

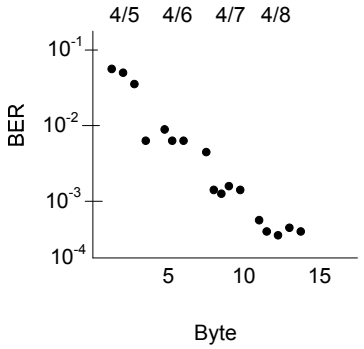

Fig 6. RCPC code performance on 128-bit source information

IV. CONCLUSIONS

A joint source and channel coding in the form of unequal error protection is implemented on a MIMO system by using rate-compatibility punctured convolutional codes (RCPC codes). Simulation is done using code rate 4/5, 4/6, 4/7 from a mother code of ½, and the code performance is measured by without taking modulation and interleaving into account. A single user Rayleigh fading enviroment is assumed. Result shows that RCPC enables unequal error protection, in which more significant bits are given stronger protection by rate ½ to get BER of 10^{-4}. Further investigation is planned to include modulation and multiplexing scheme in various conditions.

REFERENCES

[1] N. Seshadri and J.H. Winters, "Two Schemes For Improving The Performance Of Frequency-Division Duplex (FDD) Transmission System Using Transmitter Antenna Diversity," *International Journal on Wireless Information Networks,* vol. 1, pp. 49-60, January 1994.

[2] V. Tarokh, et.al, "Space-time Codes for High Data Rate Wireless Communication Performance Criterion and Code Construction," *IEEE Transactions on Information Theory,* vol. 44, pp. 744-765, March 1998

[3] S. Alamouti, "Space block coding: A simple transmitter diversity technique for wireless communications," *IEEE Journal on Selected Areas in Communications,* vol. 16 pp. 1451-1458, October 1998

[4] C.E. Shannon, "A Mathematical Theory of Communication," *Bell System Tech. Journal*, vol. 27, 1948

[5] S. Vembu and S. Verdu, "The Source-Channel Separation Theory Revisited", *IEEE Transactions of Information Theory*, vol. 41, no. 1, pp. 44-54, January 1995

[6] D. Gunduz and E. Erkip, "Joint Source-Channel Coding for MIMO Block Fading Channel", *IEEE International Symposium on Information Theory*, Seattle, July 2006.

[7] J. Hagenauer, "Rate-Compatible Punctured Convolutional Codes (RCPC Codes) and Their Applications", *IEEE Transactions on Communications,* Vol. 36, No.4, April 1988

[8] A.J. Viterbi and J.K Omura, *Principles of Digital Communication and Coding*, New York: McGraw Hill, 1979.